DEVELOPMENT OF FUNCTIONAL NEAR-INFRARED SPECTROSCOPY ANALYSIS METHODS TO SUPPORT BIOMARKER INVESTIGATION FOR DISORDERED CHILDREN

by

Stephanie Liana Utami Sutoko

A dissertation submitted to the Graduate School of Science and Engineering,

Civil, Human and Environmental Science and Engineering Course, Chuo University

in partial fulfillment of the requirements for the degree of

Doctor of Philosophy

in

Engineering

June 2020

Table of Contents

List of Tables

List of Figures

List of Abbreviations

AD	Alzheimer's disease
ADHD	attention-deficit/hyperactivity disorder
ANG	angular gyrus
ASD	autism spectrum disorder
ATX	atomoxetine
CFP	cingulo-frontal-parietal
CPT	continuous performance test
CW	continuous wave
dACC	dorsal anterior cingulate cortex
DF	degree of freedom
DLPFC	dorsolateral prefrontal cortex
DSM	Diagnostic and Statistical Manual of Mental Disorders
EDA	exploratory data analysis
EEG	electroencephalography
ERP	event-related potential
FC	functional connectivity
FD	frequency-domain
FDR	false discovery rate
FIR	finite impulse response
fMRI	functional magnetic resonance imaging
fNIRS	functional near-infrared spectroscopy
FWER	familywise error rate
GLM	general linear model
GNG	go/no-go
Hb	hemoglobin
HRF	hemodynamic response function
ICD	International Classification of Disease
IFG	inferior frontal gyrus
IQ	intelligent quotient
IQR	interquartile range
MBLL	modified Beer-Lambert law
MCI	mild-cognitive-impairment
MEG	magnetoencephalography
MFG	middle frontal gyrus
MNI	Montreal Neurological Institute

MPH	methylphenidate
MTG	middle temporal gyrus
NIR	near-infrared
OB	oddball
PCA	principal component analysis
PCC	posterior cingulate cortex
PoCG	postcentral gyrus
POTATo	Platform for Optical Topography Analysis Tools
PrCG	precentral gyrus
QoL	quality of life
ROC	receiver operating characteristic
RS	resting state
SMA	supplementary motor area
SMG	supramarginal gyrus
SNR	signal-to-noise ratio
SST	stop signal task
STG	superior temporal gyrus
SVM	support vector machine
SWC	sliding window correlation
TD	typically developing
VLPFC	ventrolateral prefrontal cortex

1   Introduction

1.1   Background

One of foremost factors of human quality of life (QoL) is health. Sick persons are unable to live their life to the fullest and consequently experience decreased QoL. Developmental disorders affecting children from the early age and being persistent over their life span will dramatically lower QoL. In 2016, 632 million children younger than 5 years old suffered developmental disorders (Olusanya et al., 2018). Prevalence of any developmental disorders for US children increased from 12.84% to 16.2–17.8% in 20 years (1997–2017) (Boyle et al., 2011; Zablotsky et al., 2019). Among developmental disorders, attention-deficit/hyperactivity disorder (ADHD) contributes to the highest prevalence rate with an increasing trend (Akinbami et al., 2011; Hill et al., 2015). ADHD patients and their family are significantly burdened by high annual medical costs ranging from $4,929–$5,651 (2004 estimates) (Matza et al., 2005) and treatment costs ($15,509–$19,281) to compensate per quality-adjusted life-year through methylphenidate (MPH) prescription (Gilmore et al., 2001). ADHD is one of global health issues, and worldwide health practitioners is striving to control this issue in purpose of improving QoL.

ADHD is characterized by age-inappropriate inattention and/or hyperactivity/ impulsivity. ADHD is commonly diagnosed based on the behavioral assessment using standard guidelines such as the Diagnostic and Statistical Manual of Mental Disorders (DSM) and the International Classification of Diseases (ICD). However, due to the diagnostic discrepancy between two standard guidelines (Döpfner et al., 2008; Adornetto et al., 2012), another perspective of biomarker is sought out to confirm ADHD pathophysiology. About 50% of parents with ADHD reported the occurrence cases of ADHD children (Starck et al., 2016). Therefore, ADHD is suggested as a hereditary disorder, and the genetic assessment is proposed to describe the ADHD phenotypes. Gene mutations related to the neurotransmitter (e.g., dopamine, noradrenaline, serotonin) and neuropeptide (e.g., oxytocin)

systems revealed the increasing risk of ADHD (Banaschewski et al., 2010; Sasaki et al., 2015). Despite those findings, the clinical practicability might be hindered by the invasive (i.e., drawing blood) and prolonged (e.g., a few days to several months) procedures.

Controlling executive functions and behaviors has been well known as one of brain functions. Therefore, the approach has been shifted to brain-based biomarkers (Fu et al., 2013; Hager et al., 2015). The non-invasive brain monitoring is provided by functional imaging techniques. Among those techniques, there are four intervention-free modalities (i.e., without tracer injection) including electroencephalography (EEG), functional magnetic resonance imaging (fMRI), functional near-infrared spectroscopy (fNIRS), and magnetoencephalography (MEG). However, by considering the practicability for children measurement, fNIRS offers benefits of natural environment measurement with moderate temporal and spatial resolutions.

fNIRS was developed for more than 25 years ago, and fNIRS studies have been attracted researchers reflected by the exponentially increasing publication number (Boas et al., 2014). fNIRS has also been applied to many application fields, such as neurology, psychiatry, psychology, and basic research (Ferrari et al., 2012). Those applications should be based on reliable analysis methods. There are two purposes in analyzing fNIRS signals: (1) removing endogenous (e.g., confounding non-neuronal components) (Germon et al., 1998; Obrig et al., 2000a; Tachtsidis et al., 2008; Tong et al., 2010) and exogenous (e.g., motion artifact) (Scholkmann et al., 2010; Brigadoi et al., 2014) noises, and (2) extracting information related to brain functions (Maki et al., 1995; Niu et al., 2014; Tak et al., 2014). As fNIRS is used for children measurement, the risk of motion artifact occurrence is heightened particularly in disordered children with hyperactive characteristics (e.g., ADHD). Extraction of brain function information from noise-affected signals will lead to inaccurate results (i.e., false positive or false negative). Prolonged measurements are sometimes done to improve the signal quality.

However, this solution may not work for disordered children that have a difficulty of attentive engagement. Furthermore, the well-established methods for extracting brain function information mainly focused on the applications of standard paradigm for normal adults. Therefore, the development of fNIRS analysis methods for disordered children measurement is inevitable. This development should consider the trade-off between measurement limitations (i.e., noise and measurement interval) and analysis accuracy. The usefulness of advanced analysis methods is then validated in exploring ADHD brain-based biomarkers. The results will clearly confirm the clinical practicability of fNIRS in pediatric studies.

1.2   Research objective

This dissertation aims to develop fNIRS analysis methods for disordered children measurement and to investigate the application of those methods on seeking potential ADHD brain-based biomarkers. These objectives are formulated in three frameworks as follows:

1. Development of noise removal algorithm to improve the conventional brain activation analysis and its application on ADHD children data (Chapter 3).

2. Development of analysis algorithm to extract the information of static functional connectivity (FC) during the performance of cognitive tasks and its application comparison to the conventional brain activation analysis for ADHD screening biomarkers (Chapter 4).

3. Investigation of dynamic FC analysis for task-based fNIRS signals and its insights into ADHD characteristics (Chapter 5).

1.3   Study outline

One of activation analyses adopted from fMRI analysis (Friston et al., 1994b) based on statistical linear model named General Linear Model (GLM) (Schroeter et al., 2004). GLM estimates the activation component following models of hemodynamic response function (HRF) (Buxton et al., 2004) that are modified

according to designated paradigms. Various HRFs, such as canonical (Worsley et al., 1995), finite impulse response (FIR) (Glover, 1999; Goutte et al., 2000), non-linear fit of two-gamma (Kruggel et al., 1999; Miezin et al., 2000), and inverse logit (Lindquist et al., 2007) models, have been created with different flexibility. In the rigid models (e.g., canonical), predetermined parameters are required, and mis-specification of parameters will greatly affect power loss. However, the most flexible model, FIR (i.e., without predetermined parameters), also results in some bias (Lindquist et al., 2009). Furthermore, the hemodynamic responses are varied across subjects, brain regions, and task paradigms (Handwerker et al., 2004; Steffener et al., 2009; Uga et al., 2014). Therefore, the simple average analysis during the task period might be more efficient to capture the task-evoked response without any assumed models. The unbiased control (i.e., baseline) task should be incorporated together in order to minimize interpretation errors.

The common experiments follow the block-design paradigm with alternating orders for control and designated (e.g., sensory, cognitive) tasks. The block-design paradigm is apparently similar to repeated boxcar functions over temporal courses with step functions representing intervals of designated task. This design results in more robust analysis with increased statistical power (Tie et al., 2009). Each interval of designated task is defined as a trial. As trials are affected by motion artifacts, trials are either corrected or rejected. Motion correction has been approached using corrective methods such as spline interpolation (Scholkmann et al., 2010), principal component analysis (PCA) (Zhang et al., 2005), wavelet filtering (Molavi et al., 2012), discrete Kalman filter (Izzetoglu et al., 2010), and correlation-based signal improvement (Cui et al., 2010). Predetermined parameters are also required, and there is no standard procedure to determine parameters. After being corrected, signal patterns may be dramatically altered, and this phenomenon raises the issue of overcorrection against correction methods. Comparisons of method effectiveness revealed inconsistent results (Robertson et al., 2010; Cooper et al., 2012; Brigadoi et al., 2014). Some factors such as artifact

types and intensities are likely influential to select optimum correction methods.

Another approach of motion rejection leads to the drawbacks of reduced trial number and statistical power. However, the risk of overcorrection and parameter assumption can be minimized. While correction methods have been widely established, a method to wisely reject motion-affected trials by considering the trade-off between remaining noises and decreased statistical power had not been addressed before. Therefore, the development of this rejection method is aimed in Chapter 3. The quantitative relationship between trial number and statistical power is initially investigate through a simulation. Variables of the strength of a phenomenon (i.e., brain activation) and the magnitude of motion artifact are added to the simulation. As the strength of a phenomenon is high, the number of trials can be minimum, and *vice versa*. The magnitude of motion artifact will disturb the equilibrium between the strength of a phenomenon and the necessary trial number. Because both variables are apparently uncontrollable during the real measurement, the statistical power are maintained to confirm the accuracy of analysis. This method focuses on the rejection of worst noisy trials and the acceptance of least noisy trials based on personalized standards. The feature of personalization brings an inclusive benefit for all children measurements with any conditions. This method is then applied to the clinical data in order to validate its applicability. The usefulness of this method as a preprocessing step is confirmed to another clinical data in purpose of searching differential diagnostic biomarkers.

In order to improve the analysis robustness, fNIRS signals are commonly averaged across trials (Tie et al., 2009). This method is relatively effective for the brain activation analysis, but the FC analysis cannot employ this method because the temporal information becomes disorganized. The development of preprocessing method to support the FC analysis is aimed in Chapter 4. This preprocessing method removes intermittent noises (e.g., motion artifacts) from continuous signals (i.e., temporal courses) and concatenates remaining signals. Therefore, the temporal information can be uniformly preserved, and the results

of FC analysis become more reliable. As ADHD children reveal impaired cognitive functions (e.g., attention and/or inhibition), brain measurements are frequently performed during the assessment of cognitive tasks with induced stimuli. Therefore, the FC analysis is possibly specified for the baseline and stimulus intervals. The alterations of FC due to stimulus-evoked responses may differ in ADHD children. These FC characteristics may be hints of ADHD neuropathophysiology. The applications of brain activation and FC characteristics for developing ADHD screening biomarkers are compared using the same optimization method. The optimization method selects the best-performing characteristics in classifying ADHD children from typically developing (TD) children. The involvement of temporal information in extracting brain functions expectedly brings merits by showing a better classification performance.

The concept of FC analysis described in Chapter 4 is the static FC analysis. The static FC analysis is a conventional method using the entire temporal information (e.g., baseline and task intervals) to figure out a single connectivity characteristic (Biswal et al., 1995). However, the assumed stationarity is seemingly farfetched because of the complex brain process. Therefore, the dynamic perspective was introduced to the FC analysis. Connectivities were found to alternate across the temporal course (Liu et al., 2013). The dynamic FC analysis was initiated based on fMRI study [see (Hutchison et al., 2013; Preti et al., 2017) for reviews]. The temporal resolution of fNIRS is better than that of fMRI. Therefore, the dynamic FC analysis is also potential to be applied on fNIRS signals. In a fNIRS study (Li et al., 2015), shifted connectivities have been revealed during the resting state (RS). The characteristics of RS dynamic FCs based on the fNIRS measurement also significantly showed the differences between mild-cognitive impairment (MCI) and Alzheimer's disease (AD) patients (Niu et al., 2019). Despite the recent interest, the dynamic FC analysis is still minorly assessed in fNIRS signals. To date, the dynamic FC analysis has not been implemented on fNIRS signals during task performances.

Chapter 5 discusses the application of dynamic FC analysis on task-based fNIRS measurements. The aforementioned preprocessing method for the static FC analysis is incompatible for the dynamic FC analysis. The concatenation of noise-free signals disorders the sequentially required temporal information for the dynamic FC analysis. Therefore, noise-affected signals should be corrected in a minimum effort to maintain the originality of signal pattern. The dynamic FC analysis evaluates connectivities between all measured regions (i.e., dynamic FC maps) in a short and shifted window across the temporal course. The global relationship among connectivities is defined by the term of connectivity states. Because the measurement is controlled by a uniform task, a hypothesis is proposed – there are several connectivity states that are commonly occurred and robust for all subjects. Therefore, the common and robust connectivity states should be initially found. An unsupervised clustering named *k*-means clustering is applied on the entire temporal course of dynamic FC maps for all subjects. A dynamic FC map is then assigned to a particular connectivity states in accordance with the pattern similarity. The occurrence probability for each connectivity state is assessed during baseline and stimulus intervals. Brain dysfunctions in ADHD children may lead to different occurrence probabilities for some connectivity states compared to TD children.

All results are arranged following the study outline and summarized in Chapter 6. Furthermore, how this dissertation contributes to more applicable fNIRS analysis for both clinical and research is also briefly described in Chapter 6.

2   Review of Literature

2.1   Brain and cognitive developments

From infants to adolescents, human brain volume increases fourfold (Johnson, 2001). For cerebral hemispheres, there are two developmental types: continuous growths and discrete growth spurts at specific brain regions and developmental periods (Thatcher et al., 1987). Discrete growth spurts within 6–12 months are found to be cyclical process for about 2 to 4 years (Thatcher, 1992). This phenomenon suggests that the cerebral development is a non-linear process [see (Durston et al., 2001; Taki et al., 2012) for reviews]. The cortical maturation process also happens in sequence following two scenarios – the maturation progress from a back-to-front direction for the anterior half of the brain, and *vice versa* for the posterior half of the brain (Gogtay et al., 2004). After the maturation for cortices related to lower-order processing (i.e., sensory, motor) has been completed, the maturation process for higher-order associated cortices is initiated (Gogtay et al., 2004). The maturation rates for subcortical and cortical regions are found to be different (Johnson, 2001). The maturation process from childhood to adolescence is identified by increases of white matter volume (Pfefferbaum et al., 1994; Bartzokis et al., 2001). While the volume of white matter linearly increases (Giedd et al., 1999) and remains constant in adulthood, the volume of gray matter increases in the early life (Pfefferbaum et al., 1994; Giedd et al., 1999) and gradually decreases (Sowell et al., 1999). The developmental trajectories for gray matter are gender-dependent (Lenroot et al., 2007) and region-specific (Sowell et al., 2003) as described by the U-shaped and inverted U-shaped functions. The delayed maturation is found in left posterior temporal cortices (Sowell et al., 2003). The mechanism behind the decreased volume of gray matter is still unknown; however, there are two proposed hypotheses – synaptic elimination (Huttenlocher et al., 1982; Huttenlocher, 1984) and axonal myelination (Benes, 1989; Benes et al., 1994). The structural development of cerebellum is found to be a non-linear and gender-dependent process as well (Diamond, 2000; Tiemeier et al., 2010).

The development of cognitive abilities is also observed from infants to adulthood. One of the famous cognitive development theories postulated by Jean Piaget described the developmental course into four stages – sensorimotor, pre-operational, concrete operational, and formal operational period (Piaget et al., 1969). In the sensorimotor stage (birth to 2 years old), babies perceive the knowledge of their surroundings using their sensing (e.g., visual, auditory, tactile). The second stage named pre-operational begins as children start learning to speak (2–7 years old). The development of cognitive functions is concentrated in symbolic and intuitive thinking with the egocentric characteristic. The next stage, concrete operational, happens in middle childhood and pre-adolescence (7–11 years old). In this stage, the function of inductive reasoning on concrete events is progressed, and the egocentrism is eliminated. Abstract and hypothetical thinking is developed in the last stage of formal operational (12 years old to adulthood).

Even though the framework of Piaget's cognitive development has been well-structured, there is a crucial argument. Piaget's cognitive development stages formulates the discontinuous concept (van der Maas et al., 1992) which the transition between stages is clear, and the development of cognitive function is described in particular periods. Another concept, namely, the continuous development oppositely hypothesizes the gradual development without distinct stages, and the early developed abilities are shown as basic skills for the further development.

Apart from the above argument, researchers tried to explain the course of cognitive development through the brain maturation concept. Gradual synaptic elimination with the strengthened connections of remaining synapsis may explain perceived cognitive functions during childhood (Casey et al., 2000). The functional imaging method evidenced the relationship between functional and cognitive developments. Children showed low memory performances; however, their brain activity in the dorsolateral prefrontal cortex found to be greater than that of adults (Cohen et al., 1994a; Casey et al., 1995). The similar phenomenon,

high activation volume in the prefrontal cortex for children, was also observed during the go/no-go (GNG) task (Casey et al., 1997). Even though similar brain regions may be activated for both children and adults, high activation magnitude and volume suggests the lacked sensitivity in accommodating and recruiting regions for children (Casey et al., 2000). Furthermore, the development of reasoning ability may coincide with the formation of structural connectivity between rostolateral prefrontal cortex and inferior parietal lobe (Wendelken et al., 2017).

Various parameters, such as nutritional intake (Ip et al., 2017; Yao et al., 2019), activity (Zeng et al., 2017), breastfeeding (Fonseca et al., 2013; Koh, 2017), environmental stimulation (Peyre et al., 2016), maternal depressive risk (Liu et al., 2017; Firk et al., 2018), preterm birth (Beauregard et al., 2018), and individual variability (de Ribaupierre, 2015; de Ribaupierre et al., 2018), have been reported to bring impacts on the cognitive development. Effects of those parameters on the brain maturation are still unclear. However, this point suggests that the cognitive development is unable to be simply explained using the theory of brain maturation (Stiles, 2011). Therefore, Bjorklund proposed the metatheory of developmental biology for a better understanding of cognitive development (Bjorklund, 2018).

2.2   Attention-deficit/hyperactivity disorder brain

Studies on ADHD brain attract researchers to unveil a better understanding related to relationships between structural/functional brain and symptoms [see (Rubia et al., 2014) for review]. ADHD children experience not only symptomatic behaviors but also delayed cognitive developments, such as verbal comprehension, expressive and receptive language, gross motor coordination, emotion understanding, and working memory (Dyck et al., 2014). These developmental delays may be associated with the late cortical maturation (i.e., the peak of cortical thickness and surface area) prominently in the prefrontal region (Shaw et al., 2007). ADHD children also reveal aberrant white matter connectivity within

fronto-parietal cortical networks (Silk et al., 2009) and cerebellar regions (Ashtari et al., 2005). Makris et. al. then showed the evidence of persistent abnormalities into adulthood (Makris et al., 2008). Total cortical and gray matter volume reduced for adolescents with ADHD. Volumetric reduction was found to be significant in lateral orbitofrontal, left inferior parietal, right caudal middle frontal, right medial orbitofrontal, and right superior frontal gyri (Noordermeer et al., 2017). These reductions are likely caused by cortical thinning (i.e., increased thinning rate) (Makris et al., 2007; Shaw et al., 2013).

Because attention and inhibition control (i.e., impulsivity) lacks are substantial ADHD symptoms, brain functions related to those behaviors are commonly examined. Several regions [i.e., dorsal anterior midcingulate cortex, dorsolateral prefrontal cortex (DLPFC), ventrolateral prefrontal cortex (VLPFC), parietal cortex, striatum, and cerebellum] involved in the cognitive-attention networks become evaluation interests (Bush, 2010). While performing any attentive and inhibitory tasks, ADHD subjects showed hypoactivation in those regions (Monden et al., 2012b; Hart et al., 2013; Nagashima et al., 2014a; Nagashima et al., 2014b; Nagashima et al., 2014c). Multiple fMRI datasets were used in a meta-analysis showing consistent hypoactivation in regions underlying on the cingulo-fronto-parietal (CFP) and fronto-basal ganglia networks (Hart et al., 2013). ADHD adolescents also encountered a difficulty in attention shifting and the dysfunctional parietal attentional system (Tamm et al., 2006). Furthermore, the strong motor network (i.e., motor, parietal, prefrontal, and limbic) found in ADHD subjects might also be associated with poor attentive sustainability that was reflected in high intra-individual variability of behavioral performances (O'Halloran et al., 2018).

Besides cognitive-related networks, DMN during the RS is found to be aberrant for ADHD. In an EEG study, ADHD children showed the reduced delta power in the frontal, central, and parietal regions (Shephard et al., 2018). Connectivities within DMN (Castellanos et al., 2008; Uddin et al., 2008) and inter

networks (Castellanos et al., 2008) (ventromedial prefrontal cortex) also reduced for ADHD adults. The coherence between dorsal anterior cingulate cortex (dACC) and posterior cingulate cortex (PCC) was abnormal for ADHD adults (Sato et al., 2012). During the RS, compared to healthy subjects, ADHD subjects revealed more significant connectivities between bilateral dACC, thalamus, cerebellum, insula, and brainstem (Tian et al., 2006). Furthermore, the ADHD dysfunctions were highly caused by the interference of DMN (Cortese et al., 2012; Hoekzema et al., 2014) during tasks and strong coherence between the left DLPFC and DMN during the RS (Hoekzema et al., 2014). The ADHD symptomatic severity was able to be estimated from the variability measured at dorsal and ventral medial prefrontal cortex (Nomi et al., 2018). The atypical ADHD network suggested a neuropathophysiological theory of brain maturation failure (Fair et al., 2010; Sato et al., 2012). However, Mostert et al. reported contrasting results of insignificant DMN between ADHD and healthy adults despite large sample number (Mostert et al., 2016). They argued that the heterogeneity of ADHD etiology may cause these inconsistent results.

There are two common medications used to ease ADHD symptoms named MPH (Schachar et al., 2008) and atomoxetine (ATX) (Michelson et al., 2002). Osmotically released MPH showed a preferable efficacy compared to immediate release MPH and ATX (Hanwella et al., 2011). However, the medication acceptability is individual-dependent (Newcorn et al., 2008); a non-responsive stimulant treatment might be replaced by non-stimulant drugs, such as ATX. Combined treatments (i.e., stimulant and non-stimulant) may be feasible and bring a better efficacy for some patients (Brown, 2004). Because of impaired brain functions, pharmacological effects on neuromodulation were also evaluated. MPH induced prolonged alteration of γ-amino butyric acid level (Solleveld et al., 2017) at the prefrontal that was closely related to the inhibition mechanism (Boy et al., 2011). The observed hypoactivation and abnormality were regulated approaching the level of healthy subjects by administering MPH (Vaidya et al., 1998; Shafritz

et al., 2004; Monden et al., 2012b; An et al., 2013; Nagashima et al., 2014c) and ATX (Nagashima et al., 2014a; Nagashima et al., 2014b; Araki et al., 2015; Ota et al., 2015). Even though neuromodulation has been confirmed, medication effects on behavioral performances sometimes remained insignificant (Shafritz et al., 2004; Matsuura et al., 2014). Task difficulty should be optimized to be more personalized; therefore, the behavioral performance can be appropriately associated with the medication effect. Furthermore, accomplishing cognitive tasks may require complex (high-order) neuronal systems which medication-evoked improvements in localized regions are insufficient.

2.3 Functional imaging for attention-deficit/hyperactivity disorder biomarkers

As mentioned above, brain functions were reported to be impaired for subjects with ADHD. The use of these impairment characteristics as biomarkers were then evaluated. Non-invasive functional imaging techniques, such as EEG, fMRI, fNIRS, and MEG, become versatile for translational studies. Table 2.1 shows several studies using various modalities and measurement paradigms for finding appropriate biomarkers.

Advantageous and disadvantageous features are found for each functional imaging techniques (Santosh, 2000); multimodality measurements have been performed to emphasize the benefits and to compensate the limitations. One of multimodality studies investigated the mechanism of persistent ADHD from childhood to adulthood. The combinations of fMRI and MEG (independent measurements) successfully inferred the adolescent-persistent ADHD pathophysiology – impaired DMN on the midline regions (Sudre et al., 2017), hypoactivation in the cortical and cerebellar regions, and low theta power at the specific time window (300–400 ms) (Szekely et al., 2017).

Unfortunately, to date, the clinical application of biomarkers is limited. Compared to other functional imaging techniques, EEG is the most mature technique in investigating ADHD. EEG-based diagnostic tools was clinically

13

Table 2. 1 ADHD biomarkers from various functional neuroimaging studies

Study	Remarks		
Monastra et al. (2001) (Monastra et al., 2001)	Subjects: 96 subjects with ADHD 33 controls Age: 6–20 years old	Modality: EEG	Results:
		Paradigm: Resting with eyes open, reading, listening, and drawing	Accuracy: 91% Sensitivity: 90% Specificity: 94%
	Biomarker: θ/β ratio at Cz θ/β ratio for ADHD subjects was higher than controls. θ/β ratio was age-dependent (children, early and late adolescents)		
Magee (2005) (Magee et al., 2005)	Subjects: 253 subjects with ADHD 67 controls Age: 7–13 years old	Modality: EEG	Results:
		Paradigm: Resting with eyes closed	Accuracy: 87% Sensitivity: 89% Specificity: 80%
	Biomarkers: powers of δ, θ, α, and β bands with the implementation of logistic regression		
Quintana et al. (2007) (Quintana et al., 2007)	Subjects: 16 subjects with ADHD 10 controls Age: 6–21 years old	Modality: EEG	Results:
		Paradigm: Resting with eyes open	Accuracy: 96% Sensitivity: 94% Specificity: 100%
	Biomarker: θ/β ratio at Cz EEG biomarker was sensitive and feasible for differential diagnosis.		
Snyder et al. (2008) (Snyder et al., 2008)	Subjects: 97 subjects with ADHD 62 controls Age: 6–18 years old	Modality: EEG	Results:
		Paradigm: Resting with eyes open	Accuracy: 89% Sensitivity: 87% Specificity: 94%
	Biomarker: θ/β ratio at Cz EEG biomarker performed better than rating scales in screening. Screening based on EEG biomarker should only complement a clinical diagnosis.		

Table 2.1 (continued)

Study	Remarks		
Ahmadlou and Adeli (2010) (Ahmadlou et al., 2010)	Subjects: 47 subjects with ADHD 7 controls Age: 7–12 years old	Modality: EEG Paradigm: Resting with eyes closed	Results: Accuracy: 95.6%
	Biomarkers: powers of θ and δ bands at O2, P4, and T5 with the implementation of radial basis function neural network.		
Abibullaev and An (2011) (Abibullaev et al., 2012)	Subjects: 7 subjects with ADHD 3 controls Age: 7–12 years old	Modality: EEG Paradigm: Continuous performance test (CPT)	Results: Accuracy: 97%
	Biomarker: power ratio with the implementation of semi-supervised feature selection method based on mutual information		
Mueller et al. (2011) (Mueller et al., 2011)	Subjects: 75 subjects with ADHD 75 controls Age: 18–7 years old	Modality: EEG Paradigm: GNG	Results: Accuracy: 91%
	Biomarkers: latency and amplitude of event-related potential (ERP) components		
Ogrim et al. (2012) (Ogrim et al., 2012)	Subjects: 62 subjects with ADHD 39 controls Age: 7 – 16 years old	Modality: EEG Paradigm: Resting with eyes open and closed	Results: Accuracy: 63%
	Biomarker: θ/β ratio at Cz Powers of θ and β bands correlated with behaviors. Screening based on behavior performances (e.g., omission errors) resulted better accuracy (85%)		

Table 2.1 (continued)

Study	Remarks		
Liechti (2013) (Liechti et al., 2013)	Subjects: 54 subjects with ADHD 51 controls Age: children – adolescents (8–16) and adults (32–55)	Modality: EEG	Results: Accuracy: 73% Sensitivity: 72% Specificity: 73%
		Paradigm: Resting with eyes open and closed, and CPT	
	Biomarkers: powers of θ and β bands at Cz, θ/β ratio at Cz, ERP features at Pz, and noise level. EEG biomarkers based on only resting condition performed poor in screening (40–53% accuracy)		
Loo (2013) (Loo et al., 2013)	Subjects: 562 subjects with ADHD 309 controls Age: children (5–11), adolescents (12–18), and adults (> 19 years old)	Modality: EEG	Results: Accuracy: 38%(Lenartowicz et al., 2014) Sensitivity: 26% Specificity: 85%
		Paradigm: Resting with eyes open or closed	
	Biomarker: θ/β ratio at Cz Screening based on the EEG biomarker performed inadequately. The biomarker was age-dependent and may be mediated by the nature of subtype and comorbidity		
Buyck (2014) (Buyck et al., 2014)	Subjects: 62 subjects with ADHD 55 controls Age: - (children and adults)	Modality: EEG	Results: Accuracy: 49–55%
		Paradigm: Resting with eyes closed	
	Biomarker: θ/β ratio at Cz Screening based on the EEG biomarker performed inadequately. ADHD phenotypes were heterogeneous across the lifespan.		

Table 2.1 (continued)

Study	Remarks		
Helgadóttir et al. (2015) (Helgadóttir et al., 2015)	Subjects: 310 subjects with ADHD 351 controls Age: 5.8 – 14 years old	Modality: EEG Paradigm: Resting with eyes closed	Results: Training accuracy: 76% Test accuracy: 73 – 81%
	Biomarkers: coherence features (power and relative power for 0.5–3.5, 3.5–7.5, 7.5–9.5, 9.5–12.5, 12.5–17.5, 17.5–25, 25–40 Hz frequency bands) at inter- and intra-hemspheric regions. Age was important factor in screening.		
Snyder et al. (2015) (Snyder et al., 2015)	Subjects: 116 subjects with ADHD 11 subjects with high possibility of ADHD 118 subjects with ADHD and other disorder symptoms 30 subjects without ADHD Age: 10.1 ± 2.9 years old	Modality: EEG Paradigm: Resting with eyes open	Results: Sensitivity for ADHD: 82% Sensitivity for high possibility of ADHD: 100% Sensitivity for ADHD and other disorder symptoms: 92% Specificity: 90%
	Biomarkers: clinician evaluation and EEG feature (θ/β ratio at Cz). Cut off for θ/β ratio was age-dependent (children and adolescents; 6.00–11.99 and 12.00–17.99 years old). Integration of EEG biomarker supported better screening.		
Khadmaoui et al. (2016) (Khadmaoui et al., 2016)	Subjects: 13 subjects with ADHD 14 controls Age: 8–13 years old	Modality: MEG Paradigm: Resting (supine) with eyes closed	Results: Accuracy: 89% Sensitivity: 77% Specificity: 100%
	Biomarker: coherence measure of δ band for short-distance values at the right-central region		

Table 2.1 (continued)

Study	Remarks		
Zhu et al. (2008) (Zhu et al., 2008)	Subjects: 9 subjects with ADHD 11 controls Age: 11 – 16.5 years old	Modality: fMRI	Results: Accuracy: 85% Sensitivity: 78% Specificity: 91%
		Paradigm: Resting	
	Biomarker: regional homogeneity index with prominent regions of prefrontal cortex, anterior cingulate cortex, and thalamus		
Bohland et al. (2012) (Bohland et al., 2012)	Subjects: 272 subjects with ADHD 482 controls Age: 7 – 21 years old ADHD-200	Modality: Structural and functional MRI	Results: Accuracy: 71 – 78%
		Paradigm: Resting	
	Biomarkers: imaging (e.g., structures and networks) and non-imaging (e.g., age, gender, handedness, verbal and performance intelligent quotient (IQ), and site information) features. Combining both features performed the best in classifying ADHD subjects from controls		
Brown et al. (2012) (Brown et al., 2012)	Subjects: 316 subjects with ADHD 523 controls Averaged age: 11.4 – 12.4 years old ADHD-200	Modality: fMRI	Results: Accuracy: 70 – 75% Accuracy: 64 – 69% (multiclass; controls and ADHD subtypes)
		Paradigm: Resting	
	Biomarkers: FC, temporal intensity, and non-imaging features (site information, gender, age, handedness, verbal and performance IQ, and Full 4 IQ) Non-imaging features classified (subtypes) ADHD from controls better than imaging features		

Table 2.1 (continued)

Study	Remarks		
Chang et al. (2012) (Chang et al., 2012)	Subjects: 210 subjects with ADHD 226 controls Age: 12.12 ± 2.95 years old ADHD-200	Modality: Structural MRI	Results: Accuracy: 70%
		Paradigm: Resting	
	Biomarker: isotropic local binary patterns on three orthogonal planes of whole-brain data		
Cheng et al. (2012) (Cheng et al., 2012)	Subjects: 98 subjects with ADHD 141 controls Age: 12.08 ± 2.05 and 11.43 ± 1.86 years old for ADHD and control, respectively ADHD-200	Modality: fMRI	Results: Accuracy: 76% Sensitivity: 63% Specificity: 85%
		Paradigm: Resting	
	Biomarkers: temporal and spatial FC, fractional amplitude of low-frequency fluctuation, and regional homogeneity with prominent frontal and cerebellar regions		
Dey et al. (2012) (Dey et al., 2012)	Subjects: 344 subjects with ADHD 561 controls Age: $7 - 26$ years old ADHD-200	Modality: fMRI	Results: Accuracy: $64 - 70\%$ Sensitivity: $37 - 49\%$ Specificity: $80 - 87\%$
		Paradigm: Resting	
	Biomarker: network features (degree, distance, cycle count, weight sum) involving regions of precuneus cortex, cingulate gyrus, temporal pole, superior temporal gyrus, inferior temporal gyrus, pre-central gyrus, lingual gyrus, and right amygdala		

Table 2.1 (continued)

Study	Remarks		
Hart et al. (2013) (Hart et al., 2014)	Subjects: 30 subjects with ADHD 30 controls Age: 10 – 17 years old	Modality: fMRI	Results: Accuracy: 77% Sensitivity: 90% Specificity: 63%
		Paradigm: Stop task	
	Biomarker: task-based activation patterns involving lateral prefrontal striatal, temporo-parietal and ventromedial fronto-limbic regions.		
Siqueira et al. (2014) (Siqueira et al., 2014)	Subjects: 269 subjects with ADHD 340 controls Age: 11.58 ± 2.88 and 11.59 ± 2.86 years old for ADHD and control, respectively ADHD-200	Modality: fMRI	Results: Sensitivity: 41% Specificity: 74%
		Paradigm: Resting	
	Biomarkers: network measures (degree, closeness, betweenness, eigenvector, Burt's constraint) with prominent networks of motor, frontoparietal, and default mode networks		
Qureshi et al. (2016) (Qureshi et al., 2016)	Subjects: 159 subjects with ADHD 53 controls Age: 7–14 years old ADHD-200	Modality: Structural MRI	Results: Accuracy: 58 – 85% Accuracy: 31 – 61% (multiclass; controls and ADHD subtypes)
		Paradigm: Resting	
	Biomarker: surface area of superior frontal lobe, and the cortical thickness, volume, and mean surface area of the whole cortex		

Table 2.1 (continued)

Study	Remarks		
Yao et al. (2018) (Yao et al., 2018)	Subjects: 112 subjects with ADHD 77 controls Age: 25.93 ± 4.86 and 26.04 ± 3.94 years old for ADHD and control, respectively	Modality: fMRI	Results: Accuracy: 80% Sensitivity: 91% Specificity: 65%
		Paradigm: Resting	
	Biomarkers: FC involving frontoparietal, default mode, salience, basal ganglia, and cerebellum networks		
Ishii-Takahashi et al. (2014) (Ishii-Takahashi et al., 2014)	Subjects: 19 subjects with ADHD 21 controls Age: 30.6 ± 7.4 and 28.8 ± 5.5 years old for ADHD and control, respectively	Modality: fNIRS	Results: Accuracy: 78.8% Sensitivity: 84.2% Specificity: 76.2%
		Paradigm: Stop signal task (SST)	
	Biomarker: task-evoked activation at the right presupplementary motor area and premotor area		
Monden et al. (2015) (Monden et al., 2015)	Subjects: 30 subjects with ADHD 30 controls Age: 6 – 15 years old	Modality: fNIRS	Results: Accuracy: 85% Sensitivity: 90% Specificity: 70%
		Paradigm: GNG	
	Biomarker: task-evoked activation at the right inferior and middle frontal gyri		

proposed (Monastra et al., 2001; Helgadóttir et al., 2015); however, some studies argued the readiness of EEG biomarkers for the clinical utility due to the observed ADHD heterogeneity (Loo et al., 2012; Liechti et al., 2013). Univariate biomarkers developed using any techniques likely encounter the similar problem (Lenartowicz et al., 2014). Furthermore, the limited success of clinical application was found in other imaging studies because those biomarkers have been drawn from small datasets. Biomarkers obtained from the biggest dataset so far (i.e., ADHD-200) also revealed high variability. Clinical screening solely using biomarkers is still optimistic; the feasible application is currently a supporting tool for screening. Continuous effort is being done to collect more datasets and to verify any obtained biomarkers in cohort studies.

2.4   Requirements for children measurement

Even though functional imaging techniques have been contributed to the understanding of ADHD pathophysiology and biomarker development, all practical, technical, and analytical aspects (Raschle et al., 2012) should be well planned and performed to obtain successful measurements. Selecting an imaging technique crucially determines subjects' convenience and analytical appropriateness (O'Malley et al., 2016). Table 2.2 shows the comparisons between imaging techniques (Lystad et al., 2009; Koike et al., 2013). While EEG and MEG directly measure the neural activity, fMRI and fNIRS detect the hemodynamic responses on neural activity. Therefore, the time resolution of EEG and MEG is more superior than that of fNIRS and fMRI. fMRI is one of tomographic techniques; the imaging process is performed by the axial scanning, and 3D imaging is constructed later on. fMRI provides the whole brain measurement from the deepest part of brainstem to the outermost part of cortex with the remarkable spatial resolution. On the other hand, EEG, MEG, and fNIRS only manage the cortical measurement with the modest spatial resolution. On the basis of subjects' convenience, fNIRS is able to offer the least measurement burden; fMRI

Table 2. 2 Comparisons between functional neuroimaging techniques

Parameters	EEG	MEG	fMRI	fNIRS
Signal property	Neural activity	Neural activity	Hemodynamic response	Hemodynamic response
Measured area	Cortices	Cortices	Whole brain	Cortices
Time resolution	1–10 ms	1–10 ms	2–5 s	0.1–1 s
Spatial resolution	10–20 mm	5–10 mm	2–5 mm	20 mm
Confinement	No	No	Yes	No
Head restraint	No	No	Yes	No
Motion tolerant	No	No	No	Yes

unfortunately requires the delicate environment with controlled movement (e.g., head restrainer) and confinement.

Figure 2.1 presents the diagram of spatial against temporal resolutions for each imaging technique (Cohen et al., 1994b; Bunge et al., 2009). fMRI is able to result in a fine resolution (~0.1 mm); however, the measurement time should be extended to several hours. In order to acquire the best quality measurement, the simultaneous measurement using EEG and fMRI can be a promising option. In present, the simultaneous measurement for MEG and fMRI practically infeasible because both instruments are bulky and cannot be fit together. This option is advantageous particularly for healthy adults who are unlikely burdened by discomforts of multimodality measurement. The application of simultaneous multimodality measurement on disordered children may be challenging. Children have already been burdened by fMRI measurements; adding another instrument, such as EEG, may elevate subject inconveniences. Therefore, the single instrument measurement supporting a trade-off between spatial and temporal resolutions is highly preferable. According to Figure 2.1, fNIRS accommodates both moderate spatial and temporal resolutions. fNIRS can be an appropriate substitute to fMRI especially for designed experiments targeting the monitoring of cortical functions (Cui et al., 2011). Therefore, fNIRS is considerably an optimum technique to perform pediatric studies. Currently, there has been a limited number of fNIRS studies compared to fMRI studies; however, researchers have been attracted to applying fNIRS on their studies in order to improve the
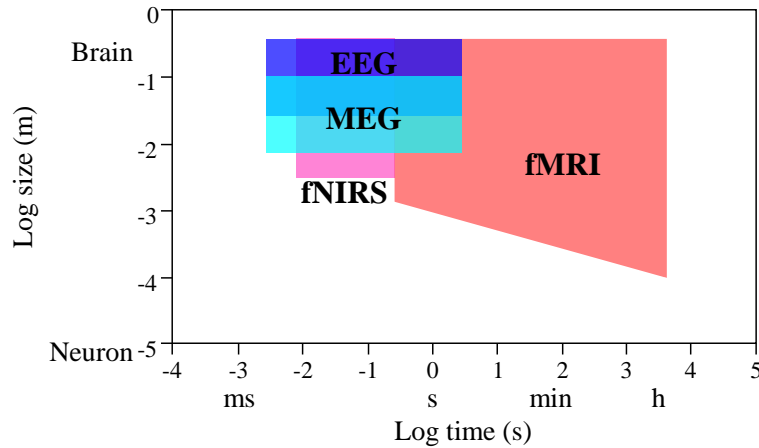
Figure 2. 1 Diagram of spatial against temporal resolutions for EEG, MEG, fMRI, and fNIRS

clinical translation and utility.

2.5   Functional near-infrared spectroscopy

The biological tissue measurement using near-infrared (NIR; 650–950 nm) lights was reported by Frans Jöbsis in 1977 for the first time (Jöbsis, 1977). NIR properties allow lights to penetrate (a few centimeters) and to transmit across biological tissues. Some portions of light are absorbed, and the absorbed light dominantly interacts with oxygenated (O_2Hb) and deoxygenated (HHb) hemoglobin (i.e., chromophores) (Strangman et al., 2002). Several parameters, such as (O_2Hb, HHb, and Hb-total) hemoglobin concentration changes (Maki et al., 1995; Delpy et al., 1997), oxygenation index (Grassi et al., 1999), tissue O_2 saturation (Franceschini et al., 2002; Quaresima et al., 2002), hemodynamic response resolution (Chance et al., 1992), blood flow (Owen-Reece et al., 1999), and blood volume (Owen-Reece et al., 1999), are derived from those interactions [see (Ferrari et al., 2004) for review]. All parameters relatively interpret the cellular activity. The application of NIR lights revealed the ability to monitor cellular activity in non-invasive and real-time manners. Figure 2.2 presents the scheme of NIR light transmission passing through the extracerebral and cortical layers.

24
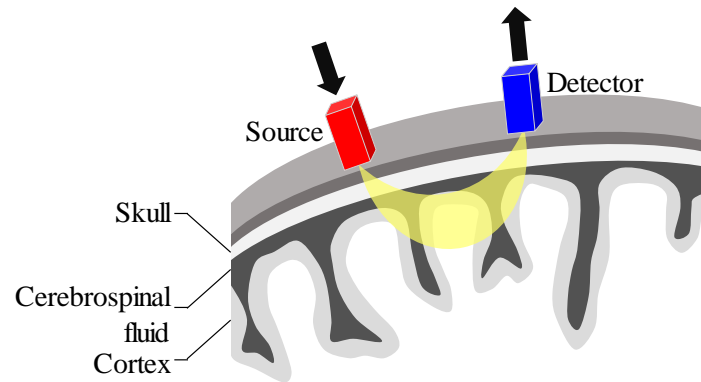
Figure 2. 2 Scheme of NIR light transmission

Commercial fNIRS instruments had been advanced for more than two decades. The first instrument incorporated only a single channel; the development has progressed to multi-channel and wireless instrument (Atsumori et al., 2009) [see (Ferrari et al., 2012) for more development history]. Those instruments majorly adapted the continuous wave (CW) system that the light is continuously emitted with the constant intensity (Nioka et al., 1997; Siegel et al., 1999; Schmitz et al., 2000). The CW system is unable to determine the scattering coefficient and the optical path length; thus, the absolute parameter measures cannot be defined. The practical use of parameters commonly involves the temporal derivation against the calibration level (e.g., ΔC) (Maki et al., 1995; Koizumi et al., 2003). In order to resolve this issue, frequency- and time-domain systems are approached. The frequency-domain (FD) system emitted the light with fluctuated intensities across the temporal course; the detected intensity light is modulated by a shifted phase (Fantini et al., 1994; Poque et al., 1994; Jiang et al., 1995; Gratton et al., 1997; Franceschini et al., 2000). This shifted phase represents the travel time of photon as being emitted, transmitted, and detected back. Compared to the CW system, the FD system reconstructs better images with a deeper penetration depth, but significantly requires longer data acquisition time (Lu et al., 2015) with more noisy signals (Davies et al., 2017). Some instruments with the FD system has been available in the market. Meanwhile, the time-domain system irradiates the short

25

pulse of light, and the time function of transmitted light intensity is then obtained (Benaron et al., 1993; Hebden et al., 1997; Jelzow et al., 2011). Compared to the CW and FD systems [see (Strangman et al., 2002; Ferrari et al., 2004) for further comparisons], the time-domain system offers the most superior absorption-scattering separation and spatial resolution with the promising feature of 3D tomography (Contini et al., 2007). Despite the benefits of frequency- and time-domain systems, the systems are packed in bulky instruments (Ferrari et al., 2004), and the computation expenses are high (Scholkmann et al., 2014) making those less practical and commercial. Furthermore, measured parameters using the CW system are well correlated with those of the FD (Davies et al., 2017) and time-domain (Diop et al., 2010) systems. Therefore, the CW system is still the most viable method.

In order to quantify more than a single chromophore, multiple wavelengths should be employed. The selection of optimum wavelength is essential because it highly influences the quality of measurement. The trends of absorption coefficient are opposite for O_2Hb and HHb. The absorption coefficient of HHb is greater than that of O_2Hb in 650–800 nm window. The HHb absorption coefficient gradually decreases, while the O_2Hb absorption coefficient increases and even surpasses the HHb absorption coefficient in 800–950 nm window. At around 800 nm, the absorption coefficients for both chromophores are the same (i.e., isosbestic). The use of isosbestic point should be avoided because the absorption for specific chromophores becomes unknown. Therefore, a wavelength is selected from the window of 650–800 nm, and another one is selected from the window of 800–950 nm. Several methods, such as Monte Carlo simulation (Strangman et al., 2003; Okui et al., 2005), error propagation approach (Yamashita et al., 2001), and empirical method (Sato et al., 2004), were performed to investigate the optimum wavelengths (see (Scholkmann et al., 2014) for review). The selected wavelengths were relatively robust across the optimization methods (~690 and 830) (Strangman et al., 2003; Sato et al., 2004; Okui et al., 2005; Kawaguchi et al.,

2008). In order to measure water and lipid for additional chromophores, three–five wavelengths were implemented on an fNIRS instrument (Corlu et al., 2003; Corlu et al., 2005). The instrument with more than two wavelengths is scarcely seen in the market. One of reasons is low signal-to-noise ratio (SNR) because of the reduced efficiency of incident light separation between channels (Scholkmann et al., 2014). Therefore, the most commercial instruments only adopt the two-wavelength system.

2.6   Analysis methods for functional near-infrared spectroscopy

The biological parameters are commonly determined following the modified Beer-Lambert Law (MBLL) (Delpy et al., 1988; Maki et al., 1995). According to the MBLL, the concentration change is proportional to the logarithm of ratio between the detected light intensity after passing through the biological tissue and the initial light intensity as shown in below equation.

$$-\log_{10}\left(\frac{I}{I_0}\right) = \sum_i \varepsilon_{i,\lambda}(C_i \cdot L) + G \qquad \text{(Eq. 1)}$$

where I_0 is the initial light intensity, I is the detected light intensity, i is the chromophore types (e.g., O_2Hb and HHb), ε is the molecular extinction coefficient $\left(\frac{1}{M \cdot cm}\right)$ specific for each chromophore i and wavelength λ, C is the concentration of chromophores (M), L is the optical pathlength, and G is the scattered portion. The optical pathlength cannot be absolutely quantified by using only the CW system; therefore, the effective parameter represents the product of concentration and optical pathlength ($C \cdot L$). The scattered portion (G) is small compared to the absorbed portion; G is assumed to be time-invariant (Scholkmann et al., 2014). Due to the disadvantageous CW system, the biological parameters are identified as the time function of concentration change ($\Delta C \cdot L$). The operation of MBLL should also be supported by the homogeneity assumption (Cope et al., 1988; Cope et al., 1991); however, the risk of assumption violation is elevated because the skull thickness is varied depending on brain regions. Despite some limitations,

MBLL is still the practical and feasible approach in determining biological parameters particularly for the commercial CW systems.

After the estimation of biological parameters (e.g., $\Delta C_{O2Hb} \cdot L$, $\Delta C_{HHb} \cdot L$) is done, signal preprocessing [see (Tak et al., 2014) for further reading] is required to appropriately infer brain measures (Tachtsidis et al., 2016). Signal preprocessing includes the decomposition process because the obtained parameters are unavoidably confounded by the mixture between neuronal and non-neuronal (i.e., physiological) components. The non-neuronal components also come from both superficial (e.g., scalp) and cortical layers (Erdoğan et al., 2014; Funane et al., 2014). Afterwards, the signal preprocessing is continued with the noise removal process. Motion artifact is one of common noises occurred during the fNIRS measurement; its noise occurrence is not as high as fMRI noise occurrence though. The effect of motion artifact on signals does not promptly subside (Robertson et al., 2010; Cooper et al., 2012); the signal baseline may shift either visibly or subtly. This baseline shift is also categorized as one of noises.

Decomposition process. Several attempts were done to distinctively separate the neuronal component from other mixtures. The simplest way is to filter out physiological components. The heartbeat pulsation is confined within 0.6–2 Hz and straightforwardly filtered. However, other physiological noises, including respiratory activity (0.15–0.4 Hz), arterial blood pressure (i.e., Mayer waves; 0.05–0.2 Hz), spontaneous fluctuation (<0.1 Hz), happen in the lower frequency window in which overlaps with the frequency window of neuronal component (0.01–0.2 Hz) (Fekete et al., 2011). Therefore, the decomposition algorithms, such as PCA and ICA, are sometimes applied on fNIRS signals (Zhang et al., 2005; Kohno et al., 2007; Katura et al., 2008). Furthermore, direct physiological measurements are approached to provide more accurate regressors for the decomposition process (Birn et al., 2006; Kirilina et al., 2012). Those were carried out using multimodality systems for either each independent component (e.g., respiratory belt, cuff) or integrated components (e.g., peripheral

photoplethysmography at finger, earlobe) (Sutoko et al., 2019a). Another attempt used the multi-distance source-detector system to measure the superficial layer (Gagnon et al., 2008; Saager et al., 2011); thus, the non-neuronal components could be modeled and removed from the cortical layer (Gagnon et al., 2008; Saager et al., 2011). However, the statistical inferences were unlikely violated even without the advanced decomposition process (Sutoko et al., 2019a).

Noise removal process. In general, there are two methods in mitigating noises – completely rejecting (i.e., not use) and correcting noisy signals. Several correction algorithms require supplementary data that usually come from expected noise sources. For example, while the brains got measured, an accelerometer was also attached on subjects to monitor motions. Supplementary data are inessential for other corrective algorithms (Scholkmann et al., 2010; Cooper et al., 2012; Brigadoi et al., 2014; Hu et al., 2015; Jahani et al., 2018), such as filtering (e.g., wavelet, Kalman), regression-interpolation (e.g., spline, GLM), and reduction of component dimensionality (PCA, ICA). Meanwhile, the conventional way in performing noise rejection is to detect noises through the visual judgment by raters following the pre-set criteria, such as sudden and discontinuous signal changes.

After performing the signal preprocessing, the analysis to extract brain measures is carried out. Brain measures can be categorized into brain activation and connectivity. Brain activation quantifies the effect of stimulus-evoked responses on $\Delta C_{O2Hb} \cdot L$ and $\Delta C_{HHb} \cdot L$, whereas brain connectivity identifies the relationships between brain regions (i.e., networks). One of typical brain activation methods averages the signal amplitude during the baseline and stimulus intervals, and the averaged baseline value is compared to the averaged stimulus value to evaluate the stimulus effect (Tak et al., 2014). Another method, namely, GLM (Friston et al., 1994a) assumes that the fNIRS signals consist of a linear combination of stimulus-related and other components following below equation.

$$y = x\beta + \varepsilon \qquad\qquad \text{(Eq. 2)}$$

where *y* is the temporal course of fNIRS measurement, *x* is the regressor matrix

(convolution between a boxcar function and HRF (Schroeter et al., 2004) together with its derivative functions for stimulus-related components), β is the estimated linear regressor of x, and ε is the error that is presumed normally distributed with 0 mean and σ^2 variance (Friston et al., 1995). The activation assessment for the subject level can be performed for both typical activation and GLM methods. The typical activation method examines the significance of stimulus effects across trials; the GLM method evaluates the significance of stimulus-related regressors (Friston et al., 1994b; Monti, 2011; Pinti et al., 2017). For the group analysis, Student's *t*-test and ANOVA (with a *post hoc* analysis) are applied on subject-wise activation values (i.e., averages of stimulus minus baseline values across trials) and β values for the typical activation and GLM methods, respectively. Compared to the typical activation method, the GLM method may be less sensitive especially in noisy signals. Furthermore, inappropriate stimulus-related regressors become drawbacks for the GLM method.

As subjects are measured under the natural environment without any stimuli (i.e., RS), the measure of brain activation is bias. Therefore, the measure of brain connectivity is evaluated during the RS; the stimulus-evoked connectivity is also allowed. Brain connectivity is functionally interpreted as a measure of a relationship between brain regions. The fMRI connectivity was a pioneering approach proposed by Biswal et al. (Biswal et al., 1995), who reported strong connectivities between low-frequency-oscillation signals in regions associated with the motor network. Common approaches for brain connectivity are seed-based correlation (Lu et al., 2010; Zhang et al., 2010b; Niu et al., 2011), whole-brain correlation (Homae et al., 2010; Sasai et al., 2011; Zhang et al., 2012), and ICA-based method (Zhang et al., 2010a). In the case of seed-based correlation, the 'seed', usually the region of interest, is determined in advance, and the seed signal is temporally correlated (Pearson's correlation r) to signals from other regions. Meanwhile, the whole-brain (or whole measured-regions) correlation do not require the seed selection. In the ICA-based method, the specific network

components are determined from the decomposed components using PCA and ICA algorithms beforehand. Furthermore, the weights of specific network components estimate the relationship between brain regions and those network components. Another approach utilizes the graph theory (Niu et al., 2012; Niu et al., 2013) to investigate network metrics (Rubinov et al., 2010), such as global and local networks, network clustering, modularity, and path length. The repeated measurement enables the evaluation of connectivity measures in the subject level. For the group analysis, similar to the brain activation analysis, Student's *t*-test and ANOVA are applied on subject-wise temporal correlation coefficients and network metrics (Xu et al., 2015).

By providing more channels, the measured regions are widened. However, the risk of type I error may be elevated due to the problem of multiple hypothesis comparison. Therefore, controlling either familywise error rate (FWER) (Hochberg et al., 1987) or false discovery rate (FDR) (Benjamini et al., 1995) is common to resolve this risk even in neuroimaging studies. Bonferroni correction was applied to evaluate the statistical significance of stimulus-evoked responses (Plichta et al., 2006; Hofmann et al., 2008). Besides the Bonferroni correction (Dunn, 1961), other correction approaches are applicable (Miller, 1981). In order to investigate the localized activation, the FDR method was applied on *p*-values of channel-wise activation (Okamoto et al., 2006; Singh et al., 2006). The FDR approach is more powerful giving the optimum controls (Nichols et al., 2003), while the FWER is considered to be excessively strict (Singh et al., 2006). Even though these corrections have been well used in the statistical evaluation of brain activation, the multiple comparison issue in brain connectivity has only been addressed in a limited way.

As the instrument advancement is growing, the computational analysis packages have been developed as well. Several packages, such as HomER (Huppert et al., 2009), NIRS-SPM (Ye et al., 2009), fOSA (Koh et al., 2007), NinPy (Strangman et al., 2009), NAP (Fekete et al., 2011), and POTATo (Sutoko

et al., 2016), are available for researchers for a free use. These packages provide functions of signal preprocessing, brain measure extraction, and statistical analyses for subject and group levels. Furthermore, an analysis tool particularly for the brain connectivity was established by Xu et al. (Xu et al., 2015). One of differences among packages is the feature of analysis tool – whether the analysis tools feasibly allow the exploratory data analysis (EDA) or not. For example, POTATo was developed to accommodate varied demands from a quick analysis with pre-set tools to an advanced analysis supporting EDA, so that researchers are empirically able to investigate their data (Sutoko et al., 2016). On the other hand, HomER offers a relatively standardized analysis which is beneficial for a practical use (Huppert et al., 2009).

3 Algorithm Development for Removing Noisy Activation Signals and Its Implementation[*]

3.1 Introduction

fNIRS has been recently used for pediatric studies (Peña et al., 2003; Sugiura et al., 2011; Monden et al., 2012a) because of its flexibility (Cui et al., 2011), such as no confinement, no head restrainer, and not necessarily putting subjects in a supine condition. fNIRS is also motion tolerable on condition of which probes are securely adhered on the scalp (Hoshi et al., 2005; Koike et al., 2013). Despite its advantages, pediatric studies manage challenging subjects, infants and children. Less comfortable conditions and/or measurement engagement (i.e., attention) will trigger a restless situation for infants and children. An extreme movement will cause a lousy contact between probes and the scalp; motion artifacts unavoidably occur. The measurement of disordered children with symptomatic hyperactivity (e.g., ADHD) worsens the risk of motion artifact.

To date, there is no golden approach to detect and remove noises. While the prolonged measurement is unfavorable for infants and children, the noise correction method is preferably selected over the noise rejection method because of maintained samples (Cooper et al., 2012). However, the noise correction algorithms require parameters that should be specified prior to applications. The performances of those algorithms were found to be unstable across datasets, and it may be caused by the improper selection of algorithm parameters. Furthermore, the incorporation of multimodality measurement to estimate motion artifacts involves more attached probes. The risk of motion likely increases, and the measurement practicability is reduced (Robertson et al., 2010; Virtanen et al., 2011; Barker et al., 2013; Chiarelli et al., 2015). Therefore, the noise rejection method is re-approached.

The conventional noise rejection method is laborious and less objective. Due

---

[*] The work in Chapter 3 has been published in two journal articles (Sutoko et al., 2018; Sutoko et al., 2019c).

to the inter-subject variability of noise levels (i.e., how severe do noises affect signals), raters may subconsciously adjust the pre-set noise criteria to maintain subject data and sufficient sample number. A novel algorithm of noise rejection method is introduced in this chapter. This algorithm was named "adaptive rejection algorithm". Following its name, this algorithm aimed to adaptively accommodate a trade-off between the rejection control and personal noise levels. To simply put, the adaptive rejection algorithm tried to maintain the least noisy signals and to obtain the sufficient sample number.

The application of the adaptive rejection algorithm should be versatile; thus, the algorithm was designed based on the bottom-up process which algorithm variables (e.g., noise criteria, rejection control rate/acceptance rate) could be flexibly set. Even though this feature improved the algorithm flexibility, the algorithm performance may be influenced by the set algorithm variables. In order to avoid this problem, the algorithm variables were selected through the optimization process. By repetitively re-doing the optimization process, the algorithm variables will be re-tuned, and the applicable variables will be eventually obtained.

The algorithm performances were evaluated in synthetic and human measurement datasets. The synthetic datasets were used to confirm the algorithm concept and to simulate effects of noise level and phenomenon strength on the algorithm performance. The human measurement datasets came from TD and ADHD children that had been analyzed and reported before (Nagashima et al., 2014b; Nagashima et al., 2014c). The algorithm application on TD and ADHD data might suggest the algorithm feasibility in managing different noise levels (i.e., risk of motion artifacts in ADHD > TD). This algorithm can be performed in an automatic manner; the algorithm application for a substitute to the conventional visual judgment is highly expected.

Noise removal is commonly done during the signal preprocessing. Therefore, the application of the adaptive noise algorithm for one of signal processing steps

was confirmed on the new dataset. After applying the algorithm, the analysis was continued to develop biomarkers for differentially diagnosing ADHD children with autism spectrum disorder (ASD) comorbidity. The well-performed biomarkers not only suggested the successful development of supporting differential diagnostic tools but also confirmed the practicability of the adaptive rejection algorithm for a signal processing step.

Besides ADHD, ASD is also one of the most prevalent neurodevelopmental disorders. Within 12 years, the prevalence rate of ASD increased more than doubled from 0.67 to 1.46% (2000–2012) (Christensen et al., 2016). Subjects with ASD show symptomatic social and communication impairments with restricted interests and repetitive behaviors. ADHD and ASD are identified as completely different disorders according to the DSM-IV. The comorbidity between ADHD and ASD was also not explained. Despite independently interpreted phenotypes, ADHD and ASD symptoms were found to co-occur. Primarily ASD-diagnosed subjects (30–50%) revealed ADHD symptoms (Goldstein et al., 2004; Gadow et al., 2006; Lee et al., 2006), and *vice versa* for ADHD-diagnosed subjects (66%) (Mulligan et al., 2009).

In the updated DSM-5 (American Psychiatric Association, 2013), the comorbidity between ADHD and ASD is clinically recognized. Its comorbidity was modeled in three mechanisms (Sokolova et al., 2017): (1) dysfunction of social information perception caused by impulsivity, (2) hyperactivity associated with stereotypic and repetitive behavior, and (3) accumulative effects between inattention, difficulties of social information perception, and verbal IQ. Besides its comorbidity, the age of symptomatic onset for diagnosing ADHD was re-defined from seven to twelve years old. This change elevated the ADHD diagnosis rate from 7.38% to 10.84% particularly in the inattentive dimension (Vande Voort et al., 2014).

Diagnosing either primary or comorbid disorders is never an easy work even using standard diagnostic guidelines. The difference of diagnosis rate between the

DSM-IV and ICD-10 was substantial by about five times (Döpfner et al., 2008; Adornetto et al., 2012). The accurate diagnosis and therapeutic assessment require the longitudinal behavioral monitoring from multiple respondents, such as parents and teachers (Soma et al., 2009). The clinical application of biomarkers will speed up the diagnosis process and the evaluations for prognosis and pharmacological efficacy.

The understanding of disorder characteristics and the development of biomarkers based on fNIRS measurements have been pursued separately for ADHD and ASD. Compared to control subjects (i.e., healthy children, adolescents, and adults), subjects with ADHD revealed hypoactivation in responses to inhibition (Monden et al., 2012a; Ishii-Takahashi et al., 2014), attention (Nagashima et al., 2014c), verbal fluency (Matsuo et al., 2014), and facial recognition (Ichikawa et al., 2014) tasks. Using these characteristics, ADHD biomarkers were developed, resulting in 78.8–85% accuracy (Ishii-Takahashi et al., 2014; Monden et al., 2015). The comparison of brain activation between control and ASD subjects showed divergent results depending on performed tasks. During the inhibition GNG (Xiao et al., 2012; Ikeda et al., 2018b), own-face recognition (Kita et al., 2011), gaze recognition (Ikeda et al., 2018a), and perception of person's expression (Iwanaga et al., 2013) tasks, hypoactivation was observed for ASD children. Meanwhile, the activations during the Stroop (Xiao et al., 2012; Yasumura et al., 2014), and expression of an object's characteristics (Iwanaga et al., 2013) tasks were similar for both control and ASD children. Furthermore, ASD children was successfully characterized by 83.3% accuracy based on their weak efficiency for the network between bilateral PFC and bilateral temporal cortices during the visual stimulus (i.e., watching a cartoon) (Li et al., 2016b). High diagnostic performance (81.6% sensitivity and 94.6% specificity) was also found by identifying the weak bilateral FC and the strong fluctuation magnitude during the RS for ASD children (Li et al., 2016a). In spite of previous findings, the biomarker for comorbidity diagnosis has never been addressed.

The distinct characteristics between ADHD and ASD-comorbid ADHD children had been reported. The activation responses on the GNG task and the neuropharmacological effects were contrast between ADHD and ASD-comorbid ADHD children (Tokuda et al., 2018). However, the biomarker for differentiating ASD-comorbid ADHD children from ADHD children has not been advanced before. Therefore, the objective for a study with the application of adaptive rejection algorithm was to investigate any effective differential diagnostic biomarkers based on activation characteristics of ADHD and ASD-comorbid ADHD children.

3.2 Materials and methods

In this chapter, the development of rejection algorithm and its application as a substitute to the visual rejection in the signal preprocessing were independently described. Therefore, 3.2 Materials and methods and 3.3 Results were arranged into two subsections.
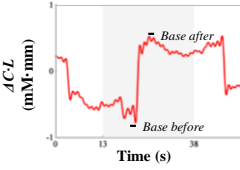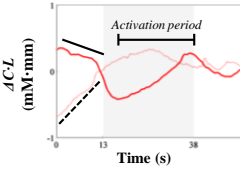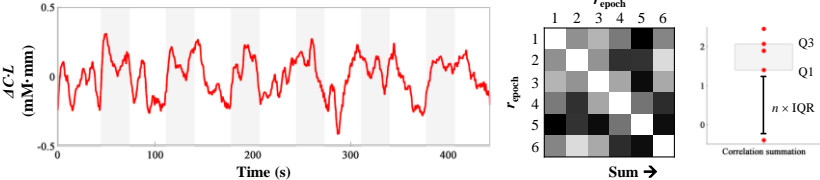
A. Development of the adaptive rejection algorithm: design and feasibility

3.2.1 Design of rejection algorithm

A rejection algorithm for suitably evaluating noises in datasets with the block-design paradigm was constructed in two processes.

1. Noise identification. Three noise criteria were initially formulated as shown in Table 3.1. Criterion 1 was the typical characteristic of motion artifact – any sudden amplitude (i.e., fNIRS signals) increases/decreases with recovery failure to the base amplitude. The greater amplitude increase/decrease was observed, the longer time was required to return to the base amplitude. If amplitude changes from two datapoints surpassed a threshold, those datapoints would be marked as the starting and ending time of a sudden amplitude increase/decrease. Furthermore, in order to confirm the recoverability, the amplitude levels before and after those datapoints were

Table 3. 1 Noise criteria. From (Sutoko et al., 2018), reproduced with permission.

No.	Criterion	Description
1.	Sudden increases/ decreases with recovery failure	$\left| \Delta C \cdot L_{(t+1)-t} \right| > threshold$ $threshold = 0.01, 0.02,\dots$ mM·mm
2.	Shifted baseline	$\left| \left(\frac{\Delta C \cdot L_{t_2-t_1}}{\Delta t} \right)_{baseline} \right| > threshold$ $threshold = 0, 0.01, \dots$ mM·mm/sec
3.	Discrepancy of correlation summation among epochs	 Q3 = upper quartile of correlation summation Q1 = lower quartile of correlation summation $IQR = Q_3 - Q_1$ $Threshold = Q1 - n \times IQR$ $n = 0, 0.5, 1, \dots$

evaluated. Epochs (i.e., shorter signals from the temporal courses corresponding to trials) containing any shifts of amplitude levels over 0.2 mM·mm were recognized as noisy ones. Criterion 2 was an extreme baseline shift before stimulus. The baseline shifts might be caused by the effects of sudden amplitude increases/decreases and/or the physiological noises (Birn et al., 2006; Chang et al., 2013; Murphy et al., 2013) with spurious signals and interlocked phases. The baseline slope was computed using a linear fitting. If epochs had slope baselines over a threshold, those epochs were marked as noisy epochs. Criteria 3 was high inter-epoch variability. Low noises likely resulted in the high inter-epoch similarity. Epoch signals were correlated with each other, and the summation of correlation coefficients represented a similarity measure. For example, if epoch 1 had noises, the summation of correlation coefficients between epoch 1 and other epochs would be low. Epochs with the outlier correlation summations were defined as noisy epochs.

The outlier range was determined by the multiplication between a threshold constant and interquartile range (IQR) of correlation summations. Criteria 1, 2, and 3 comprehensively controlled noises in datapoint, epoch, and entire temporal levels, respectively. While criteria 1 and 2 were assessed with global thresholds (i.e., same thresholds for all subjects), criteria 3 was examined using the personalized threshold (i.e., IQR).

2. Rejection judgment. The current algorithm approached the adaptive judgment based on both dataset and personal noise levels. Figure 3.1 shows the process of adaptive judgment explained in eight steps. *First*, the presence of noisy epochs was examined according to a noise criterion. *Second*, the number of
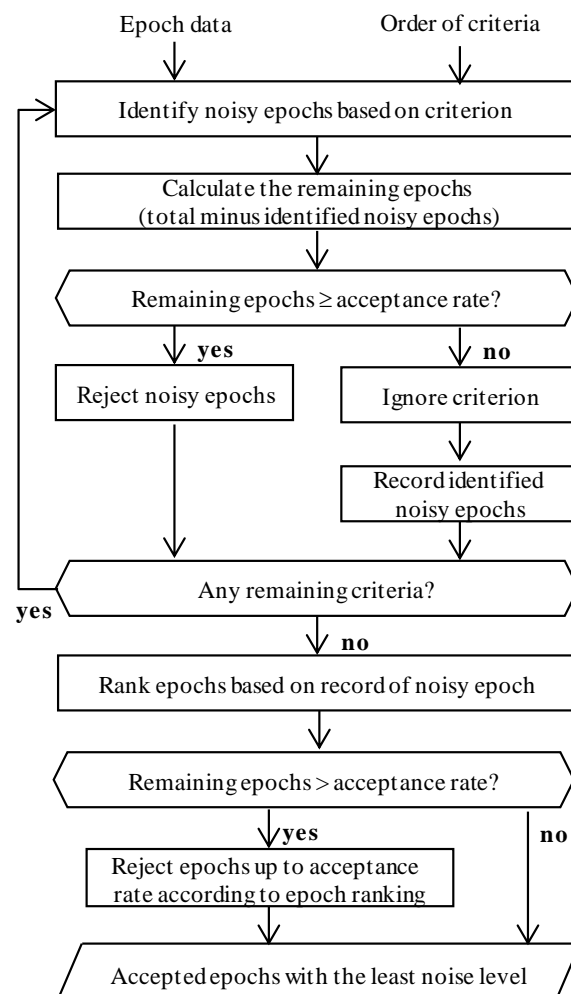
Figure 3. 1 Process flow of the adaptive rejection algorithm. From (Sutoko et al., 2018), reproduced with permission.

remaining epochs after subtracting the number of detected noisy epochs from total epochs were counted. *Third*, the number of remaining epochs was evaluated whether it was greater than or equal to the pre-set acceptance rate (i.e., the minimum expected value of remaining epochs). *Fourth*, the rejection of detected noisy epochs was executed if step 3 is met. Otherwise, the rejection was halted; however, those epochs were still labeled as noisy epochs. *Fifth*, the judgment was continued by applying other noise criteria on the remaining/non-rejected epochs. *Sixth*, steps 1–5 were repetitively done until all noise criteria had been examined. *Seventh*, in order to maintain the objectivity of judgment, the remaining epochs were ranked depending on how many times the epochs were saved from rejections but labeled as noisy epochs. If the number of remaining epochs was still greater than the pre-set acceptance rate, this ranking was re-checked. *Eighth*, if there was any remaining epochs having labels as noisy epochs, the rejection was resumed until the number of remaining epochs was equal to the pre-set acceptance rate.

To simply put, this algorithm introduced a fuzzy approach in which the epochs were labeled not only as noisy or noise-free but also as acceptably noisy epochs. This algorithm aimed to reduce noises to a tolerable level while maintaining the sufficient epoch number.

3.2.2 Datasets

Two datasets that had been collected previously used in this chapter. These datasets consisted of TD and ADHD children data (Nagashima et al., 2014b; Nagashima et al., 2014c). Table 3.2 shows the summary of dataset information. All ADHD children were clinically diagnosed based on the DSM-5 guideline and prescribed by either MPH or ATX with varied ranges of doses and intervals. The experiment was designed following the randomized, double-blind, placebo-controlled, and crossover study for ADHD children. Therefore, ADHD children underwent four measurement sessions (i.e., pre-medication, pre-placebo, post-

Table 3. 2 Demographic information. From (Sutoko et al., 2018), adapted with permission.

Parameters	Dataset I	Dataset II
TD children	22 (15 boys) 9.8 ± 2.0 years old IQ 108.0 ± 11.4	16 (14 boys) 8.9 ± 2.2 years old IQ 108.6 ± 8.1
ADHD children	22 (19 boys) 9.5 ± 2.0 years old IQ 94.4 ± 11.7	16 (14 boys) 8.9 ± 2.2 years old IQ 99.4 ± 14.4
Medication	MPH 27 ± 10.8 mg 22 ± 21 months	ATX 23.1 ± 13.6 mg 10 ± 8.0 months
Placebo	Double-blind	Double-blind
Task	Oddball	Go/no-go

medication, and post-placebo) in two measurement days (Figure 3.2A). Two measurement days were apart for about 2–30 days. In order to control medication and placebo effects, ADHD children refrained taking their medications for about 2–4 days (i.e., wash-out period) before the measurement day. In contrast, a single measurement was performed for TD children without any administration of medication or placebo. All subjects were right-handed, and the IQ was assessed using the Wechsler Intelligence Scale of Children – Third Edition (WISC-III) which IQ results were over 70 for all subjects.

In a measurement session, subjects performed either GNG or oddball (OB) task for about 6–7 min while their brains were being measured. The GNG task was done to evaluate the inhibition control, while the OB task targeted subjects' sustained attention measures (Monden et al., 2012a; Monden et al., 2012b; Nagashima et al., 2014a; Nagashima et al., 2014b; Nagashima et al., 2014c). Both GNG and OB task were constructed following the block-design paradigm with six trials (E-Prime 2.0, Psychology Software Tools). In the block-design paradigm, the entire task was categorized in baseline and stimulus tasks which were alternately performed (seven and six times for baseline and stimulus tasks, respectively; green and yellow intervals in Figure 3.2B). The 3-s instruction always preceded the baseline and stimulus tasks (gray intervals in Figure 3.2B).
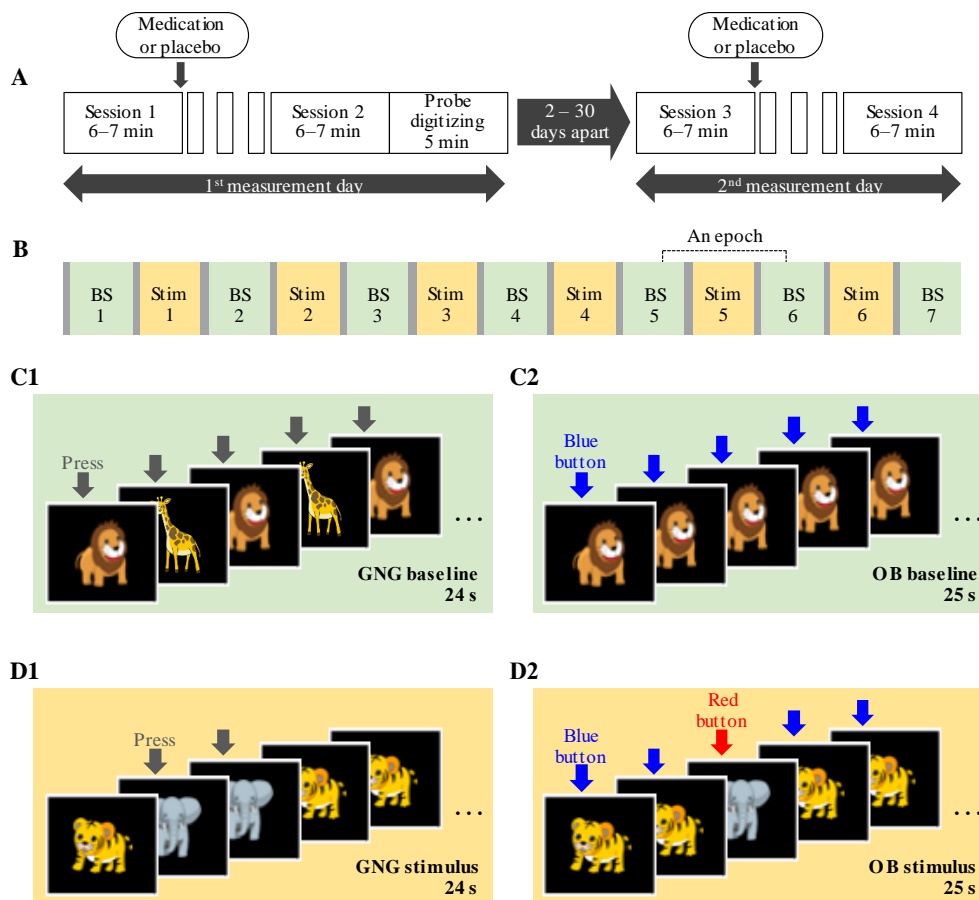
Figure 3. 2 Experimental procedure, design, and task paradigms. (A) Four measurement sessions were performed in two days. (B) Each measurement session lasted for 6–7 min with alternated baseline (BS; 24–25 s) and stimulus (Stim; 24–25 s) intervals for seven and six times, respectively. Task commands were specific for baseline (C) and stimulus (D) intervals for the GNG (C1, D1) and OB (C2, D2) tasks. From (Sutoko et al., 2018), modified with permission.

During the baseline interval(24 and 25 s for baselines of GNG and OB tasks, respectively), subjects were asked to respond to any displayed images (1-Hz frequency display; 800 and 200 ms for display and between-image waiting intervals, respectively) by pressing a designated button (Figure 3.2: C1–2). Subjects were required to inhibit their responses to the no-go images (e.g., tiger) and to specifically respond to the go images (e.g., elephant) by pressing a designated button during the stimulus interval of GNG (Figure 3.2D1; 24 s; 1-Hz frequency display; 800 and 200 ms for display and between-image waiting intervals, respectively). The ratio between no-go and go occurrences was 1:1. Meanwhile, subjects were asked to press specific buttons as standard (the blue

42

button, similar to the pressed button during the baseline) and target (the red button) images displayed during the stimulus interval of OB (Figure 3.2D2; 25 s; 1-Hz frequency display; 800 and 200 ms for display and between-image waiting intervals, respectively). The ratio between standard and target occurrences was 4:1.

The brain measurement was performed using the multichannel fNIRS system (ETG-4000, Hitachi, Ltd., Japan). Two plane probes were connected to this dual-wavelength fNIRS system (695 and 830 nm). Figure 3.3 shows the probe arrangement and placement on the brain template. A probe plane consisted of eight emitters (red circles in Figure 3.3) and seven detectors (yellow squares in Figure 3.3) that were alternately placed constructing the 3×5 arrangement. The measurement sites named channels (black circles in Figure 3.3) were estimated at the middle of an emitter and a detector. In total, two plane probes measured 44 channels. These probes were put to cover bi-hemispheric lateral prefrontal to inferior parietal cortices following the standard placement (Garavan et al., 1999; Liddle et al., 2001; Rubia et al., 2003; Herrmann et al., 2004; Herrmann et al., 2005). The probe position on the head was digitized for all subjects after the first measurement session; the channel locations were approximated and spatially registered to the Montreal Neurological Institute (MNI) space (Okamoto et al., 2004; Jurcak et al., 2005; Okamoto et al., 2005; Singh et al., 2005; Tsuzuki et al.,
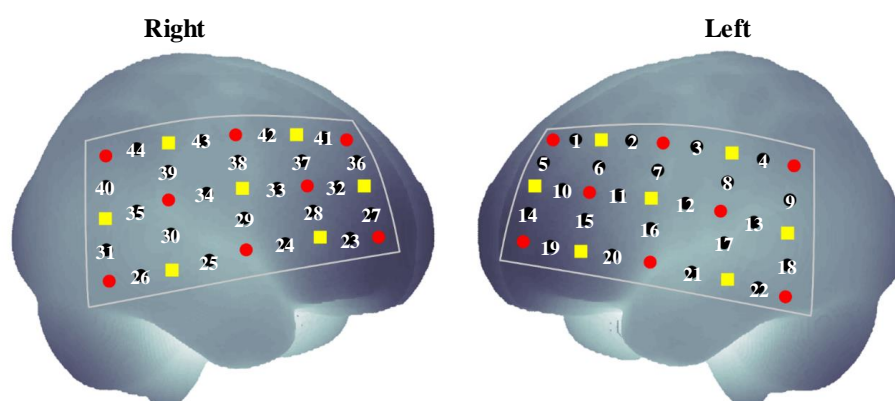
Figure 3. 3 Two-plane probe configuration with 16 emitters (red circles), 14 detectors (yellow squares), and 44 channels (numbered black circles). From (Sutoko et al., 2019b), reproduced with permission.

2007; Okamoto et al., 2009). The experimental procedures were described elsewhere in detail (Nagashima et al., 2014b; Nagashima et al., 2014c).

3.2.3 fNIRS signal preprocessing and analysis

Signal preprocessing was done on the MATLAB-based (Mathworks, Inc.) software Platform for Optical Topography Analysis Tools (POTATo, Hitachi, Ltd., Research & Development Group) (Sutoko et al., 2016). The detected optical intensity was converted to the product of hemoglobin (Hb) concentration change and optical path length ($\Delta C_{O2Hb} \cdot L$, $\Delta C_{HHb} \cdot L$, and $\Delta C_{Hb\text{-}total} \cdot L$ for oxygenated, deoxygenated, and total Hbs, respectively) (Maki et al., 1995; Koizumi et al., 2003) as being imported to the POTATo analysis platform. The conversion was done following the MBLL (Delpy et al., 1988; Maki et al., 1995). The obtained $\Delta C \cdot L$ signals were fitted to a first-degree line to correct the global baseline shift. Afterwards, FIR band-pass filter was implemented on the signals to remove low-frequency drift (< 0.01 Hz) and cardiac pulsation (> 0.8 Hz). In order to analyze each single trial, the entire temporal signal was segmented into six shorter signals (i.e., epochs) for each channel. An epoch signal consisted of 10-s pre-stimulus baseline, 3-s pre-stimulus instruction, 24- or 25-s stimulus, 3-s post-stimulus instruction, and 10-s post-stimulus baseline (Figure 3.2B). The developed rejection algorithm was then applied on these epochs. Noise-affected epochs were eliminated; the activation analysis was performed on the remaining epochs. Before computing the activation analysis, the epochs were fitted by the averaged amplitude of 10-s baseline. Afterwards, the activation values were acquired by averaging inter-epoch signals within activation interval (i.e., 4 s after stimulus onset to the end of stimulus) for each channel.

3.2.4 Dataset quality

As mentioned above (see 3.2.1), noise criteria determined the status of epochs (i.e., noisy) based on thresholds. The values of thresholds were optimized to

appropriately evaluate noises in the current datasets. Therefore, the dataset quality should be examined in advance. There were four parameters related to noise criteria – SNR, amplitude change between two datapoints (criterion 1), epoch baseline slope (criterion 2), and dispersion of correlation summation (criterion 3). Those parameters were evaluated for all datasets, subjects, channels, and signal types (i.e., $\Delta C_{O2Hb} \cdot L$ and $\Delta C_{HHb} \cdot L$) before (blue histograms in Figure 3.4: A–D) and after (red histograms in Figure 3.4: B–D) the signal preprocessing. The SNR of a single channel and signal type was calculated as follows:

$$\text{SNR} = 20 \times \log_{10} \frac{\mu_{\left[(\Delta C \cdot L)_{(t) \to t\ activation}\right]}}{\sigma_{\left[(\Delta C \cdot L)_{(t) \to t\ baseline}\right]}} \qquad \text{(Eq. 3)}$$

where μ is the average of $\Delta C \cdot L$ signal within the $t_{activation}$ interval (i.e., 4 s after stimulus onset to the end of stimulus) and σ is the standard deviation of $\Delta C \cdot L$
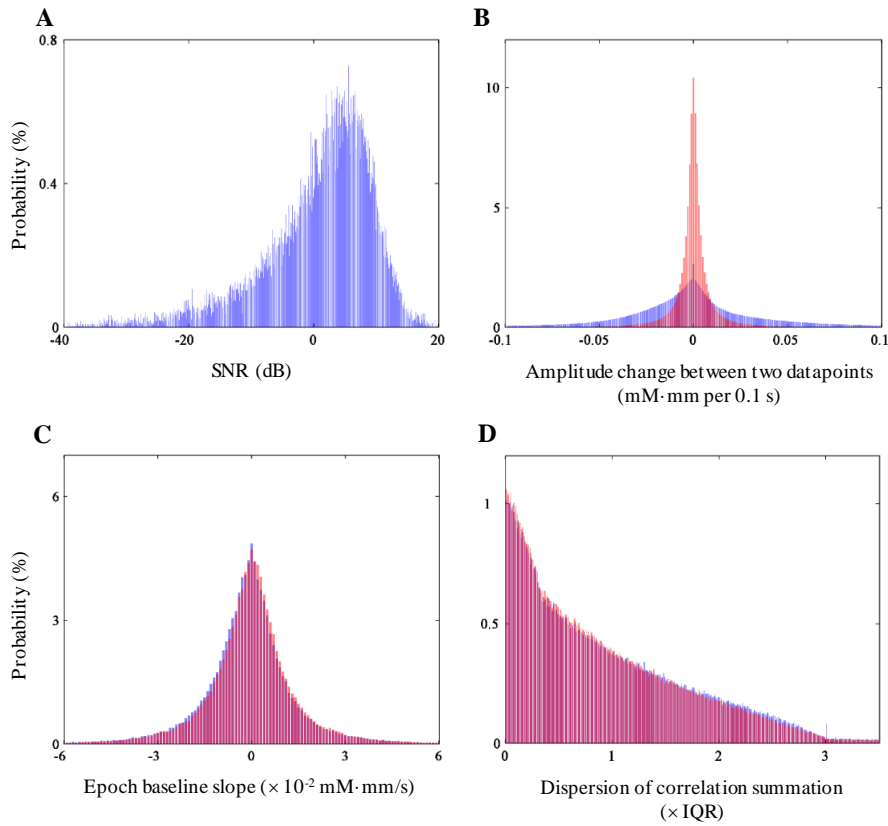
Figure 3. 4 Dataset characteristics – SNR (A), amplitude difference between two datapoints (B), epoch baseline slope (C), and dispersion of inter-epoch correlation summation (D). From (Sutoko et al., 2018), modified with permission.

signal within the $t_{baseline}$ interval (i.e., 10-s epoch baseline). The negative skewness was found in the distribution of SNR (Figure 3.4A). The signal preprocessing brought the greater kurtosis and smaller standard deviation for the distribution of amplitude changes between two datapoints (Figure 3.4B). Meanwhile, there was no preprocessing effects on parameters of epoch baseline slope (Figure 3.4C) and dispersion of correlation summation (Figure 3.4D). Thresholds for noise criteria were then optimized with 95% or 97.5% of two- or one-tail accumulative distributions as the upper optimization limits. Therefore, the optimization ranges for criteria 1 and 2 were 0.01 – 0.05 mM·mm with 0.001 in steps, and 0–3 ($\times$ IQR) with 0.1 in steps for criterion 3. The visual judgment for rejecting noises had been previously done in the current datasets. On the basis of visual judgment, all epochs were survived in 35% of total data (channels $\times$ subjects), either one- or two-epoch rejection happened in more than 60% of total data, and less than 1% of total data underwent three-epoch rejection.

3.2.5 Simulation of random epoch rejection

In order to evaluate the effects of signal quality and random rejection on statistical power, a simulation analysis was performed. The synthetic brain signals were initially created following two methods.

1. Synthetic brain signal (Figure 3.5). A HRF ($h(t)$, Figure 3.5A), adopted from the gamma function(Boynton et al., 1996) (Eq. 4), was used to model a brain activation.

$$h(t) = \left(\frac{t}{\tau}\right)^{n-1} \frac{e^{\left(-\frac{t}{\tau}\right)}}{(n-1)!\tau} \tag{Eq. 4}$$

where t is time, τ is 1.08, and n is 3 (Tanaka et al., 2013). The HRF was convolved with the boxcar function ($b(t)$, Figure 3.5B) in the six-trial paradigm with 24–25 s of stimulus intervals and 25–26 s of inter-trial intervals. The activation degree was manipulated by varying the boxcar amplitude ($\mu = 0.14$–0.3; $\sigma = 0$–0.16; and $\frac{\mu}{\sigma} = 0.85, 1, 2$) across six trials.
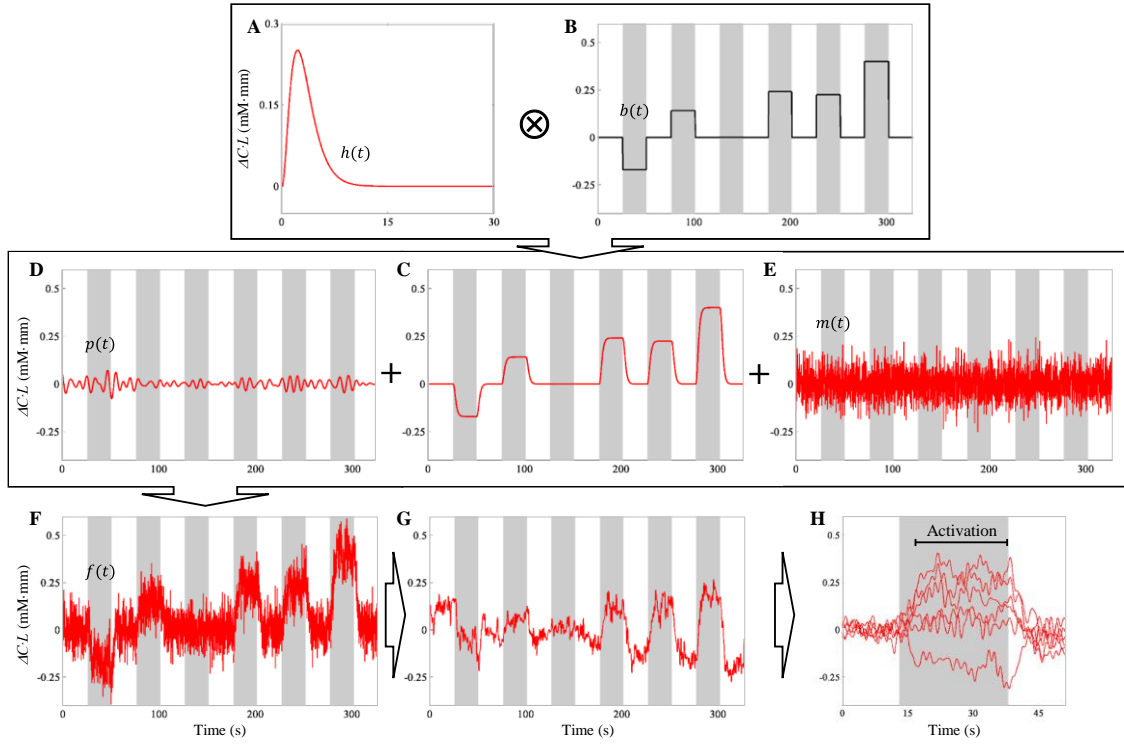
Figure 3. 5 Generation of synthetic brain signal. HRF (A) was convolved with the boxcar function (B) resulting in task-related hemodynamic response signal (C). The physiological component (D) and machine noise (E) were subsequently added constructing the typical fNIRS signal (F). After preprocessing (G), the epoch signals (H) were extracted from the continuous signal. Gray areas represent the stimulus interval. From (Sutoko et al., 2018), reproduced with permission.

This manipulation was done to mimic the variant stimulus-evoked responses. The average of boxcar amplitude (μ) was selected based on the characteristics of datasets. Furthermore, the $\frac{\mu}{\sigma}$ variables were set following the average (i.e., 0.85) and maximum (i.e., 2) ratios in the TD data with positive activations. The physiological noise ($p(t)$, Figure 3.5D) was modeled by the filtered random Gaussian noise ($\mu = 0$; $\sigma = \frac{1}{6}$) using bandpass filtering (0.08–0.15 Hz; 4th order Butterworth) (Pinti et al., 2017). Meanwhile, the machine noise ($m(t)$, Figure 3.5E) was represented by the random Gaussian noise ($\mu = 0$) without filtering. The variance of random Gaussian noise was controlled to simulate the SNR parameter within a range of -40–20dB (2dB interval). The synthetic brain signal ($f(t)$, Figure 3.5F) was created by adding $p(t)$ and $m(t)$ to the

normalized $h(t) * b(t)$ (Figure 3.5C).

2. Synthetic brain signal with motion artifacts (Figure 3.6). Two artifact characteristics, such as spikes and epoch baseline shifting, were added to synthetic brain signals. Spikes were generated by convolving the modified first derivative of the gamma function ($h'(t)$, Figure 3.6A) with the rebound step function ($s(t)$, Figure 3.6B). In order to establish the unrecoverable spike model, the modification of first derivative of the gamma function was done as the following equation.

$$h'(t) = \left[h'(t)_{t=1 \to \max_t h'(t)}, \left(2 \times h'(t)_{t=\max_t h'(t) \to end} \right) - \max_t h'(t) \right]$$

(Eq. 5)

The spike amplitude was varied within 0.14–0.48, and the spike direction was
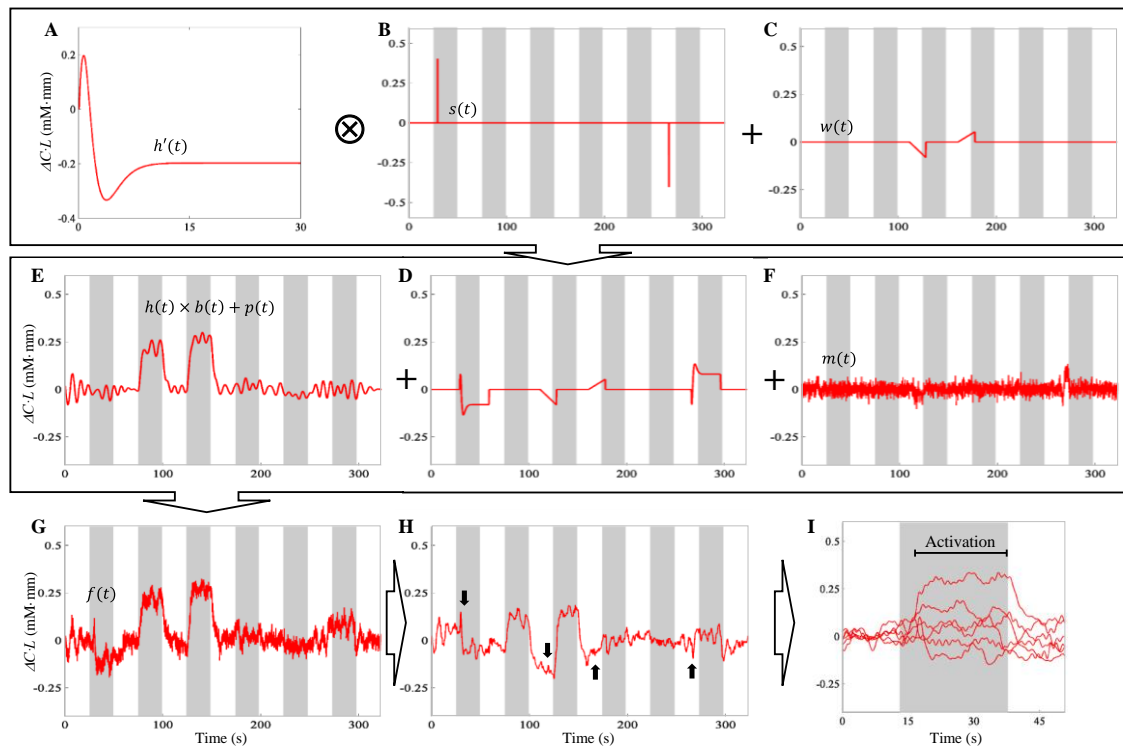
Figure 3. 6 Generation of synthetic brain signal with motion artifacts. Spikes were modeled by convolving the first derivative HRF (A) with rebound step function (B). The model of epoch baseline shift (C) was also added. All noise models (D) were composed together with the task-related signal (E; physiological components $p(t)$ included) and machine noise (F) resulting in the typical fNIRS (G). After preprocessing (H), the epoch signals (I) were extracted from the continuous signal. Gray areas and black arrows represent the stimulus interval and modeled noises, respectively. From (Sutoko et al., 2018), reproduced with permission.

48

set either positive or negative. Epoch baseline shifting ($w(t)$, Figure 3.6C) was constructed by manipulating the epoch baseline interval (13 s before the stimulus onset) with either a positive or negative slope ($\mu = 0.025$ mM·mm/s, $\sigma = 0$–0.025 mM·mm/s). The number of occurred artifact (1–6 times), artifact types, and temporal artifact event were randomized. All artifact components (Figure 3.6D) were added to the activation signal ($h(t) \times b(t)$) with the physiological noise ($h(t) \times b(t) + p(t)$; Figure 3.6E) and the machine noise (Figure 3.6F) resulting in the synthetic brain signal with motion artifacts ($f(t)$, Figure 3.6G).

One-thousand synthetic brain signals (i.e., with and without motion artifacts) were generated for each value of SNR parameter. Those signals were preprocessed (see 3.2.2, Figures 3.5H, 3.6G) and compartmentalized into six epoch data (Figures 3.5H, 3.6I). The random rejection (0–4 epoch rejection) was applied on those epoch data, and the activation analysis was performed on the remaining epoch data. The activation values were then statistically evaluated (*t*-test). Because the boxcar amplitudes were set to be greater than 0 on average, the average of activation values should be significantly found greater than 0 (5% significance level). The occurrence of insignificant results (i.e., out of 1000 synthetic brain signals) presented the probability of false negative rate (β).

3.2.6 Confirmation of algorithm feasibility

Algorithm feasibility was assessed in both synthetic signals with motion artifacts and the real datasets. A synthetic dataset ($N = 98$, $\frac{\mu}{\sigma} = 1$) was created following the SNR distribution of the real datasets. The rejection algorithm was then applied on the artificial dataset using all noise criteria with associated optimization threshold ranges. Three epochs were selected as the pre-set acceptance rate due to the upper limit of three epochs rejection in the real datasets. The optimization objective was to find the optimum threshold values resulting in

the lowest false negative rate. Furthermore, HRF recovery was evaluated in the results of the adaptive rejection algorithm and the process without any rejection.

While the information of HRF was controlled in the synthetic dataset, noise-free HRF was unknown in the real datasets. Because the current datasets had been previously analyzed, the statistical results for group analyses were available. Therefore, the optimization objective in the real datasets was to find the optimum algorithm variables that were able to reproduce statistical results (one-tail sample t-test; $\alpha = 0.025$) of group analyses as listed in Table 3.3. In accordance with previous studies (Inoue et al., 2012; Monden et al., 2012b; Ishii-Takahashi et al., 2014; Nagashima et al., 2014a; Nagashima et al., 2014b; Nagashima et al., 2014c; Araki et al., 2015; Ota et al., 2015), TD children revealed the significant O_2Hb activation ($p < 0.025$) at the right inferior frontal gyrus/middle frontal gyrus (IFG/MFG; channel 32 in Figure 3.3) as performing GNG and OB tasks. ADHD children without any medication showed null O_2Hb activation ($p \geq 0.025$). However, the medication (MPH and ATX) effects in neuromodulating O_2Hb activation ($p < 0.025$) have also been confirmed. The O_2Hb activation was not regulated by the placebo administration ($p \geq 0.025$), and the medication effects were greater than the effect of placebo on O_2Hb activation ($p < 0.025$). The difference between medication and placebo effects was defined by 'inter-administration' term.

Table 3. 3 Significances of right IFG/MFG activation as training and validation targets. From (Sutoko et al., 2018), modified with permission.

Feasibility steps	1. Training in an ADHD dataset	2. Validation in another ADHD dataset	3. Validation in TD datasets	
Samples	22 ADHD (dataset I)	16 ADHD (dataset II)	22 TD (dataset I)	16 TD (dataset II)
Task	Oddball	Go/no-go	Oddball	Go/no-go
Medication	MPH	ATX	—	—
Pre-administration	$p \geq 0.025$	$p \geq 0.025$	$p < 0.025$	$p < 0.025$
Post-medication	$p < 0.025$	$p < 0.025$	—	—
Post-placebo	$p \geq 0.025$	$p \geq 0.025$	—	—
Inter-administration	$p < 0.025$	$p < 0.025$	—	—

There were four algorithm variables that were simultaneously optimized – (1) acceptance rate (e.g., three and four epochs following the visual rejection of the real datasets), (2) number of noise criteria (e.g., one, two, and three criteria), (3) noise criteria (e.g., criteria 1, 2, and 3), and (4) criteria threshold. A conventional approach without the pre-set acceptance rate was also performed to evaluate the effectiveness of adaptive judgment. Furthermore, the OB task may be more prone to noise than the GNG task due to the demand of repetitive responses. Therefore, the task-dependent possibility of acceptance rates was also examined. In total, there were 35 combinations of algorithm variables (Table 3.4) optimized in the real datasets.

Training and validation steps were incorporated in the optimization process to confirm the feasibility and robustness of algorithm applications across tasks (e.g., OB vs. GNG), medications (MPH vs. ATX), and population (ADHD vs. TD children). The optimization process was done in two ways – independent for each training and validation steps (Figure 3.7A) and sequential with the order of training and validation steps (Figure 3.7B). In the sequential way, combinations
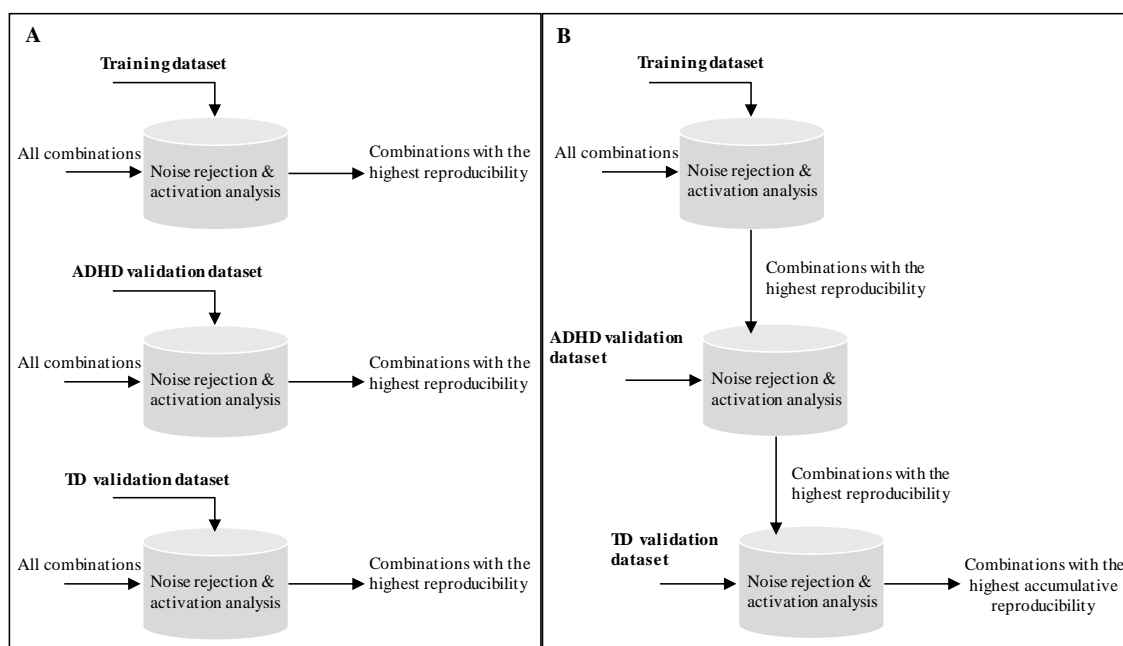
Figure 3. 7 Independent (A) and sequential (B) optimization processes. From (Sutoko et al., 2018), modified with permission.

Table 3. 4 Combinations of algorithm variables. Blue and gray-colored rows indicate combinations with three and two noise criteria, respectively. From (Sutoko et al., 2018), modified with permission.

Combination	Oddball task						Go/no-go task					
	Acceptance rate			Noise criteria			Acceptance rate			Noise criteria		
	3 epochs	4 epochs	None	Criterion 1	Criterion 2	Criterion 3	3 epochs	4 epochs	None	Criterion 1	Criterion 2	Criterion 3
1		✓		✓	✓	✓		✓		✓	✓	✓
2		✓		✓	✓			✓		✓	✓	
3		✓		✓		✓		✓		✓		✓
4		✓		✓				✓		✓		
5		✓			✓	✓		✓			✓	✓
6		✓			✓			✓			✓	
7		✓				✓		✓				✓
8	✓			✓	✓	✓	✓			✓	✓	✓
9	✓			✓	✓		✓			✓	✓	
10	✓			✓		✓	✓			✓		✓
11	✓			✓			✓			✓		
12	✓				✓	✓	✓				✓	✓
13	✓				✓		✓				✓	
14	✓					✓	✓					✓
15			✓	✓	✓	✓			✓	✓	✓	✓
16			✓	✓	✓				✓	✓	✓	
17			✓	✓		✓			✓	✓		✓
18			✓	✓					✓	✓		
19			✓		✓	✓			✓		✓	✓
20			✓		✓				✓		✓	
21			✓			✓			✓			✓
22	✓			✓	✓	✓	✓			✓	✓	✓
23	✓			✓	✓		✓			✓	✓	
24	✓			✓		✓	✓			✓		✓
25	✓			✓			✓			✓		
26	✓				✓	✓	✓				✓	✓
27	✓				✓		✓				✓	
28	✓					✓	✓					✓
29		✓		✓	✓	✓	✓			✓	✓	✓
30		✓		✓	✓		✓			✓	✓	
31		✓		✓		✓	✓			✓		✓
32		✓		✓			✓			✓		
33		✓			✓	✓	✓				✓	✓
34		✓			✓		✓				✓	
35		✓				✓	✓					✓

of algorithm variables that only satisfied 100% (or the highest) reproducibility in the training subset were survived and used for optimizing the validation subsets.

3.2.7 Comparison between visual and algorithm rejections

Besides the reproducibility of statistical results, rejection performances were evaluated in three factors. *First*, the rejection accuracy – how accurate could the adaptive rejection algorithm reject the noisy epochs that were previously labeled by visual raters? The current application solely focused on optimizing noise

rejection for $\Delta C_{O2Hb} \cdot L$ signals because $\Delta C_{O2Hb} \cdot L$ is more pronounced compared to $\Delta C_{HHb} \cdot L$ (Hoshi et al., 2001; Strangman et al., 2002; Hoshi, 2003). However, to confirm the feasibility of this algorithm in different signal types, the rejection accuracy was also evaluated in $\Delta C_{HHb} \cdot L$ and $\Delta C_{Hb\text{-}total} \cdot L$ signals using the optimum algorithm variables. Note that the visual judgment was only processed on $\Delta C_{O2Hb} \cdot L$ signals. *Second*, the temporal correlation (i.e., Pearson's correlation) – how similar were the resulted waveforms after the visual rejection to those after the algorithm rejection? *Third*, the correlation of activation value (i.e., Spearman's rank correlation) – how close were the resulted activation values after the visual rejection to those after the algorithm rejection? Those activation values were statistically examined (one-sample *t*-test) to confirm whether the visual and algorithm rejections significantly brought different interferences or not. An analysis of variance (ANOVA) was also conducted to evaluate the effects of signal types on rejection performances. These three factors were independently computed for each population, administration status, and task (i.e., TD, ADHD pre-administration, ADHD post-medication, and ADHD post-placebo data during OB and GNG tasks). These evaluations were performed to confirm the ability of the adaptive rejection algorithm to be a substitute for the visual rejection.

B. Application of the adaptive rejection algorithm as a signal preprocessing step

3.2.8 Subjects and experimental design

Thirty-two medication-naïve children participated in this study. All children were right-handed and diagnosed with ADHD based on the DSM-5. Twenty-one children (7.8 ± 1.7 years old) presented only ADHD symptoms while 11 children (8.2 ± 2.1 years old) also presented ASD symptoms based on what the DSM-5 refers to as ASD-comorbid ADHD children. All subject's IQs were over 70 (WISC-III or WISC-IV); however, ASD-comorbid ADHD children (103.2 ± 14.5) had significantly higher IQs ($t_{(30)} = 2.08$, $p < 0.05$, Cohen's $d = 0.77$) than ADHD children (92.8 ± 12.9). Age and gender were matched for both ADHD and ASD-

comorbid ADHD groups. This dataset had been collected and previously reported by Tokuda et al. (Tokuda et al., 2018). A technical problem unexpectedly occurred during data saving; thus, the affected data (i.e., two behavioral performance data and an fNIRS measurement data) were excluded in the analysis.

The experiment was designed following the randomized, double-blind, placebo-controlled, and crossover study. All subjects were administered by 18-mg MPH and placebo in two different measurement days. Therefore, both ADHD and ASD-comorbid ADHD children underwent four measurement sessions with pre-medication, post-medication, pre-placebo, post-placebo conditions (i.e., two measurement sessions in a measurement day). Two measurement days were at least four days apart. In each measurement session, the GNG task was performed while the subject's brain was also measured using the ETG-4000 fNIRS system. The GNG task was designed following the block-design paradigm with six trials (Monden et al., 2012a; Monden et al., 2012b; Nagashima et al., 2014b). The experimental design, task paradigm, and measurement system were same as mentioned above (see 3.2.2). The channels were spatially registered in the brain template (Figure 3.8) and labeled as the LONI Probabilistic Brain Atlas (Shattuck et al., 2008) and the Brodmann's atlas (Rorden et al., 2000), as listed in Table 3.5.
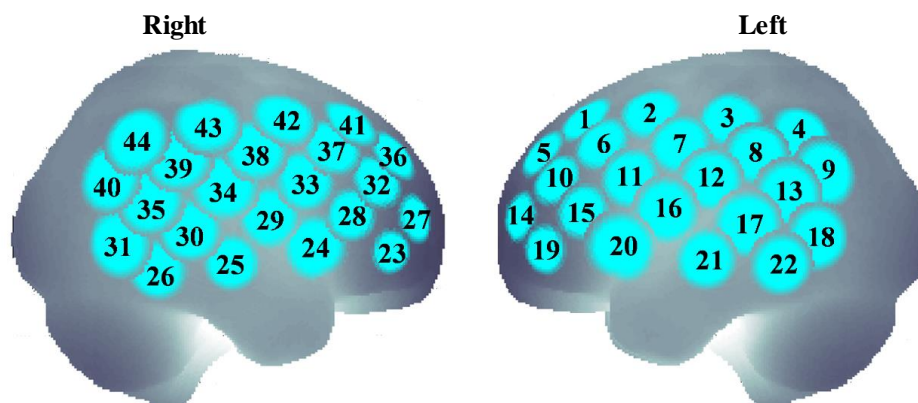
Figure 3. 8 Spatially registered channels on bilateral hemispheres. From (Sutoko et al., 2019c), reproduced with permission.

Table 3. 5 Estimated brain regions for each channel. Coordinates 0 for *x*-, *y*-, and *z*-axes are determined at the midline vertex, the lateral vertex (left-to-right preauricular points), and the Fp point, respectively. From (Sutoko et al., 2019c), reproduced with permission.

Channel	x (mm)	y (mm)	z (mm)	σ (mm)	Macroanatomy (Probability)
1	-27	36	51	14	L-MFG (0.52) L-SFG (0.48)
2	-47	9	55	14	L-MFG (0.68) L-PrCG (0.32)
3	-59	-25	52	14	L-SMG (0.55) L-PoCG (0.45)
4	-58	-55	46	14	L-ANG (0.86) L-SMG (0.14)
5	-24	55	38	13	L-MFG (0.85) L-SFG (0.15)
6	-46	30	42	13	L-MFG (1.00)
7	-60	-4	41	14	L-PrCG (0.52) L-PoCG (0.46) L-SMG (0.02)
8	-67	-36	38	14	L-SMG (0.96) L-ANG (0.04)
9	-59	-65	30	15	L-ANG (0.78) L-MOG (0.20) L-SMG (0.02) L-MTG (0.01) L-STG (0.00)
10	-42	48	26	12	L-MFG (0.99) L-IFG (0.01)
11	-58	17	27	14	L-IFG (0.42) L-PrCG (0.33) L-STG (0.11)
12	-68	-17	27	14	L-PoCG (0.49) L-SMG (0.40) L-STG (0.11)
13	-67	-50	21	15	L-STG (0.30) L-SMG (0.29) L-ANG (0.25) L-MTG (0.16)
14	-34	64	11	12	L-MFG (0.95) L-IFG (0.05)
15	-54	37	13	13	L-IFG (0.85) L-MFG (0.15)
16	-65	2	13	15	L-PrCG (0.51) L-PoCG (0.29) L-STG (0.14) L-IFG (0.06)
17	-70	-32	8	15	L-STG (0.63) L-MTG (0.38)
18	-64	-62	2	15	L-MTG (0.72) L-ITG (0.16) L-MOG (0.09) L-ANG (0.03) L-IOG (0.00)
19	-46	54	-3	11	L-IFG (0.82) L-lOFG (0.18) L-MFG (0.01)
20	-56	21	-2	16	L-IFG (0.56) L-STG (0.31) L-lOFG (0.08) L-PrCG (0.05)
21	-70	-15	-7	13	L-MTG (0.77) L-STG (0.23)
22	-68	-47	-10	14	L-MTG (0.60) L-ITG (0.40)
23	50	52	-4	10	R-IFG (0.82) R-lOFG (0.17) R-MFG (0.01)
24	58	19	-2	15	R-IFG (0.45) R-STG (0.34) R-PrCG (0.15) R-lOFG (0.03) R-MTG (0.02)
25	72	-16	-9	12	R-MTG (0.79) R-STG (0.21)
26	69	-48	-12	14	R-MTG (0.54) R-ITG (0.46)
27	40	63	10	11	R-MFG (0.76) R-IFG (0.24)
28	58	35	12	12	R-IFG (1.00)
29	67	0	11	14	R-PoCG (0.39) R-STG (0.35) R-PrCG (0.26) R-IFG (0.01)
30	73	-33	5	14	R-MTG (0.53) R-STG (0.47)
31	63	-63	0	16	R-MTG (0.39) R-MOG (0.31) R-ITG (0.30) R-ANG (0.00)
32	48	46	26	13	R-MFG (0.63) R-IFG (0.38)
33	63	15	26	14	R-PrCG (0.74) R-IFG (0.24) R-MFG (0.02) R-PoCG (0.01)
34	70	-19	24	15	R-SMG (0.41) R-PoCG (0.31) R-STG (0.27) R-ANG (0.02)
35	68	-50	18	15	R-MTG (0.39) R-ANG (0.31) R-STG (0.24) R-SMG (0.06) R-MOG (0.01) R-ITG (0.00)
36	31	53	37	14	R-MFG (0.97) R-SFG (0.03)
37	51	27	40	14	R-MFG (0.84) R-IFG (0.11) R-PrCG (0.05)
38	65	-6	39	14	R-PoCG (0.49) R-SMG (0.27) R-PrCG (0.24)
39	68	-38	36	15	R-SMG (0.65) R-ANG (0.29) R-STG (0.06)
40	58	-68	27	16	R-ANG (0.62) R-MOG (0.37) R-MTG (0.01)
41	34	34	50	14	R-MFG (0.88) R-SFG (0.12)
42	52	6	52	15	R-PrCG (0.55) R-MFG (0.36) R-PoCG (0.09)
43	64	-26	51	15	R-SMG (0.98) R-PoCG (0.02)
44	60	-56	44	16	R-ANG (0.95) R-SMG (0.05)

3.2.9 Analysis of fNIRS data

The conversion of the detected optical intensity based on the MBLL and the signal preprocessing (i.e., temporal fitting, filtering, and epoch making) were done identically as mentioned above (see 3.2.3). The motion artifacts were then managed by rejecting the affected epochs using the adaptive rejection algorithm. Similar to the datasets (see 3.2.2) used in developing the algorithm, the current dataset had been analyzed before; thus, the information of visually rejected epochs was available. While the above optimization of algorithm variables aimed to reproduce statistical results (see 3.2.6), the optimization objectives could be easily modified, and the current optimization objective was to obtain the highest rejection accuracy compared to the visual judgment. The optimization process revealed the optimum algorithm variables with single noise criterion (i.e., criterion 3) and the criterion threshold of $3 \times$ IQR. These optimum algorithm variables resulted in 96.1% rejection accuracy, and the high rejection accuracy was achieved even without the predetermined acceptance rate. In order to maintain the similarity of data number, channel-wise signals underwent excessive epoch rejection ($>$ two epochs) were excluded in the further analysis. The baseline epoch fitting and activation analysis were performed only for the remaining epochs (see 3.2.3).

3.2.10 Dataset features

Dataset features were extracted from behavioral performances and brain measurements. While performing the GNG task, there were five features indicating subject's behavioral performances – (1) accuracy of go response during the baseline interval (i.e., 1 – omission error), (2) accuracy of go response during the stimulus interval, (3) accuracy of no-go response during the stimulus interval (i.e., 1 – commission error), (4) response time of correct go response during the baseline interval, and (5) response time of correct go response during the stimulus interval. Furthermore, the brain features were obtained from channel-wise (O_2Hb and HHb) activation values in the conditions of pre-administration, post-MPH,

and post-placebo. Because the activation of right MFG/IFG had been prominently reported for the GNG task (Monden et al., 2012a; Monden et al., 2012b; Nagashima et al., 2014b; Tokuda et al., 2018), the brain features were focused on the right hemisphere. The effects of medication and placebo administrations in each feature were assessed against the pre-administration condition for the ADHD and ASD-comorbid ADHD groups (one-sample *t*-test). The differences between ADHD and ASD-comorbid ADHD group were statistically evaluated in each feature (two-sample *t*-test).

3.2.11 Classification optimization and cross-validation

The significantly differing features between two groups would be hints of effective classification. Therefore, only those features were used and optimized for individual classification. Extensive optimization was done for each feature type (i.e., behavioral and brain features). In the case of brain feature, the significantly differing features may occur in multiple channels. Those channels were categorized on the basis of brain regions (brain macroanatomy with the highest probability; Table 3.5). Region-wise features were computed by averaging activation values from significantly differing channels in the same regions.

Six operations, named simple, OR, AND, linear discriminant, quadratic discriminant, and support vector machine (SVM) were carried out in this optimization process. The simple operation classified subjects based on one-axis threshold – whether the ADHD group showed greater features than the ASD-comorbid ADHD group, or *vice versa*. Other operations were performed to classify subjects based on two-axis thresholds. An axis threshold was either a single feature or a combination of multiple features (i.e., averages of multiple features). Therefore, the combination between accuracy response and response time features for an axis threshold was unavailable due to different unit measures. There was no overlapping feature between axes. In the OR and AND operations, the axis thresholds were managed by different operations (Monden et al., 2015).
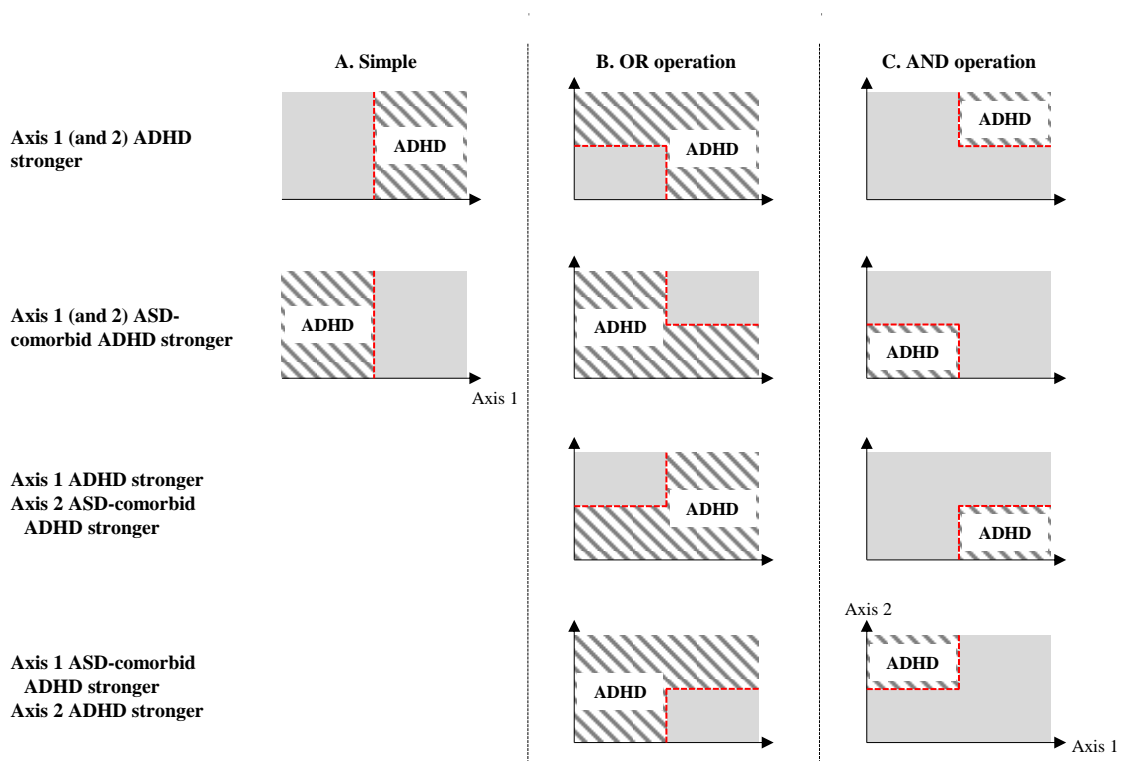
Figure 3. 9 Binary classification with simple (A), OR (B), and AND (C) operations. From (Sutoko et al., 2019c), reproduced with permission.

Several possible cases with the estimated classification axes for the simple, OR, and AND operations are shown in Figure 3.9. Leave-one-out cross validation (32 iterations; 31 training data and 1 test data) was also simultaneously done to confirm the robustness of classifying features. The optimum feature and operation were determined by high validated specificity (true ADHD) – sensitivity (true ASD-comorbid ADHD) in the training data and high accuracy in the test data. The classification performance using behavioral performances and brain features were then compared.

3.3   Results

A. Development of the adaptive rejection algorithm: design and feasibility

3.3.1   Effect of random rejection on false negative rate

Figure 3.10 shows the plots of statistical power (π; $1-\beta$) against SNR in varied
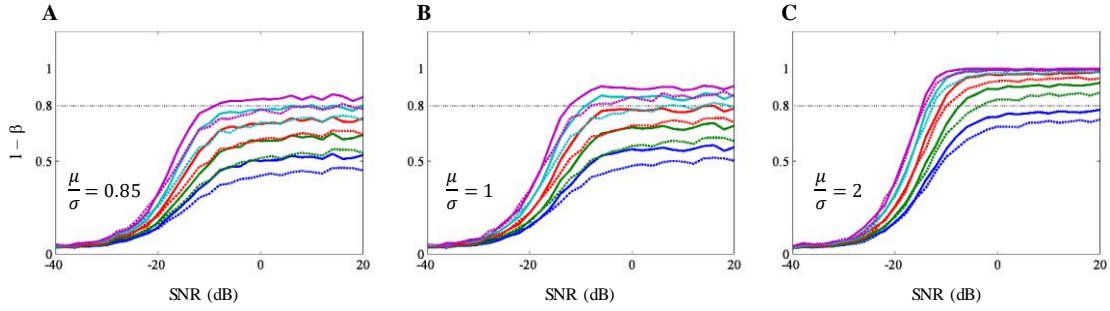
Figure 3. 10 Rejection of random epochs in synthetic brain signal without (solid lines) and with (dotted lines) noise models in three activation variances – (A) 0.85 as similar as the average of real datasets (i.e., TD children with positive activation), (B) 1, and (C) 2 as the highest value in the real datasets of TD children. Blue, green, red, cyan, and magenta plots indicate results from randomly rejected four, three, two, one, and no epochs, respectively.

activation variances ($\frac{\mu}{\sigma} = 0.85, 1, 2$). There are five points observed from the plots.

First, the evaluation of activation values from low SNR signals resulted in low statistical power and high false negative rate. *Second*, as SNR improved, the statistical power increased and reached a plateau at around -10 – -5 dB SNR. *Third*, the low activation variance (i.e., high $\frac{\mu}{\sigma}$) showed the increased statistical power, and an adequate power (i.e., 80%) could be achieved by less epochs. For example, five epochs were required at least to satisfy 80% statistical power as $\frac{\mu}{\sigma}$ was 0.85 (solid cyan line in Figure 3.10A). However, three epochs were sufficient to result in 80% statistical power as $\frac{\mu}{\sigma}$ was set to be 2 (solid green line in Figure 3.10C).

Fourth, synthetic noises decreased the statistical power (dotted lines in Figure 3.10). These decreases become less substantial as the activation variance also decreased (dotted lines in Figure 3.10: A vs. C). *Fifth*, the excessive rejection did bring reduced statistical power, and preserving more epochs was more beneficial for the statistical analysis. This simulation confirmed that the sufficient statistical power could still be maintained by a small number of epochs if the rejection was done accurately, the signal quality was adequate, and the activation phenomenon was strong.

3.3.2 Adaptive rejection algorithm application in the synthetic dataset

Without any rejection, the false negative rate was inflated up to 34%. The use of adaptive rejection algorithm could control the false negative rate at around 18%. Figure 3.11 shows the comparison of HRF recovery between the results of the adaptive rejection algorithm and no rejection. The application of the adaptive rejection algorithm could conserve the HRF (i.e., the red plot closely aligned with the black HRF plot in Figure 3.11) better than without any rejection did. This result suggested that the adaptive rejection algorithm could manage spikes which frequently occurred in the baseline (77% of total synthetic noise).

3.3.3 Optimization of algorithm variables

Figure 3.12 shows the reproducibility results obtained during the optimization process for each combination of algorithm variables. For the independent optimization, the reproducibility (0–100%) was independently assessed for ADHD training, ADHD validation, and TD validation subsets. Meanwhile, the reproducibility for the sequential optimization ranged from 0–300% because all datasets were examined cumulatively. Twenty-six out of 35 combinations of
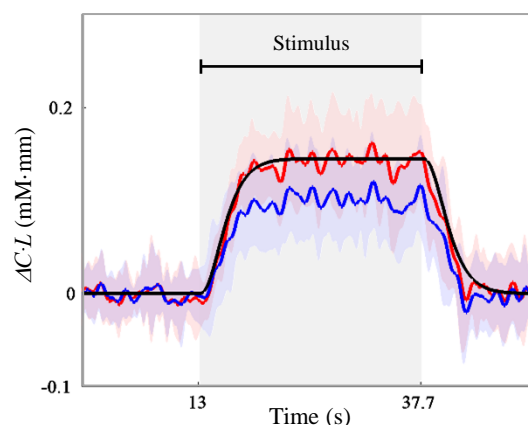
Figure 3. 11 HRF recovery from the synthetic brain signals with motion artifacts using the adaptive rejection algorithm (red plot). Black and blue plot indicate the ground truth for HRF and the HRF recovery without using the adaptive rejection algorithm, respectively. Shaded patches around plots represent the standard deviation. From (Sutoko et al., 2018), reproduced with permission.
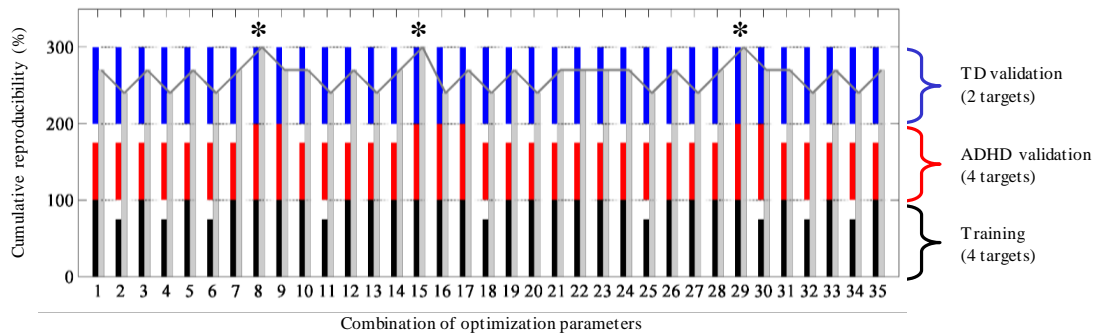
Figure 3. 12 Reproducibility results (*y*-axis) in the ADHD training (black bars), ADHD validation (red bars) and TD validation (blue bars) datasets for each combination of algorithm variables (*x*-axis) optimized using the independent and sequential (gray bars) processes. From (Sutoko et al., 2018), reproduced with permission.

algorithm variables were able to achieve the perfect reproducibility (i.e., four statistical inferences, see Table 3.3) in the ADHD training subset (black bars in Figure 3.12). However, only seven combinations of algorithm variables reproduced four statistical inferences (see Table 3.3) in the ADHD validation subset (red bars in Figure 3.12). Different with other datasets, two statistical inferences of the TD validation subset (blue bars in Figure 3.12) could completely be obtained by using any combinations of algorithm variables. Besides the different number of statistical inferences, the noise level and type were likely divergent across datasets.

Six combinations (combinations 8, 9, 15, 16, 17, and 29) of algorithm variables were able to obtain 100% reproducibility for all datasets. However, only three combinations (combinations 8, 15, and 29) reproduced all statistical inferences for all datasets (300%, gray bars with asterisks in Figure 3.12) using the same thresholds of noise criteria. Therefore, these three combinations were considerably robust compared to other combinations. Combinations 8 and 29 used three criteria in detecting noises, but the acceptance rates applied on those combinations were different. Combination 8 controlled the rejection up to three epochs in both OB and GNG datasets, and the acceptance rate of combination 29 was heterogenous depending on the datasets (four and three epochs for OB and GNG datasets, respectively).

A comparison factor, namely, the rejection accuracy (i.e., factor 1), was used to determine the most optimum combination. Among three robust combinations, combination 29 presented the highest rejection accuracy of O_2Hb epochs in both OB and GNG datasets (i.e., combinations 29 > 8 > 15; 74.5% > 67.2% > 66.3% in the OB dataset; 69.2% > 64.2% > 62.3% in the GNG dataset). Therefore, combination 29 was the most optimum combination of algorithm variables. Thereafter, the results of the adaptive rejection algorithm were based on algorithm variables used in combination 29 and obtained robust thresholds (i.e., 0.047 mM·mm, 0.029 mM·mm/s, and 0.6 × IQR for criteria 1, 2, and 3, respectively). By using the optimum algorithm variables and robust thresholds, the rejection accuracies for HHb and Hb-total epochs were evaluated. The performances were relatively similar or even better than the rejection accuracy of O_2Hb with 75.6–76% and 69–77% for HHb and Hb-total, respectively. Therefore, the adaptive rejection algorithm was applicable for any signal types.

3.3.4 Performances of adaptive rejection algorithm

Even though the adaptive rejection algorithm could reproduce all statistical inferences and resulted in about 70% rejection accuracy (i.e., factor 1), the recovery of activation waveform should be further confirmed in regard to the results of visual judgment. Beforehand, the effect of signal types on correlations between waveforms obtained from visual and adaptive judgments was evaluated (i.e., factor 2). There was no significant effect of signal types ($F = 0.02–0.74$, $p > 0.05$, DF = 2) in both OB and GNG datasets. Figure 3.13 shows the boxplots of correlation coefficients (r) for each group (i.e., TD and ADHD), administration condition (pre-administration, post-medication, and post-placebo), and task (OB and GNG). Even though some outliers were observed (i.e., cross marks in Figure 3.13), the median of correlation coefficient was greater than 0.70 for all groups, administration conditions, and tasks ($r_{median} = 0.88 \pm 0.06$). This result suggests that the waveforms resulted from the visual and algorithm rejections were similar.
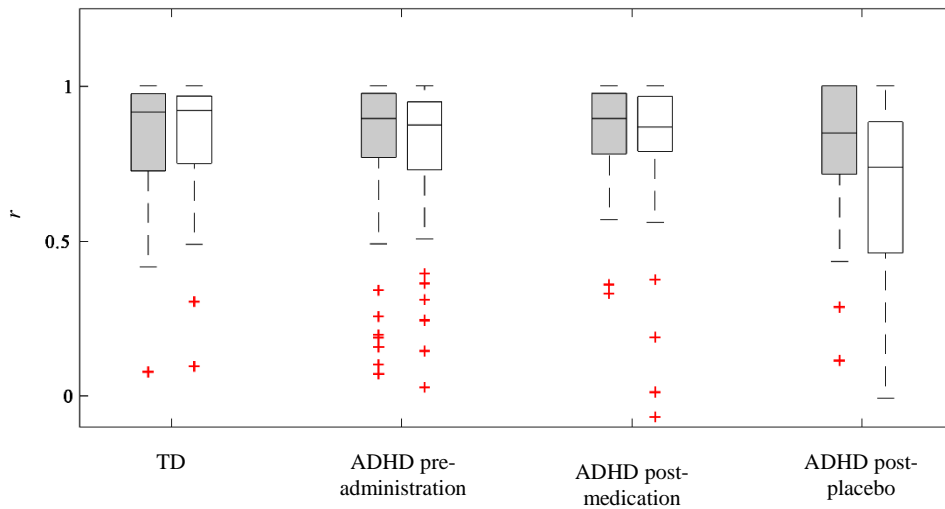
Figure 3. 13 Boxplots of temporal correlation (*r*) between resulted waveforms by the visual judgment and the adaptive rejection algorithm in datasets I (OB; filled boxes) and II (GNG; void boxes). Cross marks indicate non-parametric outliers. From (Sutoko et al., 2018), reproduced with permission.

Subject-average waveforms were compared in the raw data without any rejection and processed data through the visual and algorithm rejections as shown in Figure 3.14. No obvious spike was observed in averaged waveforms in the OB dataset (Figure 3.14: A1–D1); however, heavy spikes were found in the averaged waveforms of ADHD children at the pre-administration and post-placebo conditions during the GNG performance (arrows in Figure 3.14: B2 and D2). By rejecting noisy epochs using either the visual judgment or the adaptive rejection algorithm, noises could be controlled in the averaged waveforms of ADHD subjects at post-placebo condition (Figure 3.14D2). However, spikes still remained in the averaged waveforms of ADHD children at the pre-administration condition (Figure 3.14B2) after the epoch rejection. While the big dip at the baseline interval at the post-medication condition (arrow pointing to magenta plot in Figure 3.14C2) could be managed by Criteria 2, the result of the adaptive rejection algorithm revealed another big dip at the post-stimulus interval (arrow pointing to red plot in Figure 3.14C2).

Besides the temporal waveforms, the activation values were also compared.
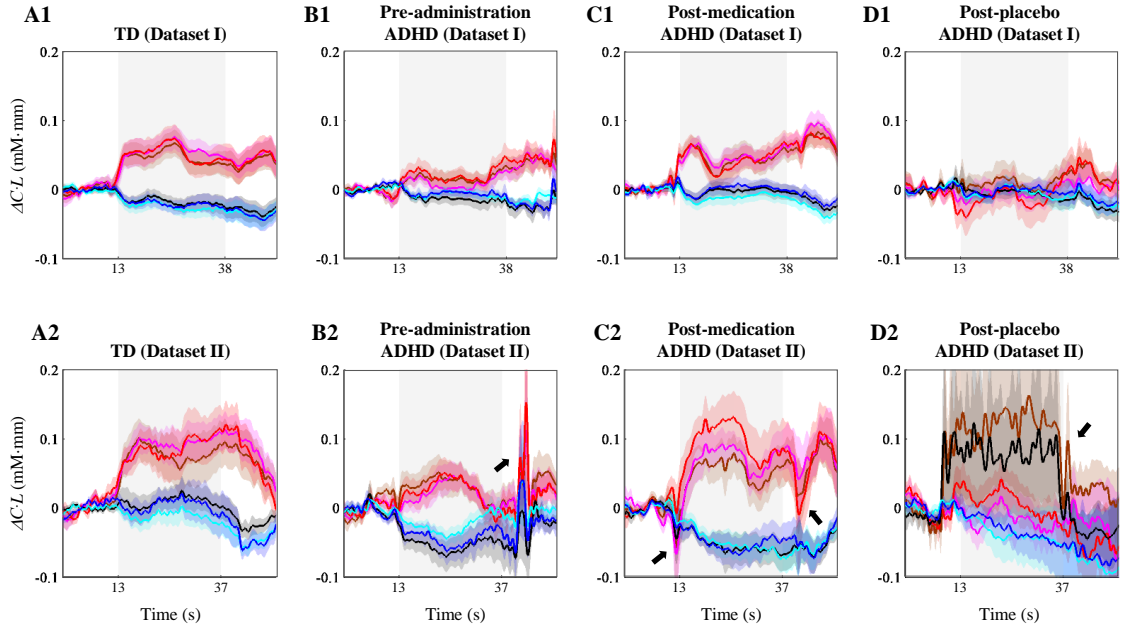
Figure 3. 14 Subject-average waveforms for TD (A1–2) and ADHD children of datasets I (A1–D1) and II (A2–D2) in the conditions of pre-administration (B1–2), post-medication (C1–2), and post-placebo (D1–2). Brown, magenta, and red plots indicate averaged $\Delta C_{O2Hb} \cdot L$ without any rejection, with the visual judgment, with the adaptive rejection algorithm, respectively. Black, cyan, and blue plots show averaged $\Delta C_{HHb} \cdot L$ without any rejection, with the visual judgment, with the adaptive rejection algorithm, respectively. Shaded patches around plots are standard errors, while gray areas represent the stimulus interval. From (Sutoko et al., 2018), reproduced with permission.

Figure 3.15 shows the correlations between activation values obtained from the visual and algorithm rejections (i.e., factor 3). All correlation coefficients were significant (Spearman's rank correlation, $p < 0.01$). Despite several substantial offsets (arrows in Figure 3.15: B1, B2, C2, and D2), the trend between activation values resulted from the visual and algorithm rejections was similar ($\rho > 0.69$). The offsets were also statistically evaluated (paired sample t-test), and the alternative hypothesis was rejected (H_i: offset is not equal to zero; $p > 0.05$, Cohen's $d = 0.03–0.23$). This result confirms the rejection similarity in activation values, and the adaptive rejection algorithm may be a potential substitute for the visual judgment.

B. Application of the adaptive rejection algorithm as a signal preprocessing step
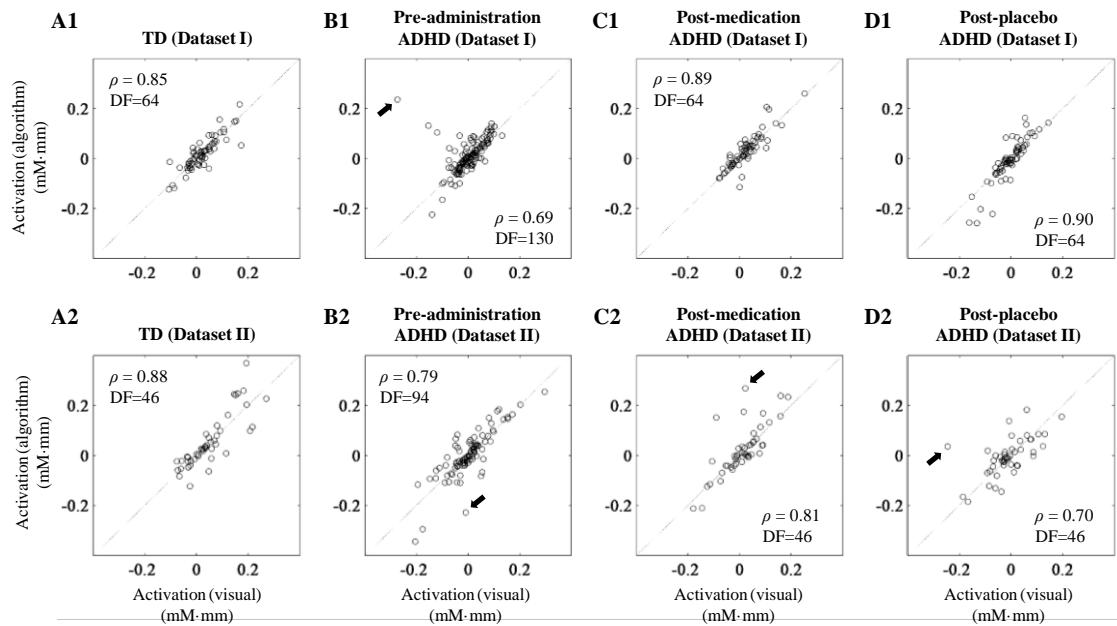
Figure 3. 15 Relationship between activation values (O_2Hb, HHb, and Hb-total) resulted from the visual judgment (*x*-axis) and the adaptive rejection algorithm (*y*-axis) for TD (A1–2), pre-administration (B1–2), post-medication (C1–2), and post-placebo (D1–2) ADHD children in datasets I (A1– D1) and II (A2–D2). Arrows indicate examples of substantial offsets. From (Sutoko et al., 2018), reproduced with permission.

3.3.5 Behavioral performance

Figure 3.16 shows the boxplots of behavioral performances for ADHD and ASD-comorbid ADHD children in each administration condition. There was no significant difference (two-sample *t*-test, p > 0.05, DF = 28–30) between ADHD and ASD-comorbid ADHD children in any behavioral performances. The effects of groups (i.e., ADHD and ASD-comorbid ADHD), behavioral performances (i.e., accuracy and response time), and administration conditions (i.e., pre-administration, post-medication, and post-placebo) were evaluated using multivariate ANOVA and *post hoc* analysis. The significant effect was brought by behavioral performances; the effects of groups and administration conditions were null. The accuracy of go response was greater ($F_{(2,271)} = 5.67$, $p < 0.01$) in the stimulus interval along with slower reaction time ($F_{(1,186)} = 87.14$, $p < 0.001$) than those in the baseline interval. These results suggested that behavioral performances was influenced by the task paradigm (e.g., baseline and stimulus)
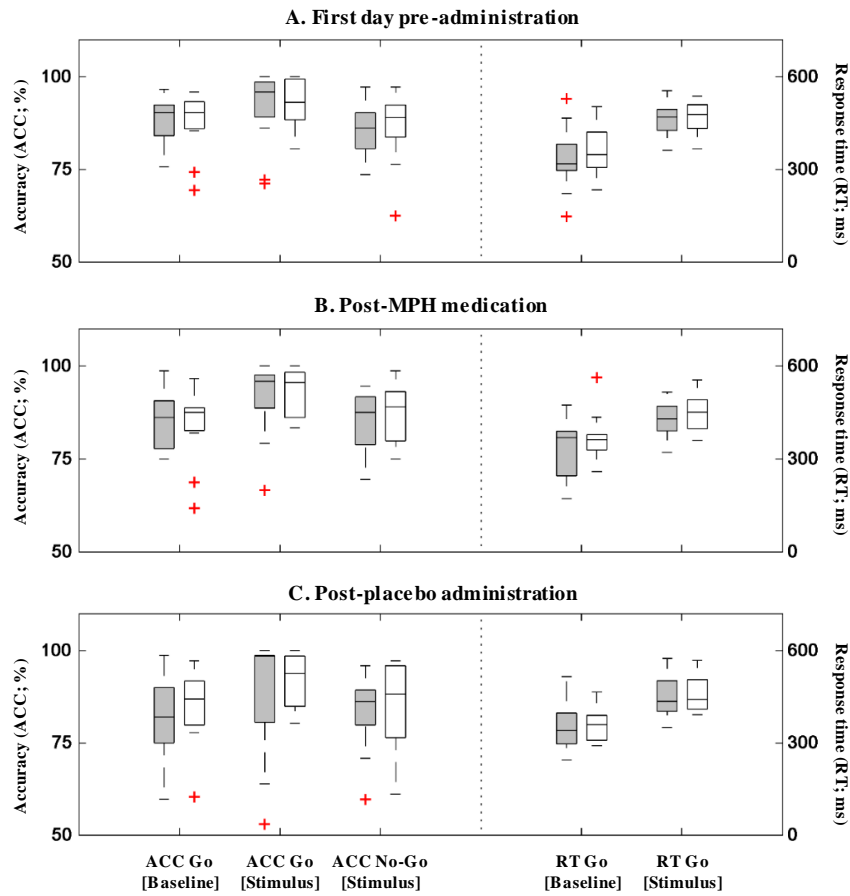
Figure 3. 16 Behavioral performances for ADHD (gray-filled boxplots) and ASD-comorbid ADHD (void-filled boxplots) children during the GNG task in the conditions of first-time measurement (A), post-MPH (B), and post-placebo (C) administrations. Cross marks indicate non-parametric outliers. From (Sutoko et al., 2019c), reproduced with permission.

rather than group characteristics or neuropharmacology effects. Because there was no between-group difference observed, behavioral performances were not included for classifying features.

3.3.6 Brain features

Figure 3.17 shows the t-maps of O_2Hb and HHb activations for ADHD and ASD-comorbid ADHD children in each administration condition. There were six highlighted points. *First*, there was no significantly increased O_2Hb activation for the ADHD group on the first day of pre-administration. *Second*, the ASD-comorbid ADHD group revealed significantly increased O_2Hb activations ($t_{(10)}$ =
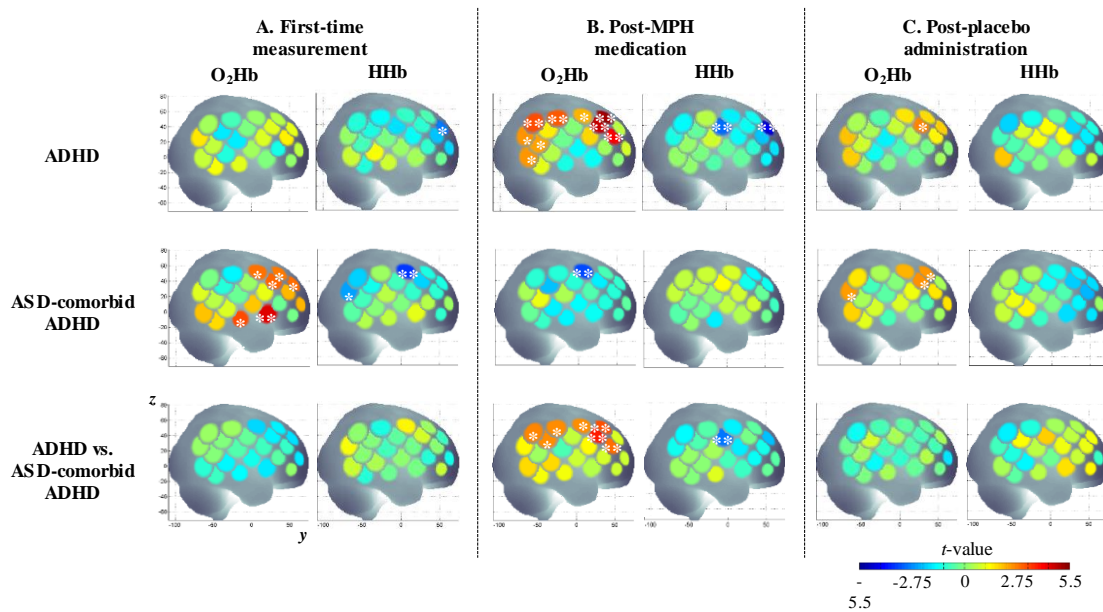
Figure 3. 17 *t*-maps of O$_2$Hb and HHb activations for ADHD children, ASD-comorbid ADHD children, and its comparisons in the conditions of first-time measurement (A), post-MPH (B), and post-placebo (C) administrations. $p < 0.05^{(*)}$; $p < 0.01^{(**)}$ for Student's *t*-test. From (Sutoko et al., 2019c), reproduced with permission.

2.91–4.48, $p < 0.05$) in the right IFG, MFG, superior temporal gyrus (STG), and precentral gyrus (PrCG) on the first day of pre-administration. *Third*, neuropharmacological effects were distinct depending on the groups. MPH administration resulted in significant increases of O$_2$Hb activations ($t_{(20)} = 2.19$–5.14, $p < 0.05$) in substantial areas of the right MFG/IFG and parts of the right PrCG, postcentral gyrus (PoCG), supramarginal gyrus (SMG), angular gyrus (ANG), STG, and middle temporal gyrus (MTG) for the ADHD group. However, the ASD-comorbid ADHD group revealed either null or significantly decreased O$_2$Hb activations (the right PrCG, $t_{(10)} = -3.35$, $p < 0.05$) in the post-MPH condition. *Fourth*, the effect of placebo on increased O$_2$Hb activations in the right MFG was similar for both ADHD ($t_{(20)} = 2.69$, $p < 0.05$) and ASD-comorbid ADHD ($t_{(10)} = 2.49$–2.57, $p < 0.05$) groups. *Fifth*, the significant HHb activations mostly differed from the significant O$_2$Hb activations in terms of group (i.e., one-sample *t*-test against baseline/zero) and between-group (i.e., two-sample *t*-test between ADHD and ASD-comorbid ADHD groups) characteristics. For example,

the significant placebo effects were only observed in the O_2Hb activations but not in the HHb activation. *Sixth*, the significant between-group difference was only brought by the MPH administration. The O_2Hb activation was significantly greater ($t_{(30)} = 2.60 - 3.84$, $p < 0.05$) for the ADHD group in the right MFG, PrCG, SMG, and ANG. The HHb activation was also found to significantly decrease ($t_{(30)} = -2.86$, $p < 0.05$) in the right PoCG for the ADHD group. Table 3.6 summarizes the significant inferences of O_2Hb and HHb activations for each group, administration condition, and brain region. Because the between-group differences were only observed in the post-MPH condition, those differences were then used as classifying features.

3.3.7 Optimization of classifying features

The features of O_2Hb activation came from seven significant activation channels; those significant activation channels were categorized into four spatial

Table 3. 6 Summary of significant O_2Hb and HHb activations for ADHD and ASD-comorbid ADHD children in the conditions of first-time measurement, post-MPH, and post-placebo administrations. From (Sutoko et al., 2019c), reproduced with permission.

		First day pre-administration		Post-MPH administration		Post-placebo administration	
		O_2Hb	HHb	O_2Hb	HHb	O_2Hb	HHb
ADHD	MTG	–	–	CH 31, 35 ($d = 0.51 - 0.54$)	–	–	–
	MFG	–	CH 36 ($d = -0.62$)	CH 32, 37, 41 ($d = 0.91 - 1.15$)	CH 36 ($d = -0.98$)	CH 37 ($d = 0.59$)	–
	PrCG	–	–	CH 42 ($d = 0.48$)	–	–	–
	PoCG	–	–	–	CH 38 ($d = -0.65$)	–	–
	SMG	–	–	CH 43 ($d = 0.69$)	–	–	–
	ANG	–	–	CH 40, 44 ($d = 0.55 - 0.72$)	–	–	–
ASD-comorbid ADHD	IFG	CH 24 ($d = 1.35$)	–	–	–	–	–
	STG	CH 25 ($d = 1.00$)	–	–	–	–	–
	MFG	CH 32, 37, 41 ($d = 0.85 - 0.92$)	–	–	–	CH 37, 41 ($d = 0.75 - 0.77$)	–
	PrCG	CH 42 ($d = 0.88$)	CH 42 ($d = -1.07$)	CH 42 ($d = -1.01$)	–	–	–
	ANG	–	CH 40 ($d = -0.72$)	–	–	CH 40 ($d = 0.74$)	–
ADHD vs. ASD-comorbid ADHD	MFG	–	–	CH 32, 37, 41 ($d = 1.10 - 1.42$)	–	–	–
	PrCG	–	–	CH 42 ($d = 0.97$)	–	–	–
	PoCG	–	–	–	CH 38 ($d = -1.07$)	–	–
	SMG	–	–	CH 39, 43 ($d = 0.97 - 0.98$)	–	–	–
	ANG	–	–	CH 44 ($d = 1.00$)	–	–	–

features, i.e., right MFG (channels 32, 37, 41), right PrCG (channel 42), right SMG (channels 39 and 43), and right ANG (channel 44). All optimization operations were applied on four features of O_2Hb activations. Meanwhile, the feature of HHb activation was extracted from a single activation channel (i.e., channel 38). Therefore, only the simple operation was able to be performed for optimizing the feature of HHb activation.

Table 3.7 presents the optimization results for each optimization operation and feature (O_2Hb and HHb activation features). The features of O_2Hb activation performed better by resulting in the higher summation of specificity and sensitivity compared to the feature of HHb activation. The comparison of classification performance among optimization operations and features was statistically evaluated using univariate ANOVA and *post hoc* analysis. The SVM operation with the optimum O_2Hb activation feature of right MFG-PrCG (channels 32, 37, 41, and 42; axis 1) and right SMG-ANG (channels 39, 43, and 44; axis 2) significantly revealed the highest specificity ($94 \pm 3.4\%$). The highest

Table 3. 7 Classification performances using optimum brain features for each operation. From (Sutoko et al., 2019c), reproduced with permission.

Characteristic	Condition	Optimization operation	Feature(s)	Specificity	Sensitivity	Accuracy
O_2Hb activation	Post-MPH medication	Simple	CH 32, 37, 41, 44	$67 \pm 1.9\%$	100%	72%
			CH 32, 37, 41, 42	$76 \pm 1.8\%$	$91 \pm 1.7\%$	75%
			CH 32, 37, 41, 42, 44	$86 \pm 1.4\%$	$82 \pm 2.3\%$	72%
		OR operation	CH 32, 37, 41, 44 (Axis 1) CH 42 (Axis 2)	$81 \pm 1.6\%$	100%	81%
			CH 32, 37, 41, 42 (Axis 1) CH 39, 43, 44 (Axis 2)	$76 \pm 1.8\%$	$91 \pm 1.7\%$	63%
		AND operation	CH 32, 37, 41, 44 (Axis 1) CH 42 (Axis 2)	$67 \pm 1.9\%$	100%	59%
			CH 32, 37, 41, 42 (Axis 1) CH 39, 43, 44 (Axis 2)	$76 \pm 1.8\%$	100%	72%
		Linear discriminant	CH 32, 37, 41, 44 (Axis 1) CH 42 (Axis 2)	$85 \pm 1.8\%$	$84 \pm 4.5\%$	84%
			CH 32, 37, 41, 42 (Axis 1) CH 39, 43, 44 (Axis 2)	$76 \pm 2.4\%$	$80 \pm 4.6\%$	75%
		Quadratic discriminant	CH 32, 37, 41, 44 (Axis 1) CH 42 (Axis 2)	$86 \pm 1.7\%$	$94 \pm 7.0\%$	81%
			CH 32, 37, 41, 42 (Axis 1) CH 39, 43, 44 (Axis 2)	$78 \pm 4.2\%$	$85 \pm 4.3\%$	72%
		Support vector machine	CH 32, 37, 41, 44 (Axis 1) CH 42 (Axis 2)	$91 \pm 2.1\%$	$92 \pm 4.5\%$	81%
			CH 32, 37, 41, 42 (Axis 1) CH 39, 43, 44 (Axis 2)	$94 \pm 3.4\%$	$57 \pm 11\%$	63%
HHb activation	Post-MPH medication	Simple	CH 38	$90 \pm 1.2\%$	$64 \pm 2.9\%$	75%

sensitivity ($100 \pm 0.0\%$) was achieved by four combinations of O_2Hb activation features using simple, OR, and AND operations (see Table 3.7). The OR and SVM operations with the optimum O_2Hb activation features of right MFG-ANG (channels 32, 37, 41, and 44; axis 1) and right PrCG (channel 42; axis 2) contributed to the highest summation of specificity and sensitivity. Furthermore, the linear discriminant operation with the same optimum feature presented the highest cross-validation accuracy. Because the sample number was currently limited, the classification error from a single sample could bring a decreased cross-validation accuracy by around 3%. Even though the best-performing operation was difficult to be determined, the O_2Hb activation features of right MFG-ANG and right PrCG were found to be robust across optimization operations resulting in $86 \pm 4.1\%$, $93 \pm 7.3\%$, $82 \pm 1.6\%$ (pooled variance) for specificity, sensitivity, and cross-validation accuracy, respectively.

Figure 3.18 shows the scatter plot of O_2Hb activations of right PrCG against right MFG-ANG and the receiver operating characteristic (ROC) graphs for the OR and AND operations. The MPH-evoked O_2Hb activations of ASD-comorbid
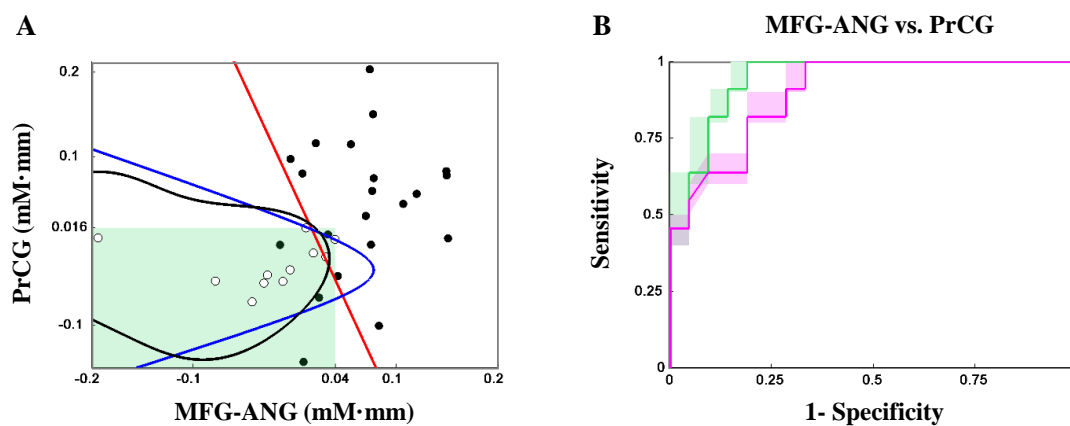
Figure 3. 18 (A) O_2Hb activations of right PrCG against right MFG-ANG for ADHD (black dots) and ASD-comorbid ADHD (white dots) children with the optimum classification – green patch (cut-off thresholds at 0.04 mM·mm and 0.016 mM·mm for axis 1 and 2, respectively), red, blue, and black lines for the OR, linear discriminant, quadratic discriminant, and SVM operations, respectively. (B) ROCs using the optimum two-axis features (MFG-ANG vs. PrCG) for the OR (green curve) and AND (magenta curve) operations. Shaded patches around curves represent the range of validation performance (minimum–to–maximum specificity and sensitivity). From (Sutoko et al., 2019c), modified with permission.
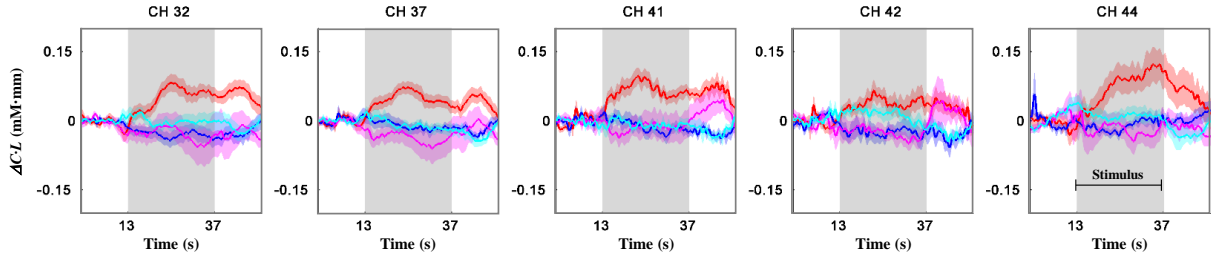
Figure 3. 19 Subject-average waveforms for ADHD (red and blue plots for $\Delta C_{O2Hb} \cdot L$ and $\Delta C_{HHb} \cdot L$, respectively) and ASD-comorbid ADHD (magenta and cyan plots for $\Delta C_{O2Hb} \cdot L$ and $\Delta C_{HHb} \cdot L$, respectively) children in the right MFG (channels 32, 37, and 41), right ANG (channel 44), and right PrCG (channel 42). Shaded patches around plots indicate standard errors. Gray areas represent the 24-s stimulus interval. From (Sutoko et al., 2019c), reproduced with permission.

ADHD group was lower than 0.04 and 0.016 mM·mm for the right MFG-ANG and right PrCG, respectively. Figure 3.19 visualizes the subject-average $\Delta C_{O2Hb} \cdot L$ and $\Delta C_{HHb} \cdot L$ waveforms of the ADHD and ASD-comorbid ADHD groups in the right MFG, ANG, and PrCG (i.e., channels 32, 37, 41, 42, and 44). The increases of $\Delta C_{O2Hb} \cdot L$ during the stimulus interval was clearly observed for the ADHD group (red plots in Figure 3.19); the ASD-comorbid ADHD group showed insignificant changes of $\Delta C_{O2Hb} \cdot L$ (magenta plots in Figure 3.19) and $\Delta C_{HHb} \cdot L$ (cyan plots in Figure 3.19) during the stimulus interval.

3.4 Discussion

3.4.1 Noise correction versus adaptive rejection algorithm

Noise correction algorithms had been frequently reported offering benefits over the noise rejection method in maintaining sufficient sample number (Robertson et al., 2010; Cooper et al., 2012; Brigadoi et al., 2014; Hu et al., 2015; Jahani et al., 2018). However, there are five arguments as to why the rejection algorithm was worthwhile to be approached and developed.

First, the temporal information was also omitted under the performance of noise correction algorithm as similar as the noise rejection method did. Noises could occur during baseline and stimulus intervals. If baseline and stimulus signals are dominantly influenced by noises, the excessive noise correction will be required,

and the results may bring the heightened risk of false positive (i.e., exaggeration of true activation) and false negative (i.e., elimination of true activation). Furthermore, the trends of temporal courses may substantially change due to overcorrecting results.

Second, unstable performances of noise correction algorithms were found (Cooper et al., 2012; Hu et al., 2015). This instability might be caused by the unmatched correction algorithms toward noise types. For example, spline interpolation performed the best to remove high frequency spikes; however, the correction become ineffective as eliminating the overlapped noises with true activation signals (Brigadoi et al., 2014; Chiarelli et al., 2015; Hu et al., 2015). The optimization of correction performance should be personalized (Brigadoi et al., 2014; Vinette et al., 2015). Furthermore, the performance of PCA depends on the noise types and the parameter of variance elimination (e.g., 80%). There is no optimum way to determine the best parameter of variance elimination. PCA is performed on the basis of the assumption of uncorrelated components (Zhang et al., 2005; Kohno et al., 2007; Katura et al., 2008). However, this assumption is likely be violated as the true activation and noises are convolved, and brain activation is confided in networks.

Third, some noise correction methods requires multiple signal sources. Even though the removal of physiological noises had been demonstrated using the single-channel ICA method (Aarabi et al., 2016), the decomposition of motion artifacts still required the multichannel measurement (Virtanen et al., 2009; Schelkanova et al., 2012; Tanaka et al., 2014). The performance efficiency will be likely reduced, if the number of independent components is more than the available signal sources (Djuwari et al., 2006).

Fourth, the performance of noise correction algorithms in an almost real-time application is still limited. The real-time application for ICA has been attempted (Esposito et al., 2003); however, this application was hindered by low data availability, limited computation time, and variances of brain signals (Soldati et

al., 2013).

Fifth, the performances of noise correction algorithms have been confirmed for the HRF recovery (Cooper et al., 2012; Yücel et al., 2014); however, the regular HRF may not be identified for the disordered children. In order to comprehensively evaluate true activation characteristics for the disordered children, the modified temporal courses caused by noise correction algorithms may not be preferable.

The adaptive rejection algorithm was developed to solve five issues above. Noise rejection may lead to the excessive loss of temporal information. However, the adaptive rejection algorithm controlled the data loss to the tolerable level of statistical requirement. The unstable performance due to diverse noise types and levels could be resolved by the personalized and adaptive judgment. The adaptive rejection algorithm may be applied on even only a channel (i.e., single signal source) in an almost real-time application. Furthermore, the adaptive rejection algorithm could retain the original trend of temporal course for supporting comprehensive evaluations of disordered brain activations.

3.4.2 Visual judgment versus adaptive rejection algorithm

There were three factors used in comparing between results of the visual judgment and the adaptive rejection algorithm. The rejection accuracy was more than 70% (i.e., factor 1) with high similarity of resulted temporal courses (i.e., factor 2) and activation values (i.e., factor 3). All factors positively suggested that the results of both methods were similar, and the adaptive rejection algorithm might potentially be a substitute for the visual judgment. While the excessive rejection (> 90%) was reported using the conventional noise rejection without the controlled rejection rate (Cooper et al., 2012), the adaptive rejection algorithm was able to control the maximum rejection rate to achieve the least noise level and the sufficient statistical power. Furthermore, this algorithm provided benefits, such as analysis speed, objectivity, and applicability for even inexperienced data

analysts.

Even though three comparison factors generally concluded the advantages of the adaptive rejection algorithm, the discrepancy between results of the visual judgment and the adaptive rejection algorithm was observed in the subject level. For example, the offsets of activation values were found to be substantial (arrows in Figure 3.15). There are three arguments related to the reasons for these offsets. *First*, the noise types differed from the noise criteria used in the adaptive rejection algorithm. Therefore, the adaptive rejection algorithm missed to identify the noisy epochs. *Second*, the number of noisy epochs was more than the maximum rejection rate (i.e., 100% - acceptance rate). The noisy epochs still then remained. *Third*, the signal quality was originally low with heavy noises in major temporal courses. In this situation, the measurement data should not be used, and the re-measurement is highly recommended. Note that the perfect reproducibility for results of the visual judgment may not always be favored because the visual judgment might be entailed by the rater's subjectivity.

The application of the adaptive rejection algorithm is exploitable and versatile. Thus, further applications can resolve above arguments. The algorithm provided the bottom-up and flexible design. The current noise criteria are able to be replaced with other criteria and different detection orders. Besides rejecting noisy epochs, this algorithm can be applied on the real-time measurement to directly evaluate the noise level and to contribute to a control command for either continuing or terminating the measurement after reaching the sufficient epoch data. Therefore, the measurement quality can be maintained in the best quality.

3.4.3 Optimum algorithm variables

After the optimization process, three noise criteria were optimally embedded on the adaptive rejection algorithm. This result suggested that the noise types were diverged across subjects. The effect of signal preprocessing (e.g., baseline correction, filtering) on the algorithm variables was not evaluated; however, the

significant effect of signal preprocessing was only observed in the threshold of noise criteria 1. Therefore, the threshold of criteria 1 should be re-tuned as the signal preprocessing is modified.

Through the sequential optimization, the robust thresholds for each criterion were found. Even though those thresholds were applicable for training and validation subsets, the different acceptance rates were observed for GNG ($\geq$ three epochs) and OB ($\geq$ four epochs) datasets. The initial hypothesis suggested the task-dependent effect on the algorithm variables. However, the complete reproducibility of the TD validation subset (i.e., GNG and OB tasks) could be achieved by either three or four epochs acceptance rates (blue bar-plots in Figure 3.12). Meanwhile, the ADHD validation subset (i.e., GNG task) only reached the complete reproducibility (combinations 8, 9, 15–17, 29, and 30; red bar-plots in Figure 3.12) when the acceptance rate was set to be either three epoch or none (i.e., non-adaptative judgment). From Figure 3.14, apparent spikes were observed in the averaged waveforms for ADHD children in the conditions of pre-administration and post-placebo. Therefore, instead of task paradigms, the noise level, that may vary across subjects, highly influenced the selection of algorithm variables.

3.4.4 Use of adaptive rejection algorithm as a signal preprocessing step

The adaptive rejection algorithm was applied on the different dataset and incorporated as one of signal preprocessing steps. In prior to the application, the algorithm variable was re-optimized to reach the highest rejection accuracy (factor 1; see 3.2.7) on the basis of the visual judgment results. Here, the different objective of optimization process was pursued and demonstrated. This demonstration addressed the application flexibility of the adaptive rejection algorithm. However, the optimum algorithm variables (i.e., number of criteria, noise criteria, acceptance rate) revealed to be different to the previously found variables during the algorithm development. This result confirmed the above logic

that the noise level affects the optimum algorithm variables. In the new dataset (i.e., ADHD and ASD-comorbid ADHD children), only single noise criterion was used in the adaptive rejection algorithm without pre-set acceptance rate. The new dataset seemingly had higher signal quality and lower noise level than the previous datasets. In order to construct a practical utility using the adaptive rejection algorithm, the tuning process for algorithm variables should be performed in various datasets with heterogeneous noise types and levels. The application of algorithm variables can be categorized depending on ranges of noise level. For example, single noise criteria is used for relatively high quality datasets, and multiple noise criteria are implemented on datasets with low quality.

3.4.5 Characteristics of ADHD and ASD-comorbid ADHD groups in inhibition response

The comparison of behavioral performances showed insignificances between ADHD and ASD-comorbid ADHD groups. While the performances related to attention tasks reportedly presented significant differences between TD, ADHD, ASD, and ASD-comorbid ADHD groups, the inhibitory performances (e.g., omission and commission errors) were comparable among groups (Sinzig et al., 2008). Furthermore, the neuropharmacological effects were not pronounced in the current behavioral performances. These results were relatively consistent with previous results. The difference between ADHD and ASD subjects was also reported to be insignificant in previous studies (Ishii-Takahashi et al., 2014; Tye et al., 2014). Furthermore, ADHD/ASD children or adolescents could perform the task equally compared to TD controls did (Kana et al., 2007; Nagashima et al., 2014b; Ikeda et al., 2018a; Ikeda et al., 2018b).

The characteristics of behavioral performances are apparently divergent. ADHD/ASD children or adolescents revealed lower accuracy responses (Monden et al., 2012b; Xiao et al., 2012; Vara et al., 2014), slower response time (Alderson et al., 2008; Xiao et al., 2012), and greater variability of response time (Smith et

al., 2006; Alderson et al., 2008; Hart et al., 2014; Tye et al., 2014) than TD controls. Despite the inferences of behavioral performances, functional imaging results (e.g., fNIRS, fMRI, MEG, EEG) could distinguish group characteristics better than behavioral performances. The current results based on the brain activation analysis was also prominent in differentiating ASD-comorbid ADHD children from ADHD children.

The observed null activation for the ADHD group was consistent with the previous results (Monden et al., 2012b; Nagashima et al., 2014b; Tokuda et al., 2018). Different to the ADHD group, the TD group showed the significant activation in the bilateral VLPFC, DLPFC (or IFG and MFG), supplementary motor area (SMA), anterior cingulate gyrus, inferior parietal and temporal lobes, caudate nucleus, and cerebellum during the GNG task (Garavan et al., 1999; Liddle et al., 2001; Menon et al., 2001; Rubia et al., 2003). The activation of right IFG has been associated with not only the GNG task but also other inhibitory tasks (Menon et al., 2001; Aron et al., 2003; Rubia et al., 2003; Aron et al., 2004). Therefore, as hypothesized before, the impairment of inhibitory response for ADHD children closely related to the brain dysfunctions particularly in the right IFG.

Vara et al. previously reported the broad activation in the frontal cortex for ASD adolescents during the inhibitory process compared to the localized activation for healthy young adults (Vara et al., 2014). However, ASD adolescents revealed poorer behavioral performances than healthy young adults performed (Belmonte et al., 2004; Schulz et al., 2004). Even though the evident activation was observed for the ASD group, contrast results were also observed. Compared to the TD group, the ASD group exhibited low activation in the bilateral DLPFC, left VLPFC, left premotor area, left pre-SMA, and frontal lobe during the inhibitory SST (Xiao et al., 2012; Ishii-Takahashi et al., 2014). Those results addressed a hypothesis of ASD neuropathophysiology related to inefficient brain recruitment or low activation.

The study of ASD-comorbid ADHD group is still limited. Chantiluke et al. hypothesized that "the comorbidity is neither an endophenocopy of the two pure disorders nor an additive pathology" (Chantiluke et al., 2014). In the pre-administration time, the ASD-comorbid ADHD group showed the increased brain activation at the right frontal lobe. The causal understanding is unclear whether the impaired recruitment was behind the significant activation for the ASD-comorbid ADHD group. Further studies are required to clarify this point.

3.4.6 Distinct MHP-evoked response in ADHD and ASD-comorbid ADHD group

The strategic treatment for ASD patient focused on the management of comorbidity condition rather than the ASD phenotypes (Davis et al., 2012; Santosh et al., 2016). For the case of ASD-comorbid ADHD children, common ADHD medications (e.g., psychostimulants and non-stimulants) (Davis et al., 2012) are often prescribed. Only 34% ASD diagnosed children take medications to ease symptoms (Frazier et al., 2011). MPH has been well used for treating ADHD symptoms. Symptomatic improvements (e.g., symptomatic rating scale) were also observed for the ASD-comorbid ADHD children; yet, the respondent rate of ADHD children (70–80%) was higher than that of ASD-comorbid ADHD children (50%) (Greenhill et al., 1996; Greenhill et al., 2006; Frazier et al., 2011). Furthermore, ASD-comorbid ADHD children revealed low tolerability against medication doses and side effects (Frazier et al., 2011). According to the improved symptomatic rating scales, MPH was suitable to manage symptoms for both ADHD and ASD-comorbid ADHD children (81.8% respondent rate based on total hyperactivity and inattentive rating scale). Note that the current dataset was limited.

The MPH-evoked responses brought the increased O_2Hb activations in the right IFG/MFG and parietal cortex for the ADHD group. While the MPH effect on right IFG/MFG was frequently reported (Monden et al., 2012a; Monden et al., 2012b), the parietal activation was rarely observed (Nagashima et al., 2014a) due

to selective MPH effects on the dopamine pathway (prefrontal and striatal regions) (Faraone et al., 1998; Bymaster et al., 2002). Medication history and pathophysiology may influence the neuropharmacological effect on brain activations. The current dataset only included medicated-naïve children being more prone to any medications, and the MPH effects were distinct between ADHD and ASD-comorbid ADHD children. In contrast with ADHD children, the decreased activation was found in the right hemisphere for the ASD-comorbid ADHD children. This result may suggest the different MPH mechanisms between ADHD and ASD-comorbid ADHD children.

Inhibitory responses in the right IFG may specifically relate to the cue recognition regardless of the involvement of inhibition output (e.g., motor response) (Hampshire et al., 2010; Aron et al., 2014). Even though the activation of right IFG and symptomatic rating scale were modulated by the MPH administration, the improvement of behavioral performance (e.g., accuracy and response time) was not expressed by ADHD children. The insignificant improvement was also observed for ASD-comorbid ADHD children (multivariate ANOVA; administration and pathophysiological status). The placebo effect was failed to reject in behavioral performances (Monden et al., 2012b; Nagashima et al., 2014b; Chantiluke et al., 2015). Therefore, neuroimaging-based analysis is a sensitive measure in evaluating pathophysiology and neuropharmacological effect.

3.4.7 MPH-evoked response as a differential feature

The anti-correlated relationship between increased O_2Hb and decreased HHb has been frequently assumed following the neurovascular coupling theorem (Obrig et al., 2000b). In the current results, the significant increases of O_2Hb activations were more prominent as similar as previous studies (Monden et al., 2012b; Ishii-Takahashi et al., 2014; Nagashima et al., 2014b) and found in the different but adjacent channels (see Figure 3.17) of significant HHb deactivation. Furthermore, the inconsistent effect of cerebral blood flow change on HHb signal

was reported compared to the robust and profound O_2Hb signal. Therefore, the current results may support the latter theorem which contributes to the minimum HHb significance and the shifted regions of HHb deactivation.

The MPH effect on brain activation reflected the most evident differences (e.g., great statistical power) between ADHD and ASD-comorbid ADHD children. Therefore, the optimum classifying features were obtained from the MPH-evoked O_2Hb activations. The diagnostic robustness have been improved by optimizing spatially categorized features. Without the spatial categorization, the selected optimum features were spurious across optimization operations (Table 3.8).

Three optimum and robust regions, including the right MFG, ANG, and PrCG, were found to differentiate ASD-comorbid ADHD children from ADHD children. In order to confirm the dependency between regions, the analysis classification was performed using activation values of those regions as three-axis features for linear discriminant, quadratic discriminant, and SVM operations (Figure 3.20). However, there was no noticeable improvement, and the decreased classification performance (i.e., sensitivity and specificity) was even observed. Therefore, the dependent relationship between right MFG and right ANG was confirmed. The MFG-ANG relation might be explained by the attentive frontal-parietal network (Chochon et al., 1999; Peers et al., 2005; Rivera et al., 2005). The attention domain should not be neglected in the inhibitory control task because this domain is

Table 3. 8 Classification performances using non-spatially categorized brain features for each operation. From (Sutoko et al., 2019c), reproduced with permission.

Characteristic	Condition	Optimization operation	Feature(s)	Specificity	Sensitivity	Accuracy
O_2Hb activation	Post-MPH medication	Simple	CH 37, 43, 44	$86 \pm 1.4\%$	$91 \pm 1.7\%$	84%
		OR operation	CH 32, 37, 39, 41, 44 (Axis 1) CH 42 (Axis 2)	$86 \pm 1.4\%$	100%	84%
		AND operation	CH 37, 41, 42, 44 (Axis 1) CH 32, 43 (Axis 2)	$86 \pm 1.4\%$	100%	84%
		Linear discriminant	CH 32, 37, 42, 44 (Axis 1) CH 43 (Axis 2)	$86 \pm 1.7\%$	$84 \pm 7.2\%$	72%
		Quadratic discriminant	CH 32, 41, 44 (Axis 1) CH 39, 42 (Axis 2)	$89 \pm 2.1\%$	100%	84%
		Support vector machine	CH 37, 39, 41, 44 (Axis 1) CH 43 (Axis 2)	$99 \pm 2.5\%$	$87 \pm 6.3\%$	69%
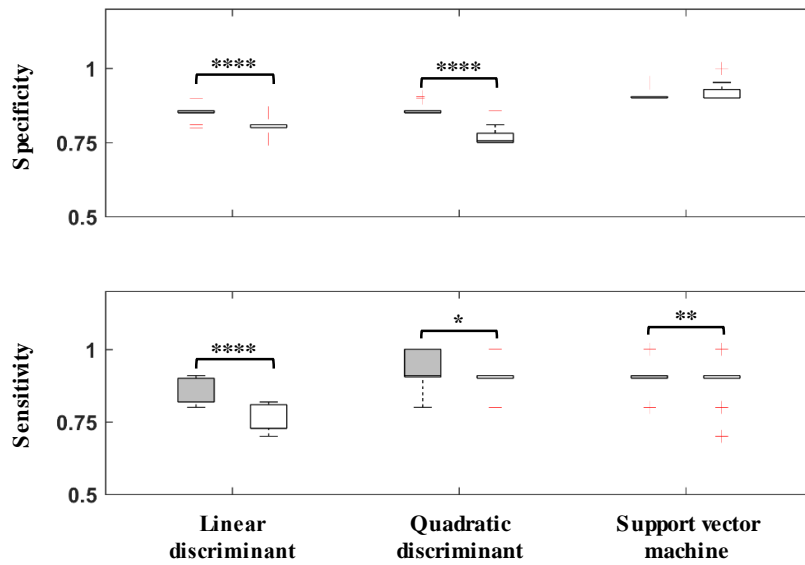
Figure 3. 20 Comparisons of classification performances between two- (MFG-ANG vs. PrCG; gray-filled boxplots) and three-axis (MFG vs. ANG vs. PrCG; void-filled boxplots) features using linear discriminant, quadratic discriminant, and SVM operations. $p < 0.05^{(*)}$; $p < 0.01^{(**)}$; $p < 0.0001^{(****)}$ for paired-sample t-test. From (Sutoko et al., 2019c), reproduced with permission.

necessitated to recognize the inhibitory targets and cues (Murphy et al., 1999; Keilp et al., 2005; Reynolds et al., 2006). Besides the inhibition and attention domains, the motor domain (i.e., arm and hand movements) might also be linked with the inhibitory response via the PrCG activation. The difference of motor-related activations (i.e., pre-SMA) between TD and ADHD children was observed during the GNG tasks (Suskauer et al., 2008). Impaired PrCG connectivity was also found in ASD children (Nebel et al., 2014).

In summary, MPH intake modulated functional domains of inhibition, attention, and motor by increasing O_2Hb activation for ADHD children; however, ASD-comorbid ADHD children experienced null O_2Hb activation. By giving only one-time MPH prescription, the differential diagnosis could be efficiently done by a support of fNIRS measurement. The MPH administration to ASD-comorbid children was also harmless, and this is commonly advised by clinical doctors.

3.4.8 Limitations

In this chapter, two limitations were described. *First*, disordered populations (ADHD, ASD-comorbid ADHD) were studied. Many understandings, including the relationships among demographic characteristics, behavioral performances, brain measurement results, pathophysiological hypotheses, and neuropharmacological mechanisms, are still unknown. Therefore, the minimum analytical assumption is preferable. However, one of noise criteria (i.e., criterion 3) tried to control the noise occurrence by evaluating inter-epoch similarity. Previous study reported that subjects with ADHD tended to show high inter-epoch variability (Klein et al., 2006; Martino et al., 2008; Buzy et al., 2009; Gmehlin et al., 2014). As the design of the adaptive rejection algorithm is flexible, criterion 3 can be changed with a more suitable criterion in future applications. *Second*, the current findings were entailed by the disadvantages of limited sample number. In order to acquire more robust algorithm variables for the adaptive rejection algorithm, a greater sample number is required for the process of variable re-tuning. Furthermore, in the biomarker development, the most well-performed operation was difficult to determine because the cross-validation accuracies were similar between operations. By providing a greater sample number, the obtained classifying features are likely more robust for managing a higher degree of subject variability.

3.5   Conclusion

In this chapter, the adaptive rejection algorithm was developed, and its practical use was confirmed in the human datasets. This algorithm particularly managed noises occurred during the measurement of block-design paradigms. The concept of noise rejection with maintained sample number was proven if only the signal quality was relatively good, and the activation phenomenon was sufficiently strong. Furthermore, the optimization process was done, and the implementation of optimum algorithm variables was able to mimic the results of

the conventional visual judgment. The application of the adaptive rejection algorithm was explored as a signal preprocessing step in a different dataset. The algorithm variables were re-tuned, and its application for a signal preprocessing step was promising because it supported the investigative analysis of differential diagnosis biomarker. The well-performed biomarker ($86 \pm 4.1\%$ specificity, $93 \pm 7.3\%$ sensitivity, and $82 \pm 1.6\%$ cross-validation accuracy) was found based on the distinct MPH-evoked O_2Hb activations in the right MFG-ANG and the right PrCG during the GNG task. ADHD children revealed the evidently modulated activation, whereas the decreased activation was observed for ASD-comorbid ADHD children.

4 Static Functional Connectivity Analysis for Task Performance: Its Benefits Compared to Activation Analysis†

4.1 Introduction

The fNIRS datasets coming from ADHD children were commonly analyzed on the basis of the activation analysis. However, another analysis, named the FC analysis, provides a perspective of brain network – how intra- and inter-regions functionally connect and communicate to each other. In general, the FC analysis was categorized into static and dynamic FC analyses. In the static FC analysis, FCs are assumed to be in a stationary condition across the entire temporal course (Biswal et al., 1995). Meanwhile, the dynamic FC analysis offers a point a view of temporarily and dynamically shifted connectivity states [see (Hutchison et al., 2013; Preti et al., 2017) for reviews]. The static FC analysis is focused on this chapter; the next chapter (i.e., Chapter 5) discussed the dynamic FC analysis for fNIRS measurement data.

The static FC analysis has been widely implemented on fMRI studies during the RS (Bohland et al., 2012; Cheng et al., 2012). The static FC characteristics were reported to be prominent in diagnosing ADHD (Uddin et al., 2017). By applying static FC characteristics during the RS, a high classification performance (80–86% accuracy) was obtained. An aggregate ADHD dataset was collected from multiple sites, and that dataset consisted of more than 900 subjects (Consortium, 2012). That dataset included the demographic information and the fMRI measurement data during the RS. From that dataset, ADHD (and its subtypes) characteristics were explored to develop accurate, effective, and robust diagnostic biomarkers. The classification performance for three ADHD subtypes (i.e., inattentive, hyperactivity, and both) using FC features was widely distributed from 37.4–60.5% accuracy (47.8% on average). Even though those biomarkers were relatively promising (i.e., classification accuracy $> \frac{100\%}{3}$), the most well-

---

† The work in Chapter 4 has been published in a journal article (Sutoko et al., 2019b).

performed biomarker with 62.5% accuracy solely used the demographic information, including age, gender, handedness, and full-scale IQ, without any brain imaging feature (Brown et al., 2012). These results were unexpected, and the robustness of RS FC features was then argued. This robustness lack may be caused by motion artifacts reducing the measurement quality (30– 50% failure rate) (Vaidya et al., 1998; Durston et al., 2003) and the uncontrolled nature of RS. Despite the low task demand of RS, intra-subject variability was found to be high, and the test-retest reliability was considerably poor (Lang et al., 2014). In order to solve this robustness lack, two strategic plans were performed.

First, instead of fMRI measurements, fNIRS measurements was carried out. Besides better motion tolerance, fNIRS also offers superior temporal resolution compared to fMRI (100 ms vs. 2–3 s). High temporal resolution is favorable for the FC analysis because signals accommodate more temporal information. The reliability of the static fNIRS FC analysis has been assessed through its comparison to the static fMRI FC analysis. From the simultaneous fMRI and fNIRS measurements, the similar static FCs in the bilateral primary motor regions were observed during the RS (Duan et al., 2012). The RS network obtained from the static fNIRS FC analysis was well-correlated with the network derived from the static fMRI FC analysis (Sasai et al., 2012). The reliability and reproducibility of the static fNIRS FC analysis were confirmed in multiple intra-subject measurement (Zhang et al., 2011; Niu et al., 2013) and various instrumentation (Niu et al., 2011). These results suggested that the application of the static FC analysis on fNIRS measurement data is plausible.

Second, the measurement protocol was modified by performing tasks during the fNIRS measurement. The performance of tasks controls task-evoked responses and narrows intra-subject variability. However, the task-based FC analysis is infrequently approached because of its more demanding protocol for a prospective cohort study. Even though incorporating tasks in a fNIRS cohort study may be technically challenging, this protocol is executable by supports of all research

elements.

Therefore, in this chapter, TD and ADHD characteristics during the visual attention OB task were evaluated based on the task-based FC analysis. While the activation analysis inferred the hypoactivation in the right IFG/MFG and the right SMG/ANG for ADHD children (Nagashima et al., 2014a; Nagashima et al., 2014c), the relationship between results of activation and task-based FC analyses would also be explained here. Because the task performance followed the block-design paradigm, the temporal course was categorized into baseline and stimulus intervals. The static FCs may differently correspond to each interval for TD/ADHD children or even both. The development of screening biomarker was also aimed for, and the effectiveness of activation- and FC-based biomarkers was then evaluated.

4.2   Materials and methods

4.2.1   Subjects and experimental design

The current datasets were acquired from two independent datasets that had been previously analyzed and reported (Nagashima et al., 2014a; Nagashima et al., 2014c). A dataset with 22 ADHD children was also used in developing the adaptive rejection algorithm (Sutoko et al., 2018) (Chapter 3; see 3.2.2). In total, the data from thirty-seven ADHD children (31 boys; 9.7 ± 2.0 years old) diagnosed by DSM-5 were included in this chapter. The children were non-medicated naïve with two prescribed medications (22 and 15 children consumed MPH 27.0 ± 10.8 mg and ATX 27.0 ± 16.0 mg, respectively). Twenty-one children also simultaneously revealed ASD symptoms; and they were defined as ASD-comorbid ADHD children. The comorbid epilepsy condition was found in a 9-year-old girl; her data was excluded in the current analysis. Both ADHD and ASD-comorbid ADHD children were then defined as the disordered children. The data of 23 TD children (15 boys; 9.8 ± 1.9 years old) from two datasets were also used in this chapter. TD children (107.0 ± 12.2) had significantly higher IQs ($t_{(57)} = 3.72$,

p < 0.05, Cohen's *d* = 0.99) than disordered children (95.8 ± 10.8).

The experimental design adopted the randomized, double-blind, placebo-controlled, and crossover study – as same as the experimental design described in Chapter 3 (see 3.2.2 and 3.2.8). However, in order to evaluate the potential of screening, only data without any interventions (i.e., the first measurement session at the first day measurement after wash-out period) were subjected to the current analysis. Those children performed the OB task (Nagashima et al., 2014a; Nagashima et al., 2014c) while their brains were measured using the multichannel fNIRS system (ETG-4000, Hitachi, Ltd., Japan). The task paradigm and probe configuration (i.e., two-plane probes on bi-hemispheric lateral prefrontal-to-inferior parietal lobes) were same as detailed above (see 3.2.2).

Behavioral parameters (e.g., response time, error rate) were recorded during the task performance, and the results have been previously reported (Nagashima et al., 2014a; Nagashima et al., 2014c). TD children could carry out the OB task faster and more attentive than disordered children. These results were indicated by the significantly faster response time and lower omission error observed in TD children [two-sample *t*-test; *p* < 0.05; degree of freedom (DF) = 28–42]. However, compared to disordered children, TD children may not respond more accurately because the difference of commission error was insignificant (two-sample *t*-test; *p* ≥ 0.05; DF = 28–42). While the neuropharmacological effects on brain activations were found consistent for both medications, the effect on behavioral performances was almost null (Nagashima et al., 2014a; Nagashima et al., 2014c). As the behavioral performances failed to classify ASD-comorbid ADHD children from ADHD children (see 3.3.4), this chapter solely explored the potential of screening biomarkers based on the brain measurement.

4.2.2 Signal preprocessing and feature extraction

As the detected optical intensity were imported to the POTATo (Sutoko et al., 2016), it was converted to the product of Hb concentration change and optical path

length ($\Delta C_{O2Hb} \cdot L$, $\Delta C_{HHb} \cdot L$, and $\Delta C_{Hb\text{-}total} \cdot L$) (Maki et al., 1995; Koizumi et al., 2003) following the MBLL (Delpy et al., 1988; Maki et al., 1995). In order to control the quality of measurement, channel-wise signals with SNRs lower than 10 dB were excluded. The SNR measure was computed by below equation.

$$SNR = 10 \log_{10} \frac{\overline{S_{0.01 \to 0.15\,Hz}}}{\overline{S_{4.5 \to 5\,Hz}}} \qquad \text{(Eq. 6)}$$

where $\bar{S}$ is the average of power spectral density within specifically assumed neuronal activation (0.01–0.15 Hz) and noise (4.5–5 Hz) frequencies. The remaining channels with sufficient SNRs may be affected by periodic noises with extremely high or low amplitudes (outlier amplitudes; $\Delta C \cdot L > \mu + 3\sigma \ \lor \ \Delta C \cdot L < \mu - 3\sigma$; μ and σ are average and standard deviation of all channels, respectively). Therefore, channels with a high number (i.e., outlier total occurrence of outlier amplitudes) of outlier amplitudes were also eliminated. Due to this control process, 12–12.5% of total channels was rejected. Afterwards, linear fitting and filtering (FIR band-pass filter; 0.01–0.8 Hz) were applied on the remaining channel-wise signals to remove baseline shift and cardiac pulsation. Even though the control process had been done, there were some possibilities that motion artifacts and/or other noises remained untreated. The developed adaptive rejection algorithm (Chapter 3) was useful for the activation analysis with the block-design paradigm. However, in the current study, the FC analysis required continuous signals. Therefore, another analytical framework suitable for the FC analysis was developed to remove motion artifacts and other noises from continuous signals. Thereafter, the activation and FC analyses were independently described and implemented in the remaining preprocessed signals.

1. Activation analysis

    The epoch signals were constructed by compartmentalizing the continuous signal on the basis of 10, 3, 25, 3, and 10 s for pre-stimulus baseline, pre-stimulus instruction, stimulus, post-stimulus instruction, and post-stimulus baseline, respectively (Figure 4.1A; six epochs for each channel). The
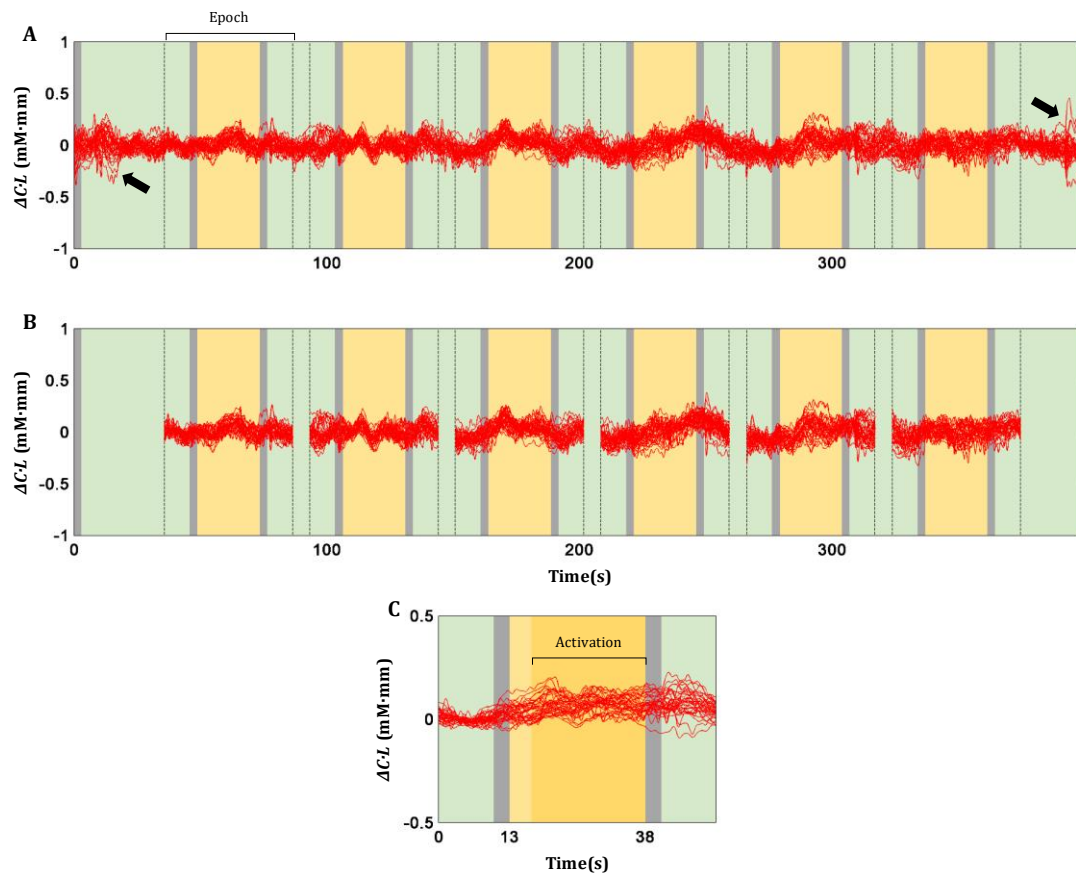
Figure 4. 1 Signal preprocessing for activation analysis. The temporal courses (A) for all channels were segmented to six epoch signals (B). Noisy epochs were rejected using the adaptive rejection algorithm. Remaining epochs were averaged for each channel (C). Green, gray, and yellow intervals represent the baseline, 3-s instruction, and stimulus intervals. The dark yellow interval (17–38 s) indicates the activation interval. Black arrows show detected spikes. From (Sutoko et al., 2019b), reproduced with permission.

rejection algorithm was applied on epochs with the previously optimized algorithm variables (criterion 3 with the threshold of $3 \times$ IQR; see 3.2.9). An epoch was rejected in maximum (6.86% of total channels; Figure 4.1B). The baseline epoch fitting and inter-epoch average were performed only for the remaining epochs (Figure 4.1C). The activation analysis was done subsequently by averaging channel-wise epoch signals from 4 s after stimulus onset to the end of stimulus (dark yellow-colored interval in Figure 4.1C),

2. FC analysis

    As mentioned above, the FC analysis required continuous signals to maintain the temporal information. Despite the improved data quality, rejecting noise-

89

affected epochs and averaging them would consequently neglect the temporal information. Therefore, instead of rejecting epochs, noise-affected datapoints were eliminated. One of noise types, spike, was detected by the sudden amplitude change (> 0.1 mM·mm) from two consecutive datapoints. The identified spikes were removed from continuous temporal data (Figure 4.2A). Channels heavily affected by outlier amplitudes had been eliminated in prior; however, the remaining channels might still contain datapoints with outlier amplitudes. Thus, datapoints with outlier amplitudes were also rejected (Figure 4.2B). The datapoint rejection was about $24.0 \pm 14.6\%$ of total datapoints across subjects. In order to compare between baseline and stimulus connectivities, the remaining datapoints were concatenated in accordance
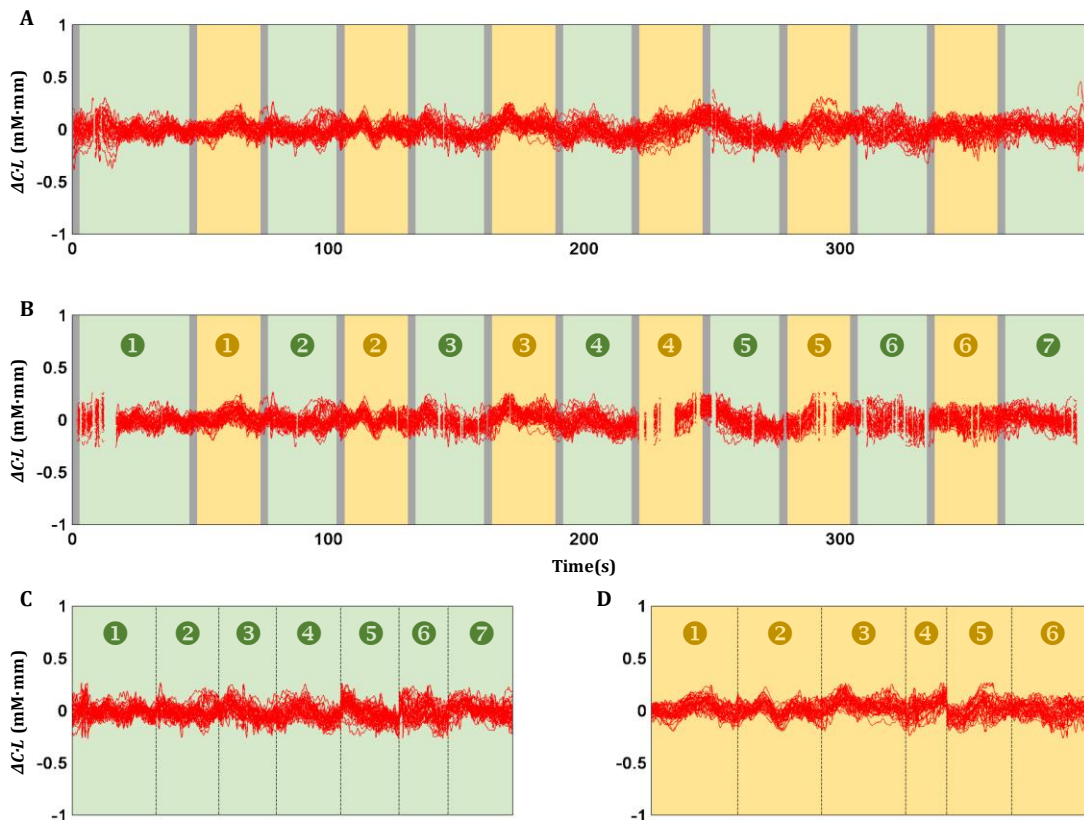
Figure 4. 2 Signal preprocessing for connectivity analysis. Detected spikes were removed from the temporal courses (A), and the recognized outlier amplitudes were also eliminated from the temporal courses (B). The remaining datapoints were independently concatenated for the baseline (C) and stimulus (D) intervals. Green, gray, and yellow intervals represent the baseline, 3-s instruction, and stimulus intervals. From (Sutoko et al., 2019b), reproduced with permission.

90

with the baseline (green-colored; Figure 4.2C) and stimulus (yellow-colored; Figure 4.2D) intervals. Inter-channel connectivity was analyzed using Pearson's correlation (r) for the entire measurement, baseline, and stimulus intervals.

$\Delta C_{O2Hb} \cdot L$ and $\Delta C_{HHb} \cdot L$ signals underwent both the activation and FC analyses. Furthermore, epoch and datapoint rejections were uniform for $\Delta C_{O2Hb} \cdot L$ and $\Delta C_{HHb} \cdot L$ signals. Activation and connectivities values were potential screening features. Because low-quality and noisy channels had been removed, this may influence the inter-subject feature availability. The feature availability should be sufficient and balanced for both TD and disordered children. Therefore, features with low (<50%) and high imbalanced (>10%) availabilities were excluded from the further analysis.

4.2.3 Classification analysis

In Chapter 3, the feature optimization for differential classification was performed by the exhaustive manner. This way was impractical for the current optimization because of the abundant number of feature combinations (all combinations from $\frac{44 \times 43}{2}$ features; about 5.95×10^{284} combinations). The subject number was also relatively small compared to the number of available features; the risk of overfitting and the curse of dimensionality might be too substantial to disregard. Therefore, the feature selection method was performed to reduce the computation time and to minimize the analytical risks. In order to maintain the essential of exhaustive optimization, the feature selection was done by the stepwise-forward method, namely, adding features one-by-one (Hocking, 1976) after confirming the optimum selection criteria (e.g., classification accuracy). The cross-validation process (5-fold; 1:2 ratio of TD to disordered children in both training and test subsets) was also embedded in the feature selection process.

Figure 4.3 summarized the process flow of feature optimization and
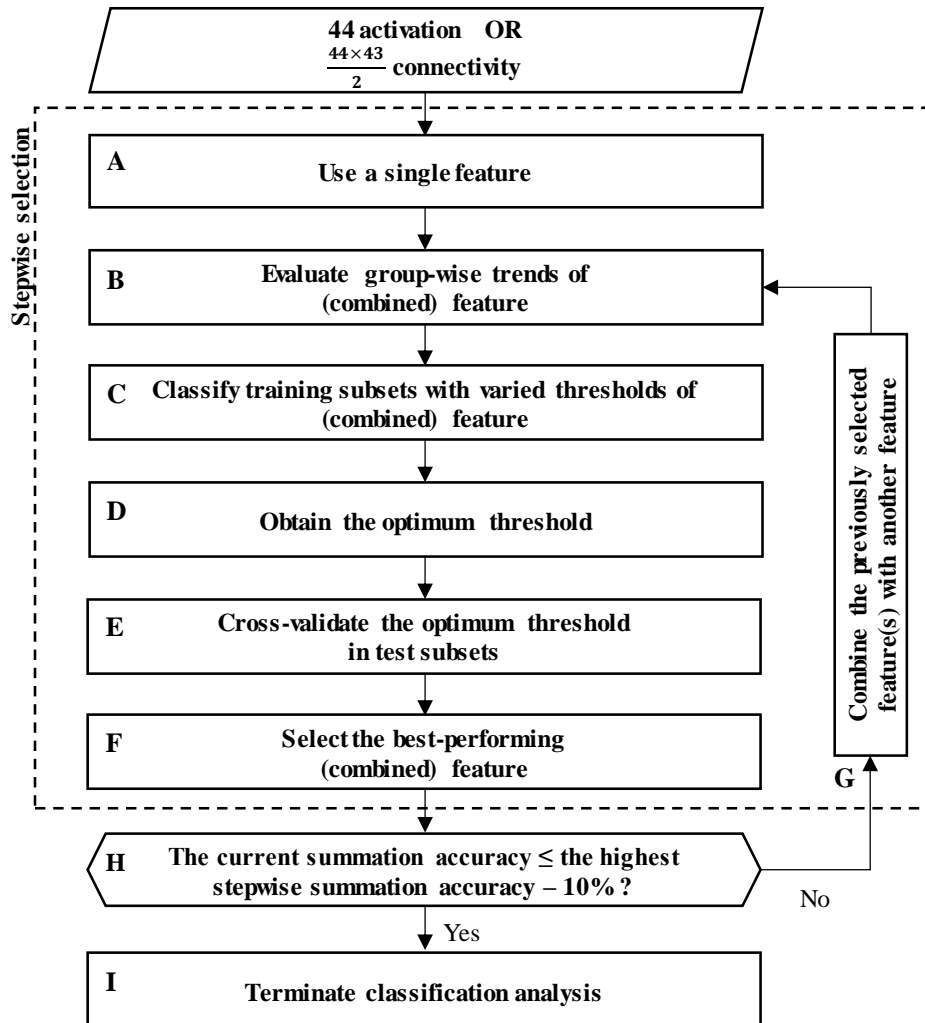
Figure 4. 3 Process flow of embedded stepwise selection and classification analysis. From (Sutoko et al., 2019b), reproduced with permission.

classification analysis. A single feature (Figure 4.3A) was statistically evaluated to characterize the feature trend (Figure 4.3B) in the training subsets (e.g., disordered children inclined to show lower feature values, and *vice versa*). Supervised and binary classification in accordance with the feature trend (Figure 4.3C) was performed by systematically changing the thresholds of feature values (in steps of 0.001). In each time of varying the thresholds of feature values, specificity (i.e., rate of true TD child) and sensitivity (i.e., rate of true disordered child) were quantified. The threshold resulting in the highest summation of specificity and sensitivity (Figure 4.3D) was then used to classify the test subsets

(Figure 4.3E). This process (Figure 4.3: A–E) was repeated for any other single feature. The feature associated with the highest summation of cross-validated and averaged accuracies (rate of true TD and disordered children) in both training and test subsets was appointed as the first selected feature (Figure 4.3F). Another single feature tried to be combined with the recently selected featured (Figure 4.3G). If two or more feature were combined, those features would be averaged (inverse of averaged Fisher-z transform for FC features). The same process (Figure 4.3: B–E) was applied on the averaged features. All two-feature combinations involving the selected feature at the first step were evaluated. Among all combinations, the two-feature combination giving the highest summation of cross-validated and averaged accuracies in both training and test subsets were selected for the second step. This process was continued to find the best-performing combinations of three features (i.e., the third step), and so on.

The optimization process continuously examined all feature combinations, unless the termination condition was set. Therefore, when the stepwise summation of training and test accuracies was 10% lower than the highest accuracy among all steps (Figure 4.3H), the optimization process would be terminated (Figure 4.3I). Optimum features were defined as the combination of features achieving the highest summation of training and test accuracies. Classification performances using activation and FC features were compared to assess the potential of screening biomarkers.

In order to confirm the usefulness of stepwise selection method, this result was also compared to the results of three other selection methods: best-performing single, significant between-group, and all available features. The selected feature at the first step of stepwise optimization was designated as the best-performing single feature. The features revealing the significant differences between TD and disordered children were then defined as the significant between-group features. The performances of all available features without applying any selection methods were included as standard comparisons.

4.3 Results

4.3.1 Characteristics of functional connectivity

O_2Hb FCs well agreed with (Pearson's correlation; $r \geq 0.7$) HHb FCs in any intervals as shown in Figure 4.4. However, the strength of O_2Hb FC was found to be greater than that of HHb connectivity as represented by scattered points majorly located under the diagonal line ($\bar{r}_{HHb} = \bar{r}_{O_2Hb}$; Figure 4.4). The FC strength may be affected by the signal quality (i.e., SNR); SNR for $\Delta C_{O_2Hb} \cdot L$ signals was significantly greater (one-sample t-test, $p < 0.001$, $t_{(116)} = 3.61$) than SNR for $\Delta C_{HHb} \cdot L$ signals.

Figure 4.5 visualizes subject-average connectivity maps in the entire measurement, baseline, and stimulus interval. There are five highlighted points from these results. Points 1 and 2 describe the characteristics of FCs across baseline and stimulus intervals for the TD and ADHD groups; the differences between TD and ADHD groups are explained in points 3–5.

Point 1, significant within-region connectivities of O_2Hb and HHb (black squares in Figure 4.5: A2, B2, C2, and D2) were observed in the right MFG for both the TD and disordered groups during the baseline interval. *Point 2*, the TD group revealed insubstantial changes for intra-hemispheric, inter-hemispheric, and within-region connectivities during the stimulus interval. On the other hand, bilateral intra- and inter-hemispheric connectivities were found to significantly
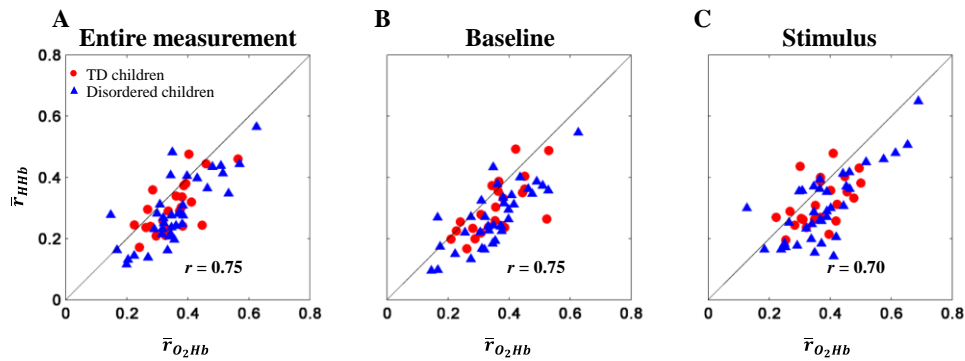
Figure 4. 4 Relationships between connectivities drawn from $\Delta C_{O_2Hb} \cdot L$ and $\Delta C_{HHb} \cdot L$ in the entire measurement (A), baseline (B) and stimulus (C) intervals for TD (red circles) and disordered (blue triangles) children.
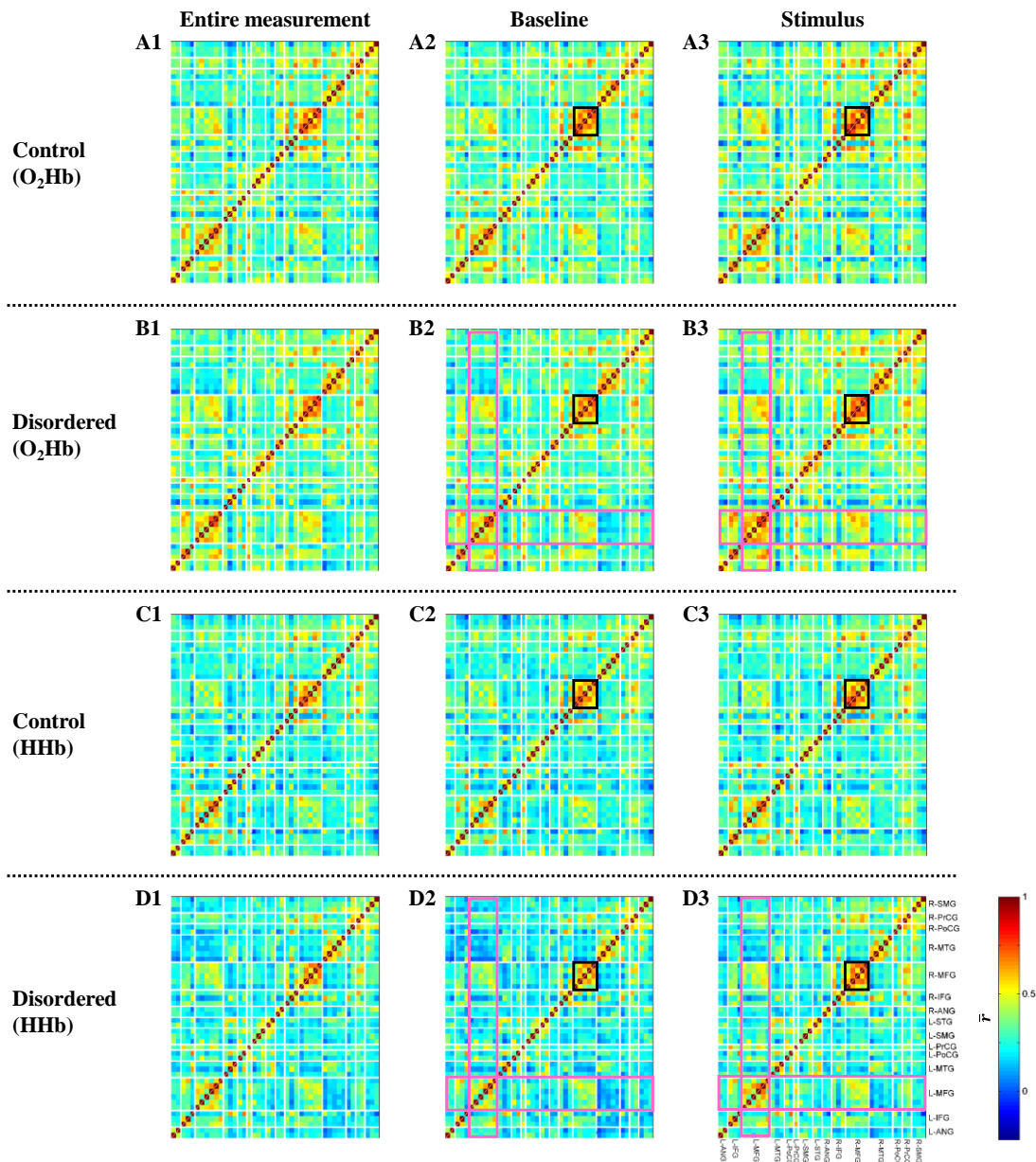
Figure 4. 5 Maps of O₂Hb (A–B) and HHb (C–D) connectivities, averaged across TD (A, C) and disordered (B, D) children, in the entire measurement (A1–D1), baseline (A2–D2), and stimulus (A3–D3) intervals. Black and magenta squares represent the within-region of right MFG and the left hemispheric MFG FCs, respectively. Color bar represents the strength of connectivity ($\bar{r}$) between two regions (i.e., channels). Cortical areas: angular gyrus (ANG), inferior frontal gyrus (IFG), middle frontal gyrus (MFG), middle temporal gyrus (MTG), postcentral gyrus (PoCG), precentral gyrus (PrCG), supramarginal gyrus (SMG), and superior temporal gyrus (STG). From (Sutoko et al., 2019b), modified with permission.

increase during the stimulus interval for the disordered group. Therefore, stimulus-evoked responses on FCs were more prominent in the disordered group than in the TD group. This result may also suggest that the TD group relatively

95

preserved the FCs in both baseline and stimulus intervals.

Point 3, even though the disordered group showed strong within-region connectivity (black squares in Figure 4.5: B2, D2, B3, D3) of right MFG during the baseline and stimulus intervals, the FC strength was still weaker compared to that of the TD group (some channels in right MFG, black squares in Figure 4.5: A2–D2 vs. A3–D3, two-sample *t*-test, $p < 0.05$, $t_{(47-50)} = 2.34$–3.08). *Point 4*, besides the within-region connectivity of right MFG, the connectivity between the right MFG and the right MTG was found to be weak for the disordered group during the stimulus interval. *Point 5*, left intra-hemispheric connectivity (left MFG, magenta squares in Figure 4.5: B2 vs, B3 and D2 vs. D3, one-sample *t*-test, p < 0.05, $t_{(17-34)} = 2.08$–4.58) increased during the stimulus interval for the disordered group. By referring to points 2–5, the disordered groups experienced impairments in connectivity maintenance across the baseline-stimulus interval and weak right MFG-related connectivity.

4.3.2 Optimization of feature selection

Stepwise optimization results for both training and test accuracies are shown in Figure 4.6. Four points are summarized from those results. *First*, the training accuracies drawn from activation features were significantly low compared to those of FC features in all intervals (76% vs. 88% on average; one-way ANOVA; $F_{(3,16)} = 30.2$–33.8; $\eta^2 = 0.85$–0.86; $p < 0.001$). *Second*, there was no effect of feature observed on the test accuracies (one-way ANOVA; $F_{(3,16)} = 2.2$–2.3; $\eta^2 = 0.3$; $p > 0.05$). Even though the averages of cross-validated test accuracy using FC features were greater than those of using activation features (75–78% vs. 83–91%), the variances were found to be high. Therefore, the null hypothesis (H_0: no effect of feature on the test accuracy) was failed to reject. *Third*, among connectivity intervals, the lowest performance for training accuracy was brought by the O_2Hb FC features from the entire measurement interval (one-way ANOVA; $F_{(5,24)} = 4.2$; $\eta^2 = 0.47$; $p < 0.01$). *Fourth*, the difference between O_2Hb and HHb
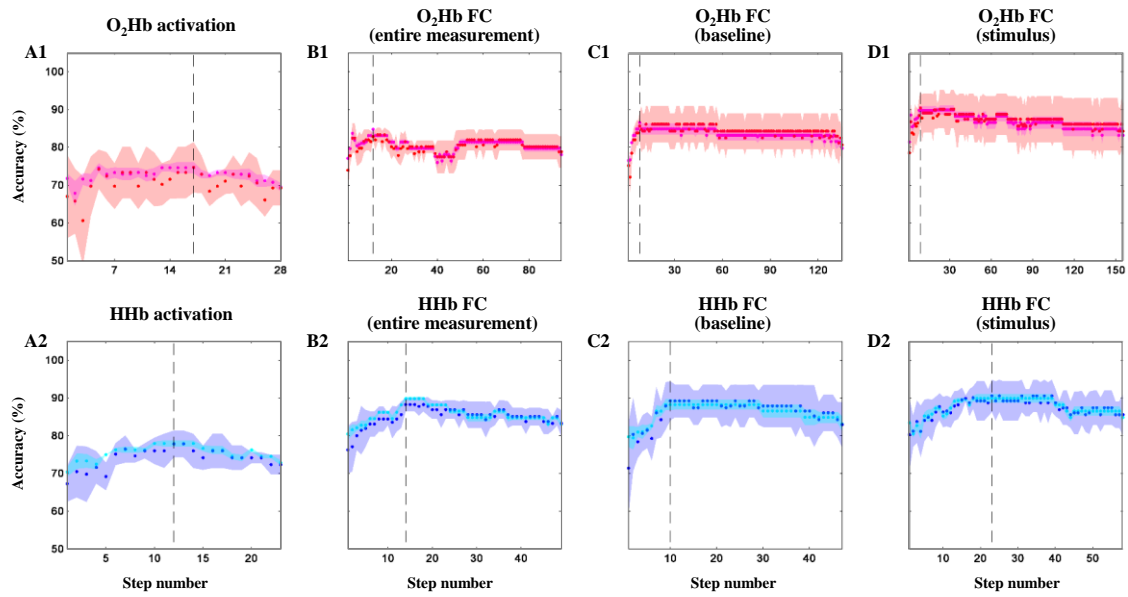
Figure 4. 6 Stepwise optimizations for training (magenta and cyan plots) and test (red and blue plots) classifications using activation (A) and FC features in the entire measurement (B), baseline (C), and stimulus (D) intervals of O_2Hb (A1–D1; magenta and red plots) and HHb (A2–D2; cyan and blue plots). Shaded patches around plots represent standard errors. Dashed vertical lines indicate the optimum step giving the highest summation of cross-validated training and test accuracies. From (Sutoko et al., 2019b), reproduced with permission.

connectivity on the training and test accuracies was only observed if those FC features were from the entire measurement interval (Figure 4.6: B1 vs. B2; HHb > O_2Hb; two-sample t-test; $t_{(8)}$ = 2.7–7.7; Cohen's d = 1.7–4.9; $p < 0.05$). In summary, despite the limitation of high variance in the measure of test accuracy, all points addressed the superiority of FC features in purpose of group classification. These results were unlikely caused by the number of selected features (12–17 vs. 8–23 features for activation and FC features, respectively). Even though the availability of FC features was much greater than that of activation features, the number of selected FC features was moderate, and those features resulted in better classification performances than the activation features did.

To evaluate the benefit of stepwise selection method, the optimum training and test accuracies were compared to those of other methods, such as best-performing single, significant between-group, and all available features. As shown

in Figure 4.7, using all FC features would not improve the performances of training and test accuracies. Therefore, the feature selection method is necessary especially for the high number of classifying features (i.e., FC features). The comparison between performances of the best-performing single feature and the significant between-group features was majorly found to be insignificant for both training and test accuracies (Tukey-Kramer *post hoc* analysis). Furthermore, the training performances of the stepwise selection method were significantly the highest among feature selection methods (one-way ANOVA; $F_{(3,16)} = 7.6–170.0$; $p < 0.01$). The benefit of feature selection methods was also substantial for the test accuracy (one-way ANOVA; $F_{(3,16)} = 3.7–35.3$; $p > 0.05$), but the advantages were not specifically observed for the stepwise selection method. The issue of high variance was still observed; the variance of test performances resulted from the stepwise selection method was relatively lower though. The limited sample number may be a reason.
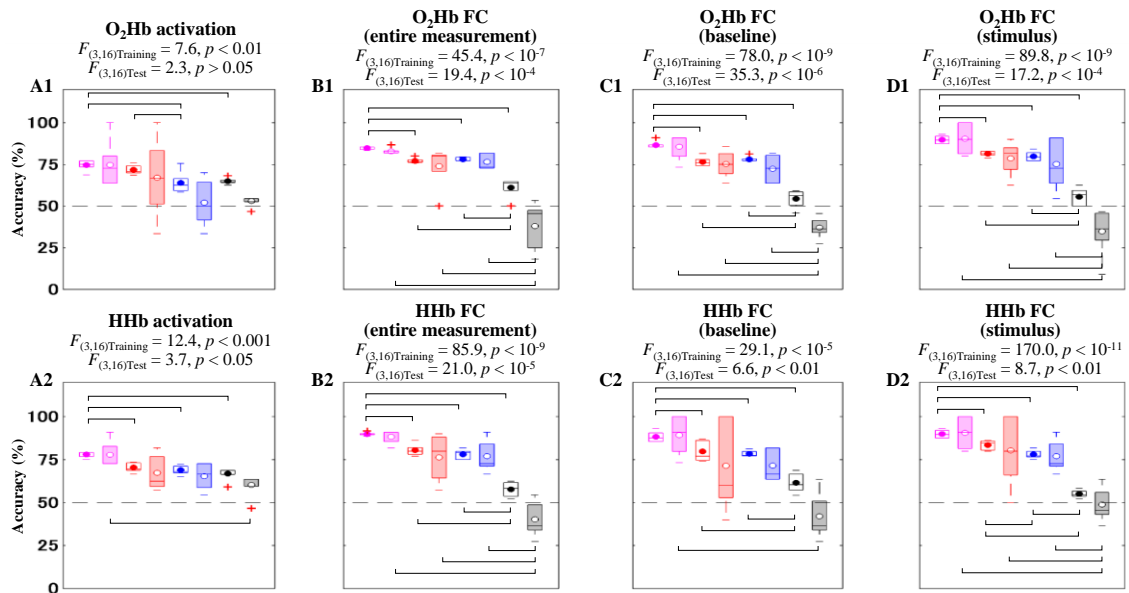
Figure 4. 7 Comparisons of classification performances (void- and color-filled boxplots for cross-validated training and test accuracies, respectively) between feature selection methods, such as optimum stepwise features (magenta boxplots), best-performing single feature (red boxplots), significant between-group features (blue boxplots), and all available features (black boxplots). Black brackets indicate the significant difference of classification performance between two methods (Tukey-Kramer *post hoc* analysis).

According to above results, the FC features were more superior than the activation features, and the stepwise selection method was beneficial particularly in the training performances. Thereafter, the optimum features are focused on the FC features.

4.3.3 Performance of optimum functional connectivity features

Besides the classification accuracies, the performances of specificity and sensitivity were assessed. The well-performing features should offer both high specificity and sensitivity (i.e., measure of separability). As varying the thresholds of feature values (e.g., O_2Hb and HHb FC features in all intervals) during the training process, specificity and sensitivity were quantified across 5-fold cross-validation as shown in ROCs of Figure 4.8. The measure of area under ROCs was also calculated. Table 4.1 summarizes the measures of training and test performances. The effects of connectivity intervals and signals types were significant on specificity, sensitivity, and area under ROC for training subsets (one-way ANOVA; $F_{(5,24)} = 5.3–14.7$; $\eta^2 = 0.52–0.75$; $p < 0.01$). The significant effects were also present in the differences between specificity and sensitivity (one-way ANOVA; $F_{(5,24)} = 4.48$; $\eta^2 = 0.48$; $p < 0.01$). However, those effects were not observed for test subsets (one-way ANOVA; $F_{(5,24)} = 0.4–1.7$; $\eta^2 = 0.07–0.26$;

Figure 4. 8 ROCs resulted from varying optimum O_2Hb (red curves) and HHb (blue curves) FC features in the entire measurement (A), baseline (B), and stimulus (C) intervals. From (Sutoko et al., 2019b), reproduced with permission.

Table 4. 1 Summary of classification performances in the training and test datasets using O_2Hb and HHb FCs in the entire measurement, baseline, and stimulus intervals
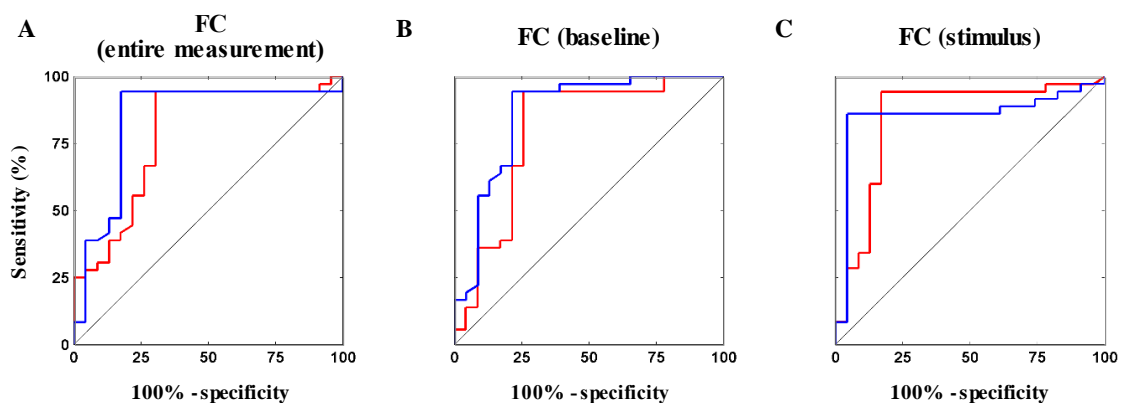
	FC (entire measurement)		FC (baseline)		FC (stimulus)		Statistic result
	O_2Hb	HHb	O_2Hb	HHb	O_2Hb	HHb	
Training subsets							
Specificity	69.5±2.3%	82.4±4.1%	74.3±7.8%	78.6±5.7%	83.0±6.5%	95.6±2.5%[*]	$F_{(5,24)}$=14.7 $p<0.001$
Sensitivity	94.4±1.9%	94.5±1.9%	94.4±1.9%	94.5±1.9%	94.3±3.2%	86.2±4.1%[*]	$F_{(5,24)}$=8.2 $p<0.001$
Area under ROC	78.5±2.1%	83.6±2.2%	79.9±3.6%	86.2±2.8%	84.5±3.7%	85.3±3.4%	$F_{(5,24)}$=5.3 $p<0.01$
Test subsets							
Specificity	69.3±10.9%	80.0±11.2%	73.6±20.3%	81.4±18.5%	86.4±19.6%	95.0±11.2%	$F_{(5,24)}$=1.7 $p > 0.05$
Sensitivity	91.4±7.8%	92.1±11.4%	94.3±7.8%	94.6±7.4%	94.3±12.8%	86.8±15.3%	$F_{(5,24)}$=0.38 $p > 0.05$

$p > 0.05$). Tukey-Kramer *post hoc* analysis was performed on the measures of training performances. Among connectivity intervals and signal types, the HHb FC features in the stimulus interval brought the highest specificity and the lowest sensitivity. Furthermore, the discrepancy between O_2Hb and HHb FC performances (i.e., training specificity) was found for the FC features in the entire measurement interval (two-sample *t*-test, $t_{(8)} = 2.58$; Cohen's $d = 1.6$; $p < 0.05$) as similarly implied above (see 4.3.2). Therefore, the use of either baseline or stimulus FC features is preferable for group classification, and the use of either O_2Hb and HHb FC features during the stimulus interval may depend on the classification demands (i.e., O_2Hb FC features for high sensitivity, and HHb FC features for high specificity)

4.3.4 Characteristics of classifying features

The optimum FC features for the TD and disordered groups are shown in Figure 4.9. There are two classifying characteristics –TD > disordered groups and TD < disordered groups. The stronger FCs for the TD group were found in the HHb FC features in all intervals and the O_2Hb FC features in the entire measurement interval (Figure 4.9: A, B2, and C2). The opposite characteristic was

Figure 4. 9 O_2Hb (A1–C1) and HHb (A2–C2) FC features in the entire measurement (A), baseline (B), and stimulus (C) intervals for TD (void-filled boxplots) and disordered (color-filled boxplot) children. From (Sutoko et al., 2019b), modified with permission.

revealed by the O_2Hb FC features in the baseline and stimulus intervals (Figure 4.9: B1 and C1). The optimum thresholds were found to be around 0.2–0.3. The different classifying characteristics were tried to be explained by the selected optimum FC features as shown in Figure 4.10. The strong FCs for the TD group were associated with the connectivity of bilateral frontal and left parietal lobes (Figure 4.10: A, B2, and C2); the FCs between bilateral parietal and left frontal lobes were related to the strong FCs for the disordered group. This finding was consistent with the strong left intra-hemispheric FC for the disordered group as mentioned above (see 4.3.1). The O_2Hb and HHb FC features in the entire measurement interval were overlapped (79–91% overlapped nodes; Figure 4.10: A1 and A2) in the right MFG, right MTG, right IFG, right PoCG, left SMG, left STG, and left ANG. The FCs between left ANG, right PoCG, and right MTG were robustly found for the HHb FC features in all intervals (Figure 4.10: A2, B2, and C2).

101

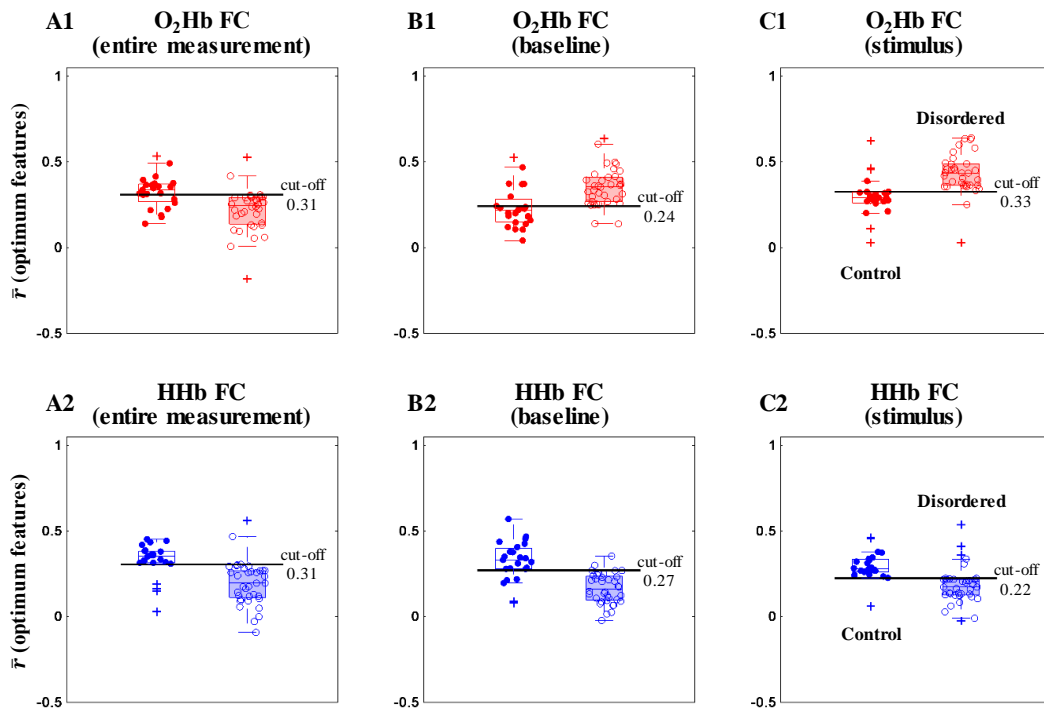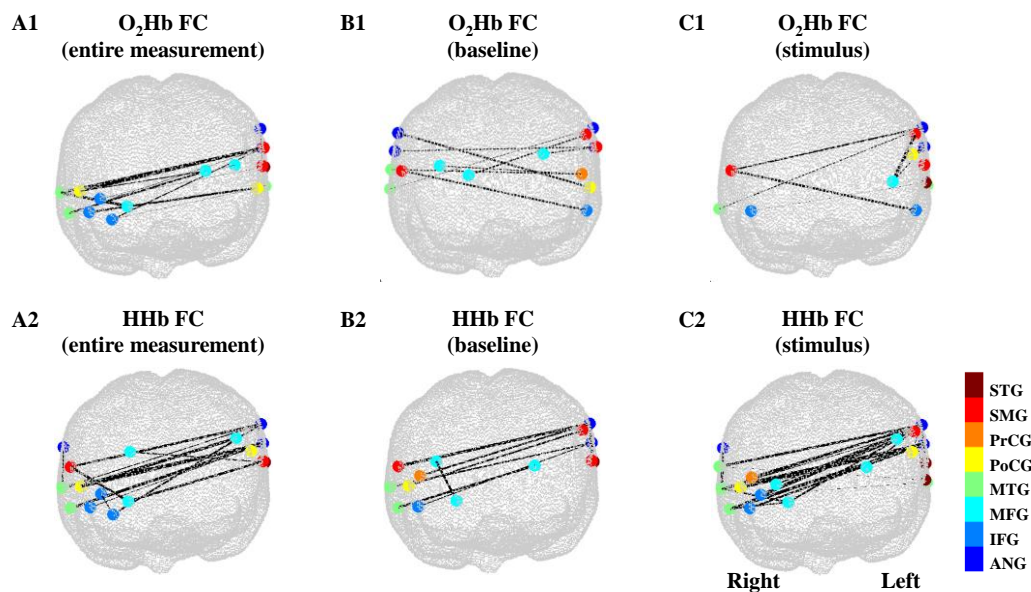Figure 4. 10 Optimum classifying O_2Hb (A1–C1) and HHb (A2–C2) FC features in the entire measurement (A), baseline (B), and stimulus (C) intervals. Cortical areas: angular gyrus (ANG), inferior frontal gyrus (IFG), middle frontal gyrus (MFG), middle temporal gyrus (MTG), postcentral gyrus (PoCG), precentral gyrus (PrCG), supramarginal gyrus (SMG), and superior temporal gyrus (STG). From (Sutoko et al., 2019b), reproduced with permission.

The difference between two classifying characteristics was caused by the differently selected feature trend at the first optimization step. In order to confirm the robustness of classifying characteristics, the first optimization step was manipulated to select the optimum O_2Hb FC feature in the stimulus interval with the specific FC trend of TD > disordered groups. Figure 4.11 shows the optimum O_2Hb FC features resulted from the manipulated optimization process. The strong FCs for the TD group were observed in the FCs between bilateral frontal and left parietal lobes. Therefore, the optimum FC features were considerably robust.

4.4   Discussion

4.4.1   Attentive activation and connectivity

Based on the fMRI measurement during the OB task, healthy adolescents revealed greater activations in the fronto-superior parietal lobes, posterior cingulate cortex, and putamen than ADHD adolescents (Tamm et al., 2006). The

102
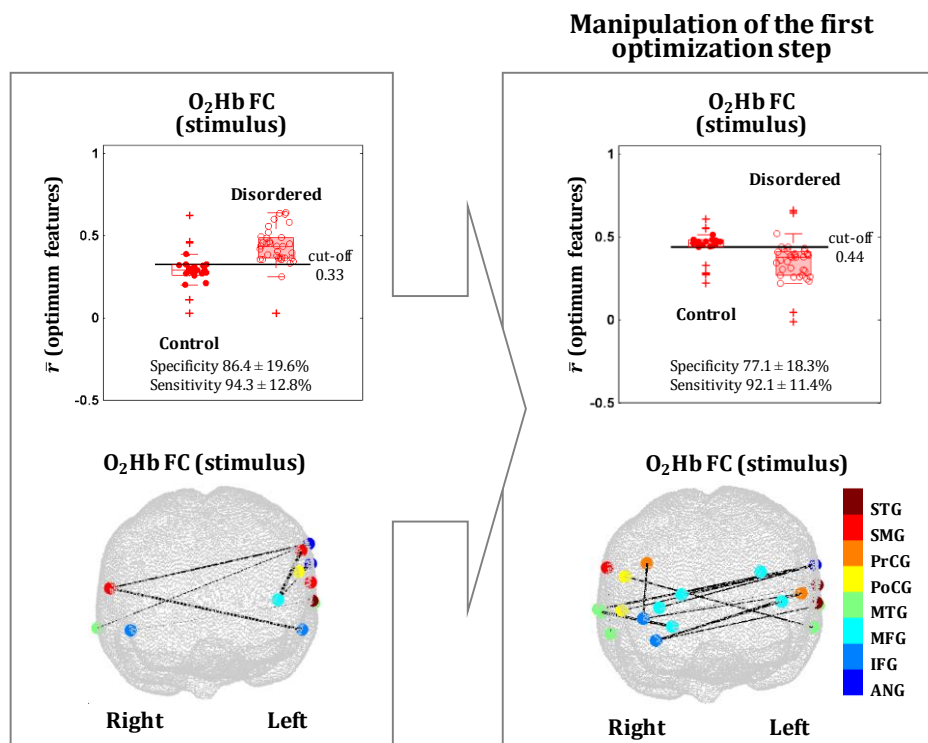
Figure 4. 11 Manipulation result for the first step of optimization using O_2Hb FC features in the stimulus interval. Cortical areas: angular gyrus (ANG), inferior frontal gyrus (IFG), middle frontal gyrus (MFG), middle temporal gyrus (MTG), postcentral gyrus (PoCG), precentral gyrus (PrCG), supramarginal gyrus (SMG), and superior temporal gyrus (STG).

experiments of visual and auditory tasks on human and animal subjects inferred the increases of transient event-related activations in the bilateral MFG, inferior parietal lobe, and inferior part of posterior cingulate gyrus (Paller et al., 1992; McCarthy et al., 1997). According to the current results, the disordered group showed low activation in the right MFG/IFG and the right SMG/ANG compared to the TD group (Nagashima et al., 2014a; Nagashima et al., 2014c). Both previous and current studies suggested the activation dysfunction for the disordered children during the performance of OB task.

During the baseline interval, the strong within-region connectivity of right MFG was observed for the TD group. This result could imply that the within-connectivity of right MFG may not be specifically associated with the OB task. Instead, any attentive engagement on tasks evoked this within-connectivity. Furthermore, there was no substantial change of stimulus-evoked FC for the TD

group.

The disordered group revealed the stimulus-evoked increases of FC strength in the regions aligned with the previously observed baseline FCs for the TD group. The stimulus apparently induced the disordered group to construct FCs approaching the TD's FCs. However, the low FC strength was still found for the disordered group. Subjects with ADHD are hypothesized having the impairment of adaptive reflexive processing that are required during the OB task (Kiehl et al., 2005). It means that those subjects encountered a difficulty of strategic adaptation to correspond to any upcoming tasks (e.g., altered responses during baseline and stimulus intervals). The failure in maintaining attentive FCs during the baseline interval may be caused by this impairment. Besides, the dysfunctions of CFP network and the right superior-inferior parietal lobes were reported for the disordered group (Vance et al., 2007; Bush, 2010; Bush, 2011).

Even though the reason behind the failure of FC maintenance likely linked to the impaired immediate adaptation above, another argument may be associated with the chronic neuromodulation effect. Long-term MPH administration (> 1 year) revealed lasting improvement of behavioral performances (Huang et al., 2012). While the effect of psychostimulants (e.g., MPH) was reported on the stable alteration for structural and functional brains (Spencer et al., 2013), the chronic effect of non-stimulant drugs (e.g., ATX) had not been described before. A further assessment with longitudinal monitoring for the entire treatment course is required.

4.4.2 Functional connectivity feature for a screening biomarker

The effectiveness of FC features was confirmed over the activation features by providing better screening performances (82.8–90.6 vs. 74.6–78.0% accuracy). The benefit of FC features was not relied on the abundant number of available features because the number of optimally selected FC features was comparable to that of the activation features. Therefore, the FC features provided more profound

characteristics of the TD and disordered groups. The activation features had been explored to investigate its potential for screening and differential diagnostic biomarkers. The biomarker performances was about 80% accuracy (Monden et al., 2015; Sutoko et al., 2019c). The current classification performance using the activation features was also about 70–80% accuracy. The previously developed biomarker required the MPH intervention to evoke distinct medication effects on between-group responses (Sutoko et al., 2019c). Meanwhile, the current screening biomarkers were technically evaluated in the least burden condition (i.e., without any intervention) for both TD and disordered children.

The FC features was reported showing not only the well-performed classification but also the robust classifying characteristics. The TD group revealed stronger FCs in the right frontal, left frontal, and left parietal lobes and weaker FCs in the left frontal, left parietal, and right parietal lobes compared to the disordered group (Figure 4.10). One of robust FC features was found in the FCs between the left ANG (BA 39), right PoCG(BA 3/1/2), and right MTG (BA 21/22), and those FCs were consistently observed in the attention network (Kiehl et al., 2005; Tamm et al., 2006).

4.4.3 Comparison between resting state and task-based connectivity

Previous FC studies highly investigated the RS FCs using fMRI due the minimum risk of task disengagement for disordered children. Due to the simple experimental design, the data collection could be vastly done in three continents (Consortium, 2012). As a result, the ADHD pathophysiology has been modeled following the hypothesis of DMN abnormalities (Castellanos et al., 2006; Castellanos et al., 2008; Choi et al., 2013). Those abnormalities was observed by either decreased connectivities (Castellanos et al., 2008) between the anterior cingulate and precuneus/posterior cingulate cortices or increased FCs (Tian et al., 2006) between the anterior cingulate and extensive region of thalamus, cerebellum, insula, and brainstem. Barttfeld et al. reported that numerous conscious level

happened and shifted during the RS (Barttfeld et al., 2015). Furthermore, the classification performance using the RS FC features was unstable, ranging from 37–86% accuracy (Consortium, 2012; Siqueira et al., 2014; Yao et al., 2018). The reasons were the analytical factors (i.e., anti-phase correlation and seed selection), the different populations (adolescents vs. adults) (Castellanos et al., 2009), and the disadvantage of uncontrolled RS. In addition, the fMRI measurement quality for pediatric studies was questioned due to heavy motion artifacts.

In order to solve the issues of uncontrolled RS and heavy motion artifacts, the task-based FCs based on fNIRS measurements were pursued. For a brief comparison, the classification results for both RS and task-based FC features were evaluated. The task-based FC features performed better screening than the RS FC features. Note that the sample number was imbalance, and unmatched symptomatic severity levels, comorbidity types, and subtypes were found. Therefore, the task-based FC features may as a complement or a substitute for the RS FC features in purpose of screening biomarkers.

4.4.4 Limitations

Despite the promising findings of FC-based screening biomarkers, the understanding of pathophysiological disorders (i.e., ADHD and ASD-comorbid ADHD) was still unclear. Besides the limited sample number as mentioned above (see 3.4.8), there was a drawback related to the protocol of data collection. Longitudinal monitoring with medication history (i.e., from medicated-naïve to prescribed conditions) is highly suggested for the cohort study design (Bossuyt et al., 2012; Linnet et al., 2012). The study completion requires a great effort and dedication though. Another limitation comes from the technical factor of the feature selection method. Even though the stepwise selection method currently worked well, the selection was irreversible, and the risk of mistaken selection is likely heightened in the small dataset. More advanced feature selection methods, such as random forest and mutual information-based methods, are worth to try.

4.5 Conclusion

In this chapter, the static FC analysis was applied on fNIRS signals during the performance of OB task. In order to control noises, another framework for noise removal was suitably developed for the static FC analysis. TD and ADHD children revealed distinct FC characteristics indeed. TD children was able to maintain the similar FCs during baseline and stimulus interval. ADHD children oppositely showed the stimulus-evoked changes by strengthening FCs; the strength of FCs was significantly weaker than that for TD children though. Furthermore, the within-region connectivity of right MFG was highly associated with the attention network. That network excited during any task performance rather than specifically for the stimulus-evoked response. It was suggested that ADHD children impaired in maintaining the required FCs during the baseline interval; the stimulus may help them to re-regulate the FCs, but the connectivity strength was still inferior compared to TD children. The results of activation and task-based FC analyses were not positively related. The screening biomarker on the basis of the task-based FC features was more effective than that of the activation feature by providing more accurate classification. The task-based FC biomarkers were specified for either FCs of right frontal, left frontal, and left parietal lobes (TD > ADHD) or FCs of left frontal, left parietal, and right parietal lobes (ADHD > TD).

5 Dynamic Functional Connectivity Analysis for Functional Near-infrared Spectroscopy Signals During Task Performance[‡]

5.1 Introduction

The dynamic FC analysis has been briefly mentioned above. The dynamic concept was introduced as several connectivity states were found to alternate across the temporal course (Liu et al., 2013). "Connectivity state" defines the fluctuation of FC strength between two brain regions during the measurement. Connectivity state also extensively explains the temporally altered relationships between FCs (i.e., networks). For example, a connectivity state represented by positively correlated ACC and negatively correlated right inferior frontal operculum with PCC was occasionally observed during the measurement (Chang et al., 2010). However, in another time, another connectivity state with opposite relationships of PCC connectivity was found. Connectivity states are task-dependent (Gonzalez-Castillo et al., 2015; Gonzalez-Castillo et al., 2018). During the process of cognitive adaptability, frontal networks were re-configured (Braun et al., 2015). This finding was technically impossible to be observed, unless the dynamic FC analysis was performed. The dynamic FC analysis had been applied on schizophrenia (Damaraju et al., 2014) and AD studies, and the developed biomarkers based on dynamic FCs performed well compared to the static FC-based biomarkers.

Even though the dynamic FC analysis was originally applied on fMRI measurement data, the potential of this analysis for fNIRS measurement data has been evaluated. Li et al. (Li et al., 2015) confirmed the feasibility of fNIRS for detecting dynamic FCs during the RS. MCI and AD biomarkers were proposed on the basis of abnormal RS connectivity states (Niu et al., 2019). Despite the practicability of the RS, it has some limitations as mentioned earlier (see 4.1). Inner experiences (Doucet et al., 2012; Hurlburt et al., 2015) (i.e., speaking, seeing,

---

[‡] The work in Chapter 5 has been published in a journal article (Sutoko et al., 2020).

thinking, sensory awareness, and feeling) are hardly controlled during the RS; the comparison of intra- and inter-subject might be less reliable. Therefore, task performances are preferably carried out to generate a more controlled measurement environment. However, to date, the task-based dynamic FCs had not been assessed from fNIRS measurements.

In this chapter, the dynamic FC analysis was applied on fNIRS measurement data coming from TD and ADHD children during the performance of the GNG task. This analysis aimed to investigate two points. *First*, the characteristics of connectivity states that dynamically shifted across the temporal course of the GNG task. In the previous chapter (i.e., Chapter 4), the static FC analysis was introduced to examine the differences between baseline and stimulus FCs (Sutoko et al., 2019b). By using the dynamic FC analysis, FCs during the transition from baseline to stimulus intervals could also be evaluated; the mechanism of task switching (baseline to stimulus) might be more clearly understood. The observation of connectivity states and its well-grounded interpretation would confirm the feasibility of the task-based dynamic FC analysis for fNIRS measurements. *Second*, the differences between TD and ADHD children. ADHD adolescents failed to specifically administer task-related networks but revealed over-expressed task-irrelevant networks during the inhibition task (van Rooij et al., 2015). Therefore, task-related and task-irrelevant connectivity states were hypothesized in the current analysis. The differences between TD and ADHD children may be brought by distinct occurrence probabilities of connectivity states. These obtained differences could comprehend the ADHD pathophysiology.

5.2   Materials and methods

5.2.1   Subjects and experimental design

The currently used dataset included 21 medication-naïve ADHD children (17 boys; 7.8 ± 1.7 years old) and 21 age-matching TD children (15 boys; 8.5 ± 1.8 years old). This dataset came from two different pre-recorded datasets. ADHD-

children data had been reported by Tokuda et al. (Tokuda et al., 2018) and Sutoko et al. (Sutoko et al., 2019c) in purposes of ADHD characterization and differential diagnosis (see Chapter 3), respectively. Meanwhile, 21 TD-children data were selected from 30 TD-children data that had been previously described by Monden et al. (Monden et al., 2015). TD children had significantly higher IQs (WISC-III) than ADHD children (two-sample t-test; $p < 0.01$; $t_{(40)} = 3.27$; 105.5 ± 12.3 vs. 92.8 ± 12.9). An ADHD-subject data was excluded from further analysis due to the problem of data saving (see 3.2.8).

The experimental design followed the randomized, double-blind, placebo-controlled, and crossover study – as same as being mentioned in the previous chapters (see 3.2.2, 3.2.8, 4.2.1). In order to focus only on the nature of ADHD and its comparisons to TD, the current study analyzed only the data without any interventions of medication or placebo (i.e., the first measurement session at the first day measurement). Those children performed the GNG task while their brains were measured using the multichannel fNIRS system (ETG-4000, Hitachi. Ltd., Japan). The task paradigm were same as explained above (see 3.2.2) and described in detail elsewhere (Monden et al., 2012b; Nagashima et al., 2014b; Ikeda et al., 2018b). The probe and channel configurations (i.e., 44 channels on bi-hemispheric lateral prefrontal-to-inferior parietal lobes) were also same as detailed above (see 3.2.2, 3.2.8).

Behavioral performances showed inconsistent results in describing the difference between TD and ADHD children. For example, the response accuracy of TD children was either similar or greater than that of ADHD children (Monden et al., 2012b; Nagashima et al., 2014b). Furthermore, ADHD children were difficult to be distinguished from TD children based on only behavioral performances. Nevertheless, the difference between TD and ADHD children on the basis of brain activations (i.e., right MFG/IFG) was found to be consistently observed in any datasets. Brain abnormalities offer better understandings for explaining TD and ADHD characteristics than behavioral performances do. Due

to the confounding interpretation of behavioral performances, the relationships between behavioral performances and brain features (i.e., dynamic connectivity states) were not pursued in this chapter.

5.2.2   Signal preprocessing

Signal preprocessing was performed on the POTATo (Sutoko et al., 2016). The products of Hb concentration change and optical path length ($\Delta C_{O_2Hb} \cdot L$, $\Delta C_{HHb} \cdot L$, and $\Delta C_{Hb\text{-}total} \cdot L$) (Maki et al., 1995; Koizumi et al., 2003) were also obtained from the detected optical intensity following the MBLL (Delpy et al., 1988; Maki et al., 1995). Channel-wise signals ($\Delta C_{O_2Hb} \cdot L$ and $\Delta C_{HHb} \cdot L$) with low quality (SNR < 10 dB; power ratio of 0.01–0.15 Hz to 4.5–5 Hz) were removed (Figure 5.1A; step 1). This step eliminated about 5% of total number of channels (i.e., total subject × 44 channels). Linear fitting and filtering (5th order Butterworth band-pass filter; 0.01–0.8 Hz) were applied on the remaining channel-wise signals (Figure 5.1B; $92.0 \pm 10.3\%$ of 44 channels across subjects)
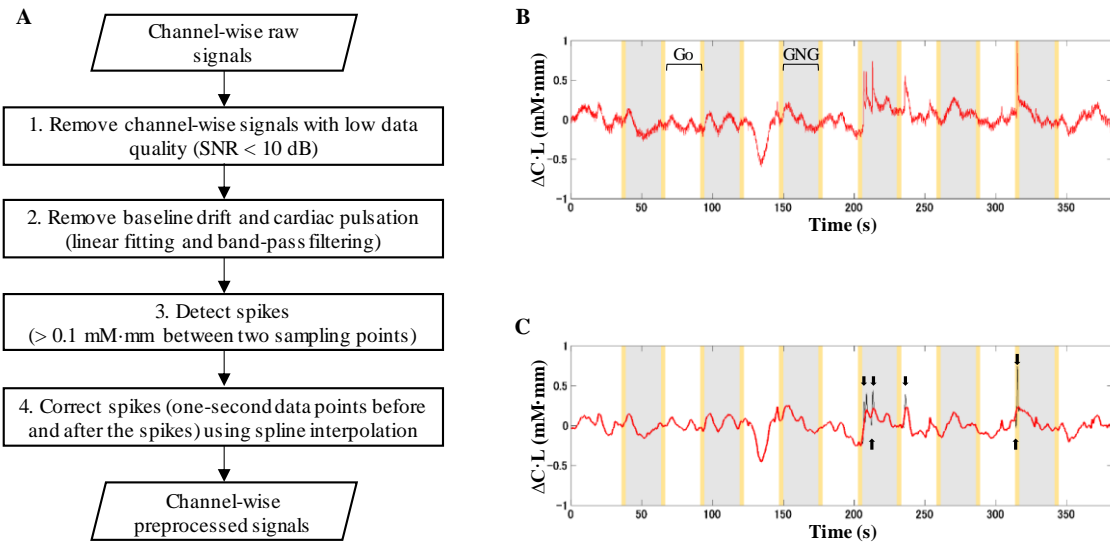
Figure 5. 1 Process flow of signal preprocessing (A) and its illustrations. A raw channel-wise signal (B) contained several spikes. After the raw signal was filtered, spikes were still remained (black arrows in C). Spikes were corrected resulting in the relatively spike-free signal. White, yellow, and gray intervals in B and C indicate the baseline, 3-s instruction, and stimulus intervals. From (Sutoko et al., 2020), modified with permission.

to remove baseline shift and cardiac pulsation (Figure 5.1A; step 2). The filtering step unlikely managed spikes. Spikes were identified by the sudden amplitude change (> 0.1 mM·mm) from two consecutive datapoints (Figure 5.1A; step 3). In the static FC analysis, spikes and other noises could be removed from the affected datapoints, and the noise-free datapoints were then concatenated (Chapter 4; see 4.2.2). However, removing datapoints was infeasible in the dynamic FC analysis because this analysis required uninterrupted datapoints. Therefore, instead of rejecting spike-affected datapoints, spikes (together with 1-s datapoints before and after the spikes) were corrected using the cubic spline interpolation (third-order polynomials; Figure 5.1A; step 4). An example result of spike correction is shown in Figure 5.1C. However, this dataset had relatively low spike occurrences by 1.11 ± 1.69% of total datapoints across subjects, and the measurement quality was reliable.

5.2.3 Dynamic functional connectivity analysis

The dynamic FC analysis adapted the sliding-window correlation (SWC) method (Hutchison et al., 2013; Preti et al., 2017). The input of this analysis was channel-wise preprocessed signals, and this analysis is explained in six steps as detailed below.

1. The channel-wise preprocessed signals were correlated (Pearson's correlation) to each other ($ch \times ch$) with window length of 12.0 s and window offset of one sampling point (0.1 s) for each subject (step 1 in Figure 5.1A, Figure 5.1B). The greater correlation coefficients (r) are observed, the stronger FCs between channels (i.e., regions) are estimated. Total number of dynamic FC maps (i.e., W) for each subject and signal type ($\Delta C_{O2Hb} \cdot L$ and $\Delta C_{HHb} \cdot L$) is given by the total datapoints (6–7 min; 3600–4200 points) minus the sliding-window points (12.0 s; 120 points). Twelve-second (i.e., 50% of baseline/stimulus interval) was selected as the window length in order to observe the transition of dynamic FC between baseline and stimulus intervals.
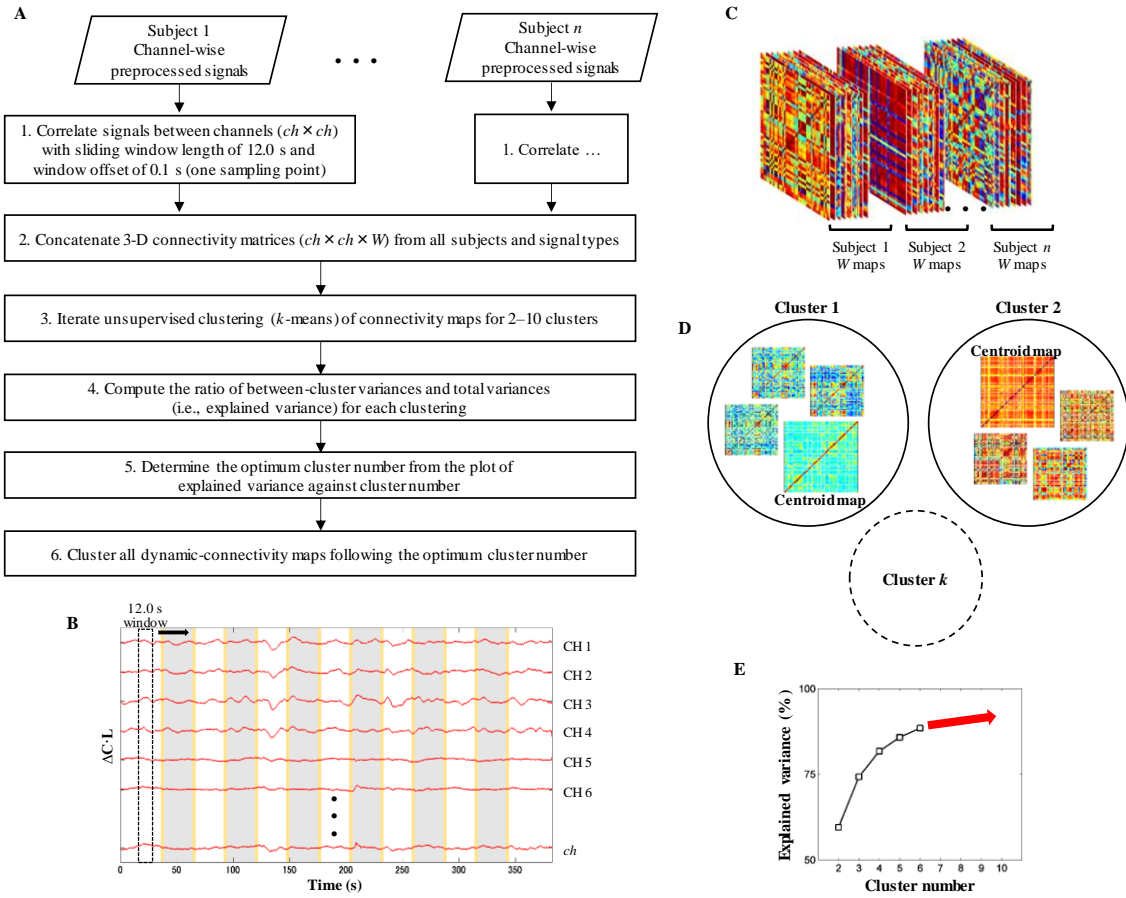
Figure 5. 2 Process flow of dynamic FC analysis (A) and its illustrations. Preprocessed signals from all channels were correlated to each other with 12.0 s sliding window length and 0.1 s window offset (B). W (total measurement minus window lengths; in points) number of $ch \times ch$ maps were obtained and concatenated across signal types (O_2Hb and HHb) and subjects (C). Clustering was performed afterwards (D; 2–10 clusters), and the cluster number was optimized following the application of the elbow method on the plot of explained variance against cluster number (E). From (Sutoko et al., 2020), modified with permission.

2. Dynamic FC maps for all temporal points, subjects, and signal types were concatenated in 3D matrices ($ch \times ch \times W$, step 2 in Figure 5.2A, Figure 5.2C).

3. The optimization process for the number of connectivity state was required because there was no presumed state. The optimization process was done by trial-and-error unsupervised clustering (k-means; two to ten clusters) across concatenated dynamic FC maps (step 3 in Figure 5.2A). However, subjects having channel-wise signals with low SNRs would construct deficient dynamic FC maps. Those deficient maps were temporarily disregarded in the

113

optimization process. Each cluster produced a centroid map. Centroid maps characterized attribute centers with the shortest total Euclidean distances of within-cluster members to the centroids (Figure 5.2D). Dynamic FC maps categorized in the same cluster were estimated to be in the same connectivity state.

4. The explained variance (given as a percentage) was computed (step 4 in Figure 5.2A) by the following equation.

$$Explained\ variance = \frac{\sum_i \sum_j |x_i - C_j| - \sum_k \sum_j |x_{(k,j)} - C_j|}{\sum_i \sum_j |x_i - C_j|} \qquad (\text{Eq. 7})$$

where x_i is the multidimensional data for each subject i, Cj is the multidimensional data of obtained centroids for each cluster j, and $x_{(k,j)}$ is the multidimensional data for each within-cluster j member k. As cluster number increases, the between-cluster variance decreases, and the explained variance gradually increases (Figure 5.2E).

5. The optimum number of cluster (i.e., connectivity state) was determined by the empirical method, namely, the elbow method on the plot of explained variance against cluster number. As the cluster number increases, the increases of explained variance become inconsiderable. This phenomenon suggests that increasing cluster number does not improve the clustering efficiency. The elbow method was used to figure out at which the cluster number revealed no longer improved clustering efficiency (step 5 in Figure 5.2A) (Tibshirani et al., 2001). That cluster number was then defined as the optimum number of connectivity state representing all dynamic FC maps.

6. Afterwards, all dynamic FC maps were clustered in accordance with the optimum cluster number (step 6 in Figure 5.2A). The deficient dynamic-connectivity maps were approximately classified into specific clusters following the highest similarity between dynamic FC and centroid maps.

5.2.4 Statistical analysis

Figure 5.3 shows an illustration of dynamic shift for four connectivity states from an ADHD child over the temporal course. Labeled dynamic FC maps were aligned to the window onset and segmented on the basis of epoch interval (10, 3, 24, 3, and 10 s for pre-stimulus baseline, pre-stimulus instruction, stimulus, post-stimulus instruction, and post-stimulus baseline, respectively). There was no overlapping connectivity window in either pre- or post-stimulus baseline. Probability occurrence was defined as the probability of specific connectivity state occurring across six epochs. Because the occurrence probability follows the discrete probability distribution, statistical tests were performed in accordance with the non-parametric manners. Kruskal-Wallis H test was applied on subject-wise median values of occurrence probability across the epoch to evaluate the effect of connectivity state. Dunn-Šidák correction was done for a *post hoc* analysis. Furthermore, Friedman test was performed to assess the effects of connectivity states and signal types on occurrence probability. The differences of occurrence probability between signal types were confirmed using Wilcoxon signed-rank test, and the differences of occurrence probability between TD and ADHD children were evaluated using Wilcoxon rank-sum test.
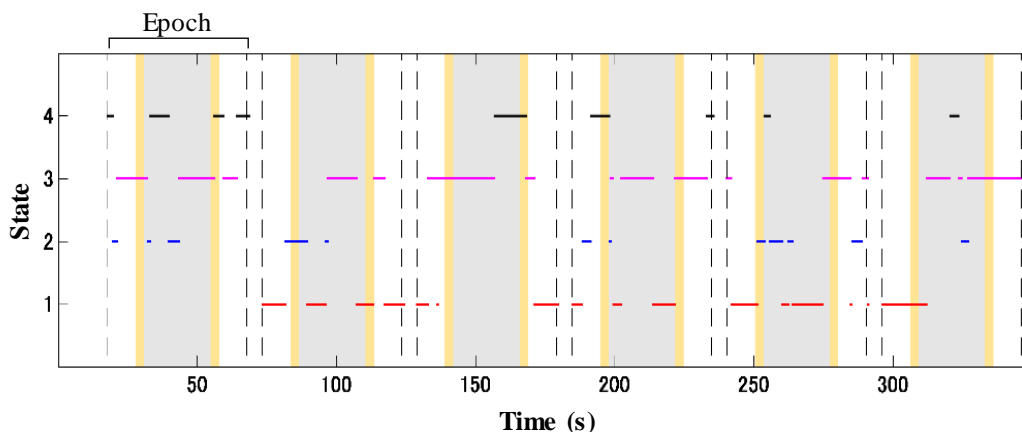
Figure 5. 3 Illustration of dynamic shifting between four connectivity states (red, blue, magenta, and black lines for states 1, 2, 3, and 4, respectively) during the temporal course. White, yellow, and gray intervals indicate the baseline, 3-s instruction, and stimulus intervals. From (Sutoko et al., 2020), reproduced with permission.

5.3 Results

5.3.1 Optimum cluster number

Figure 5.4 shows the plot of explained variance against cluster number. A non-linear positive relationship was observed. Unsupervised clustering with two clusters contributed to about 60% explained variance, and ten clusters resulted in 93% explain variance in approximate. The "elbow" was unclearly recognized; thus, the optimum cluster number was selected on the basis of the longest perpendicular distance between a linear function between points of two and 10 clusters and other points. Four clusters with the explained variance of 82% were selected as the optimum cluster number. Therefore, the number of connectivity states was also determined to be four states.

5.3.2 Connectivity states and its characteristics

After selecting the optimum cluster number, the dynamic FC maps were re-clustered into four states (i.e., clusters). Figure 5.5 visualizes the centroid maps for each state. The centroid maps of the states 2 and 3 were the least correlated
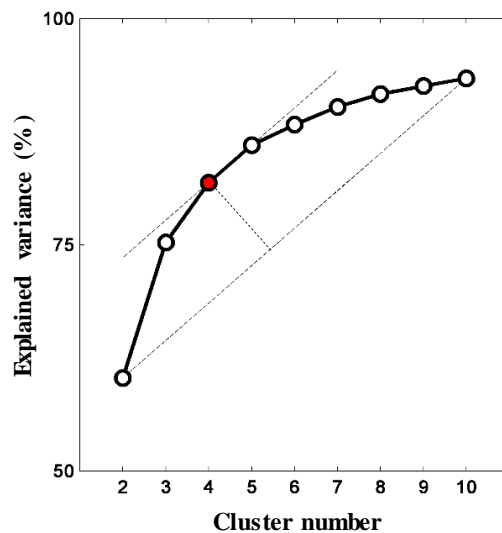
Figure 5. 4 Plot of explained variance against cluster number. According to the elbow method, four (red dot) is the optimum cluster number. From (Sutoko et al., 2020), reproduced with permission.

116

Figure 5. 5 Obtained centroid maps for each connectivity state (A–D for states 1–4, respectively). Color bar represents the strength of connectivity ($\bar{r}$) between two regions (i.e., channels). Cortical areas: angular gyrus (ANG), inferior frontal gyrus (IFG), middle frontal gyrus (MFG), middle temporal gyrus (MTG), postcentral gyrus (PoCG), precentral gyrus (PrCG), supramarginal gyrus (SMG), and superior temporal gyrus (STG). From (Sutoko et al., 2020), reproduced with permission.

(Figures 5.5: B and C, Pearson's correlation $r = 0.40$); the most-correlated centroid maps were the states 1 and 2 (Figures 5.5: A and B, $r = 0.85$). Despite its high correlation, the state 1 revealed weaker dynamic FCs for all possible connectivities ($ch \times ch$) than the state 2.

Averages of within-cluster dynamic FC maps (Fisher's z transform) are shown in Figure 5.6 for each state. There are five highlighted points as follows. *First*, the averaged dynamic FC map of the state 1 presented strong within- (i.e., bilateral MFG, bilateral IFG, bilateral SMG, right ANG, right MTG, and left STG) and between-region (i.e., right MFG – left MFG, right IFG – left IFG, intra-hemispheric PrCG and PoCG, left MTG – left STG) FCs (black-squared regions in Figure 5.6A). *Second*, similar to the centroid maps, the most correlated of averaged dynamic FC maps was found in the states 1 and 2 (Figures 5.6: A and B, $r = 0.87$). Nevertheless, the range of averaged dynamic FC strength was stronger in the state 2 (-0.07–0.62 and 0.22 – 0.77 for states 1 and 2, respectively). *Third*, the averaged dynamic FC map of the state 3 revealed the strong FCs between bilateral regions (i.e., MFG, SMG, ANG, PrCG) located on the midline vertex (black-squared regions in Figure 5.6C). *Fourth*, the averaged dynamic FC maps of the states 2 and 3 were the least correlated (Figures 5.6: B and C, $r = 0.34$).

117
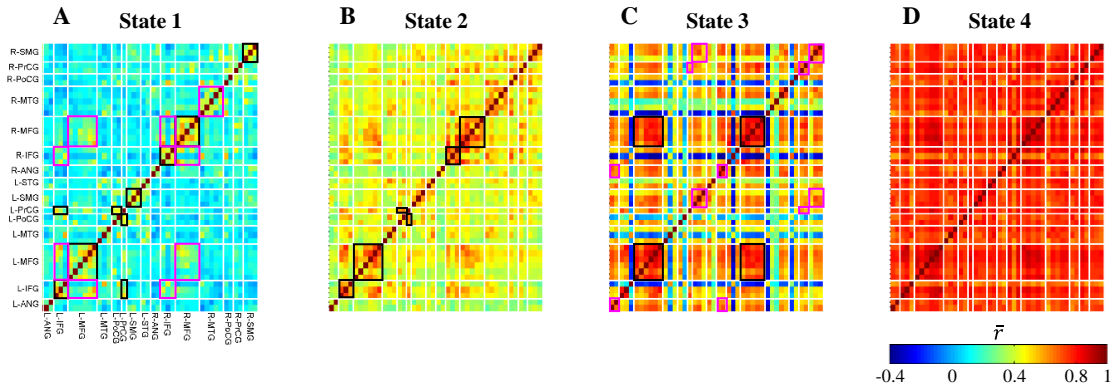
Figure 5. 6 Subject-average dynamic FC maps clustered for each connectivity state (A–D for states 1–4, respectively). Color bar represe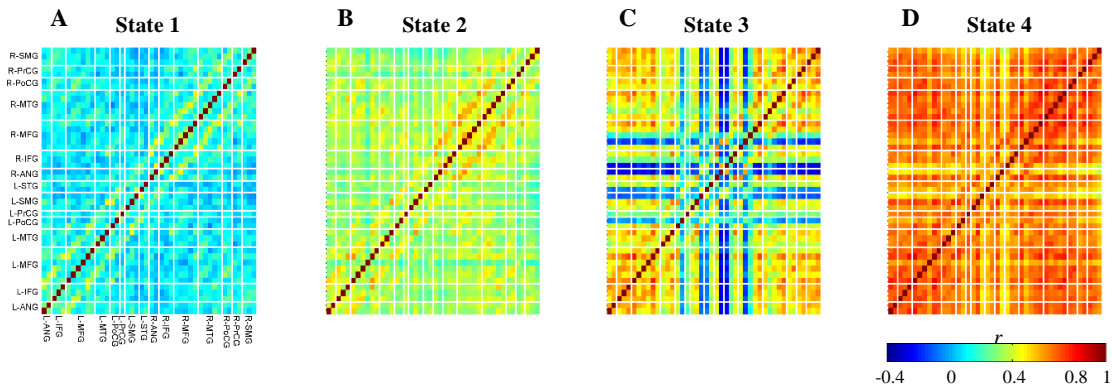nts the strength of connectivity ($\bar{r}$) between two regions (i.e., channels). Black and magenta-squared regions represent completely and partially strong within-region connectivities, respectively. Cortical areas: angular gyrus (ANG), inferior frontal gyrus (IFG), middle frontal gyrus (MFG), middle temporal gyrus (MTG), postcentral gyrus (PoCG), precentral gyrus (PrCG), supramarginal gyrus (SMG), and superior temporal gyrus (STG). From (Sutoko et al., 2020), reproduced with permission.

While the high between-state correlation may represent the similarity of dynamic FC patterns with different ranges of FC strength, the low between-state correlation may oppositely indicate that the dynamic FC patterns were dissimilar between states. For example, the strong FCs between bilateral MTG and intra-hemispheric IFG were observed in the state 2 but not in the state 3; the strong FCs of intra-hemispheric ANG and SMG were found in the state 3 but not in the state 2. *Fifth*, all possible connectivities ($ch \times ch$) were found to be massive and strong in the state 4. (Figure 5.6D, connectivity range = 0.52–0.92).

The characteristics of occurrence probabilities were evaluated for each state as shown in Table 5.1. According to these results, there are five points summed up. *First*, the highest occurrence probability was achieved in the state 1 for the dynamic HHb FC (mean of 56%; median of 67%; Dunn-Šidák post-hoc analysis of Kruskal-Wallis H test; $\chi^2_{(3,160)} = 97.5$; $p < 10^{-20}$). Among O$_2$Hb connectivity states, the occurrence probabilities of the states 1 and 2 were significantly higher than those of the states 3 and 4 (Dunn-Šidák post-hoc analysis of Kruskal-Wallis H test; $\chi^2_{(3,160)} = 51.7$; $p < 10^{-10}$). *Second*, there was no significant difference (Dunn-Šidák post-hoc analysis of Kruskal-Wallis H test; $p > 0.05$) between

118

Table 5. 1 Summary of occurrence probabilities for each O_2Hb and HHb connectivity state. From (Sutoko et al., 2020), reproduced with permission.

Signal type	State 1 (S1)	State 2 (S2)	State 3 (S3)	State 4 (S4)	Inter-state
O_2Hb	$\bar{x} = 40\%$ $\tilde{x} = 50\%$	$\bar{x} = 29\%$ $\tilde{x} = 33\%$	$\bar{x} = 15\%$ $\tilde{x} = 17\%$	$\bar{x} = 16\%$ $\tilde{x} = 17\%$	S1 ~ S2 > S3 ~ S4 $\chi^2_{(3,160)} = 51.7; p < 10^{-10}$
HHb	$\bar{x} = 56\%$ $\tilde{x} = 67\%$	$\bar{x} = 26\%$ $\tilde{x} = 17\%$	$\bar{x} = 7\%$ $\tilde{x} = 0\%$	$\bar{x} = 10\%$ $\tilde{x} = 0\%$	S1 > S2 > S3 ~ S4 $\chi^2_{(3,160)} = 97.5; p < 10^{-20}$
O_2Hb vs. HHb	$S1_{(O_2Hb)} < S1_{(HHb)}$ $z = -4.80$ $p < 10^{-6}$	$S2_{(O_2Hb)} \sim S2_{(HHb)}$ $z = 1.65$ $p > 0.1$	$S3_{(O_2Hb)} > S3_{(HHb)}$ $z = 2.95$ $p < 0.01$	$S4_{(O_2Hb)} > S4_{(HHb)}$ $z = 3.08$ $p < 0.01$	

$\bar{x}$: mean and $\tilde{x}$: median

occurrence probabilities of the states 3 (mean of 7–15%; median of 0–17%) and 4 (mean of 10–16%; median of 0–17%) for the dynamic O_2Hb and HHb FCs. *Third*, the occurrence probabilities of the states 3 and 4 for the dynamic O_2Hb FC were significantly higher (Wilcoxon signed-rank test; $z = 2.95$–3.08; $p < 0.01$) than those for the dynamic HHb FC. *Fourth*, the occurrence probability of the state 1 for the dynamic O_2Hb FC was significantly lower (Wilcoxon signed-rank test; $z = -4.80$; $p < 10^{-6}$) than that for the dynamic HHb FC. *Fifth*, the effect of connectivity states (Friedman test; $\chi^2_{(3)} = 144.95$; $p < 10^{-30}$) on occurrence probability was more prominent than that of signal types (Friedman test; $\chi^2_{(1)} = 1.65$; $p > 0.05$).

5.3.3 Differences between TD and ADHD groups in occurrence probability of connectivity state

Figure 5.7 shows the plots describing shifts of occurrence probability across baseline, stimulus, and post-stimulus intervals for each state. Even though the plots visualize the occurrence probabilities on the basis of subject averages, the statistical analysis was performed on the medians of occurrence probability between the TD and ADHD groups. The significant group effects were observed at different intervals for each state. The TD group revealed higher occurrence probability of the state 1 for the dynamic O_2Hb FC (Figure 5.7A1; Wilcoxon rank-sum test; $z = 1.99$–2.76; $p < 0.05$) than the ADHD group did during the stimulus interval. For the dynamic HHb FC, the significant group effect on occurrence probability of the state 1 was observed in the post-stimulus interval (Figure 5.7A2;
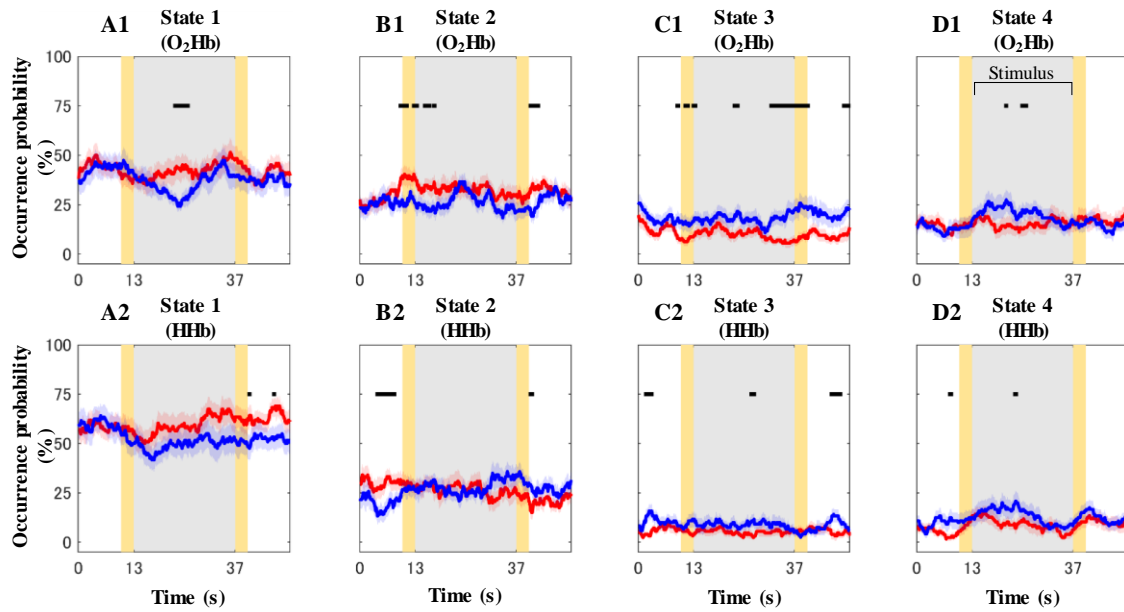
Figure 5. 7 Dynamic shifting of averaged occurrence probabilities across TD (red plots) and ADHD (blue plots) children during the epoch interval for each O$_2$Hb (A1–D1) and HHb (A2–D2) connectivity state (A–D for states 1–4, respectively). White, yellow, and gray intervals indicate the baseline, 3-s instruction, and stimulus intervals. Shaded patches around plots represent standard errors. Black squares denote the timepoints showing between-group significances. From (Sutoko et al., 2020), reproduced with permission.

Wilcoxon rank-sum test; $z = 1.99$; $p < 0.05$). The high occurrence probability of the state 2 for the dynamic O$_2$Hb FC was achieved by the TD group in the baseline, transition of baseline-to-stimulus, and post-stimulus intervals (Figure 5.7B1; Wilcoxon rank-sum test; $z = 1.96–2.68$; $p < 0.05$). However, the group effect on occurrence probability of the state 2 for the dynamic HHb FC (Figure 5.7B2) depended on the intervals. For example, the ADHD group showed decreased occurrence probability (Wilcoxon rank-sum test; $z = -2.46 - -2.97$; $p < 0.05$) in the baseline interval but increased occurrence probability (Wilcoxon rank-sum test; $z = 2.10–2.26$; $p < 0.05$) in the brief post-stimulus interval. Furthermore, the high occurrence probabilities of the states 3 and 4 for the dynamic O$_2$Hb and HHb FCs were found in a diverse time across intervals for the ADHD group (Figures 5.7: C and D; Wilcoxon rank-sum test; $z = 1.96–3.18$; $p < 0.05$). Despite the discrepancy of group effect between dynamic O$_2$Hb and HHb FCs across intervals, the high occurrence probabilities of the states 1 and 2 were associated with the TD

group, and the ADHD group contributed to the high occurrence probabilities of the states 3 and 4.

5.4 Discussion

5.4.1 Interpretation of connectivity states

Four connectivity states were dynamically shifted during the performance of the GNG task. The dominant bilateral frontoparietal network were found in two connectivity states (i.e., states 1 and 2). The functionality of frontoparietal network had been associated with attention control (Peers et al., 2005) and flexibility (Dodds et al., 2011). As described above (see 3.4.7), the attention domain may involve during the performance of inhibitory control tasks, including the GNG task. Intact attention control is required to successfully recognize the inhibitory targets and cues (Verbruggen et al., 2014; Hong et al., 2017). Furthermore, the inhibitory performances, such as omission-commission errors and response time, are also correlated with the function of attention control (Murphy et al., 1999; Keilp et al., 2005; Reynolds et al., 2006). The involvement of multiple cognitive domains during the performance of executive functions (e.g., inhibition process) is logically explained (Dodds et al., 2011; Erika-Florence et al., 2014). Therefore, the states 1 and 2 were interpreted as task-related states.

The states 1 and 2 showed the similar connectivity pattern; the differences between the states 1 and 2 came from the FC strength and occurrence probability. The hypothesis of intrinsic-transient networks may explain the occurrence of these states. Braun et al. postulated that the intrinsic network is at least preserved, and the transient network accommodates the task demands (Braun et al., 2015). Both networks are likely similar because transient networks are mainly constructed from intrinsic networks (Cole et al., 2014). Even though this hypothesis fits to the current finding, either intrinsic or transient states could not be easily deduced because the difference between the states 1 and 2 solely based on the FC strength. Furthermore, there was no clear segregation between baseline (i.e., Go blocks)

121

and stimulus (i.e., GNG blocks) intervals. The insubstantial transition-evoked change was also observed in the previous chapter (see 4.3.1) especially for TD children (Sutoko et al., 2019b). The functional differentiation within network was also found to be subtle as similar as a previous study (Verbruggen et al., 2008); Menon et al. and Hong et al. reported evident differentiation though (Menon et al., 2001; Hong et al., 2017).

Despite the strong frontoparietal network in the states 3 and 4, other networks were also prominent. Therefore, the states 3 and 4 were concluded as task-irrelevant states. The state 3 revealed strong FCs in the bilateral medial PFC and ANG. Those regions had been reported having contributions to the DMN (Raichle et al., 2001; Raichle et al., 2007). However, the frequencies of interest between the DMN (< 0.2 Hz) and the current task-based FC (0.01–0.8 Hz) were different. The DMN played a role for the task-negative network (Fox et al., 2005); its occurrence was opposite to the task-related network (Cole et al., 2014). The low occurrence probability of the state 3 (7–15% on average) strengthened this assumption. Meanwhile, the global connectivity in all measured regions was observed in the state 4. A global effect controls cerebral blood flow in a widespread manner (Roy et al., 1890; Devonshire et al., 2012) rather than the neurovascular coupling effect does localized regulations.

The disagreement between occurrence probabilities of O_2Hb and HHb connectivity states demanded some explanations. The effects of systemic components (Franceschini et al., 2003) and blood-related change sensitivity (Hoshi et al., 2001; Hirasawa et al., 2014) on O_2Hb and HHb signals were reportedly distinct. Furthermore, the analyzed frequency band may not be suitable for $\Delta C_{HHb} \cdot L$ signals. High coherence of $\Delta C_{HHb} \cdot L$ signals was observed in a lower-frequency band than the frequency of interest for $\Delta C_{O2Hb} \cdot L$ signals (Sasai et al., 2011; Fishburn et al., 2014). The mis-targeting frequency band resulted in incorrect SNR assessment (low SNR) (Sasai et al., 2011; Fishburn et al., 2014) in which $\Delta C_{HHb} \cdot L$ signals were eliminated more than $\Delta C_{O2Hb} \cdot L$ signals in the

current analysis. This addresses the requirement for an analysis standard to more accurately evaluate $\Delta C_{HHb} \cdot L$ signals.

5.4.2 Occurrence probability of connectivity state for TD and ADHD children

The significant group effects apparently interlocked with the temporal information, such as baseline, stimulus, and post-stimulus intervals. These results may suggest the different mechanisms in responding to task demands for TD and ADHD children. The assumed task-related state 1 was found to decrease, but the occurrence probabilities of the states 3 and 4 increased during the stimulus interval for ADHD children. ADHD children may experience inefficient FC recruitment which the task-irrelevant states were engaged more during the stimulus interval instead. Furthermore, the ADHD severity had been associated with the task-negative networks (e.g., DMN) (van Rooij et al., 2015). The interaction between networks (e.g., task-positive, fronto-striatal, fronto-default, sensory-motor networks) was also impaired for ADHD children (Castellanos et al., 2006; Castellanos et al., 2008; Mennes et al., 2012; Choi et al., 2013). The previous and current results proposed a hypothesis of abnormal FC recruitment happened in ADHD children.

The increased occurrence probability of the state 2 in the transition interval (i.e., baseline-to-stimulus and stimulus-to-post-stimulus) was interpreted as a response to the task switching for TD children. During the transition interval, the 3-s instruction interval provided subjects a guide to perform upcoming blocks (i.e., Go or GNG blocks). The medial frontal cortex (including SMA and pre-SMA) is responsible to task switching (Rushworth et al., 2002). The medial frontal cortex involves in the frontoparietal network, and the state 2 also showed the strong FC in the medial frontal cortex. ADHD subjects expressed the hypoactivation in the SMA/pre-SMA (Tamm et al., 2004); thus, the ADHD pathophysiology may relate to the task switching dysfunction.

123

5.4.3 Comparison between resting state and task-based dynamic functional connectivity

Niu et al. demonstrated the dynamic connectivity analysis based on RS fNIRS measurement for healthy adults, amnestic MCI patient, and AD patients (Niu et al., 2019). Even though the group effects were compared in three connectivity states, ten connectivity states were apparently found in the clustering process. This number of connectivity state was considerably high. Either patients brought the numerous and abnormal connectivity states or the RS per se contributed to this number. It has been difficult to control inter-subject consciousness level during the RS measurement (Barttfeld et al., 2015). Performing a task may be a solution to mitigate the subject variability during the RS. According to the current results, four connectivity states were robustly detected, and the TD and ADHD characteristics were observed via the occurrence probability of connectivity states. The task-based dynamic connectivity may become a promising biomarker.

5.4.4 Limitations

There were three limitations in the current study. *First*, the limited sample number was the real issue in this study. However, in this limited dataset, the findings have been eminent. The suggested cohort studies (Bossuyt et al., 2012; Linnet et al., 2012) may improve the analysis power. *Second*, the SWC implemented on the current analysis influences by several variables, such as window length, offset, and edge treatment (Shakil et al., 2016). The use of 12-s window length was seemingly fair enough. Different window lengths (e.g., 25, 50, and 100 s) were applied on the SWC analysis. Figures 5.8 and 5.9 show the optimization process for clustering and the centroid maps using different window lengths. Increasing window length did not change the optimum cluster number (i.e., four cluster) and the explained variance parameter (82–83%, Figure 5.8). Furthermore, the centroid maps were found to be similar using any window lengths ($r = 0.58$–0.89, Figure 5.9). Even though the effect of window length
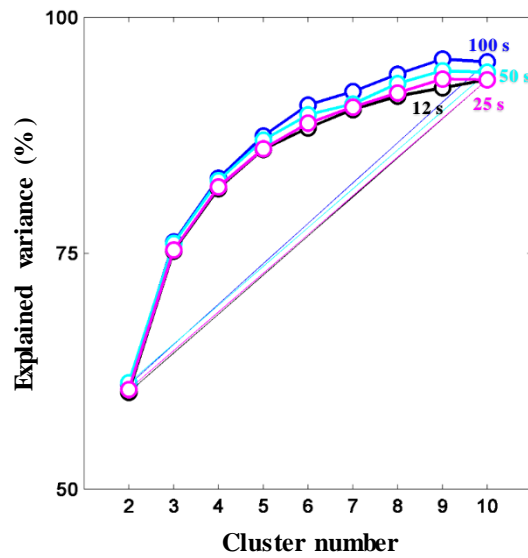
Figure 5. 8 Plots of explained variance against cluster number for various sliding window lengths (black, magenta, cyan, and blue plots for 12, 25, 50, and 100 s sliding window lengths, respectively.).

variable on clustering was null, that effect on averaged connectivity state and occurrence probability should be addressed properly. Another analysis, named hidden Markov model, was a substitute for the SWC analysis and used to predict the connectivity state (Vidaurre et al., 2017). There are still more rooms for improving the dynamic FC analysis. *Third*, the relationships between study findings were unclear. Hypoactivation (chapter 3), impaired network maintenance (chapter 4), atypical connectivity recruitment (chapter 5), and dysfunction of task switching (chapter 5) were proposed as ADHD characteristics throughout this dissertation. The interconnected relationships should be investigated further to evidently understand ADHD pathophysiology. By providing a validated model of ADHD pathophysiology, a more accurate (screening and differential diagnostic) biomarker is expected.

5.5   Conclusion

In this chapter, the dynamic FC analysis was applied on the task-based fNIRS signals for the first time. Four connectivity states were found to alternate. Two
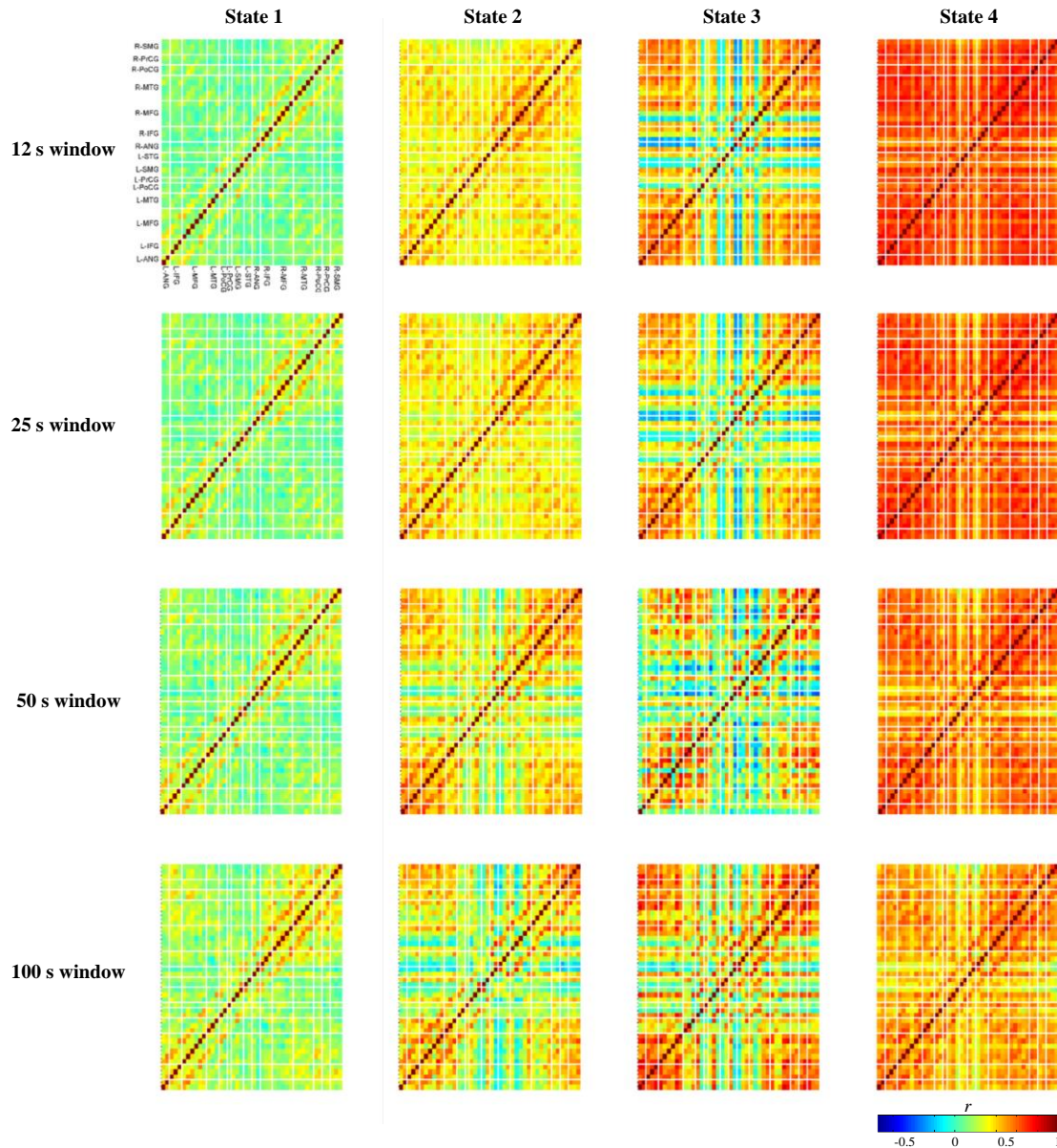
Figure 5. 9 Obtained centroid maps for each connectivity state in clustering dynamic FC maps with various sliding window lengths (e.g., 12, 25, 50, and 100 s sliding window lengths). Color bar represents the strength of connectivity ($\bar{r}$) between two regions (i.e., channels). Cortical areas: angular gyrus (ANG), inferior frontal gyrus (IFG), middle frontal gyrus (MFG), middle temporal gyrus (MTG), postcentral gyrus (PoCG), precentral gyrus (PrCG), supramarginal gyrus (SMG), and superior temporal gyrus (STG).

connectivity states (i.e., the states 1 and 2) were interpreted as the task-related connectivity states displaying the strong attentive frontoparietal network. The task-irrelevant connectivity states were assumed from the other connectivity states (i.e., the states 3 and 4) due to the detected DMN and global effect characteristics.

126

The task-related connectivity states dominantly occurred across the temporal course. TD children mainly maintained the task-related connectivity states in both baseline and stimulus intervals. Meanwhile, ADHD children showed the decreased occurrence probability of task-related connectivity states in the transition and stimulus intervals. The abnormal connectivity state recruitment for ADHD children was suggested due to the increased occurrence probabilities of task-irrelevant connectivity states particularly in the stimulus interval.

6   Concluding Remarks

6.1   Summary

This dissertation formulated three frameworks to develop fNIRS analysis methods for disordered children measurement and to investigate the application of those methods on seeking potential ADHD brain-based biomarkers. Each framework is summarized as follows:

1. Development of noise removal algorithm to improve the conventional brain activation analysis and its application on ADHD children data (Chapter 3).

   As a substitute to the laborious visual judgment and the unstably performed noise correction algorithms, the adaptive rejection algorithm was developed. This algorithm aimed to provide the objective and personalized judgment in eliminating noisy signals as well as maintaining the sample number for sufficient statistical power and minimizing the risk of overcorrection. The application of this algorithm was confirmed in both simulated synthetic and children datasets (TD and ADHD). The performance of adaptive rejection algorithm was similar (e.g., obtained waveforms, activation values, statistical inferences) to that of the visual judgment (Sutoko et al., 2018). The algorithm was applied on a different dataset acting as a signal preprocessing step. The algorithm worked well resulting in a robust activation analysis that was further explored to classify between ADHD and ASD-comorbid ADHD children. Compared to the behavioral-based biomarkers, the brain activation-based biomarkers were more sensitive tools for the differential diagnosis. The brain activation-based biomarker was associated with the neuropharmacological effects on three functionals domains, including inhibition (inferior and middle frontal gyri), attention (fronto-parietal lobes), and motor (precentral gyrus) (Sutoko et al., 2019c). The developed adaptive rejection algorithm facilitated the signal preprocessing and supported analyses with various objectives.

2. Development of analysis algorithm to extract the information of static FC

during the performance of cognitive tasks and its application comparison to the conventional brain activation analysis for ADHD screening biomarkers (Chapter 4).

In this chapter, the static FC analysis was developed to support the measurement of block-design paradigm. The static term defines that the FCs are constant and temporally independent across the measurement course. This analysis controlled intermittently occurred noises and specified between baseline and stimulus connectivities. According to this analysis, a distinct characteristic was found for TD and disordered children. TD children maintained their brain connectivities during the baseline and stimulus intervals. Meanwhile, ADHD children presented weak connectivities during the baseline interval, and the stimulus-evoked responses were observed in the increased connectivity strength. The benefit of brain connectivity was confirmed in purpose of investigating screening biomarkers. Compared to the activation-based biomarkers, the connectivity-based biomarkers were well-performed by improving about 12% screening accuracy (Sutoko et al., 2019b).

3. Investigation of dynamic FC analysis for task-based fNIRS signals and its insight into ADHD characteristics (Chapter 5).

Different with the static FC analysis, the dynamic FC analysis presumed that the FCs are non-stationary and shift across the measurement course. This chapter is a pioneering study in demonstrating the application of dynamic FC analysis on the measurement of block-design paradigm. To accommodate the dynamic FC analysis, intermittent noises should be managed differently. The suitable scheme of signal preprocessing was also developed here. According to the results, there were four connectivity states alternately shifted during the baseline and stimulus intervals. Those connectivity states were assumed as task-related and task-irrelevant connectivity states. The ADHD characteristics was found in the increased occurrence probability for task-irrelevant connectivity states, whereas the TD children was identified by the

increased occurrence probability for task-related connectivity states that involved the bilateral frontal-to-parietal network. These findings suggested a neuropathophysiological theorem of atypical connectivity recruitment for ADHD children (Sutoko et al., 2020).

6.2   Scope of future work

The analysis methods were developed to appropriately facilitate the noise removal (e.g., noisy epoch signals or datapoints) and the analysis requirement (e.g., continuous or epoch signals) of various brain parameters (e.g., activation, static FC, and dynamic FC). The usefulness of those method applications has been also confirmed in a limited dataset though. Compared to the activation-based biomarkers, the connectivity-based biomarkers performed better. Even though the results were promising, clinical utilities of biomarkers based on task-based connectivities measured by fNIRS are still premature. The translational studies should be carried out with a support of greater datasets. Therefore, a future work will involve a massive data collection, validation of currently obtained evidence, and research-to-clinical transitions.

In Chapter 5, characteristics of dynamic FCs for TD and ADHD children were revealed. However, the use of these characteristics for biomarkers has not been investigated. Furthermore, the biomarkers explained in Chapters 3 and 4 were developed from different tasks (i.e., GNG and OB). The clinical biomarkers should be based on uniform and controllable brain measurements (e.g., task performance), and a validated guideline is highly required for the clinical application of biomarkers. Therefore, a more efficient biomarker, that may be associated with the dynamic FC characteristics, with combined functions of screening and differential diagnosis will be aimed in a future work.

Another prospective work is closely related to the optimization of task paradigm to accommodate more relevant (static and dynamic) FC features. A previous study reported that the robustness of FC features depends on the selected

window length. The insignificant effect of window lengths on FC features was partially confirmed (see 5.4.4). Thus, the extensive assessment is still required together with an attempt to optimize the task paradigm without neglecting the essential demand of short measurement time for disordered children. By doing these milestones, validated and robust biomarkers for screening and differential diagnosis of ADHD children are expectedly feasible for a clinical application.

Acknowledgment

References

Aarabi, A., and Huppert, T.J. (2016). Characterization of the relative contributions from systemic physiological noise to whole-brain resting-state functional near-infrared spectrosocpy data using single-channel independent component analysis. *Neurophotonics* 3(2), 025004, https://doi.org/10.1117/1.NPh.3.2.025004.

Abibullaev, B., and An, J. (2012). Decision support algorithm for diagnosis of ADHD using electroencephalograms. *Journal of Medical Systems* 36, 2675–2688, https://doi.org/10.1007/s10916-011-9742-x.

Adornetto, C., Suppiger, A., In-Albon, T., Neuschwander, M., and Schneider, S. (2012). Concordances and discrepancies between ICD-10 and DSM-IV criteria for anxiety disorders in childhood and adolescence. *Child and Adolescent Psychiatry and Mental Health* 6, 40, https://doi.org/10.1186/1753-2000-6-40.

Ahmadlou, M., and Adeli, H. (2010). Wavelet-synchronization methodology: A new approach for EEG-based diagnosis of ADHD. *Clinical EEG and Neuroscience* 41(1), 1–10, https://doi.org/10.1177/155005941004100103.

Akinbami, L.J., Liu, X., Pastor, P.N., and Reuben, C.A. (2011). Attention deficit hyperactivity disorder among children aged 5–17 years in the United States, 1998–2009. *NCHS Data Briefs* 70, 1–8.

Alderson, R.M., Rapport, M.D., Sarver, D.E., and Kofler, M.J. (2008). ADHD and behavioral inhibition: A re-examination of the stop-signal task. *Journal of Abnormal Child Psychology* 36, 989–998, https://doi.org/10.1007/s10802-008-9230-z.

American Psychiatric Association (2013). *Diagnostic and statistical manual of mental disorders (5th ed.).* Washington, DC: Author.

An, L., Cao, X.H., Cao, Q.J., Sun, L., Yang, L., Zou, Q.H., Rubia, K., Zang, Y.F., and Wang, Y.F. (2013). Methylphenidate normalizes resting-state brain dysfunction in boys with attention deficit hyperactivity disorder. *Neuropsychopharmacology* 38(7), 1287–295, https://doi.org/10.1038/npp.2013.27.

Araki, A., Ikegami, M., Okayama, A., Matsumoto, N., Takahashi, S., Azuma, H., and

Takahashi, M. (2015). Improved prefrontal activity in AD/HD children treated with atomoxetine: A NIRS study. *Brain and Development* 37(1), 76–87, https://doi.org/10.1016/j.braindev.2014.03.011.

Aron, A.R., Fletcher, P.C., Bullmore, E.T., Sahakian, B.J., and Robbins, T.W. (2003). Stop-signal inhibition disrupted by damage to right inferior frontal gyrus in humans. *Nature Neuroscience* 6(2), 115–116, https://doi.org/10.1038/nn1003.

Aron, A.R., Robbins, T.W., and Poldrack, R.A. (2004). Inhibition and the right inferior frontal cortex. *Trends in Cognitive Sciences* 8(4), 170–177, https://doi.org/10.1016/j.tics.2004.02.010.

Aron, A.R., Robbins, T.W., and Poldrack, R.A. (2014). Inhibition and the right inferior frontal cortex: One decade on. *Trends in Cognitive Sciences* 18(4), 177–185, https://doi.org/10.1016/j.tics.2013.12.003.

Ashtari, M., Kumra, S., Bhaskar, S.L., Clarke, T., Thaden, E., Cervellione, K.L., Rhinewine, J., Kane, J.M., Adesman, A., Milanaik, R., J., M., Diamond, A., Szeszko, P., and Ardekani, B.A. (2005). Attention-deficit/hyperactivity disorder: A preliminary diffusion tensor imaging study. *Biological Psychiatry* 57(5), 448–455, https://doi.org/10.1016/j.biopsych.2004.11.047.

Atsumori, H., Kiguchi, M., Obata, A., Sato, H., Katura, T., Funane, T., and Maki, A. (2009). Development of wearable optical topography system for mapping the prefrontal cortex activation. *Review of Scientific Instruments* 80(4), 043704–043706, https://doi.org/10.1063/1.3115207.

Banaschewski, T., Becker, K., Scherag, S., Franke, B., and Coghill, D. (2010). Molecular genetics of attention-deficit/hyperactivity disorder: An overview. *European Child and Adolescent Psychiatry* 19(3), 237–257, https://doi.org/10.1007/s00787-010-0090-z.

Barker, J.W., Aarabi, A., and Huppert, T.J. (2013). Autoregressive model based algorithm for correcting motion and serially correlated errors in fNIRS. *Biomedical Optics Express* 4(8), 1366–1379, https://doi.org/10.1364/BOE.4.001366.

Barttfeld, P., Uhrig, L., Sitt, J.D., Sigman, M., Jarraya, B., and Dehaene, S. (2015).

Signature of consciousness in the dynamics of resting-state brain activity. *Proceedings of the National Academy of Sciences of the United States of America* 112(3), 887–892, https://doi.org/10.1073/pnas.1418031112.

Bartzokis, G., Beckson, M., Lu, P.H., Nuechterlein, K.H., Edwards, N., and Mintz, J. (2001). Age-related changes in frontal and temporal lobe volumes in men. *Archives of General Psychiatry* 58(5), 461–465, https://doi.org/10.1001/archpsyc.58.5.461.

Beauregard, J.L., Drews-Botsch, C., Sales, J.M., Flanders, W.D., and Kramer, M.R. (2018). Preterm birth, poverty, and cognitive development. *Pediatrics* 141(1), e20170509, https://doi.org/10.1542/peds.2017-0509.

Belmonte, M.K., Allen, G., Beckel-Mitchener, A., Boulanger, L.M., Carper, R.A., and Webb, S.J. (2004). Autism and abnormal development of brain connectivity. *Journal of Neuroscience* 24(42), 9228–9231, https://doi.org/10.1523/JNEUROSCI.3340-04.2004.

Benaron, D.A., and Stevenson, D.K. (1993). Optical time-of-flight and absorbance imaging of biologic media. *Science* 259(5100), 1463–1466, https://doi.org/10.1126/science.8451643.

Benes, F.M. (1989). Myelination of cortical-hippocampal relays during late adolescence. *Schizophrenia Bulletin* 15(4), 585–593, https://doi.org/10.1093/schbul/15.4.585.

Benes, F.M., Turtle, M., and Khan, Y. (1994). Myelination of a key relay zone in the hippocampal formation occurs in the human brain during childhood, adolescence, and adulthood. *Archives of General Psychiatry* 51(6), 477–484, https://doi.org/10.1001/archpsyc.1994.03950060041004.

Benjamini, Y., and Hochberg, Y. (1995). Controlling the false discovery rate: A practical and powerful approach to multiple testing. *Journal of the Royal Statistical Society. Series B, Statistical Methodology* 57(1), 289–300, https://doi.org/10.1111/j.2517-6161.1995.tb02031.x.

Birn, R.M., Diamond, J.B., Smith, M.A., and Bandettini, P.A. (2006). Separating respiratory-variation-related fluctuations from neuronal-activity-related

fluctuations in fMRI. *NeuroImage* 31(4), 1536–1548, https://doi.org/10.1016/j.neuroimage.2006.02.048.

Biswal, B., Yetkin, F.Z., Haughton, V.M., and Hyde, J.S. (1995). Functional connectivity in the motor cortex of resting human brain using echo-planar MRI. *Magnetic Resonance in Medicine* 34(4), 537–541, https://doi.org/10.1002/mrm.1910340409.

Bjorklund, D.F. (2018). A metatheory for cognitive development (or "Piaget is dead" revisited). *Child Development* 89(6), 2288–2302, https://doi.org/10.1111/cdev.13019.

Boas, D.A., Elwell, C.E., Ferrari, M., and Taga, G. (2014). Twenty years of functional near-infrared spectroscopy: Introduction for the special issue. *NeuroImage* 85, 1–5, https://doi.org/10.1016/j.neuroimage.2013.11.033.

Bohland, J.W., Saperstein, S., Pereira, F., Rapin, J., and Grady, L. (2012). Network, anatomical, and non-imaging measures for the prediction of ADHD diagnosis in individual subjects. *Frontiers in Systems Neuroscience* 6, 78, https://doi.org/10.3389/fnsys.2012.00078.

Bossuyt, P.M.M., Reitsma, J.B., Linnet, K., and Moons, K.G.M. (2012). Beyond diagnostic accuracy: The clinical utility of diagnostic tests. *Clinical Chemistry* 58(12), 1636–1643, https://doi.org/10.1373/clinchem.2012.182576.

Boy, F., Evans, C.J., Edden, R.A.E., Lawrence, A.D., Singh, K.D., Husain, M., and Sumner, P. (2011). Dorso-lateral prefrontal γ-amino butyric acid in men predicts individual differences in rash impulsivity. *Biological Psychiatry* 70(9), 866–872, https://doi.org/10.1016/j.biopsych.2011.05.030.

Boyle, C.A., Boulet, S., Schieve, L.A., Cohen, R.A., Blumberg, S.J., Yeargin-Allsopp, M., Visser, S.N., and Kogan, M.D. (2011). Trends in the prevalence of developmental disabilities in US children, 1997-2008. *Pediatrics* 127(6), 1034–1042, https://doi.org/10.1542/peds.2010-2989.

Boynton, G.M., Engel, S.A., Glover, G.H., and Heeger, D.J. (1996). Linear systems analysis of functional magnetic resonance imaging in human V1. *Journal of*

Neuroscience 16(13), 4207–4221, https://doi.org/10.1523/JNEUROSCI.16-13-04207.1996.

Braun, U., Schäfer, A., Walter, H., Erk, S., Romanczuk-Seiferth, N., Haddad, L., Schweiger, J.I., Grimm, O., Heinz, A., Tost, H., Meyer-Lindenberg, A., and Bassett, D.S. (2015). Dynamic reconfiguration of frontal brain networks during executive cognition in humans. *Proceedings of the National Academy of Sciences of the United States of America* 112(37), 11678–11683, https://doi.org/10.1073/pnas.1422487112.

Brigadoi, S., Ceccherini, L., Cutini, S., Scarpa, F., Scatturin, P., Selb, J., Gagnon, L., Boas, D.A., and Cooper, R.J. (2014). Motion artifacts in functional near-infrared spectroscopy: A comparison of motion correction techniques applied to real cognitive data. *NeuroImage* 85, 181–191, https://doi.org/10.1016/j.neuroimage.2013.04.082.

Brown, M.R.G., Sidhu, G.S., Greiner, R., Asgarian, N., Bastani, M., Silverstone, P.H., Greenshaw, A.J., and Dursun, S.M. (2012). ADHD-200 Global Competition: Diagnosing ADHD using personal characteristic data can outperform resting state fMRI measurements. *Frontiers in Systems Neuroscience* 6, 69, https://doi.org/10.3389/fnsys.2012.00069.

Brown, T.E. (2004). Atomoxetine and stimulants in combination for treatment of attention deficit hyperactivity disorder: Four case reports. *Journal of Child and Adolescent Psychopharmacology* 14(1), 129–136, https://doi.org/10.1089/104454604773840571.

Bunge, S.A., and Kahn, I. (2009). Cognition: An overview of neuroimaging technique. *Encyclopedia of Neuroscience* 2, 1063–1067, https://doi.org/10.1016/B978-008045046-9.00298-9.

Bush, G. (2010). Attention-deficit/hyperactivity disorder and attention networks. *Neuropsychopharmacology* 35(1), 278–300, https://doi.org/10.1038/npp.2009.120.

Bush, G. (2011). Cingulate, frontal and parietal cortical dysfunction in attention-

deficit/hyperactivity disorder. *Biological Psychiatry* 69(12), 1160–1167, https://doi.org/10.1016/j.biopsych.2011.01.022.

Buxton, R.B., Uludağ, K., Dubowitz, D.J., and Liu, T.T. (2004). Modeling the hemodynamic response to brain activation. *NeuroImage* 23(Suppl 1), S220–S233, https://doi.org/10.1016/j.neuroimage.2004.07.013.

Buyck, I., and Wiersema, J.R. (2014). Resting electroencephalogram in attention deficit hyperactivity disorder: Developmental course and diagnostic value. *Psychiatry Research* 216(3), 391–397, https://doi.org/10.1016/j.psychres.2013.12.055.

Buzy, W.M., Medoff, D.R., and Schweitzer, J.B. (2009). Intra-individual variability among children with ADHD on a working memory task: An Ex-Gaussian approach. *Child Neuropsychology* 15(5), 441–459, https://doi.org/10.1080/09297040802646991.

Bymaster, F.P., Katner, J.S., Nelson, D.L., Hemrick-Luecke, S.K., Threlkeld, P.G., Heiligenstein, J.H., Morin, S.M., Gehlert, D.R., and Perry, K.W. (2002). Atomoxetine increases extracellular levels of norepinephrine and dopamine in prefrontal cortex of rat: A potential mechanism for efficacy in attention deficit/hyperactivity disorder. *Neuropsychopharmacology* 27(5), 699–711, https://doi.org/10.1016/S0893-133X(02)00346-9.

Casey, B.J., Cohen, J.D., Jezzard, P., Turner, R., Noll, D.C., Trainor, R.J., Giedd, J., Kaysen, D., Hertz-Pannier, L., and Rapoport, J.L. (1995). Activation of prefrontal cortex in children during a nonspatial working memory task with functional MRI. *NeuroImage* 2(3), 221–229, https://doi.org/10.1006/nimg.1995.1029.

Casey, B.J., Giedd, J.N., and Thomas, K.M. (2000). Structural and functional brain development and its relation to cognitive development. *Biological Psychology* 54(1–3), 241–257, https://doi.org/10.1016/S0301-0511(00)00058-2.

Casey, B.J., Trainor, R.J., Orendi, J.L., Schubert, A.B., Nystrom, L.E., Giedd, J.N., Castellanos, F.X., Haxby, J.V., Noll, D.C., Cohen, J.D., Forman, S.D., Dahl, R.E., and Rapoport, J.L. (1997). A developmental functional MRI study of prefrontal activation during performance of a go-no-go task. *Journal of Cognitive*

Neuroscience 9(6), 835–847, https://doi.org/10.1162/jocn.1997.9.6.835.

Castellanos, F.X., Clare Kelly, A.M., and Milham, M.P. (2009). The restless brain: attention-deficit/hyperactivity disorder, resting state functional connectivity and intrasubject variability. *Canadian Journal of Psychiatry* 54(10), 665–672, hrrps://doi.org/10.1177/070674370905401003.

Castellanos, F.X., Margulies, D.S., Clare Kelly, A.M., Uddin, L.Q., Ghaffari, M., Kirsch, A., Shaw, D., Shehzad, Z., di Martino, A., Biswal, B., Sonuga-Barke, E.J.S., Rotrosen, J., Adler, L., and Milham, M.P. (2008). Cingulate - Precuneus interactions: A new locus of dysfunction in adult attention-deficit/hyperactivity disorder. *Biological Psychiatry* 63(3), 332–337, https://doi.org/10.1016/j.biopsych.2007.06.025.

Castellanos, F.X., Sonuga-Barke, E.J.S., Milham, M.P., and Tannock, R. (2006). Characterizing cognition in ADHD: Beyond executive dysfunction. *Trends in Cognitive Sciences* 10(3), 117–123, https://doi.org/10.1016/j.tics.2006.01.011.

Chance, B., Dait, M.T., Zhang, C., Hamaoka, T., and Hagerman, F. (1992). Recovery from exercise-induced desaturation in the quadriceps muscles of elite competitive rowers. *American Journal of Physiology* 262, C766–C775, https://doi.org/10.1152/ajpcell.1992.262.3.C766.

Chang, C., and Glover, G.H. (2010). Time-frequency dynamics of resting-state brain connectivity measured with fMRI. *NeuroImage* 50(1), 81–98, https://doi.org/10.1016/j.neuroimage.2009.12.011.

Chang, C., Metzger, C.D., Glover, G.H., Duyn, J.H., Heinze, H.J., and Walter, M. (2013). Association between heart rate variability and fluctuations in resting-state functional connectivity. *NeuroImage* 68, 93–104, https://doi.org/10.1016/j.neuroimage.2012.11.038.

Chang, C.W., Ho, C.C., and Chen, J.H. (2012). ADHD classification by a texture analysis of anatomical brain MRI data. *Frontiers in Systems Neuroscience* 6, 66, https://doi.org/10.3389/fnsys.2012.00066.

Chantiluke, K., Barret, N., Giampietro, V., Santosh, P., Brammer, M., Simmons, A.,

Murphy, D.G., and Rubia, K. (2015). Inverse fluoxetine effects on inhibitory brain activation in non-comorbid boys with ADHD and with ASD. *Psychopharmacology* 232(12), 2071–2082, https://doi.org/10.1007/s00213-014-3837-2.

Chantiluke, K., Chistakou, A., Murphy, C.M., Giampietro, V., Daly, E.M., Ecker, C., Brammer, M., Murphy, D.G., the MRC AIMS Consortium, and Rubia, K. (2014). Disorder-specific functional abnormalities during temporal discounting in youth with attention deficit hyperactivity disorder (ADHD), autism, and comorbid ADHD and ASD. *Psychiatry Research: Neuroimaging* 223(2), 113–120, https://doi.org/10.1016/j.pscychresns.2014.04.006.

Cheng, W., Ji, X., Zhang, J., and Feng, J. (2012). Individual classification of ADHD patients by integrating multiscale neuroimaging markers and advanced pattern recognition techniques. *Frontiers in Systems Neuroscience* 6, 58, https://doi.org/10.3389/fnsys.2012.00058.

Chiarelli, A.M., Maclin, E.L., Fabiani, M., and Gratton, G. (2015). A kurtosis-based wavelet algorithm for motion artifact correction of fNIRS data. *NeuroImage* 112, 128–137, https://doi.org/10.1016/j.neuroimage.2015.02.057.

Chochon, F., Cohen, L., van de Moortele, P.F., and Dehaene, S. (1999). Differential contributions of the left and right inferior parietal lobules to number processing. *Journal of Cognitive Neuroscience* 11(6), 617–630, https://doi.org/10.1162/089892999563689.

Choi, J., Jeong, B., Lee, S.W., and Go, H.J. (2013). Aberrant development of functional connectivity among resting state-related functional networks in medication-naive ADHD children. *PLoS One* 8(12), e83516, https://doi.org/10.1371/journal.pone.0083516.

Christensen, D.L., Baio, J., Braun, K.V., Bilder, D., Charles, J., Constantino, J.N., Daniels, J., Durkin, M.S., Fitzgerald, R.T., Kurzius-Spencer, M., Lee, L.C., Pettygrove, S., Robinson, C., Schulz, E., Wells, C., Wingate, M.S., Zahorodny, W., and Yeargin-Allsopp, M. (2016). Prevalence and characteristics of autism spectrum disorder

among children aged 8 years - autism and developmetal disabilities monitoring network, 11 sites, United States, 2012. *Morbidity and Mortality Weekly Report Surveillance Summaries* 65(No. SS-3), 1–23, http://dx.doi.org/10.15585/mmwr.ss6503a1.

Cohen, J.D., Forman, S.D., Braver, T.S., Casey, B.J., Servan-Schreiber, D., and Noll, D.C. (1994a). Activation of prefrontal cortex in a nonspatial working memory task with functional MRI. *Human Brain Mapping* 1(4), 293–304, https://doi.org/10.1002/hbm.460010407.

Cohen, M.S., and Bookheimer, S.Y. (1994b). Localization of brain function using magnetic resonance imaging. *Trends in Neuroscience* 17(7), 268–277, https://doi.org/10.1016/0166-2236(94)90055-8.

Cole, M.W., Bassett, D.S., Power, J.D., Braver, T.S., and Petersen, S.E. (2014). Intrinsic and task-evoked network architectures of the human brain. *Neuron* 83(1), 238–251, https://doi.org/10.1016/j.neuron.2014.05.014.

The ADHD-200 Consortium. (2012). The ADHD-200 Consortium: A model to advance the translational potential of neuroimaging in clinical neuroscience. *Frontiers in Systems Neuroscience* 6, 62, https://doi.org/10.3389/fnsys.2012.00062.

Contini, D., Spinelli, L., Torricelli, A., Pifferi, A., and Cubeddu, R. (2007). Novel method for depth-resolved brain functional imaging by time-domain NIRS. *Proceedings of SPIE* 6629, 662908, https://doi.org/10.1117/12.728104.

Cooper, R.J., Selb, J., Gagnon, L., Phillip, D., Schytz, H.W., Iversen, H.K., Ashina, M., and Boas, D.A. (2012). A systemic comparison of motion artifact correction techniques for functional near-infrared spectroscopy. *Frontiers in Neuroscience* 6, 147, https://doi.org/10.3389/fnins.2012.00147.

Cope, M., and Delpy, D.T. (1988). System for long-term measurement of cerebral blood and tissue oxygenation on newborn infants by near infra-red transillumination. *Medical and Biological Engineering and Computation* 26(3), 289–294, https://doi.org/10.1007/BF02447083.

Cope, M., van der Zee, P., Essenpreis, M., Arridge, S.R., and Delpy, D.T. (1991). Data

analysis methods for near infrared spectroscopy of tissue: Problems in determining the relative cytochrome AA3 concentration. *Proceedings of SPIE* 1431, 251–262, https://doi.org/10.1117/12.44196.

Corlu, A., Choe, R., Durduran, T., Lee, K., Schweiger, M., Arridge, S.R., Hillman, E.M.C., and Yodh, A.G. (2005). Diffuse optical tomography with spectral constraints and wavelength optimization. *Applied Optics* 44(11), 2082–2093, https://doi.org/10.1364/AO.44.002082.

Corlu, A., Durduran, T., Choe, R., Schweiger, M., Hillman, E.M.C., Arridge, S.R., and Yodh, A.G. (2003). Uniqueness and wavelength optimization in continuous-wave multispectral diffuse optical tomography. *Optics Letters* 23(28), 2339–2341, https://doi.org/10.1364/OL.28.002339.

Cortese, S., Kelly, C., Chabernaud, C., Proal, E., Di Martino, A., Milham, M.P., and Castellanos, F.X. (2012). Towards systems neuroscience of ADHD: A meta-analysis of 55 fMRI studies. *American Journal of Psychiatry* 169(10), 18, https://doi.org/10.1176/appi.ajp.2012.11101521.

Cui, X., Bray, S., Bryant, D.M., Glover, G.H., and Reiss, A.L. (2011). A quantitative comparison of NIRS and fMRI across multiple cognitive tasks. *Neuroimage* 54(4), 2808–2821, https://doi.org/10.1016/j.neuroimage.2010.10.069.

Cui, X., Bray, S., and Reiss, A.L. (2010). Functional near infrared spectroscopy (NIRS) signal improvement based on negative correlation between oxygenated and deoxygenated hemoglobin dynamics. *NeuroImage* 49(4), 3039–3046, https://doi.org/10.1016/j.neuroimage.2009.11.050.

Döpfner, M., Breuer, D., Wille, N., Erhart, M., and Ravens-Sieberer, U. (2008). How often do children meet ICD-10/DSM-IV criteria of attention deficit-/hyperactivity disorder and hyperkinetic disorder? Parent-based prevalence rates in a national sample-results of the BELLA study. *European Child and Adolescent Psychiatry* 17(Suppl 1), 59–70, https://doi.org/10.1007/s00787-008-1007-y.

Damaraju, E., Allen, E.A., Belger, A., Ford, J.M., McEwen, S., Mathalon, D.H., Mueller, B.A., Pearlson, G.D., Potkin, S.G., Preda, A., Turner, J.A., Vaidya, J.G., van Erp,

T.G., and Calhoun, V.D. (2014). Dynamic functional connectivity analysis reveals transient states of dysconnectivity in schizophrenia. *NeuroImage: Clinical* 5, 298–308, https://doi.org/10.1016/j.nicl.2014.07.003.

Davies, D.J., Clancy, M., Lighter, D., Balanos, G.M., Lucas, S.J.E., Dehghani, H., Su, Z., Forcione, M., and Belli, A. (2017). Frequency-domain vs continuous-wave near-infarred spectroscopy devices: A comparison of clinically viable monitors in controlled hypoxia. *Journal of Clinical Monitoring and Computing* 31, 967–974, https://doi.org/10.1007/s10877-016-9942-5.

Davis, N.O., and Kollins, S.H. (2012). Treatment for co-occuring attention deficit/hyperactivity disorder and autism spectrum disorder. *Neurotherapeutics* 9(3), 518–530, https://doi.org/10.1007/s13311-012-0126-9.

de Ribaupierre, A. (2015). Why should cognitive developmental psychology remember that individuals are different? *Research in Human Development* 12, 237–245, https://doi.org/10.1080/15427609.2015.1068059.

de Ribaupierre, A., and Lecerf, T. (2018). On the importance of intraindividual variability in cognitive development. *Journal of Intelligence* 6(2), 17, https://doi.org/10.3390/jintelligence6020017.

Delpy, D.T., and Cope, M. (1997). Quantification in tissue near-infrared spectroscopy. *Philosophical Transactions of the Royal Society B: Biological Sciences* 352(1354), 649–659, https://doi.org/10.1098/rstb.1997.0046.

Delpy, D.T., Cope, M., van der Zee, P., Arridge, S., Wray, S., and Wyatt, J. (1988). Estimation of optical pathlength through tissue from direct time of flight measurement. *Physics in Medicine and Biology* 33(12), 1433–1442, https://doi.org/10.1088/0031-9155/33/12/008.

Devonshire, I.M., Papadakis, N.G., Port, M., Berwick, J., Kennerley, A.J., Mayhew, J.E.W., and Overton, P.G. (2012). Neurovascular coupling is brain region-dependent. *NeuroImage* 59(3), 1997–2006, https://doi.org/10.1016/j.neuroimage.2011.09.050.

Dey, S., Rao, A.R., and Shah, M. (2012). Exploiting the brain's network structure in

identifying ADHD subjects. *Frontiers in Systems Neuroscience* 6, 75, https://doi.org/10.3389/fnsys.2012.00075.

Diamond, A. (2000). Close interrelation of motor development and cognitive development and of the cerebellum and prefrontal cortex. *Child Development* 71(1), 44–56, https://doi.org/ 10.1111/1467-8624.00117.

Diop, M., Tichauer, K.M., Elliott, J.T., Miqueis, M., Lee, T.Y., and Lawrence, K.S. (2010). Comparison of time-resolved and continuous wave near-infarred techniques for measuring cerebral blood flow in piglets. *Journal of Biomedical Optics* 15(5), 057004, https://doi.org/10.1117/1.3488626.

Djuwari, D., Kumar, D.K., and Palaniswami, M. (2006) Limitations of ICA for artefact removal. *Conference Proceedings IEEE Engineering in Medicine and Biology Society* 2005, 4685–4688, https://doi.org/10.1109/IEMBS.2005.1615516.

Dodds, C.M., Morein-Zamir, S., and Robbins, T.W. (2011). Dissociating inhibition, attention, and response control in the frontoparietal network using functional magnetic resonance imaging. *Cerebral Cortex* 21(5), 1155–1165, https://doi.org/ 10.1093/cercor/bhq187.

Doucet, G., Naveau, M., Petit, L., Zago, L., Crivello, F., Jobard, G., Delcroix, N., Mellet, E., Tzourio-Mazoyer, N., Mazoyer, B., and M., J. (2012). Patterns of hemodynamic low-frequency oscillations in the brain are modulated by the nature of free thought during rest. *NeuroImage* 59(4), 3194–3200, https://doi.org/10.1016/j.neuroimage.2011.11.059.

Duan, L., Zhang, Y.J., and Zhu, C.Z. (2012). Quantitative comparison of resting-state functional connectivity derived from fNIRS and fMRI: A simultaneous recording study. *NeuroImage* 60(4), 2008–2018, https://doi.org/10.1016/ j.neuroimage.2012.02.014.

Dunn, O.J. (1961). Multiple comparisons among means. *Journal of the American Statistical Association* 56(293), 52–64, https://www.jstor.org/stable/2282330.

Durston, S., Hulshoff, H.E., Casey, B.J., Giedd, J.N., Buitelaar, J.K., and van Engeland, H. (2001). Anatomical MRI of the developing human brain: What have we

learned? *Journal of the American Academy of Child and Adolescent Psychiatry* 40(9), 1012–1020, https://doi.org/10.1097/00004583-200109000-00009.

Durston, S., Tottenham, N.T., Thomas, K.M., Davidson, M.C., Eigsti, I.M., Yang, Y., Ulug, A.M., and Casey, B.J. (2003). Differential patterns of striatal activation in young children with and without ADHD. *Biological Psychiatry* 53(10), 871–878, https://doi.org/10.1016/S0006-3223(02)01904-2.

Dyck, M.J., and Piek, J.P. (2014). Developmental delays in children with ADHD. *Journal of Attention Disorders* 18(5), 466–478, https://doi.org/10.1177/1087054712441832.

Erdoğan, S.B., Yücel, M.A., and Akin, A. (2014). Analysis of task-evoked systemic interference in fNIRS measurements: Insights from fMRI. *NeuroImage* 87, 490–504, https://doi.org/10.1016/j.neuroimage.2013.10.024.

Erika-Florence, M., Leech, R., and Hampshire, A. (2014). A functional network perspective on response inhibition and attentional control. *Nature Communications* 5, 4073, https://doi.org/10.1038/ncomms5073.

Esposito, F., Seifritz, E., Formisano, E., Morrone, R., Scarabino, T., Tedeschi, G., Cirillo, S., R., G., and Di Salle, F. (2003). Real-time independent component analysis of fMRI time-series. *NeuroImage* 20(4), 2209–2224, https://doi.org/10.1016/j.neuroimage.2003.08.012.

Fair, D.A., Posner, J., Nagel, B.J., Bathula, D., Costa Dias, T.G., Mills, K.L., Blythe, M.S., Giwa, A., Schmitt, C.F., and Nigg, J.T. (2010). Atypical default network connectivity in youth with ADHD. *Biological Psychiatry* 68(12), 1084–1091, https://doi.org/10.1016/j.biopsych.2010.07.003.

Fantini, S., Franceschini, M.A., and Gratton, E. (1994). Semi-infinite-geometry boundary problem for light migration in highly scattering media: A frequency-domain study in the diffusion approximation. *Journal of the Optical Society of America B* 11(10), 2128–2138, https://doi.org/10.1364/JOSAB.11.002128.

Faraone, S.V., and Biederman, J. (1998). Neurobiology of attention-deficit hyperactivity disorder. *Biological Psychiatry* 44(10), 951–958, https://doi.org/10.1016/S0006-

3223(98)00240-6.

Fekete, T., Rubin, D., Carlson, J.M., and Mujica-Parodi, L.R. (2011). The NIRS Analysis Package: Noise reduction and statistical inference. *PLoS One* 6(9), e24322, https://doi.org/10.1371/journal.pone.0024322.

Ferrari, M., Mottola, L., and Quaresima, V. (2004). Principles, techniques, and limitations of near infrared spectroscopy. *Canadian Journal of Applied Physiology* 29(4), 463–487, https://doi.org/10.1139/h04-031.

Ferrari, M., and Quaresima, V. (2012). A brief review on the history of human functional near-infrared spectroscopy (fNIRS) development and fields of application. *NeuroImage* 63(2), 921–935, https://doi.org/10.1016/j.neuroimage.2012.03.049.

Firk, C., Konrad, K., Herpertz-Dahlmann, B., Scharke, W., and Dahmen, B. (2018). Cognitive development in children of adolescent mothers: The impact of socioeconomic risk and maternal sensitivity. *Infant Behavior and Development* 50, 238–246, https://doi.org/10.1016/j.infbeh.2018.02.002.

Fishburn, F.A., Norr, M.E., Medvedev, A.V., and Vaidya, C.J. (2014). Sensitivity of fNIRS to cognitive state and load. *Frontiers in Human Neuroscience* 8, 76, https://doi.org/10.3389/fnhum.2014.00076.

Fonseca, A.L.M., Albernaz, E.P., Kaufmann, C.C., Nevez, I.H., and de Figueiredo, V.L. (2013). Impact of breastfeeding on the intelligence quotient of eight-year-old children. *Journal of Pediatrics* 89(4), 346–353, https://doi.org/10.1016/j.jpedp.2012.12.013.

Fox, M.D., Snyder, A.Z., Vincent, J.L., Corbetta, M., Van Essen, D.C., and Raichle, M.E. (2005). The human brain is intrinsically organized into dynamic, anticorrelated functional networks. *Proceedings of the National Academy of Sciences of the United States of America* 102(27), 9673–9678, https://doi.org/10.1073/pnas.0504136102.

Franceschini, M.A., Boas, D.A., Zourabian, A., Diamond, S.G., Nadgir, S., Lin, D.W., Moore, J.B., and Fantini, S. (2002). Near-infrared spiroximetry: Noninvasive measurements of venous saturation in piglets and human subjects. *Journal of*

Applied Physiology 92(1), 372–384, https://doi.org/10.1152/jappl.2002.92.1.372.

Franceschini, M.A., Fantini, S., Thompson, J.H., Culver, J.P., and Boas, D.A. (2003). Hemodynamic evoked response of the sensorimotor cortex measured noninvasively with near-infrared optical imaging. *Psychophysiology* 40(4), 548–560, https://doi.org/10.1111/1469-8986.00057.

Franceschini, M.A., Toronov, V., Filiaci, M., Gratton, E., and Fantini, S. (2000). On-line optical imaging of the human brain with 160-ms temporal resolution. *Optics Express* 6(3), 49–57, https://doi.org/10.1364/oe.6.000049.

Frazier, T.W., Shattuck, P.T., Narendorf, S.C., Cooper, B.P., Wagner, M., and Spitznagel, E.L. (2011). Prevalence and correlates of psychotropic medication use in adolescents with an autism spectrum disorder with and without caregiver-reported attention-deficit/hyperactivity disorder. *Journal of Child and Adolescent Psychopharmacology* 21(6), 571–579, https://doi.org/10.1089/cap.2011.0057.

Friston, K.J., Holmes, A.P., Poline, J.B., Grasby, P.J., Williams, S.C.R., Frackowiak, R.S.J., and Turner, R. (1995). Analysis of fMRI time-series revisited. *NeuroImage* 2(1), 45–53, https://doi.org/10.1006/nimg.1995.1007.

Friston, K.J., Holmes, A.P., Worsley, K.J., Poline, J.P., Firith, C.D., and Frackowiak, R.S.J. (1994a). Statistical parametric maps in functional imaging: A general linear approach. *Human Brain Mapping* 2(4), 189–210, https://doi.org/10.1002/hbm.460020402.

Friston, K.J., Jezzard, P., and Turner, R. (1994b). Analysis of functional MRI time-series. *Human Brain Mapping* 1(2), 153–171, https://doi.org/10.1002/hbm.460010207.

Fu, C.H.Y., and Costafreda, S.G. (2013). Neuroimaging-based biomarkers in psychiatry: Clinical opportunities of a paradigm shift. *Canadian Journal of Psychiatry* 58(9), 499–508, https://doi.org/10.1177/070674371305800904.

Funane, T., Atsumori, H., Katura, T., Obata, A.N., Sato, H., Tanikawa, Y., Okada, E., and Kiguchi, M. (2014). Quantitative evaluation of deep and shallow tissue layers' contribution to fNIRS signal using multi-distance optodes and independent component analysis. *NeuroImage* 85, 150–165, https://doi.org/10.1016/

j.neuroimage.2013.02.026.

Gadow, K.D., DeVincent, C.J., and Pomeroy, J. (2006). ADHD symptom subtypes in children with pervasive developmental disorder. *Journal of Autism and Developmental Disorders* 36(2), 271–283, https://doi.org/10.1007/s10803-005-0060-3.

Gagnon, L., Gauthier, C., Hoge, R.D., Lesage, F., Selb, J., and Boas, D.A. (2008). Double-layer estimation of intra- and extracerebral hemoglobin concentration with a time-resolved system. *Journal of Biomedical Optics* 13(5), 054019, https://doi.org/10.1117/1.2982524.

Garavan, H., Ross, T.J., and Stein, E.A. (1999). Right hemispheric dominance of inhibitory control: An event-related functional MRI study. *Proceedings of the National Academy of Sciences of the United States of America* 96(14), 8301–8306, https://doi.org/10.1073/pnas.96.14.8301.

Germon, T.J., Evans, P.D., Manara, A.R., Barnett, N.J., Wall, P., and Nelson, R.J. (1998). Sensitivity of near infrared spectroscopy to cerebral and extra-cerebral oxygenation changes is determined by emitter-detector separation. *Journal of Clinical Monitoring and Computing* 14(5), 353–360, https://doi.org/10.1023/A:1009957032554.

Giedd, J.N., Blumenthal, J., Jeffries, N.O., Castellanos, F.X., Liu, H., Zijidenbos, A., Paus, T., Evans, A.C., and Rapoport, J.L. (1999). Brain development during childhood and adolescence: A longitudinal MRI study. *Nature Neuroscience* 2(10), 861–863, https://doi.org/10.1038/13158.

Gilmore, A., and Milne, R. (2001). Methylphenidate in children with hyperactivity: Review and cost–utility analysis. *Pharmacoepidemiology and Drug Safety* 10(2), 85–94, https://doi.org/10.1002/pds.564.

Glover, G.H. (1999). Deconvolution of impulse response in event-related BOLD fMRI. *NeuroImage* 9(4), 416–429, https://doi.org/10.1006/nimg.1998.0419.

Gmehlin, D., Fuermaier, A.B.M., Walther, S., Debelak, R., Rentrop, M., Westermann, C., Sharma, A., Tucha, L., Koerts, J., Tucha, O., Weisbrod, M., and Aschenbrenner,

S. (2014). Intraindividual variability in inhibitory function in adults with ADHD - An Ex-Gaussian approach. *PLoS One* 9(12), e112298, https://doi.org/10.1371/journal.pone.0112298.

Gogtay, N., Gledd, J.N., Lusk, L., Hayashi, K.M., Greenstein, D., Vaituzis, C.A., Nugent III, T.F., Herman, D.H., Clasen, L.S., Toga, A.W., Rapoport, J.L., and Thompson, P.M. (2004). Dynamic mapping of human cortical development during childhood through early adulthood. *Proceedings of the National Academy of Sciences of the United States of America* 101(21), 8174–8179, https://doi.org/10.1073/pnas.0402680101.

Goldstein, S., and Schwebach, A.J. (2004). The comorbidity of pervasive developmental disorder and attention deficit hyperactivity disorder: Results of a retrospective chart review. *Journal of Autism and Developmental Disorders* 34, 329–339, https://doi.org/10.1023/B:JADD.0000029554.46570.68.

Gonzalez-Castillo, J., and Bandettini, P.A. (2018). Task-based dynamic functional connectivity: Recent findings and open questions. *NeuroImage* 180(Pt B), 526–533, https://doi.org/10.1016/j.neuroimage.2017.08.006.

Gonzalez-Castillo, J., Hoy, C.W., Handwerker, D.A., Robinson, M.E., Buchanan, L.C., Saad, Z.S., and Bandettini, P.A. (2015). Tracking ongoing cognition in individuals using brief, whole-brain functional connectivity patterns. *Proceedings of the National Academy of Sciences of the United States of America* 112(28), 8762–8767, https://doi.org/10.1073/pnas.1501242112.

Goutte, C., Nielsen, F.Å., and Hansen, L.K. (2000). Modeling the haemodynamic response in fMRI using smooth FIR filters. *IEEE Transactions on Medical Imaging* 19(12), 1188–1201, https://doi.org/10.1109/42.897811.

Grassi, B., Quaresima, V., Marconi, C., Ferrari, M., and Cerretelli, P. (1999). Blood lactate accumulation and muscle deoxygenation during incremental exercise. *Journal of Applied Physiology* 87, 348–355, https://doi.org/10.1152/jappl.1999.87.1.348.

Gratton, E., Fantini, S., Franceschini, M.A., Gratton, S., and Fabiani, M. (1997). Measurements of scattering and absroption changes in muscle and brain.

Philosophical Transactions of the Royal Society B: Biological Sciences 352(1354), 727–735, https://doi.org/10.1098/rstb.1997.0055.

Greenhill, L., Kollins, S., Abikoff, H., McCracken, J., Riddle, M., Swanson, J., McCGough, J., Wigal, S., Wigal, T., Vitiello, B., Skrobala, A., Posner, K., Ghuman, J., Cunningham, C., Davies, M., Chuang, S., and Cooper, T. (2006). Efficacy and safety of immediate-release methylphenidate treatment for preschoolers with ADHD. *Journal of the American Academy of Child and Adolescent Psychiatry* 45(11), 1284–1293, https://doi.org/10.1097/01.chi.0000235077.32661.61.

Greenhill, L.L., Abikoff, H.B., Arnold, L.E., Cantwell, D.P., Conners, C.K., Elliott, G., Hechtman, L., Hinshaw, S.P., Hoza, B., Jensen, P.S., March, J.S., Newcorn, J., Pelham, W.E., Severe, J.B., Swanson, J.M., Vitiello, B., and Wells, K. (1996). Medication treatment strategies in the MTA study: Relevance to clinicians and researchers. *Journal of the American Academy of Child and Adolescent Psychiatry* 35(10), 1304–1313, https://doi.org/10.1097/00004583-199610000-00017.

Hager, B.M., and Keshavan, M.S. (2015). Neuroimaging biomarkers for psychosis. *Current Behavioral Neuroscience Reports* 2, 102–111, https://doi.org/10.1007/s40473-015-0035-4.

Hampshire, A., Chamberlain, S.R., Monti, M.M., Duncan, J., and Owen, A.M. (2010). The role of the right inferior frontal gyrus: Inhibition and attentional control. *NeuroImage* 50(3), 1313–1319, https://doi.org/10.1016/j.neuroimage.2009.12.109.

Handwerker, D.A., Ollinger, J.M., and D'Esposito, M. (2004). Variation of BOLD hemodynamic responses across subjects and brain regions and their effects on statistical analyses. *NeuroImage* 21(4), 1639–1651, https://doi.org/10.1016/j.neuroimage.2003.11.029.

Hanwella, R., Senanayake, M., and de Silva, V. (2011). Comparative efficacy and acceptability of methylphenidate and atomoxetine in treatment of attention deficit hyperactivity disorder in children and adolescents: A meta-analysis. *BMC*

Psychiatry 11, 176, https://doi.org/10.1186/1471-244X-11-176.

Hart, H., Chantiluke, K., Cubillo, A.I., Smith, A.B., Simmons, A., Brammer, M.J., Marquand, A.F., and Rubia, K. (2014). Pattern classification of response inhibition in ADHD: Toward the development of neurobiological markers for ADHD. *Human Brain Mapping* 35(7), 3083–3094, https://doi.org/10.1002/hbm.22386.

Hart, H., Radua, J., Nakao, T., Mataix-Cols, D., and Rubia, K. (2013). Meta-analysis of functional magnetic resonance imaging studies of inhibition and attention in attention-deficit/hyperactivity disorder. *JAMA Psychiatry* 70(2), 185–198, https://doi.org/10.1001/jamapsychiatry.2013.277.

Hebden, J.C., Arridge, S.R., and Delpy, D.T. (1997). Optical imaging in medicine: I. Experimental techniques. *Physics in Medicine and Biology* 42(5), 825–840, https://doi.org/10.1088/0031-9155/42/5/007.

Helgadóttir, H., Gudmundsson, Ó.Ó., Baldursson, G., Magnússon, P., Blin, N., Brynjólfsdóttir, B., Emilsdóttir, Á., Gudmundsdóttir, G.B., Lorange, M., Newman, P.K., Jóhannesson, G.H., and Johnsen, K. (2015). Electroencephalography as a clinical tool for diagnosing and monitoring attention deficit hyperactivity disorder: A cross-sectional study. *BMJ Open* 5(1), e005500, https://doi.org/10.1136/bmjopen-2014-005500.

Herrmann, M.J., Ehlis, A.C., and Fallgatter, A.J. (2004). Bilaterally reduced frontal activation during a verbal fluency task in depressed patients as measured by near-infrared spectroscopy. *Journal of Neuropsychiatry and Clinical Neurosciences* 16(2), 170–175, https://doi.org/10.1176/appi.neuropsych.16.2.170.

Herrmann, M.J., Plichta, M.M., Ehlis, A.C., and Fallgatter, A.J. (2005). Optical topography during a Go-NoGo task assessed with multi-channel near-infrared spectroscopy. *Behavioural Brain Research* 160(1), 135–140, https://doi.org/10.1016/j.bbr.2004.11.032.

Hill, H.A., Elam-Evans, L.D., Yankey, D., Singleton, J.A., and Kolasa, M. (2015). National, State, and selected local area vaccination coverage among children aged

19–35 months – United States, 2014. *Morbidity and Mortality Weekly Report* 64(33), 889–896, https://doi.org/10.15585/mmwr.mm6433a1.

Hirasawa, A., Yanagisawa, S., Tanaka, N., Funane, T., Kiguchi, M., Sorensen, H., Secher, N.H., and Ogoh, S. (2014). Influence of skin blood flow and source-detector distance on near-infrared spectroscopy-determined cerebral oxygenation in humans. *Clinical Physiology and Functional Imaging* 35(3), 237–244, https://doi.org/10.1111/cpf.12156.

Hochberg, Y., and Tamhane, A.C. (1987). *Multiple comparison procedures.* John Wiley & Sons, Inc., https://doi.org/10.1002/9780470316672.

Hocking, R.R. (1976). The analysis and selection of variables in linear regression. *Biometrics* 32(1), 1–49, https://doi.org/10.2307/2529336.

Hoekzema, E., Carmona, S., Ramos-Quiroga, J.A., Richarte Fernández, V., Bosch, R., Soliva, J.C., Rovira, M., Bulbena, A., Tobeña, A., Casas, M., and Vilarroya, O. (2014). An independent components and functional connectivity analysis of resting state fMRI data points to neural network dysregulation in adult ADHD. *Human Brain Mapping* 35(4), 1261–1272, https://doi.org/10.1002/hbm.22250.

Hofmann, M.J., Herrmann, M.J., Dan, I., Obrig, H., Conrad, M., Kuchinke, L., Jacobs, A.M., and Fallgatter, A.J. (2008). Differential activation of frontal and parietal regions during visual word recognition: An optical topography study. *NeuroImage* 40(3), 1340–1349, https://doi.org/10.1016/j.neuroimage.2007.12.037.

Homae, F., Watanabe, H., Otobe, T., Nakano, T., Go, T., Konishi, Y., and Taga, G. (2010). Development of global cortical networks in early infancy. *Journal of Neuroscience* 30(14), 4877–4882, https://doi.org/10.1523/JNEUROSCI.5618-09.2010.

Hong, X., Wang, Y., Sun, J., Li, C., and Tong, S. (2017). Segregating top-down selective attention from response inhibition in a spatial cueing Go/NoGo Task: An ERP and source localization study. *Scientific Reports* 7(1), 9662, https://doi.org/10.1038/s41598-017-08807-z.

Hoshi, Y. (2003). Functional near-infrared optical imaging: Utility and limitations in

human brain mapping. *Psychophysiology* 40(4), 511–520, https://doi.org/10.1111/1469-8986.00053.

Hoshi, Y., Kobayashi, N., and Tamura, M. (2001). Interpretation of near-infrared spectroscopy signals: A study with a newly developed perfused rat brain model. *Journal of Applied Physiology* 90, 1657–1662, https://doi.org/10.1152/jappl.2001.90.5.1657.

Hoshi, Y., and Michael, F.G. (2005). Functional Near-infrared Spectroscopy: Potential and Limitations in Neuroimaging Studies. *International Review of Neurobiology* Volume 66, 237–266, https://doi.org/10.1016/S0074-7742(05)66008-4.

Hu, X.S., Arredondo, M.M., Gomba, M., Confer, N., DaSilva, A.F., Johnson, T.D., Shalinsky, M., and Kovelman, I. (2015). Comparison of motion correction techniques applied to functional near-infrared spectroscopy data from children. *Journal of Biomedical Optics* 20(12), 126003, https://doi.org/10.1117/1.JBO.20.12.126003.

Huang, Y.S., Wang, L.J., and Chen, C.K. (2012). Long-term neurocognitive effects of methylphenidate in patients with attention deficit hyperactivity disorder, even at drug-free status. *BMC Psychiatry* 12, 194, https://doi.org/10.1186/1471-244X-12-194.

Huppert, T.J., Diamond, S.G., Franceschini, M.A., and Boas, D.A. (2009). HomER: A review of time-series analysis methods for near-infrared spectroscopy of the brain. *Applied Optics* 48(10), D280–D298, https://doi.org/10.1364/AO.4.00D280.

Hurlburt, R.T., Alderson-Day, B., Fernyhough, C., and Kühn, S. (2015). What goes on in the resting-state? A qualitative glimpse into resting-state experience in the scanner. *Frontiers in Psychology* 6, 1535, https://doi.org/10.3389/fpsyg.2015.01535.

Hutchison, R.M., Womelsdorf, T., Allen, E.A., Bandettini, P.A., Calhoun, V.D., Corbetta, M., Penna, S.D., Duyn, J.H., Glover, G.H., Gonzalez-Castillo, J., Handwerker, D.A., Keilholz, S., Kiviniemi, V., Leopold, D.A., de Pasquale, F., Sporns, O., Walter, M., and Chang, C. (2013). Dynamic functional connectivity: Promise, issues, and interpretations. *NeuroImage* 80, 360–378, https://doi.org/10.1016/

j.neuroimage.2013.05.079.

Huttenlocher, P.R. (1984). Synapse elimination and plasticity in developing human cerebral cortex. *American Journal of Mental Deficiency* 88(5), 488–496.

Huttenlocher, P.R., de Courten, C., Garey, L.J., and Van der Loos, H. (1982). Synaptogenesis in human visual cortex - evidence for synapse elimination during normal development. *Neuroscience Letters* 33(3), 247–252, https://doi.org/10.1016/0304-3940(82)90379-2.

Ichikawa, H., Nakato, E., Kanazawa, S., Shimamura, K., Sakuta, Y., Sakuta, R., Yamaguchi, M.K., and Kakigi, R. (2014). Hemodynamic response of children with attention-deficit and hyperactive disorder (ADHD) to emotional facial expressions. *Neuropsychologia* 63, 51–58, https://doi.org/10.1016/j.neuropsychologia.2014.08.010.

Ikeda, T., Hirai, M., Sakurada, T., Monden, Y., Tokuda, T., Nagashima, M., Shimoizumi, H., Dan, I., and Yamagata, T. (2018a). Atypical neural modulation in the right prefrontal cortex during an inhibitory task with eye gaze in autism spectrum disorder as revealed by functional near-infared spectroscopy. *Neurophotonics* 5(3), 035008, https://doi.org/10.1117/1.NPh.5.3.035008.

Ikeda, T., Tokuda, T., Monden, Y., Hirai, M., Mizushima, S.G., Nagashima, M., Kyutoku, Y., Taniguchi, T., Shimoizumi, H., Dan, I., and Yamagata, T. (2018b). Hypoactivation of the right prefrontal cortex underlying motor-related inhibitory deficits in children with Autism Spectrum Disorder: A functional near-infrared spectroscopy study. *Japanese Psychological Research* 60(4), 251–264, https://doi.org/10.1111/jpr.12204.

Inoue, Y., Sakihara, K., Gunji, A., Ozawa, H., Kimiya, S., Shinoda, H., Kaga, M., and Inagaki, M. (2012). Reduced prefrontal hemodynamic response in children with ADHD during the Go/NoGo task: A NIRS study. *Neuroreport* 23(2), 55–60, https://doi.org/10.1097/WNR.0b013e32834e664c.

Ip, P., Ho, F.K.W., Rao, N., Sun, J., Young, M.E., Chow, C.B., Tso, W., and Hon, K.L. (2017). Impact of nutritional supplements on cognitive development of children

in developing countries: A meta-analysis. *Scientific Reports* 7(1), 10611, https://doi.org/10.1038/s41598-017-11023-4.

Ishii-Takahashi, A., Takizawa, R., Nishimura, Y., Kawakubo, Y., Kuwabara, H., Matsubayashi, J., Hamada, K., Okuhata, S., Yahata, N., Igarashi, T., Kawasaki, S., Yamasue, H., Kato, N., Kasai, K., and Kano, Y. (2014). Prefrontal activation during inhibitory control measured by near-infrared spectroscopy for differentiating between autism spectrum disorders and attention deficit hyperactivity disorder in adults. *NeuroImage: Clinical* 4, 53–63, https://doi.org/10.1016/j.nicl.2013.10.002.

Iwanaga, R., Tanaka, G., Nakane, H., Honda, S., Imaura, A., and Ozawa, H. (2013). Usefulness of near-infrared spectroscopy to detect brain dysfunction in children with autism spectrum disorder when inferring the mental state of others. *Psychiatry and Clinical Neurosciences* 67(4), 203–209, https://doi.org/10.1111/pcn.12052.

Izzetoglu, M., Chitrapu, P., Bunce, S., and Onaral, B. (2010). Motion artifact cancellation in NIR spectroscopy using discrete Kalman filtering. *BioMedical Engineering OnLine* 9, 16, https://doi.org/10.1186/1475-925X-9-16.

Jöbsis, F.F. (1977). Noninvasive, infrared monitoring of cerebral and myocardial oxygen sufficiency and circulatory parameters. *Science* 198(4323), 1264–1267, https://doi.org/10.1126/science.929199.

Jahani, S., Setarehdan, S.K., Boas, D., and Yücel, M.A. (2018). Motion artifact detection and correction in functiona near-infrared spectroscopy: A new hybrid-method based on spline interpolation method and Savitzky-Golay filtering. *Neurophotonics* 5(1), 015003, https://doi.org/10.1117/1.NPh.5.1.015003.

Jelzow, A., Tachtsidis, I., Kirilina, E., Niessing, M., Brühl, R., Wabnitz, H., Heine, A., Ittermann, B., and Macdonald, R. (2011). Simultaneous measurement of time-domain fNIRS and physiological signals during a cognitive task. *Proceedings of SPIE* 8088, 808803, https://doi.org/10.1117/12.889484.

Jiang, H., Paulsen, K.D., Osterberg, U.L., Poque, B.W., and Patterson, M.S. (1995).

Simultaneous reconstruction of optical absorption and scattering maps in turbid media from near-infrared frequency-domain data. *Optics Letters* 20(20), 2128–2130, https://doi.org/10.1364/ol.20.002128.

Johnson, M.H. (2001). Functional brain development in humans. *Nature Reviews Neuroscience* 2, 475–493, https://doi.org/10.1038/35081509.

Jurcak, V., Okamoto, M., Singh, A., and Dan, I. (2005). Virtual 10-20 measurement on MR images for inter-modal linking of transcranial and tomographic neuroimaging methods. *NeuroImage* 26(4), 1184–1192, https://doi.org/10.1016/j.neuroimage.2005.03.021.

Kana, R.K., Keller, T.A., Minshew, N.J., and Just, M.A. (2007). Inhibitory control in high-functioning autism: Decreased activation and underconnectivity in inhibition networks. *Biological Psychiatry* 62(3), 198–206, https://doi.org/10.1016/j.biopsych.2006.08.004.

Katura, T., Sato, H., Fuchino, Y., Yoshida, T., Atsumori, H., Kiguchi, M., Maki, A., Abe, M., and Tanaka, N. (2008). Extracting task-related activation components from optical topography measurement using independent components analysis. *Journal of Biomedical Optics* 13(5), 054008, https://doi.org/10.1117/1.2981829.

Kawaguchi, H., Okui, N., Sakaguchi, K., and Okada, E. (2008). Theoretical analysis of crosstalk between oxygenated and deoxygenated haemoglobin in focal brain-activation measurements by near-infrared topography. *Opto-Electronics Review* 16(4), 404–412, https://doi.org/10.2478/s11772-008-0032-1.

Keilp, J.G., Sackeim, H.A., and Mann, J.J. (2005). Correlates of trait impulsiveness in performance measures and neuropsychological tests. *Psychiatry Research* 135(3), 191–201, https://doi.org/10.1016/j.psychres.2005.03.006.

Khadmaoui, A., Gómez, C., Poza, J., Bachiller, A., Fernández, A., Quintero, J., and Hornero, R. (2016). MEG analysis of neural interactions in attention-deficit/hyperactivity disorder. *Computational Intelligence and Neuroscience* 2016, 8450241, https://doi.org/10.1155/2016/8450241.

Kiehl, K.A., Stevens, M.C., Laurens, K.R., Pearlson, G.D., Calhoun, V.D., and Liddle,

P.F. (2005). An adaptive reflexive processing model of neurocognitive function: Supporting evidence from a large scale (N = 100) fMRI study of an auditory oddball task. *NeuroImage* 25(3), 899–915, https://doi.org/10.1016/j.neuroimage.2004.12.035.

Kirilina, E., Jelzow, A., Heine, A., Niessing, M., Wabnitz, H., Bruhl, R., Ittermann, B., Jacobs, A.M., and Tachtsidis, I. (2012). The physiological origin of task-evoked systemic artefacts in functional near infrared spectroscopy. *NeuroImage* 61(1), 70–81, https://doi.org/10.1016/j.neuroimage.2012.02.074.

Kita, Y., Gunji, A., Inoue, Y., Goto, T., Sakihara, K., Kaga, M., Inagaki, M., and Hosokawa, T. (2011). Self-face recognition in children with autism spectrum disorders: A near-infrared spectroscopy study. *Brain and Development* 33(6), 494–503, https://doi.org/10.1016/j.braindev.2010.11.007.

Klein, C., Wendling, K., Huettner, P., Ruder, H., and Peper, M. (2006). Intra-subject variability in attention-deficit hyperactivity disorder. *Biological Psychiatry* 60(10), 1088–1097, https://doi.org/10.1016/j.biopsych.2006.04.003.

Koh, K. (2017). Maternal breastfeeding and children's cognitive development. *Social Science and Medicine* 187, 101–108, https://doi.org/10.1016/j.socscimed.2017.06.012.

Koh, P.H., Glaser, D.E., Flandin, G., Kiebel, S., Butterworth, B., Maki, A., Delpy, D.T., and Elwell, C.E. (2007). Functional optical signal analysis: A software tool for near-infrared spectroscopy data processing incorporating statistical parametric mapping. *Journal of Biomedical Optics* 12(6), 064010, https://doi.org/10.1117/1.2804092.

Kohno, S., Miyai, I., Seiyama, A., Oda, I., Ishikawa, A., Tsuneishi, S., Amita, T., and Shimizu, K. (2007). Removal of the skin blood flow artifact in functional near-infrared spectroscopic imaging data through independent component analysis. *Journal of Biomedical Optics* 12(6), 062111, https://doi.org/10.1117/1.2814249.

Koike, S., Nishimura, Y., Takizawa, R., Yahata, N., and Kasai, K. (2013). Near-infrared spectroscopy in schizophrenia: A possible biomarker for predicting clinical

outcome and treatment response. *Frontiers in Psychiatry* 4, 145, https://doi.org/10.3389/fpsyt.2013.00145.

Koizumi, H., Yamamoto, T., Maki, A., Yamashita, Y., Sato, H., Kawaguchi, H., and Ichikawa, N. (2003). Optical Topography: Practical Problems and New Applications. *Applied Optics* 42(16), 3054–3062, https://doi.org/10.1364/AO.42.003054.

Kruggel, F., and von Cramon, D.Y. (1999). Temporal properties of the hemodynamic response in functional MRI. *Human Brain Mapping* 8(4), 259–271.

Lang, S., Duncan, N., and Northoff, G. (2014). Resting-state functional magnetic resonance imaging: Review of Neurosurgical Applications. *Neurosurgery* 74(5), 453–464, https://doi.org/10.1227/NEU.0000000000000307.

Lee, D.O., and Ousley, O.Y. (2006). Attention-deficit hyperactivity disorder symptoms in a clinic sample of children and adolescents with pervasive developmental disorders. *Journal of Child and Adolescent Psychopharmacology* 16(6), 737–746, https://doi.org/10.1089/cap.2006.16.737.

Lenartowicz, A., and Loo, S.K. (2014). Use of EEG to Diagnose ADHD. *Current Psychiatry Reports* 16(11), 498, https://doi.org/10.1007/s11920-014-0498-0.

Lenroot, R.K., Gogtay, N., Greenstein, D.K., Wells, E.M., Wallace, G.L., Clasen, L.S., Blumenthal, J.D., Lerch, J., Zijidenbos, A.P., Evans, A.C., Thompson, P.M., and Giedd, J.N. (2007). Sexual dimorphism of brain developmental trajectories during childhood and adolescence. *NeuroImage* 36(4), 1065–1073, https://doi.org/10.1016/j.neuroimage.2007.03.053.

Li, J., Qiu, L., Xu, L., Pedapati, E.V., Erickson, C.A., and Sunar, U. (2016a). Characterization of autism spectrum disorder with spontaneous hemodynamic activity. *Biomedical Optics Express* 7(10), 3871–3881, https://doi.org/10.1364/BOE.7.003871.

Li, Y., and Yu, D. (2016b). Weak network efficiency in young children with autism spectrum disorder: Evidence from a functional near-infrared spectroscopy. *Brain and Cognition* 108, 47–55, https://doi.org/10.1016/j.bandc.2016.07.006.

Li, Z., Liu, H., Liao, X., Xu, J., Liu, W., Tian, F., He, Y., and Niu, H. (2015). Dynamic functional connectivity revealed by resting-state functional near-infrared spectroscopy. *Biomedical Optics Express* 6(7), 2337–2352, https://doi.org/10.1364/BOE.6.002337.

Liddle, P.F., Kiehl, K.A., and Smith, A.M. (2001). Event-related fMRI study of response inhibition. *Human Brain Mapping* 12(2), 100–109, https://doi.org/10.1002/1097-0193(200102)12:2<100::AID-HBM1007>3.0.CO;2-6.

Liechti, M.D., Valko, L., Müller, U.C., Döhnert, M., Drechsler, R., Steinhausen, H.C., and Brandeis, D. (2013). Diagnostic value of resting electroencephalogram in attention deficit/hyperactivity disorder across the lifespan. *Brain Topography* 26(1), 135–151, https://doi.org/10.1007/s10548-012-0258-6.

Lindquist, M.A., Loh, J.M., Atlas, L.Y., and Wager, T.D. (2009). Modeling the hemodynamic response function in fMRI: Efficiency, Bias, and Mis-modeling. *NeuroImage* 45 (Suppl 1), S187–S198, https://doi.org/10.1016/j.neuroimage.2008.10.065.

Lindquist, M.A., and Wager, T.D. (2007). Validity and power in hemodynamic response modeling: A comparison study and a new approach. *Human Brain Mapping* 28(8), 764–784, https://doi.org/10.1002/hbm.20310.

Linnet, K., Bossuyt, P.M.M., Moons, K.G.M., and Reitsma, J.B. (2012). Quantifying the accuracy of a diagnostic test or marker. *Clinical Chemistry* 58(9), 1292–1301, https://doi.org/10.1373/clinchem.2012.182543.

Liu, X., and Duyn, J.H. (2013). Time-varying functional network information extracted from brief instance of spontaneous brain activity. *Proceedings of the National Academy of Sciences of the United States of America* 110(11), 4392–4397, https://doi.org/10.1073/pnas.1216856110.

Liu, Y., Kaaya, S., Chai, J., McCoy, D.C., Surkan, P.J., Black, M.M., Sutter-Dallay, A.L., Verdoux, H., and Smith-Fawzi, M.C. (2017). Maternal depressive symptoms and early childhood cognitive development: A meta-analysis. *Psychological Medicine* 47(4), 680–689, https://doi.org/10.1017/S003329171600283X.

Loo, S.K., Cho, A., Hale, T.S., McGough, J., McCracken, J., and Smalley, S.L. (2013). Characterization of the theta to beta ratio in ADHD: Identifying potential source of heterogeneity. *Journal of Attention Disorders* 17(5), 384–392, https://doi.org/10.1177/1087054712468050.

Loo, S.K., and Makeig, S. (2012). Clinical utility of EEG in attention-deficit/hyperactivity disorder: A research update. *Neurotherapeutics* 9(3), 569–587, https://doi.org/10.1007/s13311-012-0131-z.

Lu, C.M., Zhang, Y.J., Biswal, B.B., Zang, Y.F., Peng, D.L., and Zhu, C.Z. (2010). Use of fNIRS to assess resting state functional connectivity. *Journal of Neuroscience Methods* 186(2), 242–249, https://doi.org/10.1016/j.jneumeth.2009.11.010.

Lu, Y., Darne, C.D., Tan, I.C., Zhu, B., Rightmer, R., Rasmussen, J.C., and Sevick-Muraca, E.M. (2015). Experimental comparison of continuous-wave and frequency-domain fluorescence tomography in a commercial multi-modal scanner. *IEEE Transactions on Medical Imaging* 34(6), 1197–1211, https://doi.org/10.1109/TMI.2014.2375193.

Lystad, R.P., and Pollard, H. (2009). Functional neuroimaging: A brief overview and feasibility for use in chiropractic research. *Journal of the Canadian Chiropractic Association* 53(1), 59–72.

Magee, C.A., Clarke, A.R., Barry, R.J., McCarthy, R., and Selikowitz, M. (2005). Examining the diagnostic utility of EEG power measures in children with attention deficit/hyperactivity disorder. *Clinical Neurophysiology* 116(5), 1033–1040, https://doi.org/10.1016/j.clinph.2004.12.007.

Maki, A., Yamashita, Y., Ito, Y., Watanabe, E., Mayanagi, Y., and Koizumi, H. (1995). Spatial and temporal analysis of human motor activity using noninvasive NIR topography. *Medical Physics* 22(12), 1997–2005, https://doi.org/10.1118/1.597496.

Makris, N., Biederman, J., Valera, E.M., Bush, G., Kaiser, J., Kennedy, D.N., Caviness, V.S., Faraone, S.V., and Seidman, L.J. (2007). Cortical Thinning of the attention and executive function networks in adults with attention-deficit/hyperactivity

disorder. *Cerebral Cortex* 17(6), 1364–1375, https://doi.org/10.1093/cercor/bhl047.

Makris, N., Buka, S.L., Biederman, J., Papadimitriou, G.M., Hodge, S.M., Valera, E.M., Brown, A.B., Bush, G., Monuteaux, M.C., Caviness, V.S., Kennedy, D.N., and Seidman, L.J. (2008). Attention and executive systems abnormalities in adults with childhood ADHD: A DT-MRI study of connections. *Cerebral Cortex* 18(5), 1210–1220, https://doi.org/10.1093/cercor/bhm156.

Martino, A.D., Ghaffari, M., Curchack, J., Reiss, P., Hyde, C., Vannucci, M., Petkova, E., Klein, D.F., and Castellanos, F.X. (2008). Decomposing intra-subject variability in children with attention-deficit/hyperactivity disorder. *Biological Psychiatry* 64(7), 607–614, https://doi.org/10.1016/j.biopsych.2008.03.008.

Matsuo, T., Oshima, S., Kunii, Y., Okano, T., Yabe, H., and Niwa, S.I. (2014). A preliminary near-infrared spectroscopy study in adolescent and adult patients with attention-deficit/hyperactivity disorder symptoms. *Open Journal of Psychiatry* 4(4), 396–404, https://doi.org/10.4236/ojpsych.2014.44046.

Matsuura, N., Ishitobi, M., Arai, S., Kawamura, K., Asano, M., Inohara, K., Fujioka, T., Narimoto, T., Wada, Y., Hiratani, M., and Kosaka, H. (2014). Effects of methylphenidate in children with attention deficit hyperactivity disorder: A near-infrared spectroscopy study with CANTAB®. *Child and Adolescent Psychiatry and Mental Health* 8, 273, https://doi.org/10.1186/s13034-014-0032-5.

Matza, L.S., Paramore, C., and Prasad, M. (2005). A review of the economic burden of ADHD. *Cost Effectiveness and Resource Allocation* 3, 5, https://doi.org/10.1186/1478-7547-3-5.

McCarthy, G., Luby, M., Gore, J., and Goldman-Rakic, P. (1997). Infrequent events transiently activate human prefrontal and parietal cortex as measured by functional MRI. *Journal of Neurophysiology* 77, 1630–1634, https://doi.org/10.1152/jn.1997.77.3.1630.

Mennes, M., Potler, N.V., Kelly, C., di Martino, A., Castellanos, F.X., and Milham, M.P. (2012). Resting state functional connectivity correlates of inhibitory control in

children with attention-deficit/hyperactivity disorder. *Frontiers in Psychiatry* 2, 83, https://doi.org/10.3389/fpsyt.2011.00083.

Menon, V., Adleman, N.E., White, C.D., Glover, G.H., and Reiss, A.L. (2001). Error-related brain activation during a Go/NoGo response inhibition task. *Human Brain Mapping* 12(3), 131–143, https://doi.org/10.1002/1097-0193(200103)12:3<131::AID-HBM1010>3.0.CO;2-C.

Michelson, D., Allen, A.J., Busner, J., Casat, C., Dunn, D., Kratochvil, C., Newcorn, J., Sallee, F.R., Sangal, R.B., Saylor, K., West, S., Kelsey, D., Wernicke, J., Trapp, N.J., and Harder, D. (2002). Once-daily atomoxetine treatment for children and adolescents with attention deficit hyperactivity disorder: A randomized placebo-controlled study. *American Journal of Psychiatry* 159(11), 1896–1901, https://doi.org/10.1176/appi.ajp.159.11.1896.

Miezin, F.M., Maccotta, L., Ollinger, J.M., Petersen, S.E., and Buckner, R.L. (2000). Characterizing the hemodynamic response: Effects of presentation rate, sampling procedure, and the possibility of ordering brain activity based on relative timing. *NeuroImage* 11(6), 735–759, https://doi.org/10.1006/nimg.2000.0568.

Miller, R.G.J. (1981). *Simultaneous statistical inference.* Springer-Verlag, Inc.

Molavi, B., and Dumont, G.A. (2012). Wavelet-based motion artifact removal for functional near-infrared spectroscopy. *Physiological Measurement* 33(2), 259–270, https://doi.org/10.1088/0967-3334/33/2/259.

Monastra, V.J., Lubar, J.F., and Linden, M. (2001). The development of a quantitative electroencephalographic scanning process for attention deficit-hyperactivity disorder: Reliability and validity studies. *Neuropsychology* 15(1), 136–144, https://doi.org/10.1037//0894-4105.15.1.136.

Monden, Y., Dan, H., Nagashima, M., Dan, I., Kyutoku, Y., Okamoto, M., Yamagata, T., Momoi, M.Y., and Watanabe, E. (2012a). Clinically-oriented monitoring of acute effects of methylphenidate on cerebral hemodynamics in ADHD children using fNIRS. *Clinical Neurophysiology* 123(6), 1147–1157, https://doi.org/10.1016/j.clinph.2011.10.006.

Monden, Y., Dan, H., Nagashima, M., Dan, I., Tsuzuki, D., Kyutoku, Y., Gunji, Y., Yamagata, T., Watanabe, E., and Momoi, M.Y. (2012b). Right prefrontal activation as a neuro-functional biomarker for monitoring acute effects of methylphenidate in ADHD children: An fNIRS study. *NeuroImage: Clinical* 1(1), 131–140, https://doi.org/10.1016/j.nicl.2012.10.001.

Monden, Y., Dan, I., Nagashima, M., Dan, H., Uga, M., Ikeda, T., Tsuzuki, D., Kyutoku, Y., Gunji, Y., Hirano, D., Taniguchi, T., Shimoizumi, H., Watanabe, E., and Yamagata, T. (2015). Individual classification of ADHD children by right prefrontal hemodynamic responses during a go/no-go task as assessed by fNIRS. *NeuroImage: Clinical* 9, 1–12, https://doi.org/10.1016/j.nicl.2015.06.011.

Monti, M.M. (2011). Statistical analysis of fMRI time series: A critical review of the GLM approach. *Frontiers in Human Neuroscience* 5, 28, https://doi.org/10.3389/fnhum.2011.00028.

Mostert, J.C., Shumskaya, E., Mennes, M., Onnink, A.M.H., Hoogman, M., Kan, C.C., Vasquez, A.A., Buitelaar, J., Franke, B., and Norris, D.G. (2016). Characterising resting-state functional connectivity in a large sample of adults with ADHD. *Progress in Neuro-Psychopharmacology and Biological Psychiatry* 67, 82–91, https://doi.org/10.1016/j.pnpbp.2016.01.011.

Mueller, A., Candrian, G., Grane, V.A., Kropotov, J.D., Ponomarev, V.A., and Baschera, G.-M. (2011). Discriminating between ADHD adults and controls using independent ERP components and a support vector machine: A validation study. *Nonlinear Biomedical Physics* 5, 5, https://doi.org/10.1186/1753-4631-5-5.

Mulligan, A., Anney, R.J., O'Regan, M., Chen, W., Butler, L., Fitzgerald, M., Biuitelarr, J., Steinhausen, H.-C., Rothenberger, A., Minderaa, R., Nijmeijer, J., Hoekstra, P.J., Oades, R.D., Roeyers, H., Buschgens, C., Chistiansen, H., Frankle, B., Gabriels, I., Hartman, C., Kuntsi, J., Marco, R., Meidad, S., Müller, U.C., Psychogiou, L., Rommelse, N., Thompson, M., Uebel, H., Banaschewski, T., Ebstein, R., Eisenberg, J., Manor, I., Miranda, A., Mulas, F., Sergeant, J., Sonuga-Barke, E.J.S., Asherson, P., Faraone, S.V., and Gill, M. (2009). Autism symptoms

in attention-deficit/hyperactivity disorder: A familial trait with correlates with conduct, oppositional defiant, language and motor disorders. *Journal of Autism and Developmental Disorders* 39, 197–209, https://doi.org/10.1007/s10803-008-0621-3.

Murphy, F.C., Sahakian, B.J., Rubinsztein, J.S., Michael, A., Rogers, R.D., Robbins, T.W., and Paykel, E.S. (1999). Emotional bias and inhibitory control processes in mania and depression. *Psychological Medicine* 29(6), 1307–1321, https://doi.org/10.1017/s0033291799001233.

Murphy, K., Birn, R.M., and Bandettini, P.A. (2013). Resting-state fMRI confounds and cleanup. *NeuroImage* 80, 349–359, https://doi.org/10.1016/j.neuroimage.2013.04.001.

Nagashima, M., Monden, Y., Dan, I., Dan, H., Mizutani, T., Tsuzuki, D., Kyutoku, Y., Gunji, Y., Hirano, D., Taniguchi, T., Shimoizumi, H., Momoi, M.Y., Yamagata, T., and Watanabe, E. (2014a). Neuropharmacological effect of atomoxetine on attention network in children with attention deficit hyperactivity disorder during oddball paradigms as assessed using functional near-infrared spectroscopy. *Neurophotonics* 1(2), 025007, https://doi.org/10.1117/1.NPh.1.2.025007.

Nagashima, M., Monden, Y., Dan, I., Dan, H., Tsuzuki, D., Mizutani, T., Kyutoku, Y., Gunji, Y., Hirano, D., Taniguchi, T., Shimoizumi, H., Momoi, M.Y., Watanabe, E., and Yamagata, T. (2014b). Acute neuropharmacological effects of atomoxetine on inhibitory control in ADHD children: A fNIRS study. *NeuroImage: Clinical* 6, 192–201, https://doi.org/10.1016/j.nicl.2014.09.001.

Nagashima, M., Monden, Y., Dan, I., Dan, H., Tsuzuki, D., Mizutani, T., Kyutoku, Y., Gunji, Y., Momoi, M.Y., Watanabe, E., and Yamagata, T. (2014c). Neuropharmacological effect of methylphenidate on attention network in children with attention deficit hyperactivity disorder during oddball paradigms as assessed using functional near-infrared spectroscopy. *Neurophotonics* 1(1), 015001, https://doi.org/10.1117/1.NPh.1.1.015001.

Nebel, M.B., Eloyan, A., Barber, A.D., and Mostofsky, S.H. (2014). Precentral gyrus

functional connectivity signatures of autism. *Frontiers in Systems Neuroscience* 8, 80, https://doi.org/10.3389/fnsys.2014.00080.

Newcorn, J.H., Kratochvil, C.J., Allen, A.J., Casat, C.D., Ruff, D.D., Moore, R.J., and Michelson, D. (2008). Atomoxetine and osmotically released methylphenidate for the treatment of attention deficit hyperactivity disorder: Acute comparison and differential response. *American Journal of Psychiatry* 165(6), 721–730, https://doi.org/10.1176/appi.ajp.2007.05091676.

Nichols, T., and Hayasaka, S. (2003). Controlling the familywise error rate in functional neuroimaging: A comparative review. *Statistical Methods in Medical Research* 12(5), 419–446, https://doi.org/10.1191/0962280203sm341ra.

Nioka, S., Luo, Q., and Chance, B. (1997). Human brain functional imaging with reflectance CWS. *Advances in Experimental Medicine and Biology* 428, 237–242, https://doi.org/10.1007/978-1-4615-5399-1_33.

Niu, H., and He, Y. (2014). Resting-state functional brain connectivity: Lessons from functional near-infarred spectroscopy. *The Neuroscientist* 20(2), 173–188, https://doi.org/10.1177/1073858413502707.

Niu, H., Khadka, S., Tian, F., Lin, Z.J., Lu, C., Zhu, C., and Liu, H. (2011). Resting-state functional connectivity assessed with two diffuse optical tomographic systems. *Journal of Biomedical Optics* 16(4), 046006, https://doi.org/10.1117/1.3561687.

Niu, H., Li, Z., Liao, X., Wang, J., Zhao, T., Shu, N., Zhao, X., and He, Y. (2013). Test-retest reliability of graph metrics in functional brain networks: A resting-state fNIRS study. *PLoS One* 8(9), e72425, https://doi.org/10.1371/journal.pone.0072425.

Niu, H., Wang, J., Zhao, T., Shu, N., and He, Y. (2012). Revealing topological organization of human brain functional networks with resting-state functional near infrared spectroscopy. *PLoS One* 7(9), e45771, https://doi.org/10.1371/journal.pone.0045771.

Niu, H., Zhu, Z., Wang, M., Li, X., Yuan, Z., Sun, Y., and Han, Y. (2019). Abnormal dynamic functional connectivity and brain states in Alzheimer's diseases:

Functional near-infrared spectroscopy study. *Neurophotonics* 6(2), 025010, https://doi.org/10.1117/1.NPh.6.2.025010.

Nomi, J.S., Schettini, E., Voorhies, W., Bolt, T.S., Heller, A.S., and Uddin, L.Q. (2018). Resting-state brain signal variability in prefrontal cortex is associated with ADHD symptom severity in Children. *Frontiers in Human Neuroscience* 12, 90, https://doi.org/10.3389/fnhum.2018.00090.

Noordermeer, S.D.S., Luman, M., Greven, C.U., Veroude, K., Faraone, S.V., Hartman, C.A., Hoekstra, P.J., Franke, B., Buitelaar, J.K., Heslenfeld, D.J., and Oosterlaan, J. (2017). Structural brain abnormalities of attention-deficit/hyperactivity disorder with oppositional defiant disorder. *Biological Psychiatry* 82(9), 642–650, https://doi.org/10.1016/j.biopsych.2017.07.008.

O'Halloran, L., Cao, Z., Ruddy, K., Jollans, L., Albaugh, M.D., Aleni, A., Potter, A.S., Vahey, N., Banaschewski, T., Hohmann, S., Bokde, A.L.W., Bromberg, U., Büchel, C., Quinlan, E.B., Desrivières, S., Flor, H., Frouin, V., Gowland, P., Heinz, A., Ittermann, B., Nees, F., Orfanos, D.P., Paus, T., Smolka, M.N., Walter, H., Schumann, G., Garavan, H., Kelly, C., and Whelan, R. (2018). Neural circuitry underlying sustained attention in healthy adolescents and in ADHD symptomatology. *NeuroImage* 169, 395–406, https://doi.org/10.1016/j.neuroimage.2017.12.030.

O'Malley, J., Richer, E.J., and Strawn, J.R. (2016). Neuroimaging in children and adolescents: When do you scan? With which modalities? *Current Psychiatry* 15(9).

Obrig, H., Neufang, M., Wenzel, R., Kohl, M., Steinbrink, J., Einhaupl, K., and Villringer, A. (2000a). Spontaneous low frequency oscillations of cerebral hemodynamics and metabolism in human adults. *NeuroImage* 12(6), 623–639, https://doi.org/10.1006/nimg.2000.0657.

Obrig, H., Wenzel, R., Kohl, M., Horst, S., Wobst, P., Steinbrink, J., Thomas, F., and Villringer, A. (2000b). Near-infrared spectroscopy: Does it function in functional activation studies of the adult brain? *International Journal of Psychophysiology* 35(2–3), 125–142, https://doi.org/10.1016/S0167-8760(99)00048-3.

Ogrim, G., Kropotov, J., and Hestad, K. (2012). The quantitative EEG theta/beta ratio in attention deficit/hyperactivity disorder and normal controls: Sensitivity, specificity, and behavioral correlates. *Psychiatry Research* 198(3), 482–488, https://doi.org/10.1016/j.psychres.2011.12.041.

Okamoto, M., Dan, H., Sakamoto, K., Takeo, K., Shimizu, K., Kohno, S., Oda, I., Isobe, S., Suzuki, T., Kohyama, K., and Dan, I. (2004). Three-dimensional probabilistic anatomical cranio-cerebral correlation via the international 10-20 system oriented for transcranial functional brain mapping. *NeuroImage* 21(1), 99–111, https://doi.org/10.1016/j.neuroimage.2003.08.026.

Okamoto, M., Dan, H., Singh, A.K., Hayakawa, F., Jurcak, V., Suzuki, T., Kohyama, K., and Dan, I. (2006). Prefrontal activity during flavor difference test: Application of functional near-infrared spectroscopy to sensory evaluation studies. *Appetite* 47(2), 220–232, https://doi.org/10.1016/j.appet.2006.04.003.

Okamoto, M., and Dan, I. (2005). Automated cortical projection of head-surface locations for transcranial functional brain mapping. *NeuroImage* 26(1), 18–28, https://doi.org/10.1016/j.neuroimage.2005.01.018.

Okamoto, M., Tsuzuki, D., Clowney, L., Dan, H., Singh, A.K., and Dan, I. (2009). Structural atlas-based spatial registration for functional near-infrared spectroscopy enabling inter-study data integration. *Clinical Neurophysiology* 120(7), 1320–1328, https://doi.org/10.1016/j.clinph.2009.01.023.

Okui, N., and Okada, E. (2005). Wavelength dependence of crosstalk in dual-wavelength measurement of oxy- and deoxy-hemoglobin. *Journal of Biomedical Optics* 10(1), 011015, https://doi.org/10.1117/1.1846076.

Olusanya, B.O., Davis, A.C., Wertlieb, D., Boo, N.Y., Nair, M.K.C., Halpern, R., Kuper, H., Breinbauer, C., de Vries, P.J., Gladstone, M., Halfon, N., Kancherla, V., Mulaudzi, M.C., Kakooza-Mwesige, A., Ogbo, F.A., Olusanya, J.O., Williams, A.N., Wright, S.M., Manguerra, H., Smith, A., Echko, M., Ikeda, C., Liu, A., Millear, A., Ballesteros, K., Nichols, E., Erskine, H.E., Santomauro, D., Rankin, Z., Smith, M., Whiteford, H.A., Olsen, H.E., and Kassebaum, N.J. (2018).

Developmental disabilities among children younger than 5 years in 195 countries and territories, 1990–2016: A systematic analysis for the Global Burden of Disease Study 2016. *The Lancet Global Health* 6(10), e1100–e1121, https://doi.org/10.1016/S2214-109X(18)30309-7.

Ota, T., Iida, J., Nakanishi, Y., Sawada, S., Matsuura, H., Yamamuro, K., Ueda, S., Uratani, M., Kishimoto, N., Negoro, H., and Kishimoto, T. (2015). Increased prefrontal hemodynamic change after atomoxetine administration in pedriatric attention-deficit/hyperactivity disorder as measured by near-infrared spectroscopy. *Psychiatry and Clinical Neurosciences* 69(3), 161–170, https://doi.org/10.1111/pcn.12251.

Owen-Reece, H., Smith, M., Elwell, C.E., and Goldstone, J.C. (1999). Near infrared spectroscopy. *British Journal of Anaesthesia* 82(3), 418–426, https://doi.org/10.1093/bja/82.3.418.

Paller, K.A., McCarthy, G., Roessler, E., Allison, T., and Wood, C.C. (1992). Potentials evoked in human and monkey medial temporal lobe during auditory and visual oddball paradigms. *Electroencephalography and Clinical Neurophysiology* 84(3), 269–279, https://doi.org/10.1016/0168-5597(92)90008-Y.

Peña, M., Maki, A., Kovacic, D., Dehaene-Lambertz, G., Koizumi, H., Bouquet, F., and Mehler, J. (2003). Sounds and silence: An optical topography study of language recognition at birth. *Proceedings of the National Academy of Sciences of the United States of America* 100(20), 11702–11705, https://doi.org/10.1073/pnas.1934290100.

Peers, P.V., Ludwig, C.J., Rorden, C., Cusack, R., Bonfiglioli, C., Bundesen, C., Driver, J., Antoun, N., and Duncan, J. (2005). Attentional functions of parietal and frontal cortex. *Cerebral Cortex* 15(10), 1469–1484, https://doi.org/10.1093/cercor/bhi029.

Peyre, H., Bernard, Y., Hoertel, N., Forhan, A., Charles, M.A., De Agostini, M., Heude, B., Ramus, F., and The EDEN Mother-Child Cohort Study Group (2016). Differential effects of factors influencing cognitive development at the age of 5-

to-6 years. *Cognitive Development* 40, 152–162, https://doi.org/10.1016/j.cogdev.2016.10.001.

Pfefferbaum, A., Mathalon, D.H., Sullivan, E.V., Rawles, J.M., Zipursky, R.B., and Lim, K.O. (1994). A quantitative magnetic resonance imaging study of changes in brain morphology from infancy to late adulthood. *Archives of Neurology* 51(9), 874–887, https://doi.org/10.1001/archneur.1994.00540210046012.

Piaget, J., and Inhelder, B. (1969). *The psychology of the child.* New York: Basic Books.

Pinti, P., Merla, A., Aichelburg, C., Lind, F., Power, S., Swingler, E., Hamilton, A., Gilbert, S., Burgess, P.W., and Tachtsidis, I. (2017). A novel GLM-based method for the Automatic IDentificantion of functional Events (AIDE) in fNIRS data recorded in naturalistic environments. *NeuroImage* 155, 291–304, https://doi.org/10.1016/j.neuroimage.2017.05.001.

Plichta, M.M., Herrmann, M.J., Baehne, C.G., Ehlis, A.C., Richter, M.M., Pauli, P., and Fallgatter, A.J. (2006). Event-related functional near-infrared spectroscopy (fNIRS): Are the measurements reliable? *NeuroImage* 31(1), 116–124, https://doi.org/10.1016/j.neuroimage.2005.12.008.

Poque, B.W., and Patterson, M.S. (1994). Frequency-domain optical absorption spectroscopy of finite tissue volumes using diffusion theory. *Physics in Medicine and Biology* 39(7), 1157–1180, https://doi.org/10.1088/0031-9155/39/7/008.

Preti, M.G., Bolton, T.A.W., and Van De Ville, D. (2017). The dynamic functional connectome: State-of-the-art and perspectives. *NeuroImage* 160, 41–54, https://doi.org/10.1016/j.neuroimage.2016.12.061.

Quaresima, V., Komiyama, T., and Ferrari, M. (2002). Differences in oxygen re-saturation of high and calf muscles after two treadmill stress tests. *Comparative Biochemistry and Physiology Part A: Molecular & Integrative Phsyiology* 132(1), 67–73, https://doi.org/10.1016/S1095-6433(01)00531-1.

Quintana, H., Snyder, S.M., Purnell, W., Aponte, C., and Sita, J. (2007). Comparison of a standard psychiatric evaluation to rating scales and EEG in the differential diagnosis of attention-deficit/hyperactivity disorder. *Psychiatry Research* 152(2–

3), 211–222, https://doi.org/10.1016/j.psychres.2006.04.015.

Qureshi, M.N.I., Min, B., Jo, H.J., and Lee, B. (2016). Multiclass classification for the differential diagnosis on the ADHD subtypes using recursive feature elimination and hierarchical extreme learning machine: Structural MRI study. *PLoS One* 11(8), e0160697, https://doi.org/10.1371/journal.pone.0160697.

Raichle, M.E., MacLeod, A.M., Snyder, A.Z., Powers, W.J., Gusnard, D.A., and Shulman, G.L. (2001). A default mode of brain function. *Proceedings of the National Academy of Sciences of the United States of America* 98(2), 676–682, https://doi.org/10.1073/pnas.98.2.676.

Raichle, M.E., and Snyder, A.Z. (2007). A default mode of brain function: A brief history of an evolving idea. *NeuroImage* 37(4), 1083–1090, https://doi.org/10.1016/j.neuroimage.2007.02.041.

Raschle, N., Zuk, J., Ortiz-Mantilla, S., Sliva, D.D., Franceschi, A., Grant, P.E., Benasich, A.A., and Gaab, N. (2012). Pediatric neuroimaging in early childhood and infancy: Challenges and practical guidelines. *Annals of the New York Academy of Science* 1252, 43–50, https://doi.org/10.1111/j.1749-6632.2012.06457.x.

Reynolds, B., Ortengren, A., Richards, J.B., and de Wit, H. (2006). Dimensions of impulsive behavior: Personality and behavioral measures. *Personality and Individual Differences* 40(2), 305–315, https://doi.org/10.1016/j.paid.2005.03.024.

Rivera, S.M., Reiss, A.L., Eckert, M.A., and Menon, V. (2005). Developmental changes in mental arithmetic: Evidence for increased functional specialization in the left inferior parietal cortex. *Cerebral Cortex* 15(11), 1779–1790, https://doi.org/10.1093/cercor/bhi055.

Robertson, F.C., Douglas, T.S., and Meintjes, E.M. (2010). Motion artifact removal for functional near infrared spectroscopy: A comparison of methods. *IEEE Transactions on Biomedical Engineering* 57(6), 1377–1387, https://doi.org/10.1109/TBME.2009.2038667.

Rorden, C., and Brett, M. (2000). Stereotaxic display of brain lesions. *Behavioural*

Neurology 12(4), 191–200, https://doi.org/10.1155/2000/421719.

Roy, C.S., and Sherrington, C.S. (1890). On the regulation of the blood-supply of the brain. *The Journal of Physiology* 11(1–2), 85–158.

Rubia, K., Alegria, A., and Brinson, H. (2014). Imaging the ADHD brain- disorder-specificity, medication effects and clinical translation. *Expert Review of Neurotherapeutics* 14(5), 519–538, https://doi.org/10.1113/jphysiol.1890.sp000321.

Rubia, k., Smith, A.B., Brammer, M.J., and Taylor, E. (2003). Right inferior prefrontal cortex mediates response inhibition while mesial prefrontal cortex is responsible for error detection. *NeuroImage* 20(1), 351–358, https://doi.org/10.1016/S1053-8119(03)00275-1.

Rubinov, M., and Sporns, O. (2010). Complex network measures of brain connectivity: Uses and interpretations. *NeuroImage* 52(3), 1059–1069, https://doi.org/10.1016/j.neuroimage.2009.10.003.

Rushworth, M.F.S., Hadland, K.A., Paus, T., and Sipila, P.K. (2002). Role of the human medial frontal cortex in task switching: A combined fMRI and TMS study. *Journal of Neurophysiology* 87, 2577–2592, https://doi.org/10.1152/jn.2002.87.5.2577.

Saager, R.B., Telleri, N.L., and Berger, A.J. (2011). Two-detector Corrected Near Infrared Spectroscopy (C-NIRS) detects hemodynamic activation responses more robustly than single-detector NIRS. *NeuroImage* 55(4), 1679–1685, https://doi.org/10.1016/j.neuroimage.2011.01.043.

Santosh, P.J. (2000). Neuroimaging in child and adolescent psychiatric disorders. *Archives of Disease in Childhood* 82(5), 412–419, https://doi.org/10.1136/adc.82.5.412.

Santosh, P.J., and Singh, J. (2016). Drug treatment of autism spectrum disorder and its comorbidities in children and adolescents. *BJ Psych Advances* 22(3), 151–161, https://doi.org/10.1192/apt.bp.115.014597.

Sasai, S., Homae, F., Watanabe, H., Sasaki, A.T., Tanabe, H.C., Sadato, N., and Taga, G. (2012). A NIRS-fMRI study of resting state network. *NeuroImage* 63(1), 179–193,

https://doi.org/10.1016/j.neuroimage.2012.06.011.

Sasai, S., Homae, F., Watanabe, H., and Taga, G. (2011). Frequency-specific functional connectivity in the brain during resting state revealed by NIRS. *NeuroImage* 56(1), 252–257, https://doi.org/10.1016/j.neuroimage.2010.12.075.

Sasaki, T., Hashimoto, K., Oda, Y., Ishima, T., Kurata, T., Takahashi, J., kamat, Y., Kimura, H., Niitsu, T., Komatsu, H., Ishikawa, M., Hasegawa, T., Shiina, A., Hashimoto, T., Kanahara, N., Shiraishi, T., and Iyo, M. (2015). Decreased levels of serum oxytocin in pediatric patients with attention deficit/hyperactivity disorder. *Psychiatry Research* 228(3), 746–751, https://doi.org/10.1016/j.psychres.2015.05.029.

Sato, H., Kiguchi, M., Kawaguchi, F., and Maki, A. (2004). Practicality of wavelength selection to improve signal-to-noise ratio in near-infrared spectroscopy. *NeuroImage* 21(4), 1554–1562, https://doi.org/10.1016/j.neuroimage.2003.12.017.

Sato, J.R., Hoexter, M.Q., Castellanos, F.X., and Rohde, L.A. (2012). Abnormal brain connectivity patterns in adults with ADHD: A coherence study. *PLoS One* 7(9), e45671, https://doi.org/10.1371/journal.pone.0045671.

Schachar, R., Ickowicz, A., Crosbie, J., Donnelly, G.A.E., Reiz, J., L., Miceli, P.C., Harsanyi, Z., and Darke, A.C. (2008). Cognitive and behavioral effects of multilayer-release methylphenidate in the treatment of children with attention-deficit/hyperactivity disorder. *Journal of Child and Adolescent Psychopharmacology* 18(1), 11–24, https://doi.org/10.1089/cap.2007.0039.

Schelkanova, I., and Toronov, V. (2012). Independent component analysis of broadband near-infrared spectroscopy data acquired on adult human head. *Biomedical Optics Express* 3(1), 67–74, https://doi.org/10.1364/BOE.3.000064.

Schmitz, C.H., Graber, H.L., Luo, H., Arif, I., Hira, J., Pei, Y., Bluestone, A., Zhong, S., Andronica, R., Soller, I., Ramirez, N., Barbour, S.L.S., and Barbour, R.L. (2000). Instrumentation and calibration protocol for imaging dynamic features in dense-scattering media by optical tomography. *Applied Optics* 39(34), 6466–6486,

https://doi.org/10.1364/AO.39.006466.

Scholkmann, F., Kleiser, S., Metz, A.J., Zimmermann, R., Mata Pavia, J., Wolf, U., and Wolf, M. (2014). A review on continuous wave functional near-infrared spectroscopy and imaging instrumentation and methodology. *NeuroImage* 85, 6–27, https://doi.org/10.1016/j.neuroimage.2013.05.004.

Scholkmann, F., Spichtig, S., Muehlemann, T., and Wolf, M. (2010). How to detect and reduce movement artifacts in near-infrared imaging using moving standard deviation and spline interpolation. *Physiological Measurement* 31(5), 649–662, https://doi.org/10.1088/0967-3334/31/5/004.

Schroeter, M.L., Bucheler, M.M., Muller, K., Uludag, K., Obrig, H., Lohmann, G., Tittgemeyer, M., Villringer, A., and Cramon, D.Y.V. (2004). Towards a standard analysis for functional near-infrared imaging. *NeuroImage* 21(1), 283–290, https://doi.org/10.1016/j.neuroimage.2003.09.054.

Schulz, K.P., Fan, J., Tang, C.Y., Newcorn, J.H., Buchsbaum, M.S., Cheung, A.M., and Halperin, J.M. (2004). Response inhibition in adolescents diagnosed with attention deficit hyperactivity disorder during childhood: An event-related fMRI study. *American Journal of Psychiatry* 161(9), 1650–1657, https://doi.org/10.1176/appi.ajp.161.9.1650.

Shafritz, K.M., Marchione, K.E., Gore, J.C., Shaywitz, S.E., and Shaywitz, B.A. (2004). The effects of methylphenidate on neural systems of attention in attention deficit hyperactivity disorder. *American Journal of Psychiatry* 161(11), 1990–1997, https://doi.org/10.1176/appi.ajp.161.11.1990.

Shakil, S., Lee, C.H., and Keilholz, S.D. (2016). Evaluation of sliding window correlation performance for characterizing dynamic functional connectivity and brain states. *NeuroImage* 133, 111–128, https://doi.org/10.1016/j.neuroimage.2016.02.074.

Shattuck, D.W., Mirza, M., Adisetiyo, V., Hojatkashani, C., Salamon, G., Narr, K.L., Poldrack, R.A., Bilder, R.M., and Toga, A.W. (2008). Construction of a 3D probabilistic atlas of human cortical structures. *NeuroImage* 39(3), 1064–1080, https://doi.org/10.1016/j.neuroimage.2007.09.031.

Shaw, P., Eckstrand, K., Sharp, W., Blumenthal, J., Lerch, J.P., Greenstein, D., Clasen, L., Evans, A., Giedd, J., and Rapoport, J.L. (2007). Attention-deficit/hyperactivity disorder is characterized by a delay in cortical maturation. *Proceedings of the National Academy of Sciences of the United States of America* 104(49), 19649–19654, https://doi.org/10.1073/pnas.0707741104.

Shaw, P., Malek, M., Watson, B., Greenstein, D., de Rossi, P., and Sharp, W. (2013). Trajectories of cerebral cortical development in childhood and adolescence and adult attention-deficit/hyperactivity disorder. *Biological Psychiatry* 74(8), 599–606, https://doi.org/10.1016/j.biopsych.2013.04.007.

Shephard, E., Tye, C., Ashwood, K.L., Azadi, B., Asherson, P., Bolton, P.F., and McLoughlin, G. (2018). Resting-state neurophysiological activity patterns in young people with ASD, ADHD, and ASD + ADHD. *Journal of Autism and Developmental Disorders* 48(1), 110–122, https://doi.org/10.1007/s10803-017-3300-4.

Siegel, A.M., Marota, J.J.A., and Boas, D.A. (1999). Design and evaluation of a continuous-wave diffuse optical tomography system. *Optics Express* 4(8), 287–298, https://doi.org/10.1364/OE.4.000287.

Silk, T.J., Vance, A., Rinehart, N., Bradshaw, J.L., and Cunnington, R. (2009). White-matter abnormalities in attention deficit hyperactivity disorder: A diffusion tensor imaging study. *Human Brain Mapping* 30(9), 2757–2765, https://doi.org/10.1002/hbm.20703.

Singh, A.K., and Dan, I. (2006). Exploring the false discovery rate in multichannel NIRS. *NeuroImage* 33(2), 542–549, https://doi.org/10.1016/j.neuroimage.2006.06.047.

Singh, A.K., Okamoto, M., Dan, H., Jurcak, V., and Dan, I. (2005). Spatial registration of multichannel multi-subject fNIRS data to MNI space without MRI. *NeuroImage* 27(4), 842–851, https://doi.org/10.1016/j.neuroimage.2005.05.019.

Sinzig, J., Bruning, N., Morsch, D., and Lehmkuhl, G. (2008). Attention profiles in autistic children with and without comorbid hyperactivity and attention problems. *Acta Neuropsychiatrica* 20(4), 207–215, https://doi.org/10.1111/j.1601-

5215.2008.00292.x.

Siqueira, A.D.S., Junior, C.E.B., Comfort, W.E., Rohde, L.A., and Sato, J.R. (2014). Abnormal functional resting-state networks in ADHD: Graph theory and pattern recognition analysis of fMRI data. *BioMed Research International* 2014, 380531, https://doi.org/10.1155/2014/380531.

Smith, A.B., Taylor, E., Brammer, M., Toone, B., and Rubia, K. (2006). Task-specific hypoactivation in prefrontal and temprorparietal brain regions during motor inhibition and task switching in medictaion-naive children adnd adolescents with attention deficit hyperactivity disorder. *American Journal of Psychiatry* 163(6), 1044–1051, https://doi.org/10.1176/appi.ajp.163.6.1044.

Snyder, S.M., Quintana, H., Sexson, S.B., Knott, P., Haque, A.F.M., and Reynolds, D.A. (2008). Blinded, multi-center validation of EEG and rating scales in identifying ADHD within clinical sample. *Psychiatry Research* 159(3), 346–358, https://doi.org/10.1016/j.psychres.2007.05.006.

Snyder, S.M., Rugino, T.A., Homig, M., and Stein, M.A. (2015). Integration of an EEG biomarker with a clinician's ADHD evaluation. *Brain and Behavior* 5(4), e00330, https://doi.org/10.1002/brb3.330.

Sokolova, E., Oerlemans, A.M., Rommelse, N.N., Groot, P., Hartman, C.A., Glennon, J.C., Claassen, T., Heskes, T., and Buitelaar, J.K. (2017). A causal and mediation analysis of the comorbitiy between attention deficit hyperactivity disorder (ADHD) and autism spectrum disorder (ASD). *Journal of Autism and Developmental Disorders* 47, 1595–1604, https://doi.org/10.1007/s10803-017-3083-7.

Soldati, N., Calhoun, V.D., Bruzzone, L., and Jovicich, J. (2013). ICA analysis of fMRI with real-time constraints: An evaluation of fast detection performance as function of algorithms, parameters, and a *priori* conditions. *Frontiers in Human Neuroscience* 7, 19, https://doi.org/10.3389/fnhum.2013.00019.

Solleveld, M.M., Schrantee, A., Puts, N.A.J., Reneman, L., and Lucassen, P.J. (2017). Age-dependent, lasting effects of methylphenidate on the GABAergic system of

ADHD patients. *NeuroImage: Clinical* 15, 812–818, https://doi.org/10.1016/j.nicl.2017.06.003.

Soma, Y., Nakamura, K., Oyama, M., Tsuchiya, Y., and Yamamoto, M. (2009). Prevalence of attention-deficit/hyperactivity disorder (ADHD) symptoms in preschool children: Disrepancy between parent and teacher evaluations. *Environmental Health and Preventive Medicine* 14(2), 150–154, https://doi.org/10.1007/s12199-008-0075-4.

Sowell, E.R., Peterson, B.S., Thompson, P.M., Welcome, S.E., Henkenius, A.L., and Toga, A.W. (2003). Mapping cortical change across the human life span. *Nature Neuroscience* 6(3), 309–315, https://doi.org/10.1038/nn1008.

Sowell, E.R., Thompson, P.M., Holmes, C.J., Jernigan, T.L., and Toga, A.W. (1999). *In vivo* evidence for post-adolescent brain maturation in frontal and striatal regions. *Nature Neuroscience* 2(10), 859–861, https://doi.org/10.1038/13154.

Spencer, T., Brown, A., Seidman, L.J., Valera, E.M., Makris, N., Lomedico, A., Faraone, S.V., and Biederman, J. (2013). Effect of psychostimulants on brain structure and function in ADHD: A qualitative literature review of MRI-based neuroimaging studies. *Journal of Clinical Psychiatry* 74(9), 902–917, https://doi.org/10.4088/JCP.12r08287.

Starck, M., Grünwald, J., and Schlarb, A.A. (2016). Occurrence of ADHD in parents of ADHD children in a clinical sample. *Neuropsychiatric Disease and Treatment* 12, 581–588, https://doi.org/10.2147/NDT.S100238.

Steffener, J., Tabert, M., Reuben, A., and Stern, Y. (2009). Investigating hemodynamic response variability at the group level using basis functions. *NeuroImage* 49(3), 2113–2122, https://doi.org/10.1016/j.neuroimage.2009.11.014.

Stiles, J. (2011). Brain development and the nature versus nurture debate. *Progress in Brain Research* 189, 3–22, https://doi.org/10.1016/B978-0-444-53884-0.00015-4.

Strangman, G., Boas, D.A., and Sutton, J.P. (2002). Non-invasive neuroimaging using near-infrared light. *Biological Psychiatry* 52(7), 679–693, https://doi.org/10.1016/S0006-3223(02)01550-0.

Strangman, G., Franceschini, M.A., and Boas, D.A. (2003). Factors affecting the accuracy of near-infrared spectroscopy concentration calculations for focal changes in oxygenation parameters. *NeuroImage* 18(4), 865–879, https://doi.org/10.1016/s1053-8119(03)00021-1.

Strangman, G.E., Zhang, Q., and Zeffiro, T. (2009). Near-infrared neuroimaging with NinPy. *Frontiers in Neuroinformatics* 3, 12, https://doi.org/10.3389/neuro.11.012.2009.

Sudre, G., Szekely, E., Sharp, W., Kasparek, S., and Shaw, P. (2017). Multimodal mapping of the brain's functional connectivity and the adult outcome of attention deficit hyperactivity disorder. *Proceedings of the National Academy of Sciences of the United States of America* 114(44), 11787–11792, https://doi.org/10.1073/pnas.1705229114.

Sugiura, L., Ojima, S., Matsuba-Kurita, H., Dan, I., Tsuzuki, D., Katura, T., and Hagiwara, H. (2011). Sound to language: Different cortical processing for first and second languages in elementary school children as revealed by a large-scale study using fNIRS. *Cerebral Cortex* 21(10), 2374–2393, https://doi.org/10.1093/cercor/bhr023.

Suskauer, S.J., Simmonds, D.J., Caffo, B.S., Denckla, M.B., Pekar, J.J., and Mostofwsky, S.H. (2008). fMRI of intrasubject variability in ADHD: Anomalous premotor activity with prefrontal compensation. *Journal of the American Academy of Child and Adolescent Psychiatry* 47(10), 1141–1150, https://doi.org/10.1097/CHI.0b013e3181825b1f.

Sutoko, S., Chan, Y.L., Obata, A., Sato, H., Maki, A., Numata, T., Funane, T., Atsumori, H., Kiguchi, M., Tang, T.B., Li, Y., deB. Frederick, B., and Tong, Y. (2019a). Denoising of neuronal signal from mixed systemic low-frequency oscillation using peripheral measurement as noise regressor in near-infrared imaging. *Neurophotonics* 6(1), 015001, https://doi.org/10.1117/1.NPh.6.1.015001.

Sutoko, S., Monden, Y., Funane, T., Tokuda, T., Katura, T., Sato, H., Nagashima, M., Kiguchi, M., Maki, A., Yamagata, T., and Dan, I. (2018). Adaptive algorithm

utilizing acceptance rate for eliminating noisy epochs in block-design functional near-infrared spectroscopy data: Application to study in attention deficit/hyperactivity disorder children. *Neurophotonics* 5(4), 045001, https://doi.org/10.1117/1.NPh.5.4.045001.

Sutoko, S., Monden, Y., Tokuda, T., Ikeda, T., Nagashima, M., Funane, T., Atsumori, H., Kiguchi, M., Maki, A., Yamagata, T., and Dan, I. (2020). Atypical dynamic-connectivity recruitment in attention-deficit/hyperactivity disorder children: An insight into task-based dynamic connectivity through an fNIRS study. *Frontiers in Human Neuroscience* 14, 3, https://doi.org/10.3389/fnhum.2020.00003.

Sutoko, S., Monden, Y., Tokuda, T., Ikeda, T., Nagashima, M., Funane, T., Sato, H., Kiguchi, M., Maki, A., Yamagata, T., and Dan, I. (2019b). Exploring attentive task-based connectivity for screening attention deficit/hyperactivity disorder children: A functional near-infrared spectroscopy study. *Neurophotonics* 6(4), 045013, https://doi.org/10.1117/1.NPh.6.4.045013.

Sutoko, S., Monden, Y., Tokuda, T., Ikeda, T., Nagashima, M., Kiguchi, M., Maki, A., Yamagata, T., and Dan, I. (2019c). Distinct methylphenidate-evoked response measured using functional near-infrared spectroscopy during go/no-go task as a supporting differential diagnostic tool between attention-deficit/hyperactivity disorder and autism spectrum disorder comorbid children. *Frontiers in Human Neuroscience* 13, 7, https://doi.org/10.3389/fnhum.2019.00007.

Sutoko, S., Sato, H., Maki, A., Kiguchi, M., Hirabayashi, Y., Atsumori, H., Obata, A., Funane, T., and Katura, T. (2016). Tutorial on platform for optical topography analysis tools. *Neurophotonics* 3(1), 010801, https://doi.org/10.1117/1.NPh.3.1.010801.

Szekely, E., Sudre, G., Sharp, W., Leibenluft, E., and Shaw, P. (2017). Defining the neural substrate of the adult outcome of childhood ADHD: A multimodal neuroimaging study of response inhibition. *American Journal of Psychiatry* 174(9), 867–876, https://doi.org/10.1176/appi.ajp.2017.16111313.

Tachtsidis, I., Leung, T.S., Tisdall, M.M., Devendra, P., Smith, M., Delpy, D.T., and

Elwell, C.E. (2008). Investigation of frontal cortex, motor cortex and systemic haemodynamic changes during anagram solving. *Advances in Experimental Medicine and Biology* 614, 21–28, https://doi.org/10.1007/978-0-387-74911-2_3.

Tachtsidis, I., and Scholkmann, F. (2016). False positives and false negatives in functional near-infrared spectroscopy: Issues, challenges, and the way forward. *Neurophotonics* 3(3), 031405, https://doi.org/10.1117/1.NPh.3.3.031405.

Tak, S., and Ye, J.C. (2014). Statistical analysis of fNIRS data: A comprehensive review. *NeuroImage* 85, 72–91, https://doi.org/10.1016/j.neuroimage.2013.06.016.

Taki, Y., and Kawashima, R. (2012). Brain development in childhood. *Open Neuroimaging Journal* 6, 103–110.

Tamm, L., Menon, V., and Reiss, A.L. (2006). Parietal attentional system aberration during target detection in adolescents with attention deficit hyperactivity disorder: Event-related fMRI evidence. *American Journal of Psychiatry* 163, 1033–1043, https://doi.org/10.2174/1874440001206010103.

Tamm, L., Menon, V., Ringel, J., and Reiss, A.L. (2004). Event-related fMRI evidence of frontotemporal involvement in aberrant response inhibition and task switching in attention-deficit/hyperactivity disorder. *Journal of the American Academy of Child and Adolescent Psychiatry* 43(11), 1430–1440, https://doi.org/10.1097/01.chi.0000140452.51205.8d.

Tanaka, H., Katura, T., and Sato, H. (2013). Task-related component analysis for functional neuroimaging and application to near-infrared spectroscopy data. *NeuroImage* 64, 308–327, https://doi.org/10.1016/j.neuroimage.2012.08.044.

Tanaka, H., Katura, T., and Sato, H. (2014). Task-related oxygenation and cerebral blood volume changes estimated from NIRS signals in motor and cognitive tasks. *NeuroImage* 94, 107–119, https://doi.org/10.1016/j.neuroimage.2014.02.036.

Thatcher, R.W. (1992). Cyclic cortical reorganization during early childhood. *Brain and Cognition* 20(1), 24–50, https://doi.org/10.1016/0278-2626(92)90060-Y.

Thatcher, R.W., Walker, R.A., and Giudice, S. (1987). Human cerebral hemispheres develop at different rates and ages. *Science* 236(4805), 1110–1113,

https://doi.org/10.1126/science.3576224.

Tian, L., Jiang, T.Z., Wang, Y., Zang, Y.F., He, Y., Liang, M., Sui, M.Q., Cao, Q., Hu, S., Peng, M., and Zhuo, Y. (2006). Altered resting-state functional connectvity patterns of anterior cingulate cortex in adolescents with attention deficit hyperactivity disorder. *Neuroscience Letters* 400(1–2), 39–43, https://doi.org/10.1016/j.neulet.2006.02.022.

Tibshirani, R., Walther, G., and Hastie, T. (2001). Estimating the number of clusters in a data set via the gap statistic. *Journal of the Royal Statistical Society: Series B* 63(2), 411–423, https://doi.org/10.1111/1467-9868.00293.

Tie, Y., Suarez, R.O., Whalen, S., Radmanesh, A., Norton, I.H., and Golby, A.J. (2009). Comparison of blocked and event-related fMRI designs for pre-surgical language mapping. *NeuroImage* 47(Suppl 2), T107–T115, https://doi.org/10.1016/j.neuroimage.2008.11.020.

Tiemeier, H., Lenroot, R.K., Greenstein, D.K., Tran, L., Pierson, R., and Giedd, J.N. (2010). Cerebellum development during childhood and adolescence; a longitudinal morphometric MRI study. *NeuroImage* 49(1), 63–70, https://doi.org/10.1016/j.neuroimage.2009.08.016.

Tokuda, T., Ikeda, T., Monden, Y., Mizushima, S.G., Inoue, T., Nagashima, M., Shimamura, K., Arakawa, A., Kobayashi, M., Kuroiwa, C., Ujiie, Y., Dan, H., Kyutoku, Y., Taniguchi, T., Shimoizumi, H., Yamagata, T., Yamaguchi, M.K., Kanazawa, S., Sakuta, R., and Dan, I. (2018). Methylphenidate-elicited distinct neuropharmacological activation patterns between medication-naive attention deficit hyperactivity disorder children with and without comorbid autism spectrum disorder: A functional near-infrared spectroscopy study. *Neuropsychiatry (London)* 8(3), 917–929, https://doi.org/10.4172/Neuropsychiatry.1000418.

Tong, Y., and Frederick, B.D. (2010). Time lag dependent multimodal processing of concurrent fMRI and near-infrared spectroscopy (NIRS) data suggests a global circulatory origin for low-frequency oscillation signals in human brain.

NeuroImage 53(2), 553–564, https://doi.org/10.1016/j.neuroimage.2010.06.049.

Tsuzuki, D., Jurcak, V., Singh, A.K., Okamoto, M., Watanabe, E., and Dan, I. (2007). Virtual spatial registration of stand-alone fNIRS data to MNI space. *NeuroImage* 34(4), 1506–1518, https://doi.org/10.1016/j.neuroimage.2006.10.043.

Tye, C., Asherson, P., Ashwood, K.L., Azadi, B., Bolton, P., and McLoughlin, G. (2014). Attention and inhibition in children with ASD, ADHD and co-morbid ASD + ADHD: An event-related potential study. *Psychological Medicine* 44(5), 1101–1116, https://doi.org/10.1017/S0033291713001049.

Uddin, L.Q., Clare Kelly, A.M., Biswal, B.B., Margulies, D.S., Shehzad, Z., Shaw, D., Ghaffari, M., Rotrosen, J., Adler, L.A., Castellanos, F.X., and Milham, M.P. (2008). Network homogeneity reveals decreased integrity of default-mode network in ADHD. *Journal of Neuroscience Methods* 169(1), 249–254, https://doi.org/10.1016/j.jneumeth.2007.11.031.

Uddin, L.Q., Dajani, D.R., Voorhies, W., Bednarz, H., and Kana, R.K. (2017). Progress and roadblocks in the search for brain-based biomarkers of autism and attention-deficit/hyperactivity disorder. *Translational Psychiatry* 7(8), e1218, https://doi.org/10.1038/tp.2017.164.

Uga, M., Dan, I., Sano, T., Dan, H., and Watanabe, E. (2014). Optimizing the general linear model for functional near-infrared spectroscopy: An adaptive hemodynamic response function approach. *Neurophotonics* 1(1), 015004, https://doi.org/10.1117/1.NPh.1.1.015004.

Vaidya, C.J., Austin, G., Kirkorian, G., Ridlehuber, H.W., Desmond, J.E., Glover, G.H., and Gabrieli, J.D.E. (1998). Selective effects of methylphenidate in attention deficit hyperactivity disorder: A functional magnetic resonance study. *Proceedings of the National Academy of Sciences of the United States of America* 95(24), 14494–14499, https://doi.org/10.1073/pnas.95.24.14494.

van der Maas, H.L.J., and Molenaar, P.C.M. (1992). Stagewise cognitive development: An application of catastrophe theory. *Pyschological Review* 99(3), 395–417, https://doi.org/10.1037/0033-295x.99.3.395.

van Rooij, D., Hartman, C.A., Mennes, M., Oosterlaan, J., Franke, B., Rommelse, N., Heslenfeld, D., Faraone, S.V., Buitelaar, J.K., and Hoekstra, P.J. (2015). Altered neural connectivity during response inhibition in adolescents with attention-deficit/hyperactivity disorder and their unaffected siblings. *NeuroImage: Clinical* 7, 325–335, https://doi.org/10.1016/j.nicl.2015.01.004.

Vance, A., Silk, T.J., Casey, M., Rinehart, N.J., Bradshaw, J.L., Bellgrove, M.A., and Cunnington, R. (2007). Right parietal dysfunction in children with attention deficit hyperactivity disorder, combined type: A functional MRI study. *Molecular Psychiatry* 12, 826–832, https://doi.org/10.1038/sj.mp.4001999.

Vande Voort, J.L., He, J.P., Jameson, N.D., and Merikangas, K.R. (2014). Impact of the DSM-5 attention-deficit/hyperactivity disorder age-of-onset criterion in the US adolescent population. *Journal of the American Academy of Child and Adolescent Psychiatry* 53(7), 736–744, https://doi.org/10.1016/j.jaac.2014.03.005.

Vara, A.S., Pang, E.W., Doyle-Thomas, K.A., Vidal, J., Taylor, M.J., and Anagnostou, E. (2014). Is inhibitory control a 'no-go' in adolescents with autism spectrum disorder? *Molecular Autism* 5, 6, https://doi.org/10.1186/2040-2392-5-6.

Verbruggen, F., and Logan, G.D. (2008). Response inhibition in the stop-signal paradigm. *Trends in Cognitive Sciences* 12(11), 418–424, https://doi.org/10.1016/j.tics.2008.07.005.

Verbruggen, F., Stevens, T., and Chambers, C.D. (2014). Proactive and reactive stopping when distracted: An attentional account. *Journal of Experimental Psychology. Human Perception and Performance* 40(4), 1295–1300, https://doi.org/10.1037/a0036542.

Vidaurre, D., Smith, S.M., and Woolrich, M.W. (2017). Brain network dynamics are hierarchically organized in time. *Proceedings of the National Academy of Sciences of the United States of America* 114(48), 12827–12832, https://doi.org/10.1073/pnas.1705120114.

Vinette, S.A., Dunn, J.F., Slone, E., and Federico, P. (2015). Artifact reduction in long-term monitoring of cerebral hemodynamics using near-infrared spectroscopy.

Neurophotonics 2(2), 025004, https://doi.org/10.1117/1.NPh.2.2.025004.

Virtanen, J., Noponen, T., Kotilahti, K., Virtanen, J., and Ilmoniemi, R.J. (2011). Accelerometer-based method for correcting signal baseline changes caused by motion artifacts in medical near-infrared spectroscopy. *Journal of Biomedical Optics* 16(8), 087005, https://doi.org/10.1117/1.3606576.

Virtanen, J., Noponen, T., and Merilainen, P. (2009). Comparison of principal and independent component analysis in removing extracerebral interference from near-infrared spectroscopy signals. *Journal of Biomedical Optics* 14(5), 054032, https://doi.org/10.1117/1.3253323.

Wendelken, C., Ferrer, E., Ghetti, S., Bailey, S.K., Cutting, L., and Bunge, S.A. (2017). Frontoparietal structural connectivity in childhood predicts development of functional connectivity and reasoning ability: A large-scale longitudinal investigation. *Journal of Neuroscience* 37(35), 8549–8558, https://doi.org/10.1523/JNEUROSCI.3726-16.2017.

Worsley, K.J., and Friston, K.J. (1995). Analysis of fMRI time-series revisited – Again. *NeuroImage* 2(3), 173–181, https://doi.org/10.1006/nimg.1995.1023.

Xiao, T., Xiao, Z., Ke, X., Hong, S., Yang, H., Su, Y., Chu, K., Xiao, X., Shen, J., and Liu, Y. (2012). Response inhibition impairment in high functioning autism and attention deficit hyperactivity disorder: Evidence from near-infrared spectrocopy data. *PLoS One* 7(10), e46569, https://doi.org/10.1371/journal.pone.0046569.

Xu, J., Liu, X., Zhang, J., Li, Z., Wang, X., Fang, F., and Niu, H. (2015). FC-NIRS: A functional connectivity analysis tool for near-infrared spectroscopy data. *BioMed Research International* 2015, 248724, https://doi.org/10.1155/2015/248724.

Yücel, M.A., Selb, J., Cooper, R.J., and Boas, D. (2014). Targeted principle component analysis: A new motion artifact correction approach for near-infrared spectroscopy. *Journal of Innovative Optical Health Sciences* 7(2), 1350066, https://doi.org/10.1142/S1793545813500661.

Yamashita, Y., Maki, A., and Koizumi, H. (2001). Wavelength dependence of the precision of noninvasive optical measurement of oxy-, deoxy-, and total-

hemoglobin concentration. *Medical Physics* 28(6), 1108–1114, https://doi.org/10.1118/1.1373401.

Yao, D., Guo, X., Zhao, Q., Liu, L., Cao, Q., Wang, Y., Calhoun, V.D., Sun, L., and Sui, J. (2018). Discriminating ADHD from healthy controls using a novel feature selection method based on relative importance and ensemble learning. *Conference Proceedings IEEE Engineering in Medicine and Biology Society* 2018, 4632–4635, https://doi.org/10.1109/EMBC.2018.8513155.

Yao, J., Liu, Y., and Zhou, S. (2019). Effect of eating breakfast on cognitive development of elementary and middle school students: An empirical study using large-scale provincial survey data. *Medical Science Monitor* 25, 8843–8853, https://doi.org/10.12659/MSM.920459.

Yasumura, A., Kokubo, N., Yamamoto, H., Yasumura, Y., Nakagawa, E., Kaga, M., Hiraki, K., and Inagaki, M. (2014). Neurobehavioral and hemodynamic evaluation of stropp and reverse stroop interference in children with attention-deficit/hyperactivity disorder. *Brain and Development* 36(2), 97–106, https://doi.org/10.1016/j.braindev.2013.01.005.

Ye, J.C., Tak, S., Jang, K.E., Jung, J., and Jang, J. (2009). NIRS-SPM: Statistical parametric mapping for near-infrared spectroscopy. *NeuroImage* 44(2), 428–447, https://doi.org/10.1016/j.neuroimage.2008.08.036.

Zablotsky, B., Black, L.I., Maenner, M.J., Schieve, L.A., Danielson, M.L., Bitsko, R.H., Blumberg, S.J., Kogan, M.D., and Boyle, C.A. (2019). Prevalence and trends of developmental disabilities among children in the United States: 2009–2017. *Pediatrics* 144(4), e20190811, https://doi.org/10.1542/peds.2019-0811.

Zeng, N., Ayyub, M., Sun, H., Wen, X., Xiang, P., and Gao, Z. (2017). Effects of physical activity on motor skills and cognitive development in early childhood: A systematic review. *BioMed Research International* 2017, 2760716, https://doi.org/10.1155/2017/2760716.

Zhang, H., Duan, L., Zhang, Y.J., Lu, C.M., Liu, H., and Zhu, C.Z. (2011). Test-retest assessment of independent component analysis-derived resting state functional

connectivity based on functional near-infarred spectrosocopy. *NeuroImage* 55(2), 607–615, https://doi.org/10.1016/j.neuroimage.2010.12.007.

Zhang, H., Zhang, Y.J., Lu, C.M., Ma, S.Y., Zang, Y.F., and Zhu, C.Z. (2010a). Functional connectivity as revealed by independent component analysis of resting-state fNIRS measurements. *NeuroImage* 51(3), 1150–1161, https://doi.org/10.1016/j.neuroimage.2010.02.080.

Zhang, Y., Books, D.H., Franceschini, M.A., and Boas, D.A. (2005). Eigenvector-based spatial filtering for reduction of physiological interference in diffuse optical imaging. *Journal of Biomedical Optics* 10(1), 11014, https://doi.org/10.1117/1.1852552.

Zhang, Y.J., Duan, L., Biswal, B.B., Lu, C.M., and Zhu, C.Z. (2012). Determination of dominant frequency of resting-state brain interaction within one functional system. *PLoS One* 7(12), e51584, https://doi.org/10.1371/journal.pone.0051584.

Zhang, Y.J., Lu, C.M., Biswal, B.B., Zang, Y.F., Peng, D.L., and Zhu, C.Z. (2010b). Detecting resting-state functional connectivity in the language system using functional near-infrared spectroscopy. *Journal of Biomedical Optics* 15(4), 047003, https://doi.org/10.1117/1.3462973.

Zhu, C.Z., Zang, Y.F., Cao, Q.J., Yan, C.G., He, Y., Jiang, T.Z., Sui, M.Q., and Wang, Y.F. (2008). Fischer discriminative analysis of resting-state brain function for attention-deficit/hyperactivity disorder. *NeuroImage* 40(1), 110–120, https://doi.org/10.1016/j.neuroimage.2007.11.029.